INFORMATION TO USERS

This dissertation was produced from a microfilm copy of the original document. While the most advanced technological means to photograph and reproduce this document have been used, the quality is heavily dependent upon the quality of the original submitted.

The following explanation of techniques is provided to help you understand markings or patterns which may appear on this reproduction.

1. The sign or "target" for pages apparently lacking from the document photographed is "Missing Page(s)". If it was possible to obtain the missing page(s) or section, they are spliced into the film along with adjacent pages. This may have necessitated cutting thru an image and duplicating adjacent pages to insure you complete continuity.

2. When an image on the film is obliterated with a large round black mark, it is an indication that the photographer suspected that the copy may have moved during exposure and thus cause a blurred image. You will find a good image of the page in the adjacent frame.

3. When a map, drawing or chart, etc., was part of the material being photographed the photographer followed a definite method in "sectioning" the material. It is customary to begin photoing at the upper left hand corner of a large sheet and to continue photoing from left to right in equal sections with a small overlap. If necessary, sectioning is continued again — beginning below the first row and continuing on until complete.

4. The majority of users indicate that the textual content is of greatest value, however, a somewhat higher quality reproduction could be made from "photographs" if essential to the understanding of the dissertation. Silver prints of "photographs" may be ordered at additional charge by writing the Order Department, giving the catalog number, title, author and specific pages you wish reproduced.

University Microfilms

300 North Zeeb Road
Ann Arbor, Michigan 48106

A Xerox Education Company

73-2840

HASPEL, Mitchell Stuart, 1940-
A SLOW WAVEGUIDE WITH CEM PROPAGATION AND CEF ELECTRON BEAM.

The City University of New York, Ph.D., 1972
Engineering, electrical

University Microfilms, A XEROX Company, Ann Arbor, Michigan

A SLOW WAVEGUIDE WITH CEM PROPAGATION

AND CEF ELECTRON BEAM

by

MITCHELL S. HASPEL

A dissertation submitted to the Graduate Faculty in Engineering in partial fulfillment of the requirements for the degree of Doctor of Philosophy, The City University of New York

1972

This manuscript has been read and accepted for the Graduate Faculty in Engineering in satisfaction of the dissertation requirement for the degree of Doctor of Philosophy.

7/21/72
date

Chairman of Examining Committee

7/21/72
date

Executive Officer

Supervisory Committee

Professor N. Jen

Professor P. Karmel

Professor H. Soodak

Professor M. Ettenberg, chairman

The City University of New York

DEDICATION

This work is dedicated to the Jews of the Soviet Union and to all men who struggle for spiritual and corporeal freedom.

ושב יי־הוה אלקיך את־שבותך
ורחמך ושב וקבצך מכל־העמים
אשר הפיצך יי־הוה אלקיך שמה׃
דברים ל׃ג

That then the Lord thy God will turn thy captivity, and have compassion upon thee, and will return and gather thee from all the peoples, whither the Lord thy God hath scattered thee.

Deuteronomy 30:3

תושלב"ע

ACKNOWLEDGEMENTS

בן זומא אומר: איזהו חכם, הלומד מכל אדם...
פרקי אבות ד:א

Ben Zoma said: Who is wise? He who learns from every man . . .
Ethics of the Fathers 4:1

There were many who contributed in their various ways to the completion of this work. To thank them all would be impossible, but I would be remiss if I were not to express my appreciation to those who contributed most.

Without the encouragement and help of my parents, Mr. and Mrs. Leo Haspel, I doubt if I could have completed the task.

My sincere thanks go to my advisor, Professor Morris Ettenberg, for his guidance, support and interest throughout the entire period of the research.

To Bracha Hollander, who typed and proofread the manuscript, and who always was ready to provide encouragement and moral support, I will always be indebted.

I am grateful to Professor Wilhelm Magnus, of the Courant Institute, for his aid in confirming the collapse of the Theorem due to Borg of Chapter 4.

My thankfulness goes to those who helped in the experiments and in the preparation of the manuscript. I apologize to anyone who should be listed but was omitted in error. They are: Frank Barrone, Ruth Hellinger, Dr. Stephen Kleinman, Ervin Lemberger, Mal H. Lemeshow, David Pressman, Bernard Roiss, Mrs. Ruth Rosenzweig, Joseph Siev, Fran Sussman, and the men of my advisory and examination committees.

I wish to acknowledge the financial support of the Graduate Division of the City University of New York, of the City College of New York, and of the National Science Foundation.

TABLE OF CONTENTS

LIST OF TABLES

LIST OF FIGURES

ABSTRACT

A SLOW WAVEGUIDE WITH CEM PROPAGATION AND CEF ELECTRON BEAM

by

Mitchell S. Haspel

Advisor: Professor Morris Ettenberg

An interaction mechanism is proposed between an electron beam and an electromagnetic wave with the view towards amplification of the wave at the expense of the beam energy. The beam is centrifugal-electrostatically-focused in a coaxial periodic geometry which supports a perturbation of the circular-electric-mode. The problem falls into four natural parts consisting of the interaction and three concomitant areas, namely, the solution to the wave equation and Laplace's equation and the electron dynamics and stability in the static fields.

In the solution of the wave equation the fields and dispersion of the circuit are found by a modal expansion method. In addition, an approximate method using a Hill's equation is utilized to arrive at an expression for dispersion which is simpler in form than the result of the expansion method. The results of an experimental program are given which are in very good agreement with the theoretical findings.

The solution of Laplace's equation in the periodic geometry involves solution of a mixed boundary value potential problem for the approximation of infinitesimal tooth width. This is secured using conformal mapping theory and the result is found to be accurate for a wide range of geometrical configurations, especially so for the geometry relevant to this problem. The results are verified experimentally with very good agreement.

In the area of electron dynamics in the static fields, space charge effects and stability in the uniform system is first considered. Next, neglecting space charge the nonzero thickness beam is examined to find the choice of equilibrium radius and nonlinear natural period of electron oscillation.

This latter question is tied to electron stability in the periodic fields. Addressing the question of single electron stability in the peridic system it is found that for regions where interaction might be pursued the differential equation of interest is a nonhomogenious piecewise quadratic Hill's equation. The homogeneous equation is discussed and an explicit solution found for stability. Only a few such explicit solutions have previously been found. The results are compared with several stability criteria, one of which is found to break down. The stability plane is compared with that for the Mathieu equation obtained by truncation of the Fourier series. Computer trajectories are presented for various points in the plane verifying the theoretical findings. Applying these results it is found that the motion will be stable and nonlinear period effects can improve stability. An approximate particular solution is given for the nonhomogeneous differential equation.

Finally, linear interaction is considered based upon a very simple model. Small signal gain is found and a numerical example given. The effects of the rf magnetic field are found and the consequences considered for a TE mode synchronous interaction. The need for a drastic change in the interaction model is indicated.

A discussion is given in the appendix of the calculation of the Parabolic Cylinder Functions by computer which were needed in the analysis.

CHAPTER 1

INTRODUCTION

1.1 Motivation

The interaction between electrons and electromagnetic waves is of interest because of the possible interchange of energy between the two. In microwave amplifiers and oscillators such interactions are useful in extracting energy from an electron beam and conversion into microwave energy while in modern particle accelerators the inverse process is used to increase the energy of electrons at the expense of the wave energy. This work addresses the former mechanism and investigates a particular interaction mechanism and some of its concomitant problems.

In order to obtain net interaction in traveling-wave devices the electron stream longitudinal velocity approximately equals the phase velocity of the interacting wave. To produce a wave whose phase velocity is sufficiently low requires a guiding structure which often consists of a geometry periodic with respect to the longitudinal dimension. The particular geometry and mode of operation considered herein will be seen to contain certain advantages.

To obtain useful interaction the process must occur over relatively long lengths and therefore some means must be provided to focus the electron beam and maintain its position relative to the guiding structure. Most schemes utilize magnetic fields which involve large weight and size and power consumption in the case of a solenoid. An alternative is the use of electostatic focusing methods. Chernov[1] has contrasted various focusing schemes and has favored the centrifugal-electrostatically-focused method, or CEF, which basically balances the forces on a rotating annular electron beam by the use of an external radial electrostatic field. This method is adopted here with the exception that the periodic nature of the guiding structure introduces a perturbation of the electrostatic field which requires consideration of electron stability.

Due to the requirements of synchronization and focusing the kinetic energy of the electrons as they enter the interaction region is partitioned into

longitudinal and rotational energies. Normally, the source of energy for the amplification process in traveling-wave devices[2] is the longitudinal energy and the interaction between electrons and wave occurs through a longitudinal electric field. The interaction considered here is with an electric field vector purely in the θ direction and therefore the proposed source of energy is rotational. The rf field mode considered for interaction is a perturbation of the coaxial TE_{01} mode, which we refer to as a circular-electric-mode, or CEM.

For interations with a longitudinal electric field the synchronous elecrons experience accelerating or retarding forces depending upon their phase. If we assume that they do not interact with each other we note that as the interaction progresses the electrons in a nonzero field move away from synchronous velocity. Since in the proposed scheme there is no first order coupling to the longitudinal velocity, synchronism is maintained. Since longitudinal energy can be recovered after interaction, in principle, by use of a depressed collector[3], and since the electrons will have the same energy independent of phase, the use of such a scheme in our case can be particularly effective. For longitudinal-field interactions, after the energy exchange process the electrons are no longer mono-energetic in the z direction and therefore no single value of collector potential will suffice.

As microwave tubes of normal geometry are scaled to higher frequencies the slow wave circuits become exceedingly small and therefore not capable of dissipating large amounts of intercepted beam current. In addition, the magnitude of the beam current itself is limited by maximum current densities available from cathode materials, possible convergence ratios of electron guns and values of current densities which can successfully be focused. These limiting factors on the frequency and power are obviated since in the annular geometry the beam current is distributed over an arbitrarily large cross section since the system may be constructed at an arbitrarily large radius of curvature. This is true since for large values of radius of curvature the frequency characteristics of the slow wave circuit in CEM is practically independent of the curvature and the system may be treated as planar. Modest current density can therefore lead to large total current.

From the standpoint of losses CEM is in itself well suited to high frequency.

For most waveguide modes the attenuation reaches a minimum at some frequency and increases for larger values of frequency. On the other hand, for CEM the attenuation is a monotonically decreasing function of frequency, approaching zero asymptotically.

In addition, CEM is well suited to high power applications since the electric field is zero at all metal surfaces. The maximum electric field occurs far from these boundaries, a situation which would tend to impede the production of arcs due to high power transmission.

Selective mode control is facilitated by the simple fact that for CEM the currents on the metal boundaries are in the θ direction only and so construction in a stacked ring array would damp unwanted modes which could otherwise exist.

1.2 Physical Picture of the Interaction Mechanism

For this simple picture we assume that the static field is taken to be uniform with respect to z and that the only rf force is due to the "cold" electric field. An electron enters the interaction region with the longitudinal velocity required for synchronism with the electromagnetic wave and with the angular momentum required for equilibrium in the static field at the injected radius. We assume the radial velocity to be zero on injection. The electron will experience a tangential force due to the rf electric field, the magnitude and sign of this force depending upon the time of entrance of the electron into the interaction region. Under this force the electron angular momentum will change and the orbit will vary from its heretofore helical form. As viewed in cross section the orbit will change from a circular one to one where the radius is a function of time. Those electrons in an accelerating field gain energy from the field and move to larger values of radius while those in a retarding field give up their energy to the field and move to smaller radial positions. Since the electrons are equally distributed with respect to phase we as yet have no reason to expect net interchange of energy. The interaction field, however, decreases in magnitude with increasing radius because the slow wave circuit is placed at the inner boundary. Therefore, those electrons which

remove energy from the field move to regions of weaker fields while those which give up energy move to stronger interaction. This simple picture therefore predicts that there will be a net transfer of energy from electrons to field resulting in amplification.

Based on this simple picture there is no true bunching of the electron beam in the normal sense. The electrons are merely shifted radially but the azimuthal and axial densities remain constant. The trajectories of the individual electrons are not circularly symmetric but because the beam as a whole and the interacting fields are symmetric the beam locus maintains this symmetry. The way the beam builds up in radial displacement as the interaction progresses is shown in Fig. 1-1. It is to be noted again that the simple model has neglected the magnetic field. The way that this modifies the above is discussed in Chap. 5.

1.3 Some Related Work

There have been very few attempts to use CEM for interaction. The *Ubitron*[4,5] uses magnetic undulation of an electron beam and uses no periodic structure for interaction.

The CEF focusing scheme was used in conjunction with a normal traveling-wave-tube helix[6], backward wave interaction[7,8] and θ-periodic interaction with a TEM wave, the *Helitron*[9,10]. There also has been some general discussion of these devices[11,12].

1.4 Organization

The major aspects of the problem are considered separately to obtain individual effects. The research undertaken falls into four natural parts and these are considered in the four following chapters. These areas consist of the solution of Laplace's equation and the wave equation, electron stability and dynamics in the static fields and the interaction problem.

Chapter 2 concerns itself with the solution of the wave equation. The fields

and dispersion of the circuit are found by the method of modal expansion. An approximate method using a Hill's equation is used to find an approximate dispersion equation which is far simpler in form than the modal expansion result. Experimental results are given which are in good agreement with the theoretical findings.

In Chapter 3 we are concerned with the solution of the static fields in the periodic geometry. These fields are necessary to determine stability of the electron trajectories in the periodic fields. The solution to this mixed boundary value potential problem for infinitesimal tooth width is accomplished by utilization of conformal mapping theory and the result is found to be accurate for a wide range of geometrical configurations. For the geometry consistent with the results of Chapter 2 we find excellent accuracy. The results are verified experimentally by the use of analog field plotting. We have found excellent agreement.

In Chapter 4 our attention is turned to electron dynamics in the static field situation. We consider space charge effects and stability for the uniform system. Neglecting space charge effects we examine the nonzero thickness beam to find the equilibrium radius choice and nonlinear effects upon the natural period of electron oscillation which is tied to the question of electron stability in the periodic fields. We then address the question of electron stability in the periodic fields ignoring space charge. We find that for regions where interaction might be pursued the differential equation of interest is a nonhomogeneous piecewise quadratic Hill's equation. The homogeneous equation is discussed and an explicit solution is found for the stability. This represents an explicit solution for a Hill's equation of which only a few are known. The question of coexistence would therefore be a very interesting realm of study.

The results are compared with several stability criteria, one of which is found to break down. The stability plane is compared with that for the Mathieu equation obtained by truncation of the Fourier series. Computer trajectories are presented for various points in the stability plane which verify the theoretical results.

Applying the results we find that the electron motion will be stable and nonlinear period effects improve the stability. An approximate particular solution is found for the nonhomogeneous differential equation.

In Chapter 5 linear interaction is considered based on a simple model using results found in the preceding chapters. The value of small signal gain is found and a numerical example given. A short discussion of a large signal effect follows. Finally, the effects of the magnetic field are discussed, which were ignored in the rest of the chapter.

An appendix is provided which discusses the calculation of the Parabolic Cylinder Functions needed in Chapter 4.

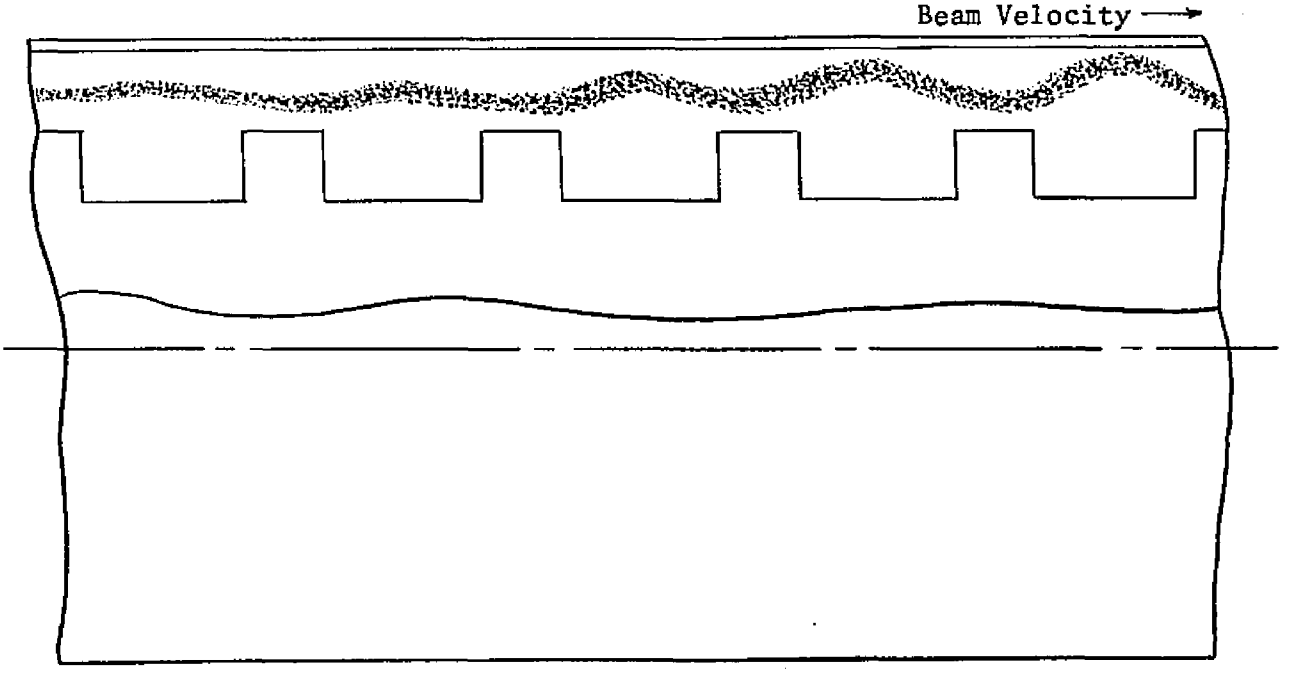

Fig. 1-1 Beam-Wave Interaction

($\beta \approx 2\pi/L$)

CHAPTER 2

THE ELECTRODYNAMIC PROBLEM

2.1 Preliminary Considerations

We will consider, as the first problem, the electrodynamic fields which exist in the guiding structure for the desired mode. Two aspects of the solution are of importance. Primarily, we are interested in the dispersion of the slow wave structure. This is the relationship between frequency of free-space propagation constant and the propagation constant of a particular space harmonic of the field. This information yields the phase velocity of that space harmonic as a function of frequency. For synchronism between the electrons and the wave, we require that the translational velocity of the electrons equal the phase velocity of the wave.

Therefore, when the system is operated as an amplifier we may calculate the required longitudinal energy of the electron beam given the frequency of the input signal. This information is required when one physically sets the voltages on the electron injection scheme. On the other hand, if one were to design an oscillator, one knows the tuning characteristics of the system, which is simply the relationship between the voltage and output frequency.

The second aspect of the solution which is of importance is the determination of the fields and space harmonic content. The transverse variation of the field with radius is important in determining the gain of the system as explained in Chap. 1.

The slow wave structure consists of an outer cylinder and an inner boundary consisting of alternating stepped cylinders of different radii. This corrugated inner boundary is therefore periodic so that the combined coaxial system forms a periodic guiding structure. The structure is assumed to be many periods in length and consequently with respect to the major body of the system we may take the circuit to be infinite in length. Except for the immediate vicinity of the ends, the solution for the fields will be accurate. The end conditions will shift the dispersion relation slightly, but it too will be quite accurate if the structure is many periods long. On the other hand, by proper matching techniques applied to both ends one may make the system seem to be infinitely long by the elimination of reflections.

The geometry of interest is of large radius of curvature. This situation follows due to the requirements of input and output schemes and the desire to have interaction take place over a large area. The differences in radii in the interaction region are therefore much less than their absolute values, that is, $\Delta r << r$. As the system radius of curvature becomes larger the geometry appears more planar. Based upon this heuristic reasoning, we conclude that we may treat the geometry as planar and obtain accurate results. We write the Laplacian in cylindrical coordinates with axially symmetric geometry and solution

$$\nabla^2\psi = \frac{\partial^2\psi}{\partial r^2} + \frac{1}{r}\frac{\partial\psi}{\partial r} + \frac{\partial^2\psi}{\partial z^2} \tag{2-1A}$$

For large radius of curvature $\frac{\partial^2\psi}{\partial r^2} >> \frac{1}{r}\frac{\partial\psi}{\partial r}$ and we have that

$$\nabla^2\psi \approx \frac{\partial^2\psi}{\partial r^2} + \frac{\partial^2\psi}{\partial z^2} \tag{2-1B}$$

Eq. 2-1B indicates that the Laplacian is approximated by the rectangular Laplacian provided we associate r with one of the rectangular coordinates.

The conclusion drawn above may be illustrated for a simple relevant example. Consider a coaxial transmission line of inner radius r_i and outer radius r_o. As is well known, the axial magnetic field for the TE_{om} mode is

$$H_z = \left[A J_o(k_c r) + B N_o(k_c r)\right] e^{i(\omega t \pm \beta z)} \tag{2-2A}$$

$$k_c^2 = k^2 - \beta^2 \tag{2-2B}$$

where J_o is the Bessel function of first kind and N_o is the Neumann function, both of zeroth order. From the condition that $\frac{\partial H_z}{\partial r}$, proportional to E_Θ, be zero at $r=r_i$ and $r=r_o$ we find the equation determining k_c

$$J_1(\lambda x) N_1(x) = J_1(x) N_1(\lambda x) \tag{2-3A}$$

$$\lambda \equiv \frac{r_o}{r_i} \tag{2-3B}$$

$$X \equiv k_c r_i \tag{2-3C}$$

As the radius of curvature increases λ approaches unity and x approaches infinity. For this situation we may use the asymptotic forms[13] for the Bessel functions

$$J_\nu(z) \approx \sqrt{\frac{2}{\pi z}}\left\{\cos\left(z - \nu\frac{\pi}{2} - \frac{\pi}{4}\right)\right\} \tag{2-4A}$$

$$N_\nu(z) \approx \sqrt{\frac{2}{\pi z}}\left\{\sin\left(z - \nu\frac{\pi}{2} - \frac{\pi}{4}\right)\right\} \tag{2-4B}$$

in 2-3A to find that the requirement reduces to

$$\sin(\lambda - 1)X \approx 0 \tag{2-5A}$$

yielding

$$k_c \approx \frac{\ell\pi}{r_o - r_i}$$

$$\ell = 1, 2, 3, \cdots \tag{2-5B}$$

which is recognized as the result for parallel plate waveguide. In particular, for the TE_{01} mode, relevant to our case, we take ℓ=1. We therefore note that for large radius of curvature the rectangular approximation is indeed accurate and will be used from this point on for all considerations. The relevant rectangular geometry is shown in Fig. 2-1.

The equivalent field pattern, existing in this structure and corresponding to the perturbed coaxial TE_{01} mode, is such that the electric field is purely in the x direction and is unidirectional with respect to variations in y, corresponding to ℓ=1, above.

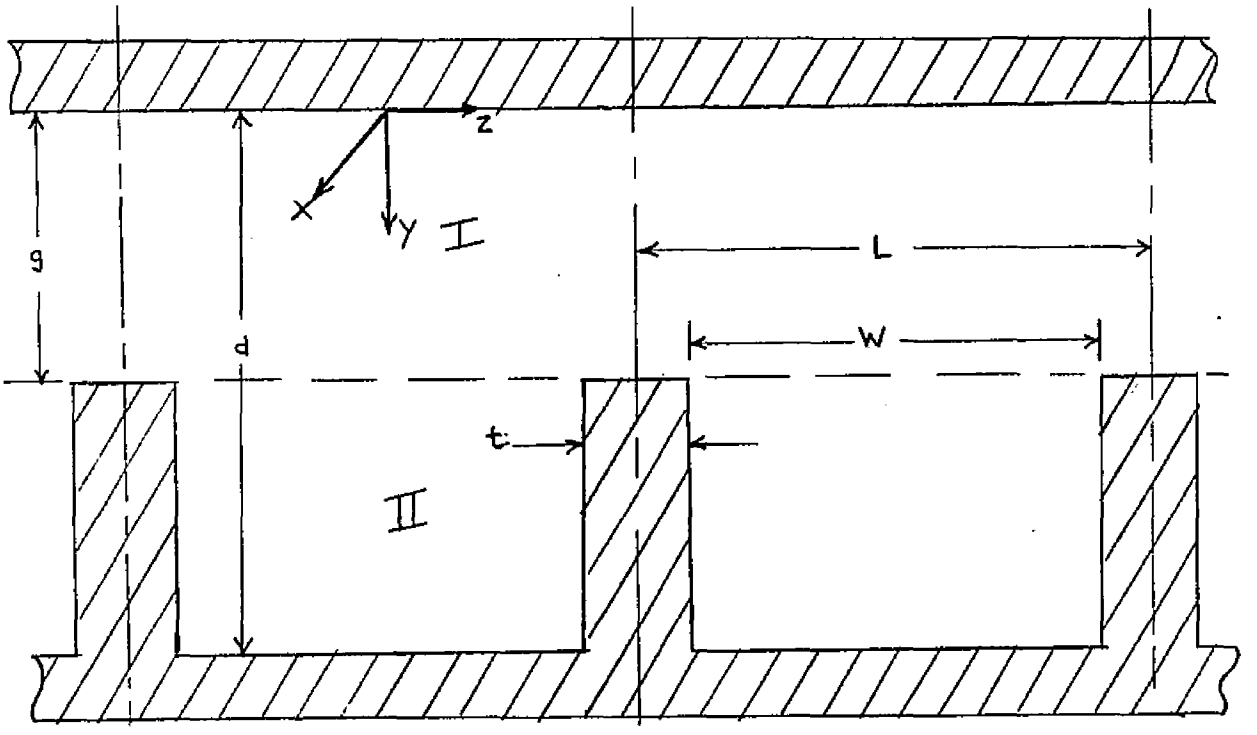

Fig. 2-1 Rectangular Geometry, $\frac{\partial}{\partial x}=0$

The situation depicted in Fig. 2-1 may be viewed as such a parallel plate waveguide which is loaded in one of two manners. If the waveguide is considered to be of width d, then it is loaded by the periodic teeth of thickness t. On the other hand, if it is considered to be of width g, then it is loaded by the periodic slots of width w. We may consider the guide width to vary between the values g and d and therefore expect the low frequency cutoff wavelength, corresponding to the so-called zero mode, to be given by

$$f_o = \frac{c}{2a_o} \tag{2-6A}$$

where

$$g < a_o < d \tag{2-6B}$$

The value of a_0 and its proximity to either of the limiting values, g and d, depends upon the relationships between the dimensions and the relative strength of loading. We expect different effects if the slot is large

enough to permit a propagating wave in the slot or not. We note also, that as the tooth width approaches zero, its effect upon the wave pattern remains finite since E_x must still be zero at the tooth edge, y=g. The result 2-6 has been shown to be borne out by the results given later and may be used as a starting point for estimating f_0 (cf., Eq. 2-41B).

The two important considerations which will determine the choice of dimensions of the circuit, in addition to that of strength of interaction, will be the frequency of operation and the desired operating voltages. The voltages applied must be kept within reasonable bounds because of insulation difficulties and simple availability of power supplies. The potential difference through which the electrons must be accelerated is larger still than that required for pure synchronism with the wave to supply the rotational energy necessary for focusing and interaction.

From what will be shown later, the normalized phase velocity of the n^{th} space harmonic may be written as

$$\frac{v_{\varphi m}}{c} = \frac{L/\lambda}{m \pm \frac{\beta_0 L}{2\pi}} \qquad (2\text{-}7)$$

where λ and c are the free space wavelength and phase velocity respectively, β_0 is the fundamental propagation constant and the positive and negative signs refer to the forward and backward wave harmonics, respectively.

If a particular circuit is dimensionally scaled, the phase velocity remains unchanged, since the dimensions and λ both change by the same constant.

$\frac{v_{\varphi m}}{c}$ is linearly proportional to L/λ, so for a fixed point of operation, $\beta_0 L/2\pi$, and for a chosen value of n, we must reduce the period of the circuit to lower the required voltage. However, reducing L will tend to reduce λ unless one makes additional modifications in the circuit dimensions.

Using this result, one may consider what period will be necessary for particular synchronous and rotational energy conditions. As an example we take the frequency to be the approximate center of x-band, 10GHz, and

assume that the dimensions are such that $\beta_0 L = 30^\circ$. We then may calculate the values of $\frac{v_{ph}}{c}$ corresponding to various space harmonics as the value of the period is changed. These results are shown in Fig. 2-2.

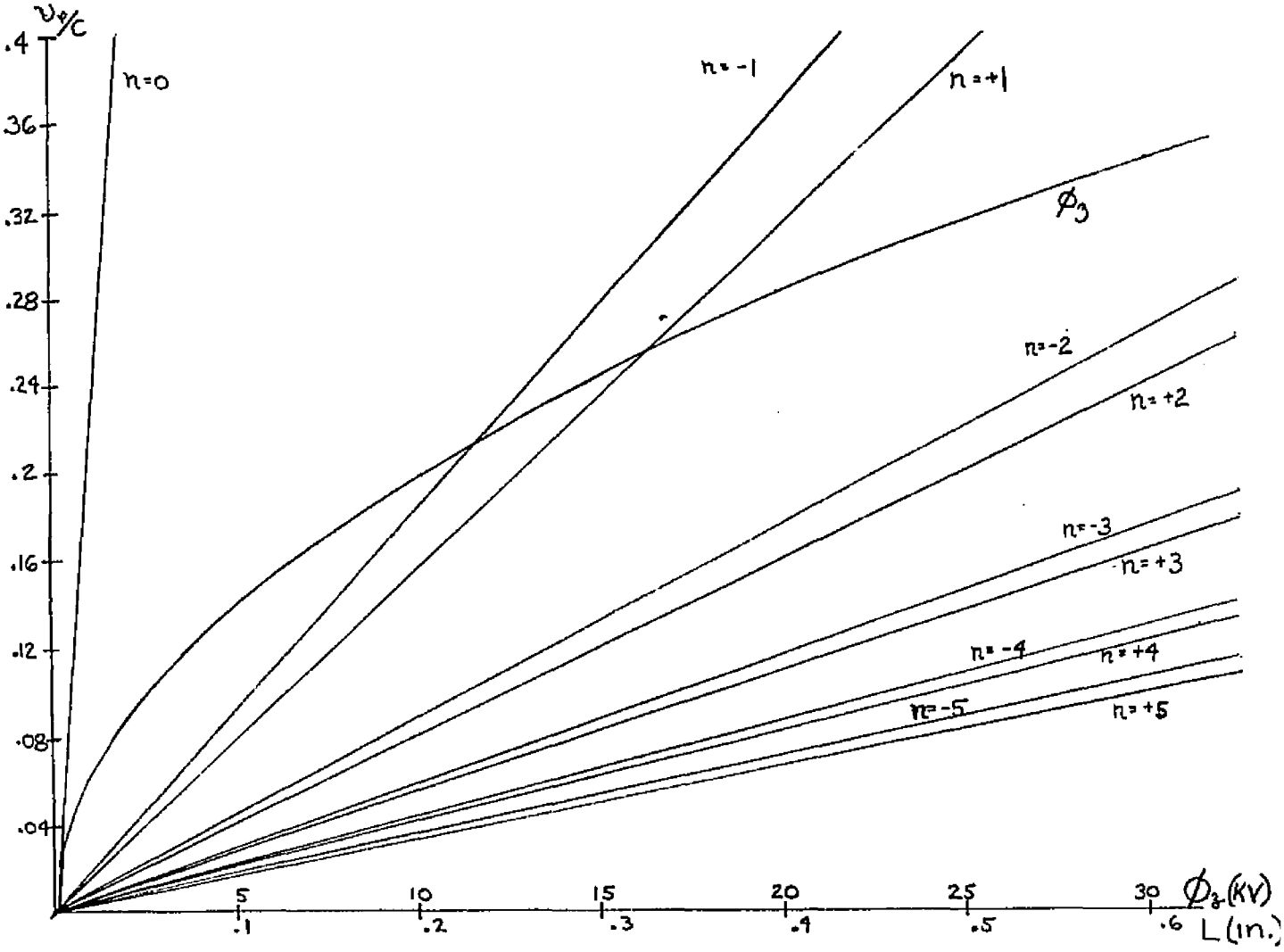

Fig. 2-2 Normalized Phase Velocity versus the Period and Synchronous Voltage {f=10Ghz and $\beta_0 L = 30^\circ$}

We note that the separation between the forward and backward waves for the same value of n decreases as the value of n is increased. This means that as the order of the harmonic is raised the relative spacing of another synchronous mode is decreased and the voltage must be held more constant.

As will be seen later when the solution is found for the fields, the strength of the harmonic decreases as the value of n increases. Moreover, the larger the value of n the more quickly the harmonic decays away from the plane

of the teeth, y=g. One should therefore choose to operate on as low a value of n as is consistent with the other previously mentioned considerations.

Neglecting relatavistic corrections one calculates the value of potential through which the electron is accelerated in order to reach velocity v_φ from

$$\frac{1}{2} m v_\varphi^2 = e \phi_z \tag{2-8A}$$

where ϕ_z is the portion of total voltage going into translational energy. We may write 2-8A approximately as

$$\frac{v_\varphi}{c} \approx \frac{\sqrt{\phi_z}}{505} \tag{2-8B}$$

The relation between ϕ_z and $\frac{v_\varphi}{c}$ is shown on Fig. 2-2 as well. Therefore, given a particular harmonic and desired value of ϕ_z, one can find the required value of period. Since the electrons must be accelerated through an additional voltage corresponding to the rotational energy, this voltage must be added to ϕ_z to determine what voltage must be supplied and what the insulation requirements will be.

2.2 Modal Analysis

The analysis of propagation through periodic structures is an outgrowth of the theory of periodic differential equations, or linear differential equations with periodically varying coefficients, in particular, of second order. The same sort of behavior is experienced to one degree or other in such analyses as the descriptions of free electrons in metals, propagation of light or electrons through a crystal lattice,[14] propagation through layered media, periodic dynamics, stability of nonlinear systems, self-excited oscillators, motion of the lunar perigee and oscillations and waves in elliptical waveguides and drumheads.

Periodic structures that may be considered for propagation of microwave energy may be of two types. The periodic variation may be in the electrical

properties of the medium[15] or in the boundaries of the structure. We are concerned with the latter. The problem of the propagation of waves through the structure of Fig. 2-1 will be treated both by a modal expansion and by approximation by a Hill's equation where we apply the theory of periodic differential equations. This theory will again be applied in Chap. 4 when the problem of stability of electrons in the periodic static fields will be considered. A different Hill's equation will then be considered.

There are certain general qualities which may be ascribed to periodic transmission structures.[16] Such structures exhibit stopband and passband characteristics. In the stopbands, waves are attenuated (excluding a non-physical growing wave) through the structure and in the passbands they propagate freely. In the case of the electron stability problem discussed in Chap. 4, the stopbands correspond to instabilities and the passbands correspond to stable motion. At a specific frequency there is no single unique phase velocity but in general an infinite number of discrete phase velocities. Each of these values of phase velocity belongs to a particular component of the Fourier decomposition of the fields, known as a space, or Hartree, harmonic. In general there will be an infinite number of space harmonics with phase velocity less than c, a necessary condition for synchronous interaction with an electron beam. All harmonics have the same group velocity indicating that they are part of the same solution.

The fundamental result[17] in the theory of periodic differential equations is given by Floquet's theorem. Similar reasoning may be applied to the structure of Fig. 2-1. Suppose we have solution for the fields in one period of the structure. For example, for the electric field

$$\bar{E} = Re\left\{\hat{E}(x,y,z)e^{i\omega t}\right\} \tag{2-9}$$

In all of the following let the multiplication by $e^{i\omega t}$ and the taking of the real part be understood. If the coordinate system is translated in z by the period L the geometry is unchanged since the structure is of infinite length. Therefore, we must be able to write the field in the new coordinates in terms of the old with only the addition of a multiplicative

constant. This constant may be written in any arbitrary way and we choose to specify it as $e^{-\gamma L}$. γ may take on any complex value so that $e^{-\gamma L}$ spans the entire finite complex plane. We have then, casting $\hat{E}$ into a more particular form

$$\hat{E}(x,y,z) = e^{-\gamma L}\hat{E}(x,y,z-L) = e^{-\gamma z}\hat{\Psi}(x,y,z) \tag{2-10}$$

so that

$$\hat{\Psi}(x,y,z) = \hat{\Psi}(x,y,z-L) \tag{2-11}$$

and $\hat{\Psi}$ is a periodic function of z with period L so that we note immediately from 2-10 that the character of γ will determine whether the state is one of stopband or passband. We expand $\hat{\Psi}$ in a Fourier series and find for $\hat{E}$

$$\hat{E}(x,y,z) = e^{-\gamma z}\sum_{m=-\infty}^{\infty}\hat{\Psi}_m(x,y)e^{-i\frac{2\pi m}{L}z} \tag{2-12A}$$

$$\hat{\Psi}_m(x,y) = \frac{1}{L}\int_{z'}^{z'+L}\hat{E}(x,y,z)e^{\gamma z}e^{i\frac{2\pi m}{L}z}\,dz \tag{2-12B}$$

yielding the various Hartree harmonics. We write the m^{th} space harmonic as

$$\hat{\Psi}_m(x,y)e^{-(\gamma + i\frac{2\pi m}{L})z}$$

If we assume that the system is lossless, in the passband γ will be purely imaginary and we may write for this condition, $\gamma \equiv i\beta_o$. Defining

$$\beta_m = \beta_o + \frac{2\pi m}{L} \tag{2-13}$$

we see that β_m is the propagation constant for the m^{th} space harmonic

and we note that the $m^{\underline{th}}$ space harmonic maintains constant phase if the coordinate system is translated with velocity $\frac{\omega}{\beta_m}$. The phase velocity of the $m^{\underline{th}}$ space harmonic is therefore

$$v_{p_m} = \frac{\omega}{\beta_m} = \frac{\omega}{\beta_0 + \frac{2\pi m}{L}} \tag{2-14}$$

so that proper choice of m will allow synchronism with an electron beam of velocity $<$ c.

The group velocity of the $m^{\underline{th}}$ space harmonic is given by

$$v_g = \frac{d\omega}{d\beta_m} = \frac{d\omega}{d\beta_0} \tag{2-15}$$

utilizing Eq. 2-13. Therefore, all the space harmonics have the same group velocity, which is to be expected since they are all part of the composite field. At the edges of the passbands, the group velocity will be zero for $\omega \neq 0$. It is shown[18] that the time average power flow in the passbands equals the group velocity multiplied by the time average stored energy per period, viz.,

$$\frac{1}{2} Re\left\{\int_S \bar{E} \times \bar{H}^* \cdot d\bar{S}\right\} = \frac{d\omega}{d\beta_0} \frac{1}{2L} \int_V \left[\frac{1}{2}\epsilon \bar{E}\cdot\bar{E}^* + \frac{1}{2}\mu \bar{H}\cdot\bar{H}^*\right] dV \tag{2-16}$$

and we see that v_g is the energy velocity in a periodic structure as it is in a uniform structure.

A very useful diagram for displaying these properties is the ω-β, or Brillouin, diagram where one plots ω as the ordinate and β as the abscissa. For example, for a simple TE or TM mode in uniform waveguide, the ω-β curve is hyperbolic, as given by $-kc^2-\beta^2+k^2=0$, and is asymptotic to the ω-β diagram for the TEM mode, straight lines passing through the origin with slopes $\pm c$. As seen from 2-14 and 2-15, the phase velocity corresponding to a particular point is simply the slope of a line drawn from the origin to that point while the group velocity is the slope of the tangent to the ω-β curve at the point in question.

For the case of the periodic structure we may infer some characteristics of the Brillouin diagram. Suppose we begin with a smooth system in the TE mode and add small periodic obstacles expecting that the ω-β diagram will depart from the hyperbolic curve in a small way. There will be small reflections caused by scattering from the small teeth of height d-g in Fig. 2-1. It is shown[19], that if the phase shift between the teeth equals $k\pi$, all the small reflections will add in phase and the summation of these from the infinity of teeth will equal the incident wave. The conclusion is that for $\beta L = k\pi$ there is no transmission, defining the location of stopbands. Hence, there will be gaps introduced into the hyperbolic curve for which there is no propagation. These results may also be shown[20] from coupled mode theory. In addition, we observe form 2-13 that a change in β of $\frac{2\pi}{L}S$, S an integer, is equivalent to a simple change of the index m. We conclude that ω is a periodic function of β with period $\frac{2\pi}{L}$. Changing the sign of β indicates a wave propagating in the -z direction so that ω is also an even function of β.

Based upon these observations we may sketch an expected shape for the ω-β curve of the system of Fig. 2-1, shown in Fig. 2-3. The branches of the diagram which are the direct perturbations of the hyperbolic curve of the uniform case are shown in solid line. It is noted that the first branch is forward wave*, a situation holding for capacitive[21] coupling. For the case of inductive coupling one finds a backward wave fundamental. The analysis and experimental results show that the fundamental is forward wave. We conclude that the coupling for the case considered is capacitive.

As the dimension g in Fig. 2-1 approaches zero, the coupling between adjacent sections approaches zero. We view this situation as a system of coupled resonant ciruits where the coupling becomes lighter until no coupling at all exists. The coupling has the effect, for n resonant systems, of introducing modes of differing resonant frequencies. For zero coupling the only possible frequency is that of a single resonant circuit. We expect, therefore, that as $g \to 0$ the bandwidth will approach zero since the zero and π-mode frequencies approach each other. In the limit the ω-β curve is reduced

---

*For a forward wave the phase velocity and group velocity have the same sign whereas for a backward wave they have opposite signs.

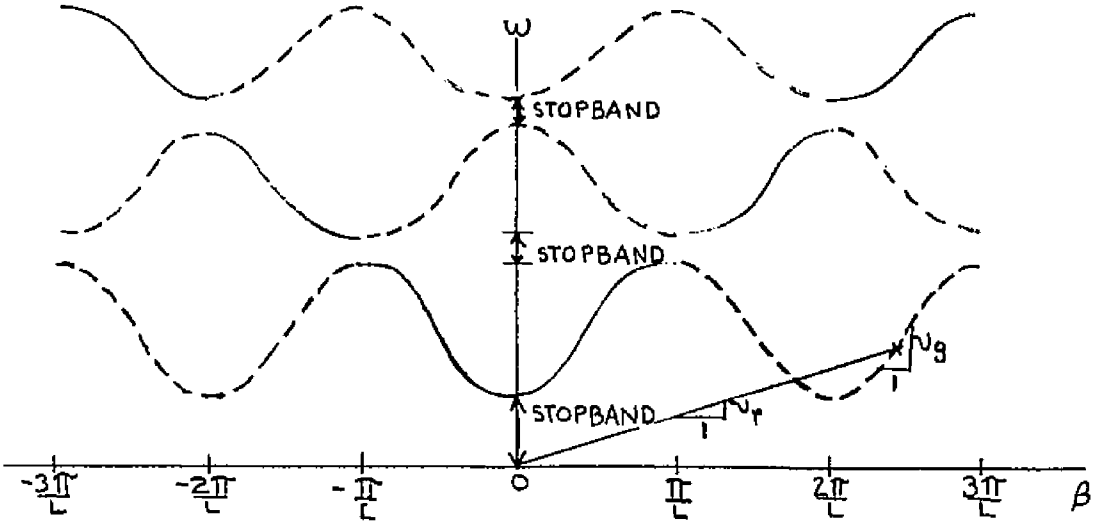

Fig. 2-3 Brillouin Diagram

to straight lines, ω =constant, with any phase shift possible between sections. This behavior is found in the later analysis.

The structure shown in Fig. 2-1 is an open structure in that a transverse dimension, x, is unbounded. It is characteristic of such structures that they can have so called "forbidden regions"[22] of the ω-β plane, where there is power flow in the unbounded transverse direction. For the mode to be considered there can be no such power flow since the electric field is always in the x direction precluding the existence of forbidden regions for the desired mode.

One may approach the problem of finding the ω versus β relationship for the geometry of Fig. 2-1 by a field analysis or by devising an equivalent circuit for the system, periodic in nature, and using circuit analysis techniques.[23] The former method produces the fields which are necessary for consideration of interaction and will be used here. The geometry is divided into two regions, defined by

$$\text{Region I} : \{x,y,z\} \ni : \quad 0 < y < g$$

$$\text{Region II} : \{x,y,z\} \ni : \quad g < y < d \quad \text{and} \quad |z - mL| < \frac{w}{2}$$

$$m = 0, \pm 1, \pm 2, \cdots$$

In the desired mode the electric field lies purely in the x direction and the magnetic field has components in the y and z directions and we consider it the dominant TE mode in the sense that it is derived by a perturbation of the TE_{10} mode of parallel plane waveguide.

The structure may sustain an infinity of other modes, among them a mode which has longitudinal electric field and is also useful for interaction with electrons in linear magnetrons.[24] The assumptions for the fields existing in the two regions for the two modes are different and the results obtained differ. For example, for the linear magnetron mode it is found that the first passband has its lower cutoff frequency equal to zero while for the case considered here it will be found that it is nonzero. Methods of mode control may be employed to damp other modes which may ordinarily propagate in the same frequency range as the desired mode. Such schemes can take advantage of the fact that the desired mode's surface current is purely in the x direction. Assembly of the inner structure from stacked rings will therefore damp modes which have longitudinal current but will not affect those with only circumferential currents. Higher order circular electric modes will be assumed not propagating in the frequency range of interest.

In region I we derive the fields from the axial magnetic field, which we write in form similar to Eq. 2-12A. For the passband we write $i\beta_0$ for γ and use $\frac{\partial}{\partial x}=0$. Thus,

$$H_z^I(y,z)=\sum_{m=-\infty}^{\infty} h_{zm}^I(y)\,e^{-i\beta_m z} \tag{2-17}$$

where multiplication by $e^{i\omega t}$ and the taking of the real part is to be understood. Now, $Hz^I(y,z)$ satisfies the wave equation

$$\nabla^2 H_z^I(y,z)+k^2 H_z^I(y,z)=0 \tag{2-18A}$$

When we substitute 2-17 into 2-18, interchange the order of differentiation and summation and recognize the orthogonality of the exponentials, we find that the $hz^In(y)$ separately satisfy the wave equation

$$\frac{d^2 h^I_{zm}}{dy^2} + \left(k^2 - \beta_m^2\right) h^I_{zm} = 0 \tag{2-18B}$$

We have for the other five components of field in region I

$$e^I_{xm} = \frac{i\omega\mu}{\beta_m^2 - k^2} \frac{\partial h^I_{zm}}{\partial y} \tag{2-19A}$$

$$h^I_{ym} = \frac{i\beta_m}{\beta_m^2 - k^2} \frac{\partial h^I_{zm}}{\partial y} \tag{2-19B}$$

$$e^I_{ym} = e^I_{zm} = h^I_{xm} = 0 \tag{2-19C}$$

where the $n^{\underline{th}}$ harmonic of each field component is derived from the $n^{\underline{th}}$ harmonic of the axial magnetic field. In the above the multiplication by $e^{-i\beta_m z}$ is to be understood to find the full spacial variation of the field harmonic.

The boundary condition on Ex is that it vanish at y=0. We may impose this boundary condition on the e^I_{xm} individually since the boundary condition must be satisfied for all z and t and we see from 2-19A that $\frac{\partial h^I_{zm}}{\partial y} = 0$ at y=0.

The form of the solution of 2-18B will depend upon the relationship of the magnitudes of k^2 and βn^2. For particular values of β_o and k that relationship is a function of the index, n. In particular, near the lower cutoff $\beta_o \approx 0$ and therefore $\beta_m \approx 0$ for n=0. Since we expect, on physical grounds, that there is a nonzero cutoff frequency for this mode, the corresponding k^2 will be different from zero. The condition, $k^2 > \beta n^2$, will obtain for n=0 for this region while for sufficiently large n the inequality will reverse. From 2-14 we see that the condition $k^2 > \beta n^2$ is equivalent to $|v_{\varphi m}| > C$ and $k^2 < \beta n^2$ denotes $|v_{\varphi m}| < C$. Therefore, the former condition implies a space harmonic which is "fast wave" and the latter a space harmonic which is "slow wave". Only the slow wave harmonics will be useful for interaction but of course all the harmonics, fast and

slow, enter into the summation to satisfy the boundary conditions. The transition solution, $k^2=\beta n^2$, corresponding to the intersection of the $\omega-\beta$ curve with the $v=c$ line, will be considered as limiting forms of the fast or slow waves.

We have for the slow waves, $|v_{\varphi m}|<C$, taking the proper function to satisfy the boundary condition at y=0, using 2-19

$$H_z^I(y,z) = e^{-i\beta_0 z}\sum_{m=-\infty}^{\infty} H_m^I \cosh\gamma_m y\, e^{-i\frac{m2\pi}{L}z} \tag{2-20A}$$

$$E_x^I(y,z) = i\omega\mu e^{-i\beta_0 z}\sum_{m=-\infty}^{\infty} H_m^I \frac{\sinh\gamma_m y}{\gamma_m} e^{-i\frac{m2\pi}{L}z} \tag{2-20B}$$

$$H_y^I(y,z) = i e^{-i\beta_0 z}\sum_{m=-\infty}^{\infty} H_m^I \frac{\beta_m \sinh\gamma_m y}{\gamma_m} e^{-i\frac{m2\pi}{L}z} \tag{2-20C}$$

$$H_x^I = E_y^I = E_z^I = 0 \tag{2-20D}$$

$$\gamma_m^2 \equiv \beta_m^2 - k^2 \tag{2-20E}$$

where it is understood that for any value of n not leading to a slow wave, we take $Hm^I=0$.

For the fast waves, $|v_{\varphi m}|>C$, in the same way

$$H_z^I(y,z) = e^{-i\beta_0 z}\sum_{m=-\infty}^{\infty} H_m'^I \cos\gamma_m' y\, e^{-i\frac{m2\pi}{L}z} \tag{2-21A}$$

$$E_x^I(y,z) = i\omega\mu e^{-i\beta_0 z}\sum_{m=-\infty}^{\infty} H_m'^I \frac{\sin\gamma_m' y}{\gamma_m'} e^{-i\frac{m2\pi}{L}z} \tag{2-21B}$$

$$H_y^I(y,z) = i e^{-i\beta_0 z}\sum_{m=-\infty}^{\infty} H_m'^I \frac{\beta_m \sin\gamma_m' y}{\gamma_m'} e^{-i\frac{m2\pi}{L}z} \tag{2-21C}$$

$$H_x^I = E_y^I = E_z^I = 0 \tag{2-21D}$$

$$\gamma_m'^2 \equiv k^2 - \beta_m^2 = -\gamma_m^2 \tag{2-21E}$$

Again, for those values of n which do not lead to fast waves, the coefficients $H_m'^I$ will be zero. Since most of the harmonics are slow waves the summations indicated in 2-21 really represent a finite sum. Either of the two forms of solution may be found as a direct extension of the other and in reality they are the same. From 2-21E we have that $\gamma_m = \pm i\gamma_m'$ so that $\cosh \gamma_m y = \cos \gamma_m' y$ and $\sinh \gamma_m y = \pm i \sin \gamma_m' y$ and the slow wave solutions transform directly to the solutions for fast waves.

The transitional solution, for $|v_{\varphi m}| = C$, is generated by a limiting process applied to either form of solution. We have

$$\lim_{\gamma_m \to 0} \cosh \gamma_m y = \lim_{\gamma_m' \to 0} \cos \gamma_m' y = 1 \tag{2-22A}$$

$$\lim_{\gamma_m \to 0} \frac{\sinh \gamma_m y}{\gamma_m} = \lim_{\gamma_m' \to 0} \frac{\sin \gamma_m' y}{\gamma_m'} = y \tag{2-22B}$$

We have then for the transition solution, $|v_{\varphi m}| = C$, which occurs for the single index, n=p,

$$H_z^I(y,z) = e^{-i\beta_0 z} H_p''^I e^{-ip\frac{2\pi}{L}z} \tag{2-23A}$$

$$E_x^I(y,z) = i\omega\mu e^{-i\beta_0 z} H_p''^I y e^{-ip\frac{2\pi}{L}z} \tag{2-23B}$$

$$H_y^I(y,z) = i e^{-i\beta_0 z} H_p''^I \beta_p y e^{-ip\frac{2\pi}{L}z} \tag{2-23C}$$

$$H_x^I = E_y^I = E_z^I = 0 \qquad (2\text{-}23D)$$

The appearance of a term in the solution given by 2-23 is fortuitous in the sense that it occurs only for a value of frequency such that the ω-β curve crosses the $v = c$ line. The possibility must be allowed for, however, when summing the solutions necessary to match the boundary conditions.

As the boundary between the two regions is approached we write the tangential fields in terms of the three types of solutions we have generated.

$$\lim_{y\to g} H_z^I(y,z) = e^{-i\beta_0 z}\left\{\sum_{m=-\infty}^{\infty}\left[H_m^I \cosh\gamma_m g + H_m'^I \cos\chi_m' g\right]e^{-im\frac{2\pi}{L}z} + H_p''^I e^{-ip\frac{2\pi}{L}z}\right\} \qquad (2\text{-}24A)$$

$$\lim_{y\to g} E_x^I(y,z) = i\omega\mu e^{-i\beta_0 z}\left\{\sum_{m=-\infty}^{\infty}\left[H_m^I \frac{\sinh\gamma_m g}{\gamma_m} + H_m'^I \frac{\sin\chi_m' g}{\chi_m'}\right]e^{-im\frac{2\pi}{L}z} + H_p''^I g e^{-ip\frac{2\pi}{L}z}\right\} \qquad (2\text{-}24B)$$

where it is understood that the Hn^I and the Hn'^I are not simultaneously present and the Hp^I term is added in the case of a transitional solution.

We turn next to region II and consider the fields in the slots of Fig.2-1. We have from 2-10 that the fields in adjacent slots differ only by the multiplicative constant $e^{-\gamma L}$, or for the case of propagation, $e^{-i\beta_0 L}$. It will be sufficient to consider only a single slot. In the slots, just as in region I, the only nonvanishing field components are taken to be Ex, Hy, and Hz. Any other component of field which would exist in the slot could not be matched at the boundary of the two regions, y=g. In region II it is useful to consider the direction of propagation the y direction and to derive the fields from Hy. We may think of the slots as parallel plane waveguides which are terminated in short circuits at y=d. Depending upon the frequency and the width of the slot, W, the modes existing in the slot may propagate or attenuate with respect to y. For a propagating mode a standing wave exists in the slot for that mode. Let the variation of a field component in the slot with respect to y be $e^{\Gamma y}$, where Γ may

be real or imaginary. We define

$$k_t^2 \equiv \Gamma^2 + k^2 \tag{2-25}$$

The value of k_t^2 is fixed by the boundary conditions at the walls of the slots. If the frequency is such that for a particular mode in the slots $k^2 > k_t^2$, then Γ is imaginary and equal to $\pm i\Gamma'$ and the solution is a standing wave. If, on the other hand, $k^2 < k_t^2$, then Γ is real and the solution is an attenuated wave existing in the cutoff slot. A transitional solution exists when the slot is at the edge of cutoff.

We consider only the slot which is centered at z=0 in Fig. 2-1. The boundary conditions on E_x demand that it vanish on the three walls of the slot, namely, y=d and $z = \pm w/2$. We find the fields in a manner similar to that used for region I. The functions are separated according to even or odd symmetry and, as usual, multiplication by $e^{i\omega t}$ and the taking of the real part is understood. We have for the cutoff modes

$$H_y^{II}(y,z) = \sum_{s=1}^{\infty}\left[a_{2s-1}\sin\frac{2s-1}{w}\pi z \sinh\Gamma_{2s-1}(y-d) - b_{2s}\cos\frac{2s\pi}{w}z\sinh\Gamma_{2s}(y-d)\right] \tag{2-26A}$$

$$E_x^{II}(y,z) = i\omega\mu\sum_{s=1}^{\infty}\left[a_{2s-1}\frac{\cos\frac{2s-1}{w}\pi z}{\frac{2s-1}{w}\pi}\sinh\Gamma_{2s-1}(y-d) + b_{2s}\frac{\sin\frac{2s\pi}{w}z}{\frac{2s\pi}{w}}\sinh\Gamma_{2s}(y-d)\right] \tag{2-26B}$$

$$H_z^{II}(y,z) = \sum_{s=1}^{\infty}\left[a_{2s-1}\Gamma_{2s-1}\frac{\cos\frac{2s-1}{w}\pi z}{\frac{2s-1}{w}\pi}\cosh\Gamma_{2s-1}(y-d) + b_{2s}\Gamma_{2s}\frac{\sin\frac{2s\pi}{w}z}{\frac{2s\pi}{w}}\cosh\Gamma_{2s}(y-d)\right] \tag{2-26C}$$

$$E_y^{II} = E_z^{II} = H_x^{II} = 0 \tag{2-26D}$$

where

$$\Gamma_{2s-1\ 2s} = \sqrt{k_{t\ 2s-1\ 2s}^2 - k^2} \tag{2-26E}$$

$$k_{t_{2s-1}}^2 = \left[\frac{2s-1}{w}\pi\right]^2 \tag{2-26F}$$

$$k_{t_{2s}}^2 = \left[\frac{2s\pi}{w}\right]^2 \tag{2-26G}$$

where the coefficients are zero for those values of s not leading to cutoff modes.

For the propagating modes we proceed in a similar manner.

$$H_y^{II}(y,z) = \sum_{s=1}^{\infty}\left[a'_{2s-1}\sin\frac{2s-1}{w}\pi z \sin\Gamma'_{2s-1}(y-d) - b'_{2s}\cos\frac{2s\pi}{w}z\sin\Gamma'_{2s}(y-d)\right] \tag{2-27A}$$

$$E_x^{II}(y,z) = i\omega\mu\sum_{s=1}^{\infty}\left[a'_{2s-1}\frac{\cos\frac{2s-1}{w}\pi z}{\frac{2s-1}{w}\pi}\sin\Gamma'_{2s-1}(y-d) + b'_{2s}\frac{\sin\frac{2s\pi}{w}z}{\frac{2s\pi}{w}}\sin\Gamma'_{2s}(y-d)\right] \tag{2-27B}$$

$$H_z^{II}(y,z) = \sum_{s=1}^{\infty}\left[a'_{2s-1}\Gamma'_{2s-1}\frac{\cos\frac{2s-1}{w}\pi z}{\frac{2s-1}{w}\pi}\cos\Gamma'_{2s-1}(y-d) + b'_{2s}\Gamma'_{2s}\frac{\sin\frac{2s\pi}{w}z}{\frac{2s\pi}{w}}\cos\Gamma'_{2s}(y-d)\right] \tag{2-27C}$$

$$E_y^{II} = E_z^{II} = H_x^{II} = 0 \tag{2-27D}$$

$$\Gamma'_{\substack{2s-1\\2s}} = \sqrt{k^2 - k_{t_{\substack{2s-1\\2s}}}^2} \tag{2-27E}$$

and $k_{t_{2s-1}}^2$ and $k_{t_{2s}}^2$ are the same as given in 2-26. The coefficients appearing in the summations vanish for those values of s yielding nonpropagating modes. As was done previously for the solutions in region I we may show that the two sets of solutions are equivalent in that one follows directly from the other with the substitution $\Gamma_m = \pm i\Gamma_m'$.

The transitional solution for the slots occurs when the frequency is such

that a mode in the slot is just at the edge of cutoff, $k^2 \rightarrow k_t^2$. Taking the limit of the solutions given in 2-26 and 2-27 gives zero for all field components. Investigation of the wave equation in the limit yields a linear solution.

Applying the boundary conditon at y=d we find, for a mode just at the edge of cutoff, a solution of the form

$$E_x^{II}(y,z) = i\omega\mu C_{2s-1} \cos\frac{2s-1}{w}\pi z\,(y-d) \tag{2-28A}$$

or

$$E_x^{II}(y,z) = i\omega\mu C_{2s} \sin\frac{2s\pi}{w} z\,(y-d) \tag{2-28B}$$

whichever is appropriate. Since the region where we apply this solution is for bounded y, we allow the linear solution. In addition, we have

$$H_y^{II}(y,z) = C_{2s-1}\,\frac{2s-1}{w}\pi \sin\frac{2s-1}{w}\pi z\,(y-d) \tag{2-28C}$$

or

$$H_y^{II}(y,z) = -C_{2s}\,\frac{2s\pi}{w}\cos\frac{2s\pi}{w} z\,(y-d) \tag{2-28D}$$

and

$$H_z^{II}(y,z) = C_{2s-1}\cos\frac{2s-1}{w}\pi z \tag{2-28E}$$

or

$$H_z^{II}(y,z) = C_{2s}\sin\frac{2s\pi}{w} z \tag{2-28F}$$

We sum the three possible solution forms and find the tangential fields at the boundary between region I and region II. In the following it is to be noted that only one of the three coefficients in each square bracket can be nonzero.

$$\lim_{y\to g} E_x^{II}(y,z) = i\omega\mu \sum_{s=1}^{\infty} \left\{ \left[\frac{a_{2s-1}}{\frac{2s-1}{w}\pi} \sinh \Gamma_{2s-1}(g-d) + \frac{a'_{2s-1}}{\frac{2s-1}{w}\pi} \sin \Gamma'_{2s-1}(g-d) + C_{2s-1}(g-d) \right] \cos \frac{2s-1}{w}\pi z \right.$$

$$\left. + \left[\frac{b_{2s}}{\frac{2s\pi}{w}} \sinh \Gamma_{2s}(g-d) + \frac{b'_{2s}}{\frac{2s\pi}{w}} \sin \Gamma'_{2s}(g-d) + C_{2s}(g-d) \right] \sin \frac{2s\pi}{w} z \right\} \qquad (2\text{-}29A)$$

$$\lim_{y\to g} H_z^{II}(y,z) = \sum_{s=1}^{\infty} \left\{ \left[\frac{a_{2s-1}\Gamma_{2s-1}}{\frac{2s-1}{w}\pi} \cosh \Gamma_{2s-1}(g-d) + \frac{a'_{2s-1}\Gamma'_{2s-1}}{\frac{2s-1}{w}\pi} \cos \Gamma'_{2s-1}(g-d) + C_{2s-1} \right] \cos \frac{2s-1}{w}\pi z \right.$$

$$\left. + \left[\frac{b_{2s}\Gamma_{2s}}{\frac{2s\pi}{w}} \cosh \Gamma_{2s}(g-d) + \frac{b'_{2s}\Gamma'_{2s}}{\frac{2s\pi}{w}} \cos \Gamma'_{2s}(g-d) + C_{2s} \right] \sin \frac{2s\pi}{w} z \right\} \qquad (2\text{-}29B)$$

At the boundary between the two regions we require the fields be continuous. It is easily shown[25] that if at the boundary between two regions the tangential components of $\bar{E}$ and $\bar{H}$ are continuous and if the fields satisfy Maxwell's equations, then the normal components of $\bar{E}$ and $\bar{H}$ are also continuous. We see, therefore, that it is necessary and sufficient to require continuity of E_x and H_z at the boundary. In addition we require E_x to vanish at the tops of the teeth. We have from 2-24 and 2-39 that for E_x

$$i\omega\mu e^{-i\beta_0 z} \left\{ \sum_{m=-\infty}^{\infty} \left[H_m^{I} \frac{\sinh \gamma_m g}{\gamma_m} + H_m'^{I} \frac{\sin \gamma'_m g}{\gamma'_m} \right] e^{-im\frac{2\pi}{L}z} + H_p''^{I} g\, e^{-ip\frac{2\pi}{L}z} \right\}$$

$$= \begin{cases} i\omega\mu \sum_{s=1}^{\infty} \left\{ \left[\frac{a_{2s-1}}{\frac{2s-1}{w}\pi} \sinh \Gamma_{2s-1}(g-d) + \frac{a'_{2s-1}}{\frac{2s-1}{w}\pi} \sin \Gamma'_{2s-1}(g-d) + C_{2s-1}(g-d) \right] \cos \frac{2s-1}{w}\pi z \right. \\ \left. + \left[\frac{b_{2s}}{\frac{2s\pi}{w}} \sinh \Gamma_{2s}(g-d) + \frac{b'_{2s}}{\frac{2s\pi}{w}} \sin \Gamma'_{2s}(g-d) + C_{2s}(g-d) \right] \sin \frac{2s\pi}{w} z \right\} & \text{for } -\frac{w}{2} < z < \frac{w}{2} \\ 0 & \text{for } -\frac{L}{2} < z < -\frac{w}{2} \text{ and } \frac{w}{2} < z < \frac{L}{2} \end{cases} \qquad (2\text{-}30A)$$

and for H_z

$$e^{-i\beta_0 z}\left\{\sum_{m=-\infty}^{\infty}\left[H_m^I \cosh\gamma_m g + H_m'^I \cos\gamma_m' g\right] e^{-im\frac{2\pi}{L}z} + H_p''^I e^{-ip\frac{2\pi}{L}z}\right\}$$

$$= \sum_{s=1}^{\infty}\left\{\left[\frac{a_{2s-1}\Gamma_{2s-1}}{\frac{2s-1}{w}\pi}\cosh\Gamma_{2s-1}(g-d) + \frac{a'_{2s-1}\Gamma'_{2s-1}}{\frac{2s-1}{w}\pi}\cos\Gamma'_{2s-1}(g-d) + C_{2s-1}\right]\cos\frac{2s-1}{w}\pi z\right.$$

$$\left.+\left[\frac{b_{2s}\Gamma_{2s}}{\frac{2s\pi}{w}}\cosh\Gamma_{2s}(g-d) + \frac{b'_{2s}\Gamma'_{2s}}{\frac{2s\pi}{w}}\cos\Gamma'_{2s}(g-d) + C_{2s}\right]\sin\frac{2s\pi}{w}z\right\}$$

$$\text{for } -\frac{w}{2} < z < \frac{w}{2} \qquad \text{(2-30B)}$$

Now the functions $e^{-im\frac{2\pi}{L}z}$ are orthogonal over the interval L so that we may determine the H^I, H'^I and H''^I coeffecients on the left side of the equations in terms of the a, a', b, b' and c coefficients on the right-hand side by an integral such as given in 2-12B applied to the boundary condition for E_x given in 2-30A. In addition, since the second boundary condition, that for H_z, holds only for $-\frac{w}{2} < z < \frac{w}{2}$ and since the $\cos\frac{2s-1}{w}\pi z$ and the $\sin\frac{2s\pi}{w}z$ functions are orthogonal over this interval we may in the same manner determine the a, a', b, b' and c set in terms of the H^I, H'^I and H''^I set. If one result is substituted into the other we have an infinite set of linear homogeneous equations to solve. In order to have a nontrivial solution for the coefficients it is necessary that the determinant vanish. The solution of this yields β_o as a function of k.

We now simplify the equations by approximating the fields in the slots by a single mode. We truncate the series appearing on the right-hand sides of 2-30 to a single leading term. Let us consider why this is a reasonable assumption. As was discussed earlier it is desirable to operate at a low value of n and a low synchronous voltage. If we refer to Fig. 2-2 we see that these considerations require that the period of the structure, L, be kept small. For the example of Fig. 2-2 the frequency of 10^{10} Hz yields a free space wavelength of 3 cm. The slots will therefore not propagate in all modes for slot widths less than approximately .59 inches. Depending

on the width of the teeth, t=L-W, the period will be somewhat larger than the slot width. We see from Fig. 2-2 that for a period of this range, the synchronous voltage becomes rather large for, say, synchronism with the n=1 forward wave space harmonic. We conclude, therefore, that all slot modes will be nonpropagating and thus the first one will be dominant in determining the value of the field in the slot. We take therefore, on the right-hand side of 2-30, only the term for s=1 with the cosinusoidal variation.

Since for a strongly cutoff slot the wave equation is approximated by Laplace's equation, we may use the result for the potential in a rectangular slot which states that if the depth of the slot becomes larger than the width the solution does not change very much. On this basis, for a cutoff slot mode we choose in later results to make the slot square, that is, d-g=w. We have then from 2-30A with the approximate right-hand side, using the orthogonality of the exponentials, and allowing for the separate possible solution forms and taking $e^{i\beta_0 z}$ constant over the slot

$$\begin{Bmatrix} H_m^I \dfrac{\sinh\gamma_m g}{\gamma_m} \\ H_m'^I \dfrac{\sin\gamma_m' g}{\gamma_m'} \\ H_m''^I g \end{Bmatrix} \approx \begin{Bmatrix} \dfrac{a_1}{\pi/w}\sinh\Gamma_1(g-d) \\ \dfrac{a_1'}{\pi/w}\sin\Gamma_1'(g-d) \\ C_1(g-d) \end{Bmatrix} \cdot \frac{2}{\pi}\frac{\frac{W}{L}\cos m\pi\frac{W}{L}}{1-4m^2\left(\frac{W}{L}\right)^2}, \quad m\neq\tfrac{1}{2}\frac{L}{W} \tag{2-31A}$$

If $\frac{L}{W}$ is an even integer, for the value of $m=\frac{L}{2W}$ the right-hand side of 2-31A is indeterminate. We have easily

$$\lim_{\frac{W}{L}\to\frac{1}{2m}} \frac{\cos m\pi\frac{W}{L}}{1-4m^2\left(\frac{W}{L}\right)^2} = \frac{\pi}{4}$$

so that for the limiting case of 2-31A

$$\begin{Bmatrix} H_{\frac{L}{2W}}^I \dfrac{\sinh\gamma_{\frac{L}{2W}} g}{\gamma_{\frac{L}{2W}}} \\ H_{\frac{L}{2W}}'^I \dfrac{\sin\gamma_{\frac{L}{2W}}' g}{\gamma_{\frac{L}{2W}}'} \\ H_{\frac{L}{2W}}''^I g \end{Bmatrix} \approx \begin{Bmatrix} \dfrac{a_1}{\pi/w}\sinh\Gamma_1(g-d) \\ \dfrac{a_1'}{\pi/w}\sin\Gamma_1'(g-d) \\ C_1(g-d) \end{Bmatrix} \cdot \frac{W}{2L} \tag{2-31B}$$

The approximation used in 2-31 is that $e^{i\beta_0 z}$ is constant over the slot and equal to its value at the slot center, unity. This approximation will be valid for the lower part of the ω-β curve, where β_0 is small. If the factor $e^{i\beta_0 z}$ were kept in the integral we would have

$$\frac{1}{L}\int_{-\frac{W}{2}}^{\frac{W}{2}} \cos\frac{\pi}{W} z\, e^{i\beta_m z}\, dz = \frac{2\frac{\pi}{W}\cos\beta_m\frac{W}{2}}{L\left[\left(\frac{\pi}{W}\right)^2-\beta_m^2\right]} \tag{2-32}$$

Now, for $|m|>0$, the larger $|m|$ becomes the better the approximation of β_m^2 by $\left(\frac{m2\pi}{L}\right)^2$, which is used in 2-31. Therefore, the most crude approximation is for m=0, the fundamental. The value of 2-32 for m=0 is

$$\frac{2}{\pi}\frac{W}{L}\frac{\cos\beta_0\frac{W}{2}}{1-\left(\frac{\beta_0 W}{\pi}\right)^2}$$

while the value obtaining from the integral when neglecting the factor $e^{i\beta_0 z}$ is $\frac{2}{\pi}\frac{W}{L}$ so that the correction factor to be applied to the fundamental coefficient is given by

$$\alpha = \frac{\cos\beta_0\frac{W}{2}}{1-\left(\frac{\beta_0 W}{\pi}\right)^2} = \frac{\cos\left[\frac{\beta_0 L}{2}\frac{W}{L}\right]}{1-\left[\frac{\beta_0 L}{\pi}\frac{W}{L}\right]^2} \tag{2-33}$$

which has no indeterminate points since for finite tooth thickness

$$0 < \frac{\beta_0 L}{2}\frac{W}{L} < \frac{\pi}{2}$$

and

$$0 < \frac{\beta_0 L}{\pi}\frac{W}{L} < 1$$

The limits of α as $\frac{\beta_0 L}{\pi}\frac{W}{L}$ approaches 0 and 1 are 1 and $\frac{\pi}{4}$ respectively.

Referring to Fig. 2-4, we see that α is very close to unity for a fairly wide range of $\frac{\beta_0 L}{\pi}\frac{W}{L}$. Thus, the approximate result given in 2-31 will be quite accurate for a fairly large segment of the ω-β curve, depending upon the particular value of $\frac{W}{L}$. For example, for a case which will be presented in detail later, it is found that the phase velocity for the n=1 space harmonic has a minimum with respect to frequency at

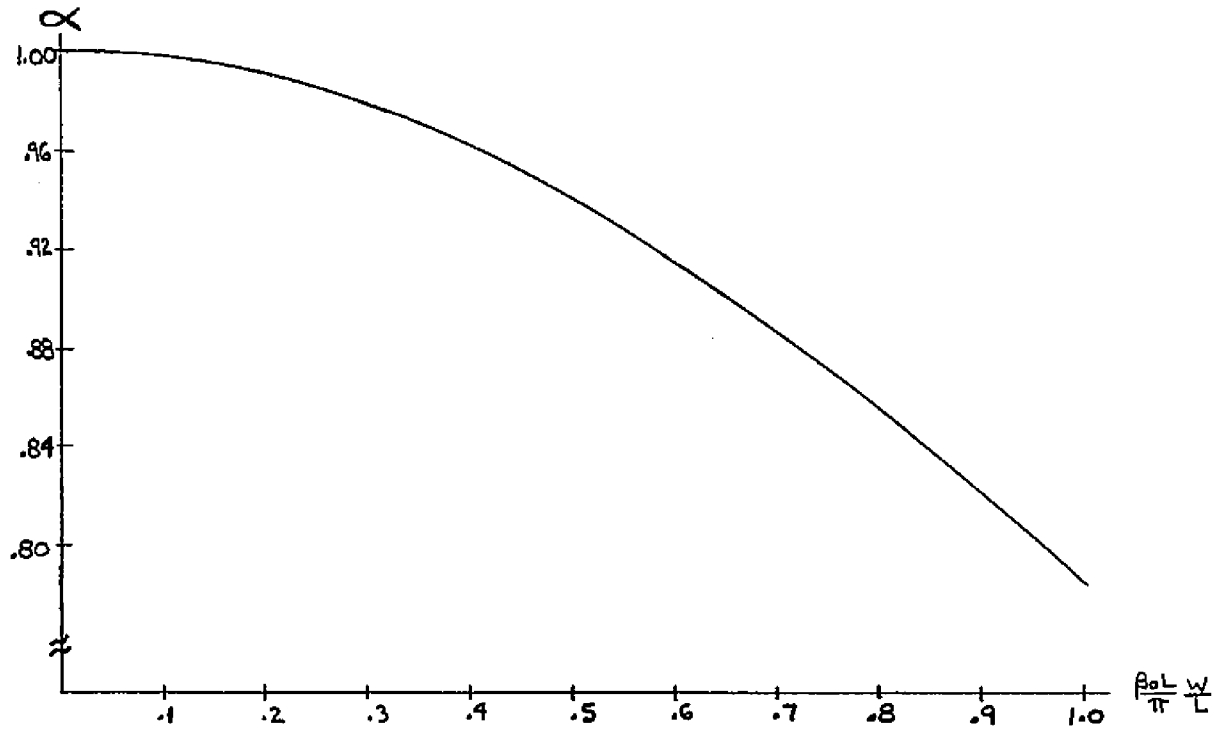

Fig. 2-4 Correction Factor

$\beta_0 L \approx 0.28\pi$. This is a desirable point to operate because of lower synchronous voltage and since $\frac{d v_g}{d\omega} = 0$ it will be relatively broadband. For this geometry $W/L = 0.625$. The value of $\frac{\beta_0 L}{\pi}\frac{W}{L}$ is then approximately 0.175 for which the value of α is larger than .99. For this condition, therefore, the approximation given in 2-31 is in error by less than 1%. In addition, it is found later from comparison of experimental and theoretical results that the two diverge most for large β_0 .

We have, then, the relation of the H^I, H'^I, and H''^I coefficients in terms of the a_1, a_1' and c_1 coefficients. The matching equation for Hz is found from 2-30B and 2-31. In the following the brackets represent the various combinative possibilities determined by the nature of the solutions in regions I and II and the general or limiting form of the coefficient which occurs for $m = \frac{L}{2W}$. In all there are eighteen possibilities. It cannot be satisfied for all values of $-\frac{W}{2} < z < \frac{W}{2}$ because only a single slot mode has been taken. There are various criteria which could be imposed.[26] They all lead to approximations which represent varying degrees of accuracy. We have,

$$e^{-j\beta z}\left\{\sum_{m=-\infty}^{\infty}\left\{\begin{array}{l}\gamma_m \coth \gamma_m g \\ \gamma_m' \cot \gamma_m' g \\ \frac{1}{g}\end{array}\right\}\left\{\begin{array}{l}\frac{2}{\pi}\frac{\frac{W}{L}\cos m\pi\frac{W}{L}}{1-4m^2(W/L)^2} \\ \frac{1}{2}\frac{W}{L}\end{array}\right\}\left\{\begin{array}{l}\frac{a_1}{\pi/W}\sinh\Gamma_1(g-d) \\ \frac{a_1'}{\pi/W}\sin\Gamma_1'(g-d) \\ C_1(g-d)\end{array}\right\}\right\} e^{-jm\frac{2\pi}{L}z} \approx \left\{\begin{array}{l}\frac{a_1\Gamma_1}{\pi/W}\cosh\Gamma_1(g-d) \\ \frac{a_1'\Gamma_1'}{\pi/W}\cos\Gamma_1'(g-d) \\ C_1\end{array}\right\}\cos\frac{\pi}{W}z$$

$$-\frac{W}{2} < z < \frac{W}{2} \qquad (2\text{-}34)$$

We will match the two sides of Eq. 2-34 at the center of the slot, z=0. Eliminating the constants of proportionality we arrive at the dispersion equation.

$$\sum_{m=-\infty}^{\infty}\left\{\frac{2}{\pi}\frac{\frac{W}{L}\cos m\pi\frac{W}{L}}{1-4m^2(W/L)^2}\right\}\left\{\begin{array}{l}\gamma_m \coth \gamma_m g \\ \gamma_m' \cot \gamma_m' g \\ \frac{1}{g}\end{array}\right\} \approx \left\{\begin{array}{l}\Gamma_1 \coth\Gamma_1(g-d) \\ \Gamma_1' \cot\Gamma_1'(g-d) \\ \frac{1}{g-d}\end{array}\right\} \qquad (2\text{-}35A)$$

where

$$\gamma_m = \sqrt{\beta_m^2 - k^2} \qquad (2\text{-}35B)$$

$$\gamma_m' = \sqrt{k^2 - \beta_m^2} \qquad (2\text{-}35C)$$

$$\Gamma_1 = \sqrt{\left(\frac{\pi}{W}\right)^2 - k^2} \tag{2-35D}$$

$$\Gamma_1' = \sqrt{k^2 - \left(\frac{\pi}{W}\right)^2} \tag{2-35E}$$

$$\beta_m = \beta_0 + m\frac{2\pi}{L} \tag{2-35F}$$

To solve for the dispersion, $k(\beta_0)$, we set β_0 at some value and then find the value of k which satisfies 2-35. To do this we vary k and find the intersection of the right-hand and left-hand sides of the equation. As k is varied the solution types on both sides of 2-35A will switch forms, the left-hand side being n-dependent.

We examine the dispersion equation as $W \to 0$. In this limit, we take the cutoff slot solution and the right-hand side of 2-35A approaches π/W and therefore has a pole. The possible poles in the left-hand side are for $\gamma_m = 0$, $\gamma_m' = 0$ and for $\gamma_m' g = P\pi$ (P an integer). The first two possibilities are excluded since $\gamma_m \coth \gamma_m g$ and $\gamma_m' \cot \gamma_m' g$ both approach $\frac{1}{g}$ in the limit. For the remaining possibility, we have from 2-35C that for $W \to 0$

$$k^2 - \beta_m^2 - \left(\frac{P\pi}{g}\right)^2 = 0$$

which is immediately recognized as the relationship for a TE_{PO} mode in uniform waveguide. We see easily from 2-35A that the same conclusions hold if $g-d \to 0$ so that in both cases the dispersion equation reduces to the uniform waveguide solution and the perturbation approaches zero.

As $\frac{W}{L} \to 1$ the thickness of the teeth approaches zero. For this situation, in contrast with the above, the dispersion does not approach that for the homogeneous boundary case. This can be seen by considering that even though the teeth become infinitesimally thin, E_x must still vanish at the edges of the teeth. This is contrasted with the TM mode of the linear magnetron at $\beta_0 = 0$, where the infinitesimally thin teeth do not perturb the field at

all. The zero thickness tooth is a useful idealization in that as we will see, a lower synchronous voltage will result for thin teeth and the space harmonic content is not zero in this limit. In practice, mechanical and beam interception considerations would dictate how small the dimension t may become. In Chap. 3 a solution is found for Laplace's equation in the rectangular geometry for this limiting case.

Let us approximate the dispersion equation. Assume that the fundamental is a fast wave and that the slot is cutoff at the frequency of interest. Further, let us take only the fundamental into the summation of 2-35A. It becomes, then

$$\frac{2}{\pi}\frac{W}{L}\sqrt{k^2-\beta_o^2}\cot\sqrt{k^2-\beta_o^2}\,g \approx \sqrt{\left(\frac{\pi}{W}\right)^2-k^2}\coth\left[\sqrt{\left(\frac{\pi}{W}\right)^2-k^2}(g-d)\right] \qquad (2\text{-}36A)$$

For a slot which is strongly cutoff the right-hand side of 2-36A is frequency independent. We have then

$$\frac{\tan\left[\sqrt{k^2-\beta_o^2}\,g\right]}{\sqrt{k^2-\beta_o^2}\,g} \approx \frac{2}{\pi^2}\frac{W}{L}\frac{W}{g}\tanh\frac{\pi(g-d)}{W} \qquad (2\text{-}36B)$$

We note that the right-hand side of 2-36B is a constant depending upon the dimensions of the circuit. The equation to be solved is of form

$$\frac{\tan\psi}{\psi} = -K \quad , \quad K \geq 0 \qquad (2\text{-}37)$$

The roots of 2-37 are equivalent to, following the notation for uniform waveguide,

$$\sqrt{k^2-\beta_o^2}\,g = \text{constant} \equiv k_c g \qquad (2\text{-}38)$$

yielding a hyperbolic ω-β curve, the solution for a uniform waveguide with a modified width, a', given by the solution of 2-37. That is, for a uniform waveguide in the TE_{mo} mode we have, denoting the m^{th} root of 2-36B as $k_{c_m} g$,

$$a' = \frac{m\pi g}{k c_m g} \tag{2-39}$$

For $\varphi \geq 0$ the smallest root of 2-37 occurs for $\frac{\pi}{2} < \varphi \leq \pi$. The function $\ln\left[-\frac{\tan\varphi}{\varphi}\right]$ is shown as a function of $\ln\left[1-\varphi/\pi\right]$ within this range in Fig. 2-5. We note a wide range of relative linearity. Since,

$$\frac{\tan\varphi}{\varphi} = -\frac{\tan(\pi-\varphi)}{\varphi} = -\frac{(\pi-\varphi) + \frac{(\pi-\varphi)^3}{3} + \frac{2(\pi-\varphi)^5}{15} + \cdots}{\varphi}$$

$$\text{for} \quad |\pi-\varphi| < \frac{\pi}{2} \tag{2-40A}$$

so that for φ close to π we have, corresponding to small values of K,

$$\frac{\tan\varphi}{\varphi} \approx -\left[1-\varphi/\pi\right] \tag{2-40B}$$

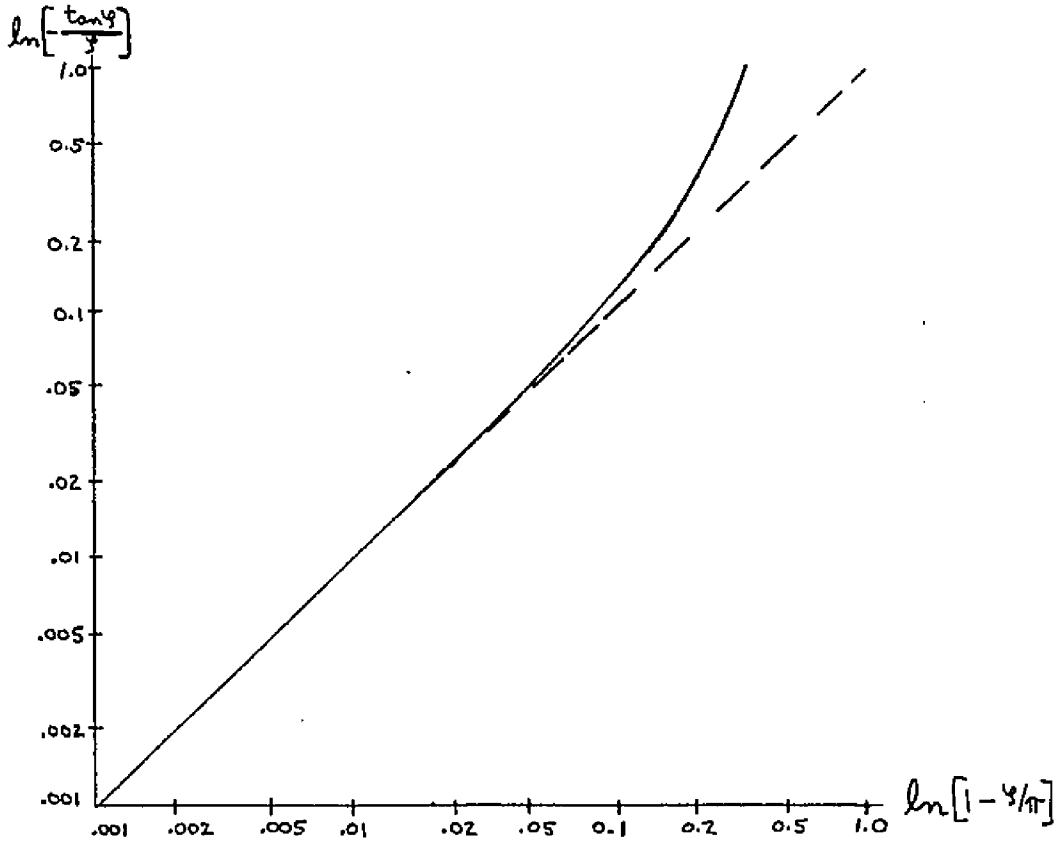

Fig. 2-5 $\ell n(-\tan\zeta/\zeta)$ as a function of $\ell n(1-\zeta/\pi)$, $\pi/2 < \zeta < \pi$

Eq. 2-28 defines the approximate Brillouin diagram where the constant is

given by the root of 2-37 as found from Fig. 2-5 or the approximation, 2-40B. The band structure is missing in this approximation as the higher order stopbands can only appear when the space harmonics are included. As $W \to 0$ or $d \to g$, K approaches zero and from 2-40B we have that $\varsigma \to \pi$, $\varsigma < \pi$. Therefore we have from 2-39, that a' approaches g from above.

For a square slot

$$\tanh \frac{\pi(g-d)}{W} = -\tanh \pi \approx -1$$

and if in addition we use the linear approximation given in 2-40B, consistent with small $\frac{2}{\pi^2}\frac{W^2}{Lg}$, we have

$$\varsigma = k_c g \approx \pi - \frac{2}{\pi}\frac{W^2}{Lg} \tag{2-41A}$$

and we have

$$a' \approx \frac{g}{1 - \frac{2}{\pi^2}\frac{W^2}{Lg}} \tag{2-41B}$$

We see that $a' > g$ so that the equivalent waveguide has a width larger than g as was postulated earlier in Eq. 2-6. As an example we take the case

W=.312 inch
L=.500 inch
g=.650 inch
d=.963 inch

for which the slot is square. We have

$$\tanh \pi \frac{g-d}{W} = \tanh[-\pi] \approx -.996$$

and we have

$$-K = \frac{2}{\pi^2}\frac{W^2}{Lg}\tanh \pi \frac{g-d}{W} \approx -.0605$$

The solution to 2-37 for this value is

$$1 - \frac{g}{\pi} = 1 - \frac{k_c g}{\pi} \approx .0565$$

The deviation from the linear approximation is about 7%. Then,

$$\frac{k_c}{\pi} \approx \frac{.9435}{g}$$

From 2-38

$$f = \frac{c}{2}\sqrt{\left(\frac{k_c}{\pi}\right)^2 + \left[\frac{\beta_0 L/\pi}{L}\right]^2} \qquad (2\text{-}42)$$

This approximate ω-β curve is shown for the dimensions of the example in Fig. 2-6. Also shown is the computer solution for the accurate dispersion equation, 2-35A. We note that for the example the approximation is good, coming within a few percent of the accurate curve. The approximation is hyperbolic and therefore the derivative does not decrease as the upper cutoff is approached. The computer solution does have such a bend although the group velocity does not go to zero even for the computer solution. Because of this behavior the two curves are seen to cross.

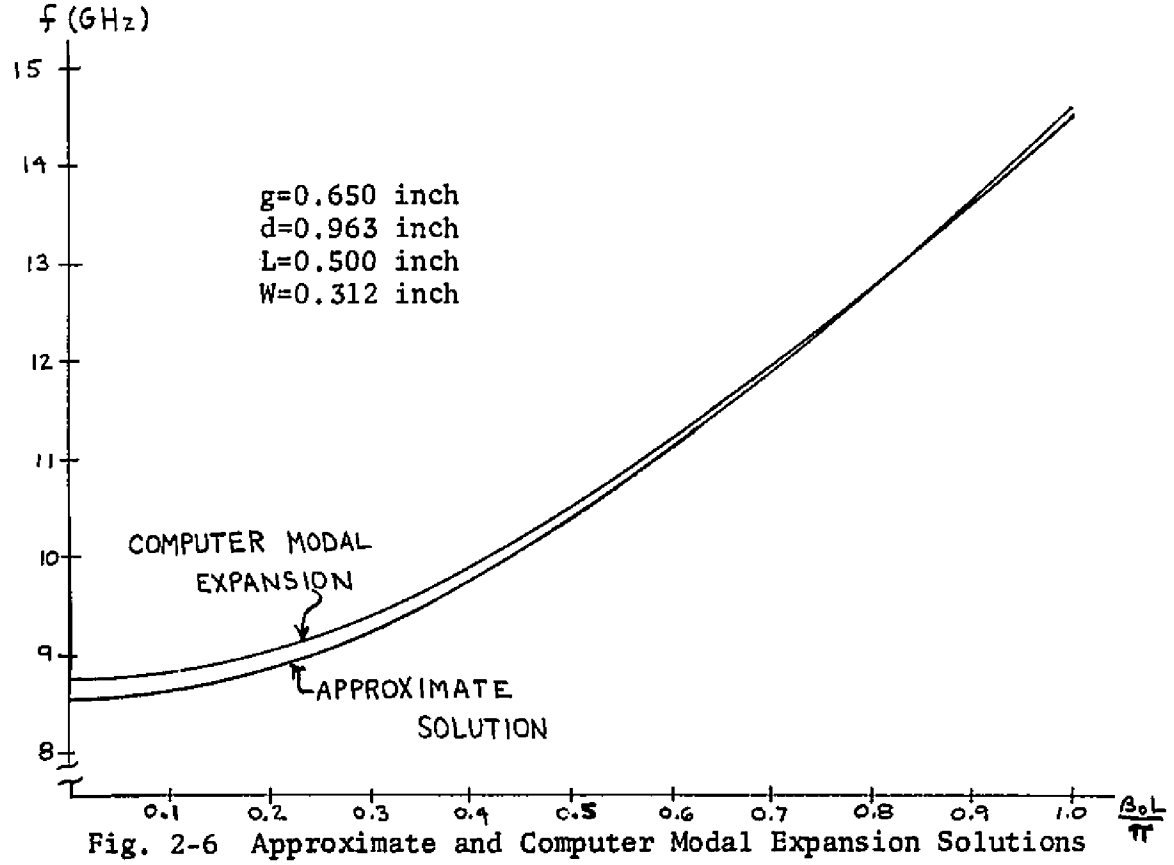

Fig. 2-6 Approximate and Computer Modal Expansion Solutions

We may write the fields existing in region I within a constant multiplier derived from the slot fields. We have, then, from 2-20, 2-21, 2-23, and 2-31

$$H_z^I(y,z) = e^{-i\beta_0 z} \sum_{m=-\infty}^{\infty} f_m \begin{Bmatrix} \gamma_m \dfrac{\cosh \gamma_m y}{\sinh \gamma_m g} \\ \gamma_m' \dfrac{\cos \gamma_m' y}{\sin \gamma_m' g} \\ \dfrac{1}{g} \end{Bmatrix} e^{-im\frac{2\pi}{L}z} \tag{2-43A}$$

$$E_x^I(y,z) = i\omega\mu e^{-i\beta_0 z} \sum_{m=-\infty}^{\infty} f_m \begin{Bmatrix} \dfrac{\sinh \gamma_m y}{\sinh \gamma_m g} \\ \dfrac{\sin \gamma_m' y}{\sin \gamma_m' g} \\ y/g \end{Bmatrix} e^{-im\frac{2\pi}{L}z} \tag{2-43B}$$

$$H_y^I(y,z) = i\, e^{-i\beta_0 z} \sum_{m=-\infty}^{\infty} f_m \begin{Bmatrix} \beta_m \dfrac{\sinh \gamma_m y}{\sinh \gamma_m g} \\ \beta_m \dfrac{\sin \gamma_m' y}{\sin \gamma_m' g} \\ \beta_m y/g \end{Bmatrix} e^{-im\frac{2\pi}{L}z} \tag{2-43C}$$

$$H_x^I = E_y^I = E_z^I = 0 \tag{2-43D}$$

and where

$$f_m = \begin{Bmatrix} \frac{2}{\pi} \dfrac{\frac{W}{L}\cos m\pi \frac{W}{L}}{1-4m^2(W/L)^2} \\ \\ \frac{1}{2}\frac{W}{L} \end{Bmatrix} \begin{Bmatrix} \dfrac{a_1}{\pi/W} \sinh \Gamma_1 (g-d) \\ \dfrac{a_1'}{\pi/W} \sin \Gamma_1' (g-d) \\ c_1 (g-d) \end{Bmatrix} \tag{2-43E}$$

If an electron beam is synchronous with, for example, the n=1 space harmonic, only this harmonic will influence the motion of the electrons, the effect of the other harmonics being negligible. To calculate the interaction and

resultant gain we must know what the amplitude of the synchronous harmonic is for given power flow through the structure. We integrate the z component of the complex Poynting vector in region I over a plane normal to the z direction and intersecting a tooth. We take the width of the structure in the x direction to be unity so that the average power calculated will be per unit width. In the case of the coaxial system, for which this analysis is intended, we multiply the result by $2\pi R_o$, where Ro is the mean radius of the structure. We have then, for a unit width, from 2-43

$$P_{avg} = \frac{1}{2} Re \int_0^g E_x^I(y,z)\, H_y^{I*}(y,z)\, dy$$

$$= \frac{\omega\mu}{2} \sum_{m=-\infty}^{\infty} \sum_{m=-\infty}^{\infty} \beta_m f_m f_m \cos(m-m)\frac{2\pi}{L} z \int_0^g \left\{ \begin{matrix} \frac{\sinh \gamma_m y}{\sinh \gamma_m g} \\ \frac{\sin \gamma_m' y}{\sin \gamma_m g} \\ y/g \end{matrix} \right\} \left\{ \begin{matrix} \frac{\sinh \gamma_m y}{\sinh \gamma_m g} \\ \frac{\sin \gamma_m' y}{\sin \gamma_m g} \\ y/g \end{matrix} \right\} dy \qquad (2\text{-}44A)$$

where we have assumed that we may interchange the orders of summation and integration. This is certainly permissible if the series are truncated, which is in fact what will be done.

We note from 2-44A that the coefficients are functions of z, but the average power must be a constant with respect to z, similar to the Fourier series of a rectangular wave. If we take the plane of integration to be at the center of a tooth, it would appear that the approximation of a single slot mode will affect the answer the least when the series is truncated. With reference to Fig. 2-1 we take $z=\frac{L}{2}$. At a particular frequency the right-hand bracket of 2-43E will be a constant which we define as B. We have, then

$$P_{avg} = \frac{B^2\omega\mu}{2} \sum_{m=-\infty}^{\infty} \sum_{m=-\infty}^{\infty} (-1)^{m-m} \beta_m \left\{ \begin{matrix} \frac{2}{\pi}\frac{W}{L}\cos m\pi\frac{W}{L} \Big/ 1-4m^2\left(\frac{W}{L}\right)^2 \\ \frac{1}{2}\frac{W}{L} \end{matrix} \right\} \left\{ \begin{matrix} \frac{2}{\pi}\frac{W}{L}\cos m\pi\frac{W}{L} \Big/ 1-4m^2\left(\frac{W}{L}\right)^2 \\ \frac{1}{2}\frac{W}{L} \end{matrix} \right\} \int_0^g \left\{ \begin{matrix} \frac{\sinh \gamma_m y}{\sinh \gamma_m g} \\ \frac{\sin \gamma_m' y}{\sin \gamma_m g} \\ y/g \end{matrix} \right\} \left\{ \begin{matrix} \frac{\sinh \gamma_m y}{\sinh \gamma_m g} \\ \frac{\sin \gamma_m' y}{\sin \gamma_m g} \\ y/g \end{matrix} \right\} dy$$

(2-44B)

We make note of the fact that 2-44B contains cross terms since the functions of y are not orthogonal. In a homogeneous waveguide, because

the modes are orthogonal with respect to integration over the cross section, the total power is the sum of the powers carried by the separate modes. In this case this is not true and the cross products do contribute to the power.

We will specialize 2-44B to obtain a useful result. For β_0 taken small enough, the fundamental will be a fast wave. We assume further that L is small enough so that all other space harmonics are slow waves. We have ruled out the possibility of a $v_\varphi = c$ wave by these assumptions. If such a wave existed, a slight frequency shift would produce the assumed situation. We approximate the power by taking the contributions of only the fundamental and the first forward and backward space harmonics, taking only the values 0, 1 and -1 for m and n. This yields nine terms in 2-44B. We will retain only the zeroth and first order terms of this set, discarding the products of $m=\pm1$ and $n=\pm1$, keeping, therefore, therefore five terms. Let us assume that $\frac{L}{W} \neq 2$ so that we avoid use of the special term $\frac{1W}{2L}$ for m, $n=\pm1$. We find that

$$P_{avg} \approx \frac{2\left(\frac{\omega}{c}\right)^2 \omega\mu B^2}{\pi^2 \sin\gamma_0' g}\left\{\frac{\beta_0}{\sin\gamma_0' g}\left[\frac{g}{2} - \frac{\sin 2\gamma_0' g}{4\gamma_0'}\right] - \frac{\cos\pi\frac{W}{L}}{1-4\left(\frac{W}{L}\right)^2}\left[\frac{(\beta_0+\beta_1)(\gamma_1 \sin\gamma_0' g \cosh\gamma_1 g - \gamma_0' \cos\gamma_0' g \sinh\gamma_1 g)}{(\sinh\gamma_1 g)(\gamma_0'^2+\gamma_1^2)}\right.\right.$$

$$\left.\left. + \frac{(\beta_0+\beta_{-1})(\gamma_{-1} \sin\gamma_0' g \cosh\gamma_{-1} g - \gamma_0' \cos\gamma_0' g \sinh\gamma_{-1} g)}{(\sinh\gamma_{-1} g)(\gamma_0'^2+\gamma_{-1}^2)}\right]\right\} \qquad (2\text{-}45A)$$

and for the total power in the coaxial system

$$P_{T_{avg}} \approx 2\pi R_0 P_{avg} \qquad (2\text{-}45B)$$

We therefore may express the n=1 space harmonic of E_x in terms of the average power. We find

$$E_{x_1}^{I}(y,z) \approx \frac{i\frac{\sqrt{2\omega\mu}}{\sinh\gamma_1 g}\sqrt{\sin\gamma_0' g}\,\frac{\cos\pi\frac{W}{L}}{1-4(W/L)^2}\sqrt{P_{avg}}\sinh\gamma_1 y\, e^{-i\left(\beta_0+\frac{2\pi}{L}\right)z}}{\sqrt{\frac{\beta_0}{\sin\gamma_0' g}\left[\frac{g}{2} - \frac{\sin 2\gamma_0' g}{4\gamma_0'}\right] - \frac{\cos\pi\frac{W}{L}}{1-4\left(\frac{W}{L}\right)^2}\left[\frac{(\beta_0+\beta_1)(\gamma_1 \sin\gamma_0' g \cosh\gamma_1 g - \gamma_0' \cos\gamma_0' g \sinh\gamma_1 g)}{(\sinh\gamma_1 g)(\gamma_0'^2+\gamma_1^2)}\right.}}$$

$$\left. + \frac{(\beta_0+\beta_{-1})(\gamma_{-1} \sin\gamma_0' g \cosh\gamma_{-1} g - \gamma_0' \cos\gamma_0' g \sinh\gamma_{-1} g)}{(\sinh\gamma_{-1} g)(\gamma_0'^2+\gamma_{-1}^2)}\right] \qquad (2\text{-}46)$$

We turn next to the solution of the dispersion equation, 2-35, by digital computer. The computer program tests to determine which term of the brackets is appropriate since the computer cannot make the smooth transition between the possibilities. For a given value of β_o , $0 \leq \beta_o \leq \pi/L$, the left-hand side of 2-35A is computed using a symmetrically truncated version of the series as k is varied, viz.,

$$\sum_{m=-\infty}^{\infty} \approx \sum_{m=-N}^{N}$$

The series is summed for a value of N such that the absolute value of the change in the summed value is less than an arbitrary percentage of the value of the sum for N-1 and such that N is greater than an arbitrary minimum value. The program was run with the minimum N equal to 50 so that a minimum of 101 terms are included in the summation. The summing process was terminated when the absolute value of the increment is less than $\frac{1}{2}\%$ of the preceding value of the sum. It was found that in most cases the initial value of N=50 was sufficient. The right-hand side of the equation is found as a function of k as well, and a common value is sought for the two sides of the equation for the same value of k, that value belonging to the assumed value of β_o .

Since the testing of the structure will be done in the x band, the geometry will be varied to obtain the zero-mode cutoff towards the lower end of this band. First we set the dimension L, the period, to be 0.500 inch since with reference to Fig. 2-2 we see that a larger period will yield too high a voltage. Next we vary the dimension d, keeping others fixed. We are interested, at this point, in only the cutoff frequencies since we wish to adjust the placement of the passband. We therefore set, in the left-hand side of the dispersion equation, β_o equal to the two values 0 and π/L .

An example of the graphical solution for one such case is shown in Fig. 2-7. The value of k where the slot becomes propagating is shown as well. We note that the dimensions given yield a passband which is far above the x band. We attempt to lower the frequency of the passband by increasing the value of d. If it were possible to do so we would expect to have good space harmonic content due to the small value of g. The variation in the passband as

d is increased while the other dimensions remain fixed is shown in Fig. 2-8. We note that the frequency of the passband is lowered only slightly as d is increased past the point of a square slot, agreeing with our earlier predictions. We also note from Fig. 2-8 that the fundamental is forward wave, which was also predicted.

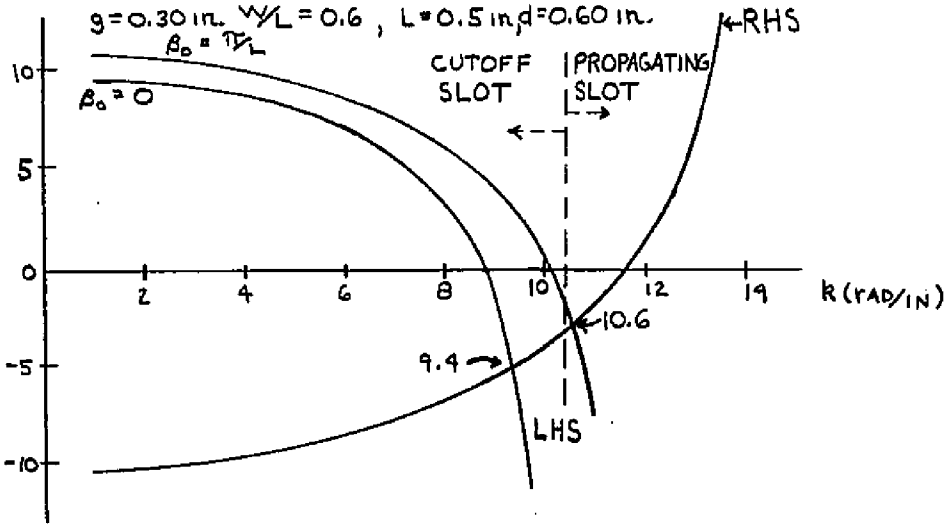

Fig. 2-7 Graphical Solution of the Dispersion Equation

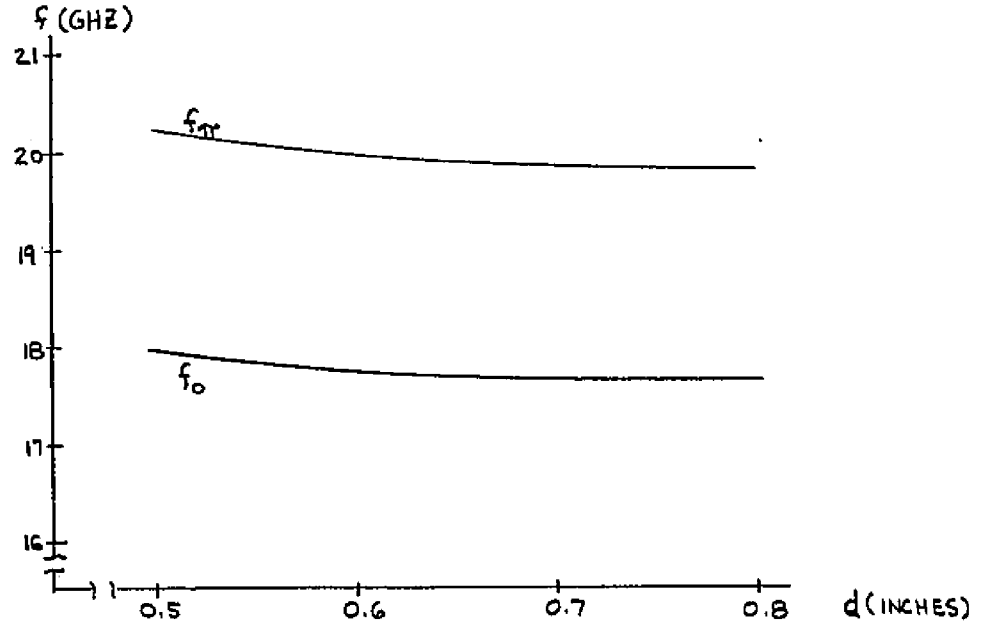

Fig. 2-8 Calculated Zero and π-Mode Frequencies as Functions of d (g=0.3 in., W/L=0.6, L=0.5 in.)

We next vary the gap dimension g while maintaining a square slot based upon the above reasoning. As g is reduced, the values of k corresponding to the solutions are increased and their separation is reduced, as shown in Fig. 2-9.

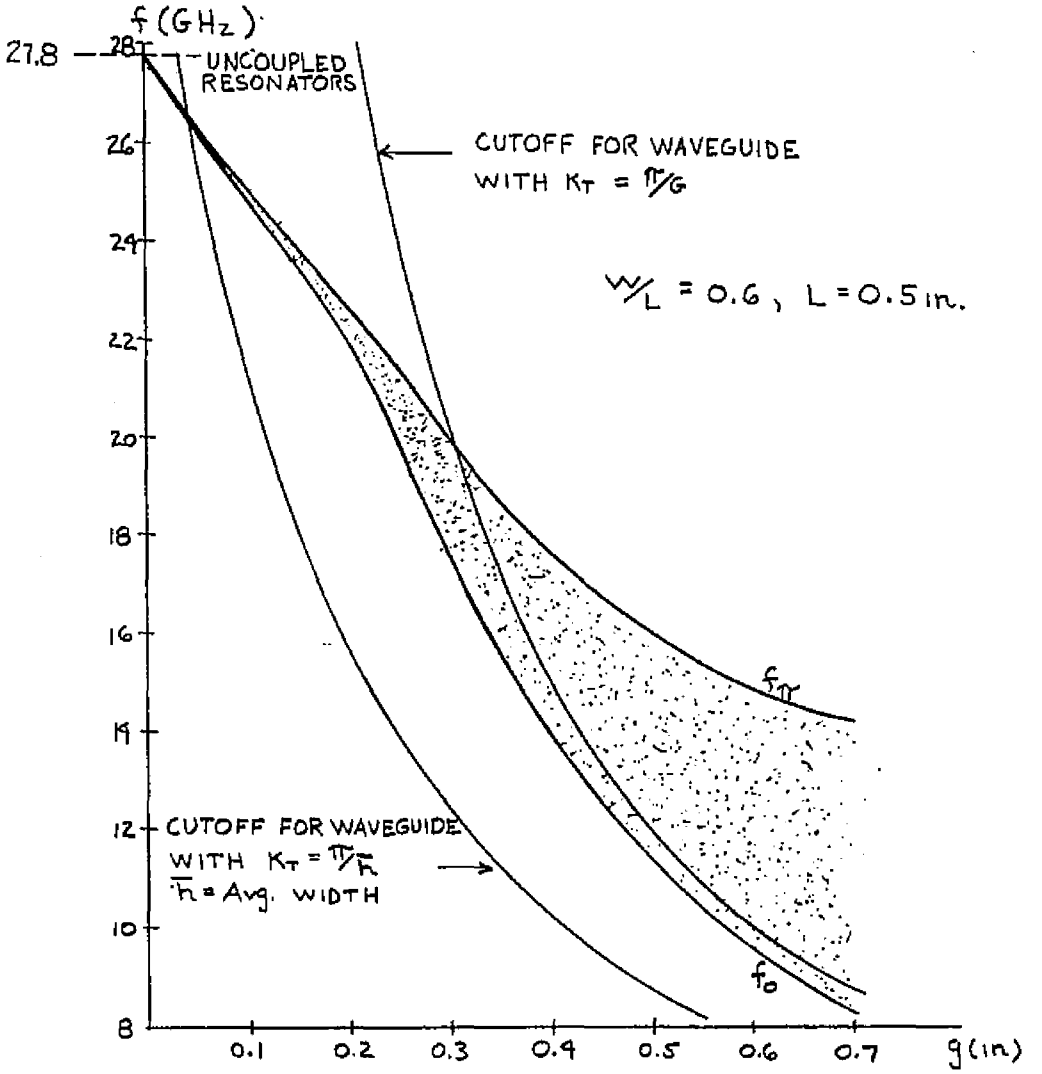

Fig. 2-9 Calculated Zero and π-Mode as a Function of g (d simultaneously varied to maintain a square slot)

We see that as $g \to 0$ the zero and π-mode frequencies coalesce into a single frequency of uncoupled resonators in consonance with earlier predictions. This frequency corresponds to a resonator of width and length equal to 0.3 inch. For comparison the cutoff frequency for a uniform waveguide of width g and of average width is shown. The average is weighted with respect to the fraction of the period where the width of guide is equal to g or d. It is noted from the figure that for large values of g the waveguide of width g is a fair approximation to obtain the zero mode frequency and the average width approximation is better for smaller values of g.

An example of the dispersion curve for fairly small g and high frequency is shown in Fig. 2-10. An approximate zero slope is noted at the lower cutoff, corresponding to the physical requirement that $v_g \to 0$ there. As

$\beta_o \rightarrow \pi/L$, the slope decreases but we do not find the behavior that $v_g \rightarrow 0$. This is no doubt a result of the approximation made that $e^{i\beta_o z}$ is approximately constant over the slot with a possible contributing factor being that for the upper 20% of $\beta_o L$ the slot is propagating, so that perhaps the assumption of a single slot mode is no longer accurate. The edges of the passband are found for parametric values of g as the aspect ratio, $A=\frac{W}{L}$, is varied with the results depicted in Fig. 2-11. The affect of the aspect ratio upon the solution is greatest for smaller values of g.

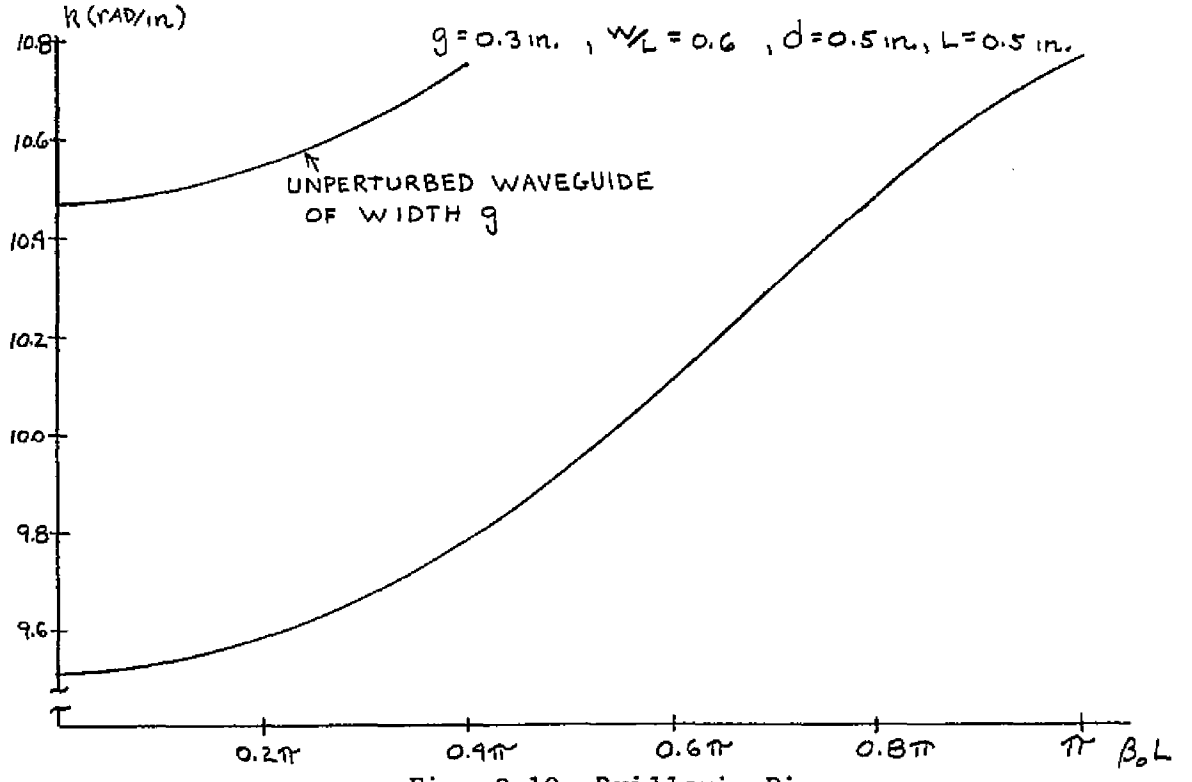

Fig. 2-10 Brillouin Diagram

The passband of the situation shown in Fig. 2-12 lies mostly in x band. We note the same observations as before with respect to group velocity. In this case, however, the slot remains cutoff throughout the passband. With reference to the $v_\phi = C$ line shown we note that the fundamental is a fast wave through the entire passband. The experimental points shown, from the results of Sec. 2.4, indicate excellent agreement with the theoretical solution. It should be noted here that the agreement is better at low β_o with slight disagreement at the higher β_o points as expected from the approximations made. The experimental points indicate that the slope of the curve will decrease as $\beta_o L$ approaches π as theoretically expected.

Experimental points for very low β_0 were not obtained due to problems of matching into the structure in this range. The upper part of the curve lay beyond the range of the measuring equipment.

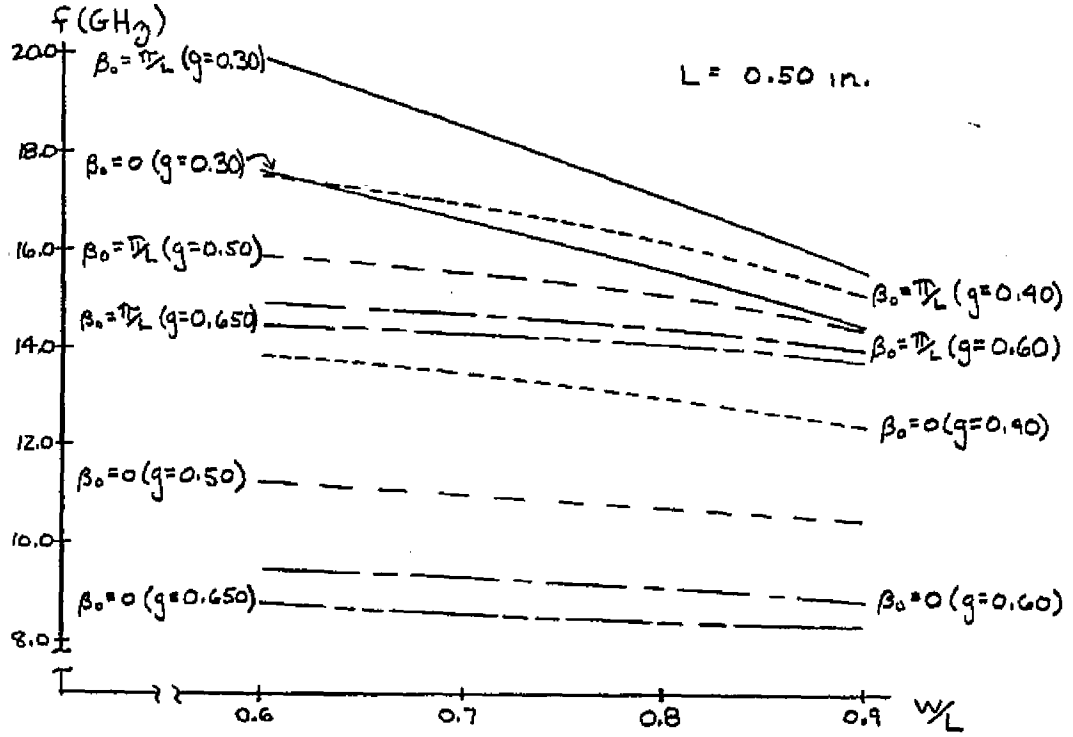

Fig. 2-11 Calculated f_0 and f_π as Functions of Aspect Ratio, $A=\frac{W}{L}$ (d simultaneously varied to maintain a square slot)

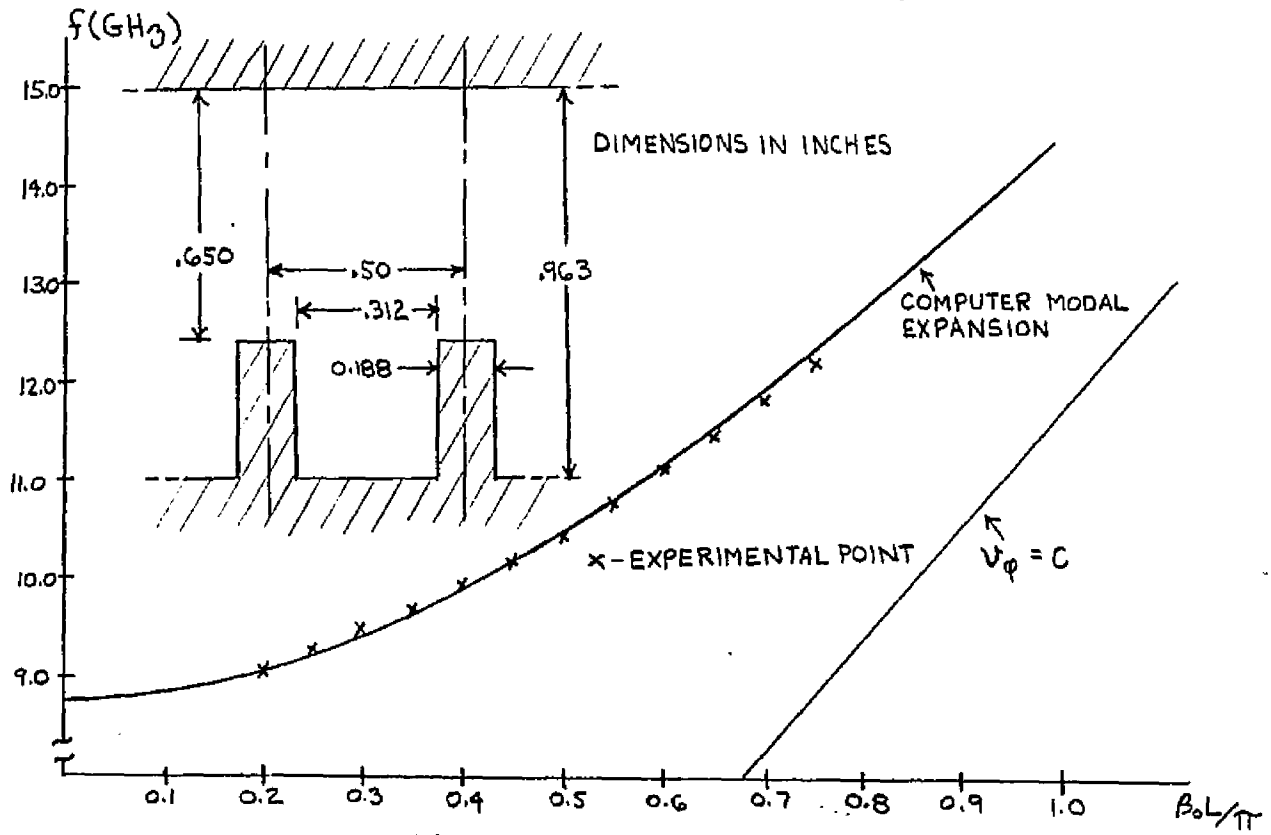

Fig. 2-12 Brillouin Diagram

We may investigate the question as to whether the result found is the perturbation of the TE_{10} mode as postulated. We note from 2-43B that the fundamental varies in the gap as $\sin \gamma_o' y$. If the fundamental has no zeros in the region $0<y<g$ we may assume that we have the required mode. We therefore wish to determine that

$$\gamma_o' g = \sqrt{k^2 - \beta_o^2}\, g < \pi \tag{2-47}$$

From Fig. 2-12 we find that the lower cutoff frequency is approximately 8.75GHz from which the value of k is found to be approximately $.585\pi$ radians/cm. At this point we find $\gamma_o' g \approx .965\pi < \pi$ verifying 2-47.

For this case we calculate the synchronous voltage as a function of frequency for the n=1 space harmonic with the result shown in Fig. 2-13. We see that from the standpoint of minimum voltage we would wish to operate at approximately 9.3-9.4GHz. This is also the best point in terms of broad-band operation since the synchronous voltage is relatively constant with respect to changes in frequency in this range. Therefore, a modulated signal would remain relatively synchronous with the beam.

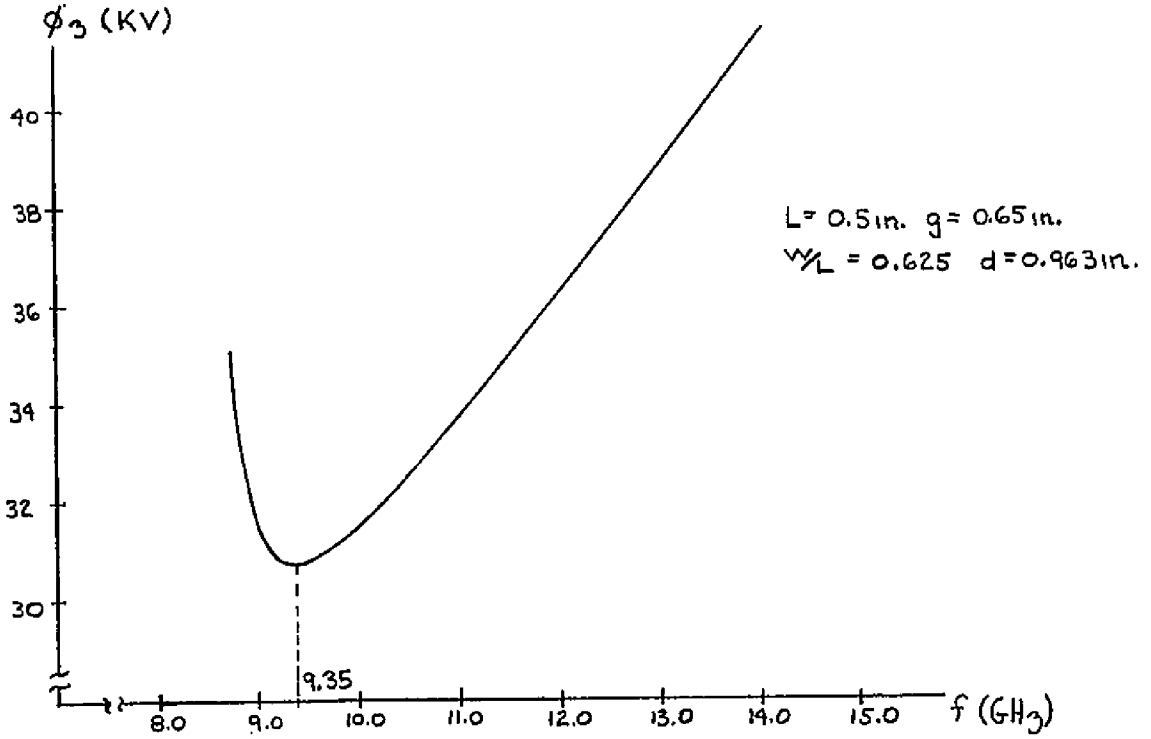

Fig. 2-13 Axial Potential As A Function of Frequency (n=+1 space harmonic)

The dimensions of Fig. 2-1 are varied to satisfy certain considerations. The passband must lie in the chosen frequency range and a harmonic must be found with a moderate value of synchronous voltage. This latter aspect involves restrictions on the value of the period. Based on the previous discussions we would choose n=1 or n=-1. The value of the gap, g, should be large enough so that the electron beam will not impinge upon the structure yet not so small as to make the space harmonic content negligible. We must also have a set of dimensions consistent with stability of the electrons in the periodic static fields, a problem taken up in Chap. 4.

There are higher order solutions of the dispersion equation, 2-35A, at higher frequency. Physically, one expects higher order solutions in one of two possible forms. For the same mode we have been discussing we expect solutions corresponding to the higher frequency branches of the Brillouin diagram shown in Fig. 2-3. In addition to these higher order branches there exist the modes which are derived from the higher order TE modes in uniform waveguide. For example, the next mode would be that derived from the TE_{20} mode and the electric field would display a null within the structure. Each of these modes would have higher order branches, similar to those shown in Fig. 2-3, as well. These solutions occur at higher frequency where the approximation of the slot fields by the single slot mode may be in doubt. For example, if two slot modes are propagating it is possible at a particular frequency for the slot depth to be a half-wavelength for the lowest mode, in which case the second mode determines the fields at the mouth of the slot. Because of this, no attempt will be made to relate the higher order intersections of 2-35A with the higher order branches of this mode or the higher order modes.

2.3 Hill's Equation Approximation

We next obtain an approximate and simpler dispersion equation for the periodic structure by making some rather crude assumptions. With respect to Fig. 2-1 we translate the coordinate axes by $\frac{W}{2}$ so that

$$\zeta \equiv z - \frac{W}{2} \tag{2-48}$$

We consider the tooth region, $0<\zeta<t$, and the slot region, $-w<\zeta<0$, as sections of uniform waveguide and make the simplifying assumption that only the dominant TE_{10} modes exist in each section. In either case these are the lowest order modes which satisfy the boundary conditions at y=0 and y=g and at y=0 and y=d. We take, therefore, the variation of E_x with respect to y for the slot region to be $\sin\frac{\pi}{d}y$ and the variation for the tooth region to be of the form $\sin\frac{\pi}{g}y$. With these assumptions we have two distinct differential equations for the two regions. That is

$$\frac{\partial^2 E_x}{\partial \zeta^2} - \left[\frac{\pi^2}{d^2} - k^2\right]E_x = 0 \qquad -w<\zeta<0 \tag{2-49A}$$

and

$$\frac{\partial^2 E_x}{\partial \zeta^2} - \left[\frac{\pi^2}{g^2} - k^2\right]E_x = 0 \qquad 0<\zeta<t \tag{2-49B}$$

We recognize, at this point, that the problem is similar to that considered by Kronig and Penney[27] as well as van der Pol and Strutt[28] for a model of the quantum mechanics of electrons in crystal lattices. The problem there is the solution of the Schroedinger equation for a rectangular potential function. Some of the results are given by Brillouin[29] and we follow his method for our case. We may write down the solutions for the two regions from the differential equations given in 2-49

$$E_x = \sin\tfrac{\pi}{d}y\,\psi_s(\zeta) = \sin\tfrac{\pi}{d}y\left[A_0 e^{\sqrt{\frac{\pi^2}{d^2}-k^2}\,\zeta} + B_0 e^{-\sqrt{\frac{\pi^2}{d^2}-k^2}\,\zeta}\right] \qquad -w<\zeta<0 \tag{2-50A}$$

$$E_x = \sin\tfrac{\pi}{g}y\,\psi_t(\zeta) = \sin\tfrac{\pi}{g}y\left[C_0 e^{\sqrt{\frac{\pi^2}{g^2}-k^2}\,\zeta} + D_0 e^{-\sqrt{\frac{\pi^2}{g^2}-k^2}\,\zeta}\right] \qquad 0<\zeta<t \tag{2-50B}$$

At this point we suppress the variation with respect to y and consider only the functions ψ_s and ψ_t which depend only on ζ. By doing this we have made the problem one-dimensional and take the ψ functions to carry the information necessary to find the dispersion. By the same reasoning

utilized in Sec. 2.2 we write for a solution of the Ψ function throughout

$$\Psi(\xi) = \Phi(\xi) e^{\mu \xi} \tag{2-51A}$$

where the $\Phi(\xi)$ is periodic with period L, and

$$\Psi(\xi) = e^{\mu L} \Psi(\xi - L) \tag{2-51B}$$

We therefore may write the solutions for the tooth region and the two slot regions to either side

$$\Psi(\xi) = A_0 e^{\sqrt{\frac{\pi^2}{d^2} - k^2}\,\xi} + B_0 e^{-\sqrt{\frac{\pi^2}{d^2} - k^2}\,\xi} \quad , \quad -w < \xi < 0 \tag{2-52A}$$

$$\Psi(\xi) = C_0 e^{\sqrt{\frac{\pi^2}{g^2} - k^2}\,\xi} + D_0 e^{-\sqrt{\frac{\pi^2}{g^2} - k^2}\,\xi} \quad , \quad 0 < \xi < t \tag{2-52B}$$

$$\Psi(\xi) = e^{\mu L}\left[A_0 e^{\sqrt{\frac{\pi^2}{d^2} - k^2}\,(\xi - L)} + B_0 e^{-\sqrt{\frac{\pi^2}{d^2} - k^2}\,(\xi - L)}\right] \quad , \quad t < \xi < L \tag{2-52C}$$

At the boundaries between the regions, $\xi = 0$ and $\xi = t$, we demand that Ψ and its derivative be continuous. Except for the variation in y, which has been dropped, this is equivalent to the requirement that E_x and $\frac{\partial E_x}{\partial y}$ be continuous. From the curl of $\bar{E}$ equation, $\frac{\partial E_x}{\partial y}$ is proportional to H_y so that we have required E_x and H_y to be continuous, neglecting the variation in y. These continuity conditions lead to four homogeneous equations for which a nontrivial solution for the coefficients A_0, B_0, C_0 and D_0 requires that the following determinant be zero:

$$\Delta = \begin{vmatrix} 1 & 1 & -1 & -1 \\ \sqrt{\frac{\pi^2}{d^2} - k^2} & -\sqrt{\frac{\pi^2}{d^2} - k^2} & -\sqrt{\frac{\pi^2}{g^2} - k^2} & \sqrt{\frac{\pi^2}{g^2} - k^2} \\ e^{\mu L} e^{-\sqrt{\frac{\pi^2}{d^2} - k^2}\,w} & e^{\mu L} e^{\sqrt{\frac{\pi^2}{d^2} - k^2}\,w} & -e^{\sqrt{\frac{\pi^2}{g^2} - k^2}\,t} & -e^{-\sqrt{\frac{\pi^2}{g^2} - k^2}\,t} \\ e^{\mu L}\sqrt{\frac{\pi^2}{d^2} - k^2} e^{-\sqrt{\frac{\pi^2}{d^2} - k^2}\,w} & -e^{\mu L}\sqrt{\frac{\pi^2}{d^2} - k^2} e^{\sqrt{\frac{\pi^2}{d^2} - k^2}\,w} & -\sqrt{\frac{\pi^2}{g^2} - k^2} e^{\sqrt{\frac{\pi^2}{g^2} - k^2}\,t} & \sqrt{\frac{\pi^2}{g^2} - k^2} e^{-\sqrt{\frac{\pi^2}{g^2} - k^2}\,t} \end{vmatrix} = 0 \tag{2-53A}$$

or, after manipulation,

$$e^{2\mu L} - e^{\mu L}\left\{2\cosh\sqrt{\frac{\pi^2}{d^2}-k^2}\,w\,\cosh\sqrt{\frac{\pi^2}{g^2}-k^2}\,t + \frac{\left(\frac{\pi^2}{g^2}-k^2\right)+\left(\frac{\pi^2}{d^2}-k^2\right)}{\sqrt{\frac{\pi^2}{d^2}-k^2}\,\sqrt{\frac{\pi^2}{g^2}-k^2}}\sinh\sqrt{\frac{\pi^2}{d^2}-k^2}\,w\,\sinh\sqrt{\frac{\pi^2}{g^2}-k^2}\,t\right\} + 1 = 0 \qquad (2\text{-}53B)$$

The product of the two solutions to this quadratic equation in $e^{\mu L}$ is unity. Thus the sum of the roots, $e^{\mu L} + e^{-\mu L} = 2\cosh \mu L$, is given by the negative of the coefficient of the term linear in $e^{\mu L}$. The dispersion equation is, then,

$$\cosh \mu L = \cosh\left[\sqrt{\frac{\pi^2}{d^2}-k^2}\,w\right]\cosh\left[\sqrt{\frac{\pi^2}{g^2}-k^2}\,t + \frac{1}{2}\left[\frac{\sqrt{\frac{\pi^2}{d^2}-k^2}}{\sqrt{\frac{\pi^2}{g^2}-k^2}} + \frac{\sqrt{\frac{\pi^2}{g^2}-k^2}}{\sqrt{\frac{\pi^2}{d^2}-k^2}}\right]\sinh\left[\sqrt{\frac{\pi^2}{d^2}-k^2}\,w\right]\sinh\left[\sqrt{\frac{\pi^2}{g^2}-k^2}\,t\right] \qquad (2\text{-}54)$$

For the computation of the right-hand side of 2-54 by digital computer the nature of the square roots is tested, since, depending upon the value of k, they may be real or imaginary. In the latter case the circular functions are used. It is easily seen that for all combinations of the various possible square roots, the right-hand side is purely real. We have,

$$\cosh \mu L = \cosh(\mu_r + i\mu_i)L = \cos \mu_i L \cosh \mu_r L + i \sin \mu_i L \sinh \mu_r L \qquad (2\text{-}55)$$

In view of the fact that the right-hand side of 2-54 is purely real we have

$$\sin \mu_i L \sinh \mu_r L = 0 \qquad (2\text{-}56A)$$

which has one or both of the following solutions

$$\mu_r = 0 \qquad (2\text{-}56B)$$

$$\mu_i L = \pm m\pi \,, \quad m = 0, 1, 2, \cdots \qquad (2\text{-}56C)$$

if $\mu_r=0$ we have

$$\cos \mu_i L = \cosh \mu L \tag{2-57A}$$

so that this holds for

$$-1 \leq \cosh \mu L \leq 1 \tag{2-57B}$$

On the other hand, if $\mu_i L=\pm m\pi$

$$(-1)^m \cosh \mu_r L = \cosh \mu L \tag{2-58A}$$

so that this is relevant for

$$\cosh \mu L \geq 1, \quad m \text{ even} \tag{2-58B}$$

and for

$$\cosh \mu L \leq -1, \quad m \text{ odd} \tag{2-58C}$$

Therefore, depending upon the value of the right-hand side of 2-54, μ is purely imaginary or complex. The nature of μ determines the passband-stopband character of the Brillouin diagram. The possibilities are summarized in Table 2-1.

For the passband situation the values of n are equivalent to the space harmonics that were derived in Sec. 2.2. In a similar manner, at the transitions between the passband and stopband, the value of m specifies the zero or π-mode cutoff depending upon whether m is even or odd, repectively. In the stopbands the value of m identifies the position of the stopband relative to the passband structure.

Table 2-1 Passband-Stopband Character

$\cosh\mu L$	μ	Condition
$-\infty<\cosh\mu L<-1$	$\frac{1}{L}\cosh^{-1}[-\cosh\mu L]\pm i\frac{m\pi}{L}$, m odd	Stopband
$\cosh\mu L=-1$	$\pm i\frac{m\pi}{L}$, m odd	π-Mode Cutoff
$-1<\cosh\mu L<1$	$\pm\frac{i}{L}(\cos^{-1}[\cosh\mu L]\pm n2\pi)$, n integer	Passband
$\cosh\mu L=1$	$\pm i\frac{m\pi}{L}$, m even	Zero-Mode Cutoff
$1<\cosh\mu L<\infty$	$\frac{1}{L}\cosh^{-1}[\cosh\mu L]\pm i\frac{m\pi}{L}$, m even	Stopband

As an example, $\cosh\mu L$ is shown in Fig. 2-14 as a function of k, for the set of dimensions of Fig. 2-10. Those values of k for which $|\cosh\mu L|<1$ correspond to passbands and we note that the width of the stopbands decreases for the higher order branches. The branches of the ω-β diagram derived from the uniform case are shown in Fig. 2-15 together with the ω-β curve for a uniform waveguide of average width, .42 inches. The two sets

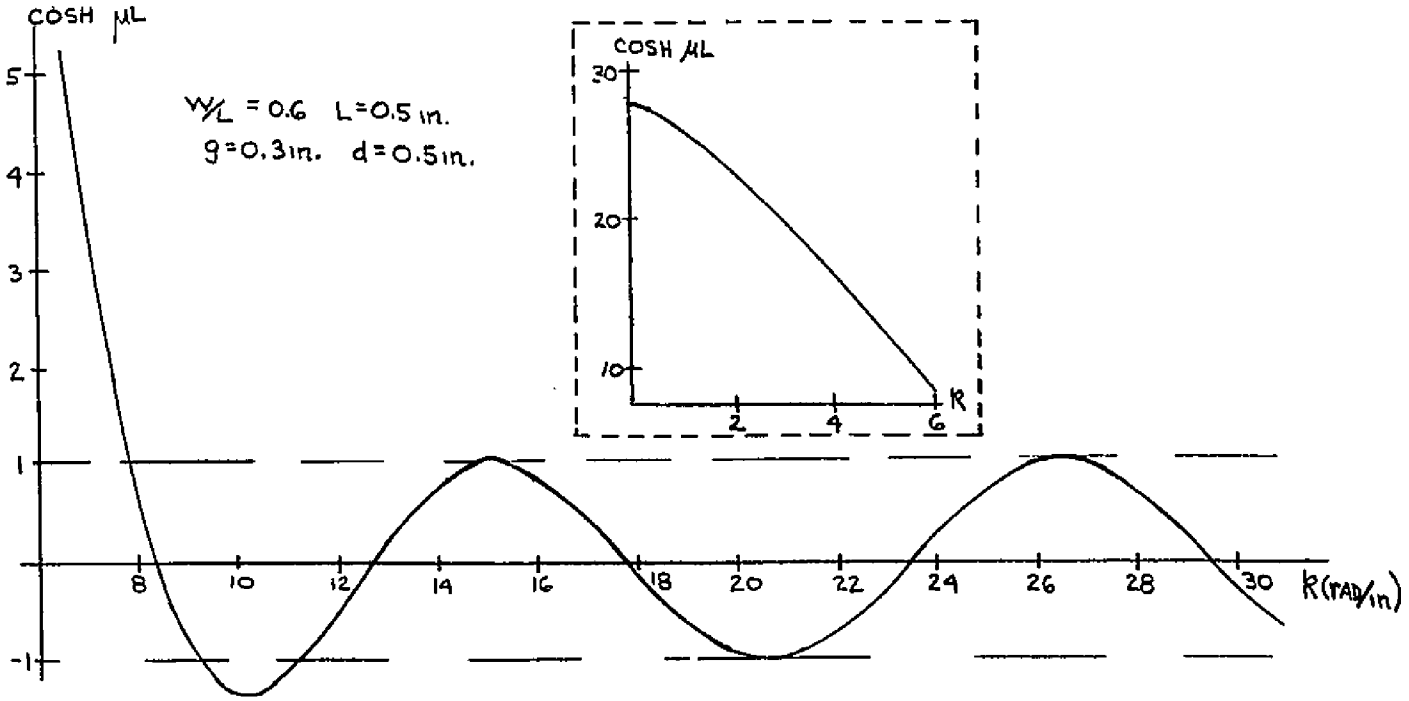

Fig. 2-14 $\cosh\mu L$ vs. k For The Hill's Equation Approximation

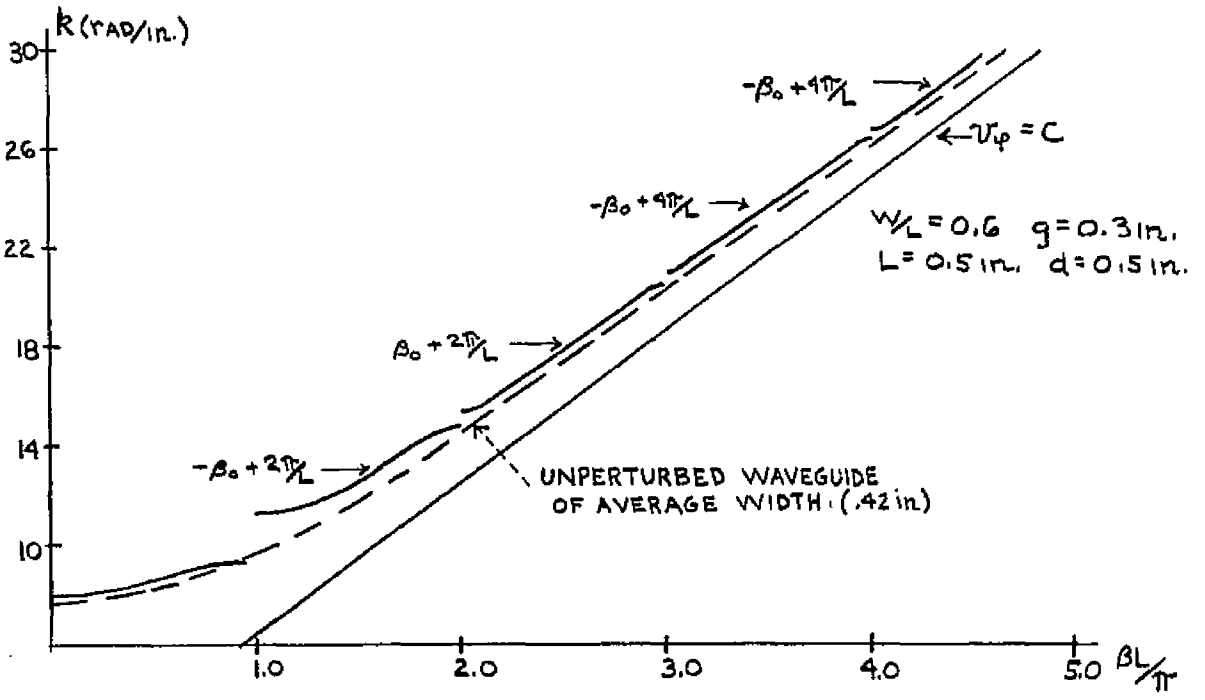

Fig. 2-15 Dispersion Curves, Hill's Equation Approximation

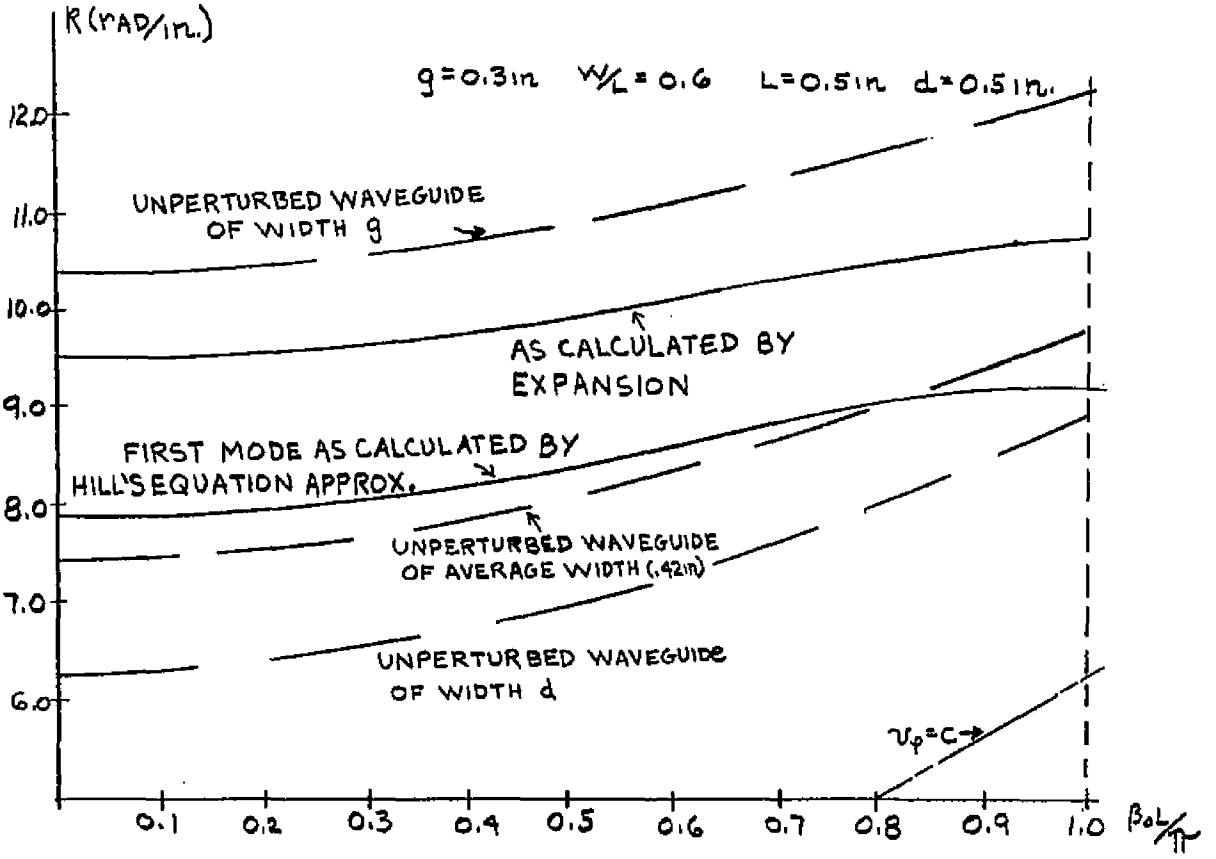

Fig. 2-16 Dispersion Curves

of curves are seen to approach each other as the frequency increases. These derived harmonics are all seen to be fast waves. In Fig. 2-16 the first passband is compared with that obtained by the method of Sec. 2.2. They are seen to differ in absolute value but to have the same basic shape. Curves are also shown for smooth waveguides of width g, d, and of average width. In Fig. 2-17 the edges of the first passband are shown as g is varied and compared with the similar result for the modal expansion method from Fig. 2-9. The dimension d is set so as to maintain a square slot. The same general shapes are found for the curves but they differ in magnitude considerably.

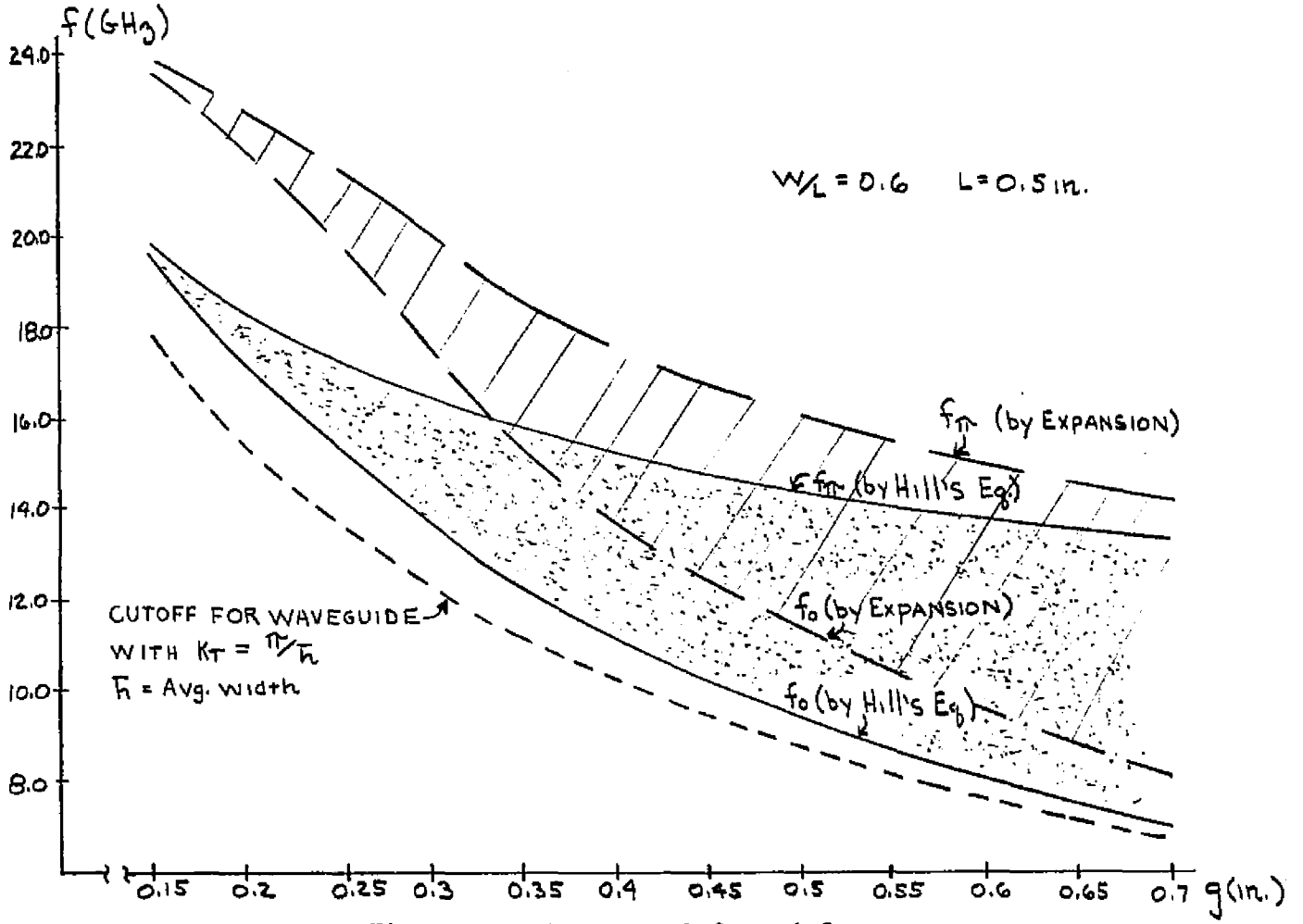

Fig. 2-17 Calculated f_0 and f_π
(d simultaneously varied to maintain a square slot)

The Hill's equation solution is shown in Fig. 2-18 for the geometry of Fig. 2-12 and the solutions are compared. It is noted that the solutions

are displaced but have similar shape. For the case shown it is known that the fields decay into the slots whereas the Hill's equation assumes a sinusoidal variation there. It therefore seems reasonable that the results would be improved if, instead of the dimension d, we used a foreshortened dimension, d'. Toward this end we calculate the dimension d' such that a uniform waveguide of average width would have a cutoff frequency equal to the zero mode frequency found from the modal expansion results. For the example the dimension d' equals 0.700 inch*. The Hill's equation solution used with this value is shown also in Fig. 2-18. Very good agreement is found for this modified Hill's equation solution.

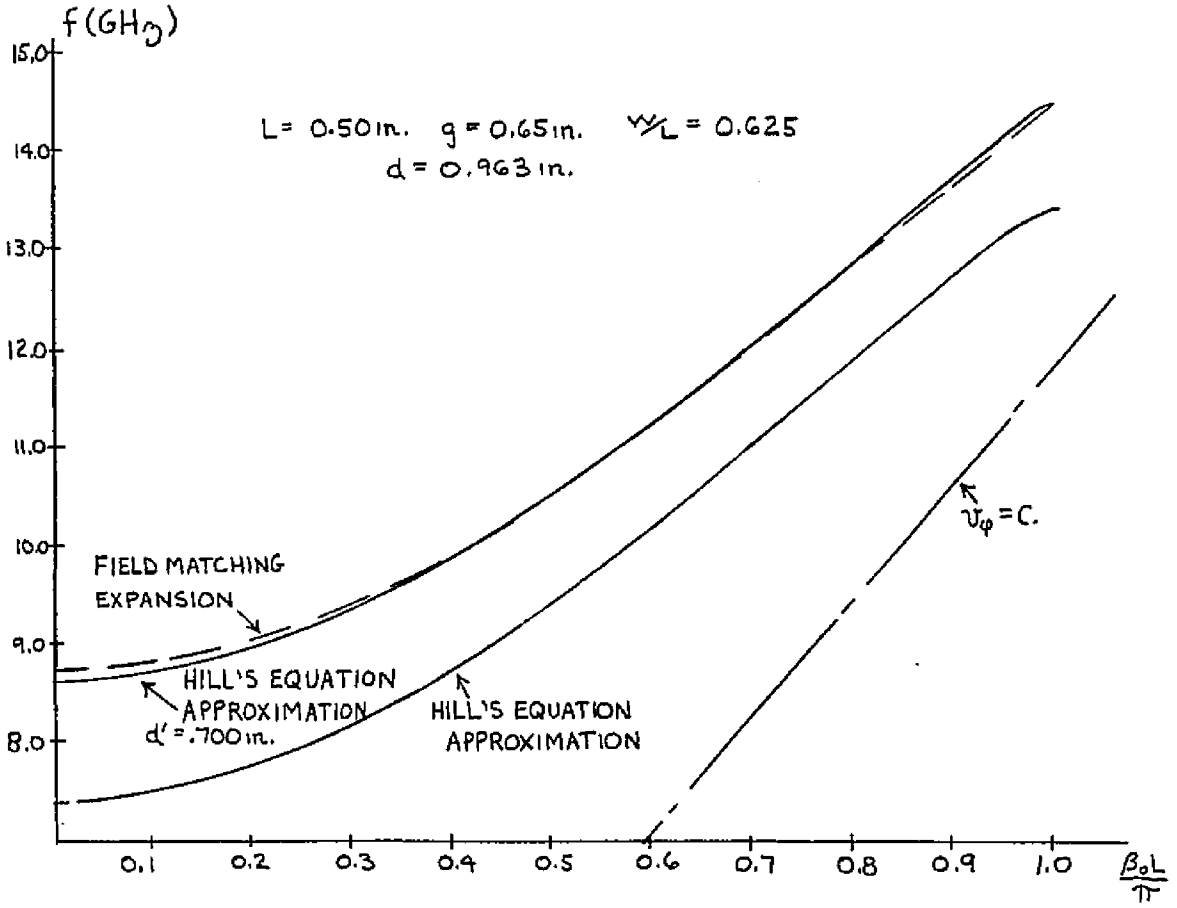

Fig. 2-18 Brillouin Diagram

---

*An alternate approach is to take a variation of form

$$b \sinh \frac{\pi}{w}(d-y)$$

in the slot and

2.4 The Resonated Structure and Experimental Results

Within the passband, $0 < \beta_o < \frac{\pi}{L}$, we write the solution for E_x for propagation in the positive and negative z directions, since β_o may not change

---

$$a \sin \frac{\pi}{d'} y$$

in region I opposite the slot. Note that the variation with respect to z has been suppressed. We require continuity of the functions and their first derivatives at y=g. A nontrivial solution for a and b exists if

$$\begin{vmatrix} \sin \frac{\pi}{d'} g & -\sinh \frac{\pi}{W}(d-g) \\ \frac{\pi}{d'} \cos \frac{\pi}{d'} g & \frac{\pi}{W} \cosh \frac{\pi}{W}(d-g) \end{vmatrix} = 0$$

or,

$$\frac{\tan \frac{\pi}{d'} g}{\frac{\pi}{d'} g} = -\frac{W}{\pi g} \tanh \frac{\pi}{W}(d-g)$$

This is the same as Eq. 2-37. For

W=.312 inch
L=.500 inch
g=.650 inch
d=.963 inch

the value of K is .152. From Fig. 2-5 we see that this point is outside the linear region. We find

$$\frac{\varphi}{\pi} = \frac{g}{d'} \approx .874$$

or

$$d' \approx .744 \text{ inch}$$

in magnitude for propagation in the two directions, as

$$E_x^{\pm}(y,z) = e^{\mp i\beta_0 z}\sum_{m=-\infty}^{\infty}\psi_m^{\pm}(y)e^{-im\frac{2\pi}{L}z} \tag{2-59}$$

The wave equation is symmetric in z since the derivative with respect to z is a second derivative. Also, with reference to Fig. 2-1 we see that z=0 defines a plane of symmetry of the structure so that the boundary conditions are the same for +z and for -z. Therefore, if $E_x^{+}(y,z)$ is a solution of the wave equation and satisfies the boundary conditions, so will $E_x^{+}(y,-z)$. Therefore,

$$\psi_m^{-}(y) = \psi_{-m}^{+}(y) \tag{2-60}$$

We sum the two solutions with arbitrary phase and seek zeros of the total solution. At the places where these zeros occur one may place infinitely conducting sheets and thereby form a resonant structure. We have,

$$E_x(y,z) = E_x^{+}(y,z) + e^{i\theta}E_x^{-}(y,z) = 2e^{i\frac{\theta}{2}}\sum_{m=-\infty}^{\infty}\psi_m^{+}(y)\cos\left[(\beta_0+m\tfrac{2\pi}{L})z+\tfrac{\theta}{2}\right] \tag{2-61}$$

Suppose that at $z=z_1$, $E_x(y,z_1)=0$. Since the $\psi_n^{+}(y)$ are different, $E_x(y,z_1)=0$ only if

$$\cos\left[(\beta_0+m\tfrac{2\pi}{L})z_1+\tfrac{\theta}{2}\right] = 0 \tag{2-62}$$

for all n such that $\psi_n^{+}(y)\neq 0$ identically. Thus, as n varies the roots must be separated by $k\pi$, or, $2n\frac{z_1}{L}=k$, an integer. If $\psi_1^{+}(y)$ is not identically zero, then we require $2\frac{z_1}{L}$ to be an integer. If an integer is added to, or subtracted from, $\frac{z_1}{L}$ such that the result, $\frac{z_1'}{L}$, lies in the closed interval [0,1], it is easily shown that $\frac{z_1'}{L}$ can only take on the values 0, $\frac{1}{2}$ or 1. The values $\frac{z_1'}{L}=0,1$ mean that the zero of the field occurs at the symmetry planes which bisect the slots. The value $\frac{1}{2}$ means that a zero can occur at the centers of the teeth.

If we let the periodic boundary be given by a function of z, and let the boundary have a plane of symmetry at z=0, we have for the Fourier series of that function

$$f(z)=\sum_{m=0}^{\infty} a_m \cos \frac{m2\pi}{L} z \tag{2-63A}$$

If we shift the origin and define $z \equiv \epsilon L+\varphi$, $0 \leq \epsilon \leq 1$, we have

$$f(\epsilon L+\varphi)=\sum_{m=0}^{\infty} a_m\left[\cos(2m\pi\epsilon)\cos\left(m\frac{2\pi}{L}\varphi\right)-\sin(2m\pi\epsilon)\sin\left(m\frac{2\pi}{L}\varphi\right)\right] \tag{2-63B}$$

which is an even function of φ if and only if $2n\pi\epsilon = m\pi$. By reasoning similar to that used before, if $a_1 \neq 0$, we must have

$$\epsilon = 0, \frac{1}{2}, 1 \tag{2-64}$$

Thus, the only other plane of symmetry is at $z=\frac{L}{2}$ and we make the general statement that the zero of the field occurs only at a plane of symmetry. Therefore, if a resonator is constructed by placing shorting planes at two planes of symmetry, z_1 and z_2, the resultant field will consist of a superposition of the two wave solutions of the infinite structure. Such a resonator is used to experimentally determine points of the Brillouin diagram. We have,

$$z_2 = z_1 + \frac{m}{2}L \tag{2-65}$$

where m is an integer. If m is even the shorting plane is placed at the same relative plane of symmetry, for odd m the short is positioned at the alternate plane of symmetry. From 2-61 we require that

$$\cos\left[\left(\beta_0+\frac{m2\pi}{L}\right)z_2+\frac{\theta}{2}\right] = \cos\left[\left(\beta_0+m\frac{2\pi}{L}\right)z_1\right]\cos\left[\beta_0\frac{m}{2}L+m\pi\right]$$
$$-\sin\left[\left(\beta_0+m\frac{2\pi}{L}\right)z_1\right]\sin\left[\beta_0\frac{m}{2}L+m\pi\right]=0 \tag{2-66}$$

In view of 2-62 the first term on the right-hand side of 2-66 is zero and since, if 2-62 is satisfied,

$$\sin\left[\left(\beta_0 + m\tfrac{2\pi}{L}\right)z_1\right] \neq 0$$

so that 2-66 requires that

$$\sin\left[\beta_0 \tfrac{m}{2} L + m\pi\right] = 0 \qquad \text{(2-67A)}$$

or

$$\beta_0 \tfrac{m}{2} L = p\pi \qquad \text{(2-67B)}$$

Therefore, if we construct a resonator of length equal to $\frac{m}{2}$ periods with shorting planes placed at planes of symmetry of the structure, the values of β_0 which satisfy the boundary conditions are given by 2-67B and the resonant frequencies measured correspond to those values of β_0. The values of β_0 lie in $(0, \frac{\pi}{L})$ so that the values that p may take on in 2-67B are limited by

$$1 \leq p < \tfrac{m}{2} \qquad \text{(2-67C)}$$

For even m, corresponding to an integral period length resonator, there are $\frac{m}{2}$-1 possible values of p, or $\frac{m}{2}$-1 resonant frequencies within the first passband. For odd m, yielding a resonator length equal to an integer plus one-half periods, there are $\frac{m-1}{2}$ possible p values, the number of resonant frequencies within the first passband. If the positions of the shorting planes are not at planes of symmetry of the structure then the measured resonant frequencies will not correspond to the ω-β diagram of the infinite structure.

At the band edges, the form of solution changes so the preceding does not apply. However, as the number of sections increases, the measured resonant frequencies approach the zero and π-mode frequencies and therefore they may be approximated quite accurately. This is especially true since the

ω -β curve has zero slope at the cutoff frequencies.

Models were built in both the planar and coaxial geometries. The planar models were preferred for experimentation since they were smaller and easier to manipulate. Dielectric probing to identify the value of $\beta 0$, to be described, was far easier in the planar case. There the perturbation was accomplished with a small disc rather than a large diameter annular ring, difficult to maintain perpendicular to the axis of the structure. In addition, the problem of extraneous modes was more of a problem in the large size coaxial system. The coaxial system was used to find a proper coupling scheme for the actual structure and to verify the results of the planar analyses and experiments. The verification was found to be good.

The first step in the experimental procedure was to identify the resonant frequencies of a section of resonant periodic structure. The resonant frequency structure was found by use of the experimental arrangement shown in Fig. 2-19 which, in essence, compares the reflected power from the resonated periodic structure with the incident power. At frequencies approximately equal to the resonant frequencies the reflected power is small since most of the power incident is dissipated by the resonant structure. The higher the Q of the structure, the narrower will be the frequency interval over which this occurs. This type behavior is noted in Fig. 2-21 and Fig. 2-25b. At a value of frequency relatively far from a resonant value most of the power is reflected from the structure. The swept frequency source produces a microwave signal whose frequency varies with time and at the same time sweeps the oscilloscope at a rate proportional to the sweep rate of the frequency. The oscilloscope trace represents the comparison of the reflected and incident powers as a function of frequency.

The planar structure is built in rectangular form, that is, with terminating walls at two values of x in Fig. 2-1. Its essential form is that of a toothed structure which fits into what is basically a section of x-band waveguide with one narrow wall removed. The structure is terminated by a shorting block and coupling is provided by an aperture in a thin shorting plate. A photograph of the rectangular structure is shown in Fig. 2-20. Three experimental geometries are shown, each having a square slot. A

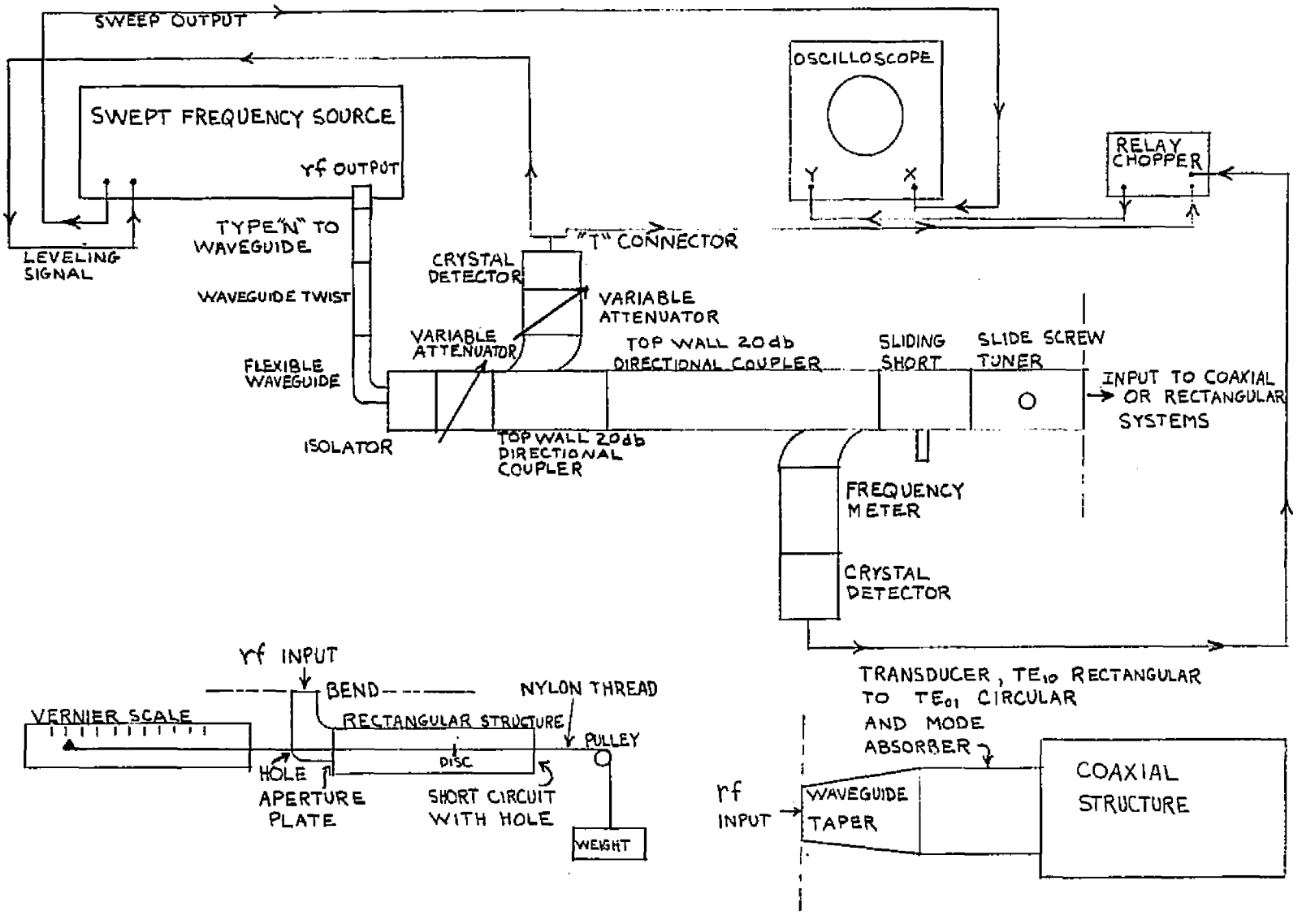

Fig. 2-19 Experimental Arrangement

dielectric perturbing disc is shown on a thin nylon thread. This disc is translated through the structure, as indicated in Fig. 2-19, to explore the field structure. A section of the frequency spectrum as obtained from the oscilloscope is shown in Fig. 2-21. Only the reflected power is shown, the traces are inverted, and frequency increases from right to left. The three cases represent, from top to bottom; undercoupled, critically coupled for the high frequency resonances, and overcoupled. The coupling is increased by increasing the diameter of the aperture hole.

One tests the resonances by dielectric and loss probing. If dielectric material is inserted into the structure, either in the form of the disc previously mentioned, or in the form of a dielectric rod inserted through a hole in the termination block, those resonances will move to lower frequency which are connected with the resonant circuit. Those which are connected with some other part of the setup of Fig. 2-19 will not be perturbed. This discriminates among the resonances measured. Loss may be inserted into the circuit in the form of a thin metallic coating on mylar, or fiberglass, sheet. This material loads the circuit when the electric field is tangent to its surface and no loss is presented for the electric field normal to the surface. By changing the orientation of a strip of such material, one determines the polarization of the electric field. By doing this we have determined that the mode of interest was indeed present. The effect of loss is to lower the Q of the resonant structure and therefore lower or eliminate completely the peaks of Fig. 2-21. For orientation such that the electric field is normal to the surface of the strip there is no noticeable change.

For use with the coaxial structure, a mode transducer from TE_{10} rectangular to TE_{01} circular consists essentially of changing the boundary of the waveguide in a very slow manner with respect to wavelength. This transducer is used in tandem with a mode absorber which is used to assure purity of the circular-electric-mode. Such mode filters consisted of crossed loss sheet or circumferentially grooved circular waveguide with lossy material suitably placed. The TE_{01} circular mode is coupled to the TE_{01} coaxial system through radial slots distributed uniformly around the circumference as shown in Fig. 2-22.

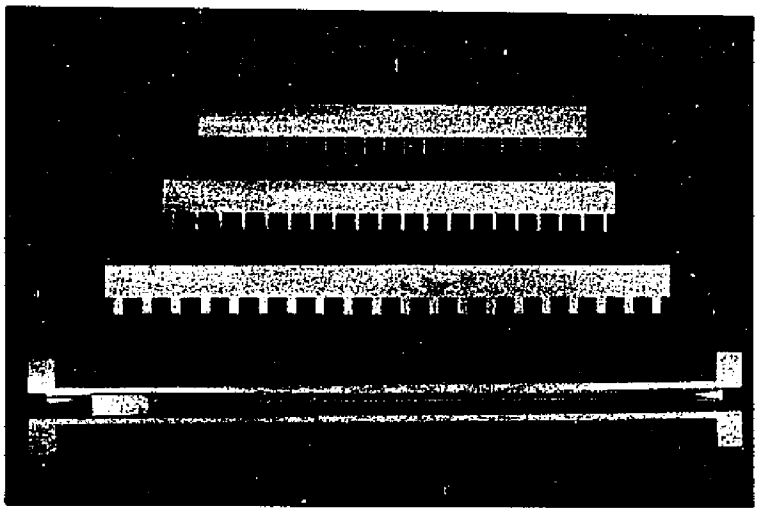

Fig. 2-20 Rectangular Models

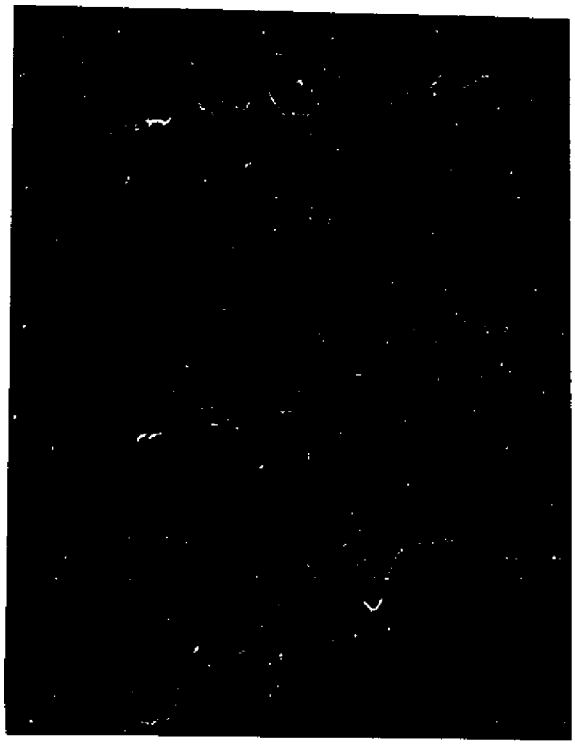

Fig. 2-21 Reflected Power Traces for Rectangular Model
(g=.650 inch, d=.963 inch, W=.312 inch, t=.032 inch)

Fig. 2-22 Radial Coupling Slots

An assembly drawing of the coaxial model is shown in Fig. 2-23. The diameter of the central cylindrical waveguide is made equal to the diameter of the transducer, which is twice the large dimension of the oversize rectangular waveguide used to couple to the transducer. The radial coupling slots, shown also in Fig. 2-22, are made one-half guide wavelength long in radial extent at 10GHz to minimize their effect at the approximate frequency of operation. The slots cannot be made thin because of the required radial extent of the slow wave structure. The width of the slots, in the axial direction, is made equal to the width of x-band waveguide. There are two degrees of tuning flexibility provided through the two pistons. The circuit geometry is varied by changing the annular rings of which the slots and teeth are composed. This stacked ring construction will provide damping to modes which have longitudinal currents and therefore provide a natural mode filter for both the model and the actual electron tube. Probing of the fields is accomplished through a hole in the termination block. Uniformity of the fields was checked by rotation of the perturbing rod through the full 360° and noting any inhomogeneity in the perturbation. Within the accuracy of this method the fields were found to be uniform. The circumferential spacing of the slots is made small enough so that the high order circumferential mode which might be excited in the coaxial waveguide will not propagate at the highest frequency to be used in x-band. The mean

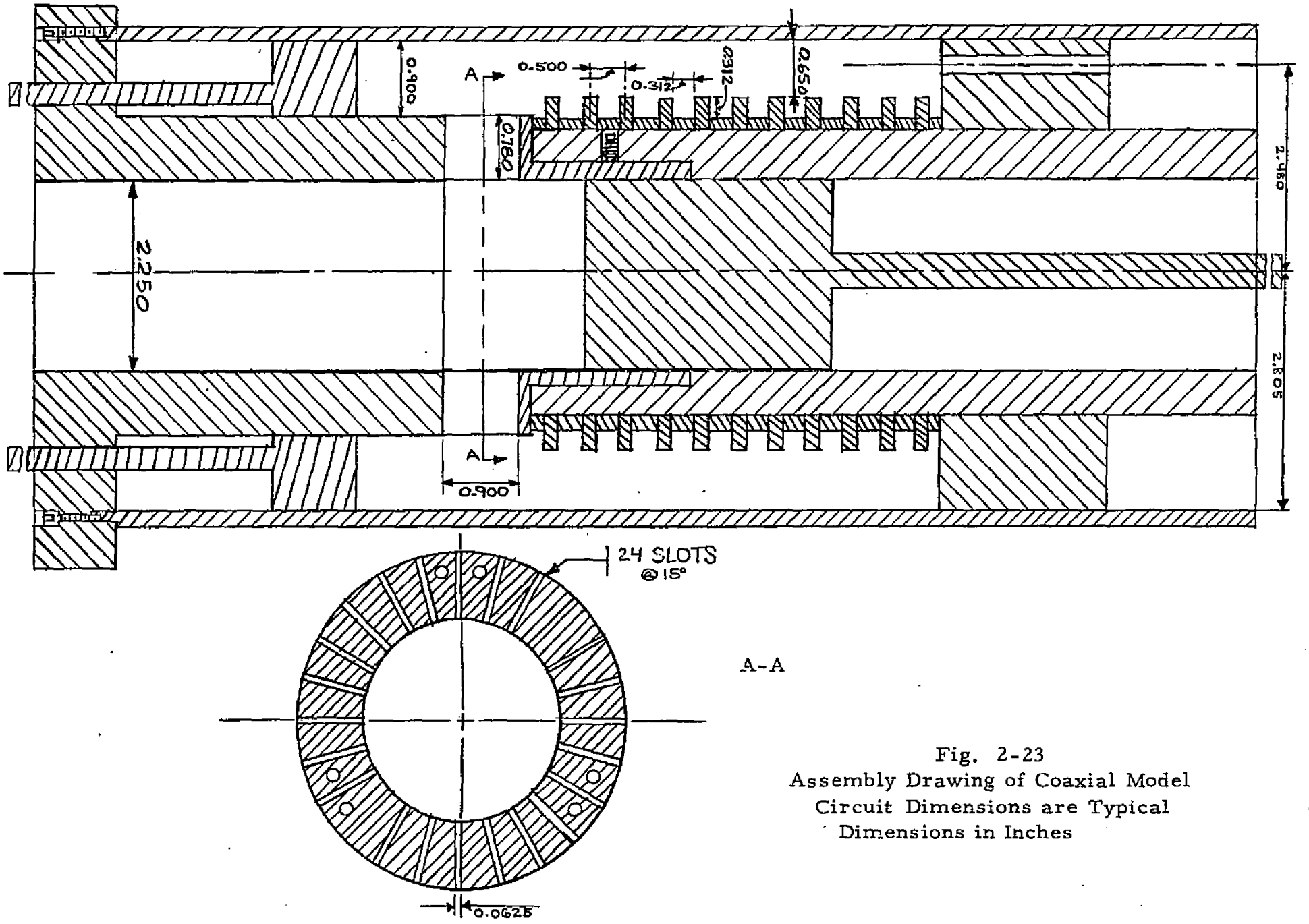

Fig. 2-23
Assembly Drawing of Coaxial Model
Circuit Dimensions are Typical
Dimensions in Inches

diameter is used for this calculation and the planar approximation applied. It is found that slots spaced at 15°, or 24 slots over the full circumference, provides a good safety factor for this calculation. As mentioned before, the fields were found to be uniform with respect to Θ. Finally, the angular width of the slots was made small enough, 0.0625 inch, to provide adequate provision for mounting.

The partly assembled model is shown in Fig. 2-24. Note the presence of the mylar loss ring which was used as a termination for the circuit to check matching into an infinite structure, or what is more applicable, matching in and out of the structure in a symmetrical way. An example of such a match condition is shown in Fig. 2-25, where the modification in the reflected power is shown when the termination is changed from a shorting plane to a loss ring.

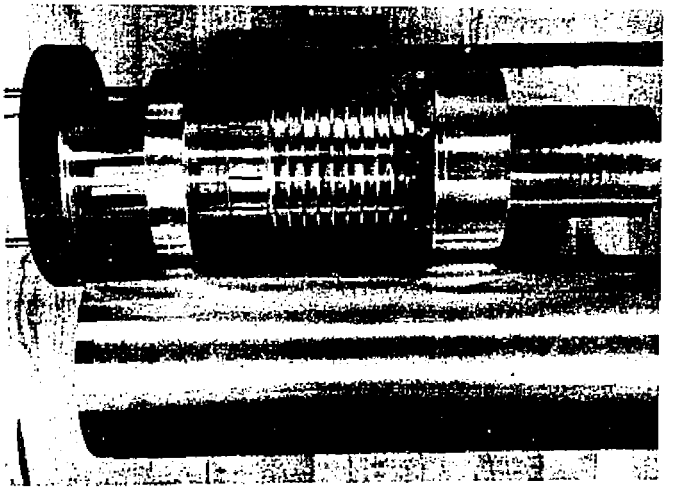

Fig. 2-24 Coaxial Model

The correspondence between the resonant frequencies and the particular values of β_0 is made by exploring the electric field by means of a perturbing object.[30] The perturbing object used in this experiment was a dielectric disc which was translated through the rectangular structure as indicated in Fig. 2-19. The orientation of the disc was in the xy plane and its dimensions were a 0.275 inch diameter and a 0.050 inch thickness.

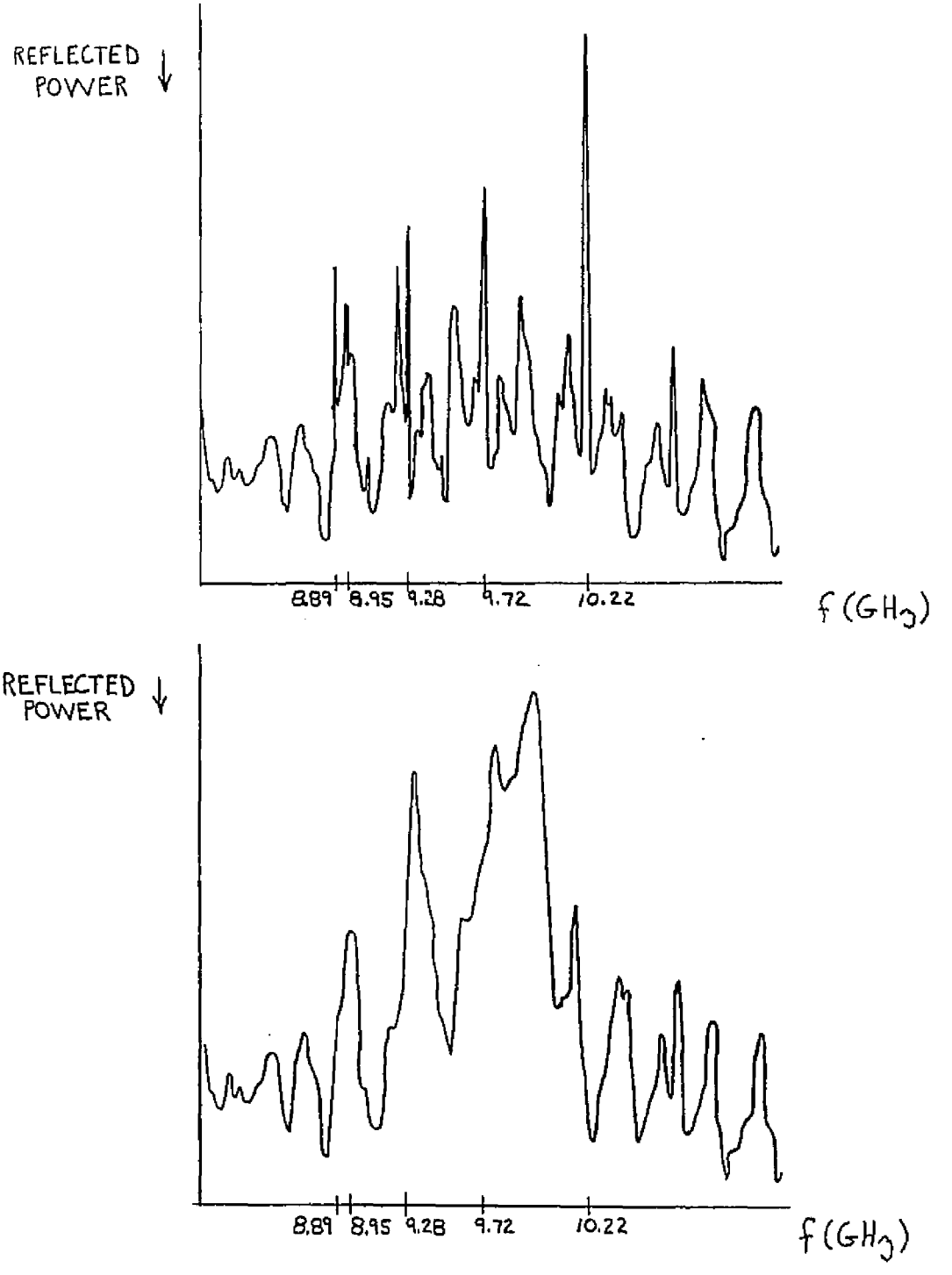

Fig. 2-25 Match of the Circuit
a) Termination in a Shorting Plane
b) Termination in a Loss Ring

The material was assumed to be alumina. As the disc is moved through the structure it perturbs only the electric field to first order. The perturbation of the resonant frequency will be zero for an infinitely thin disc when the disc is at a position of zero electric field. For the small but finite thickness used, the frequency shift will be near zero at the nodes. We assume that the electric field pattern is unchanged outside the disc, while inside it is reduced by requiring continuity of D_N. One may show, by the Slater perturbation theorem[31], that the relative frequency shift, $\frac{\Delta f}{f_o}$, is proportional to

$$\frac{1}{W}\int E^2 d\tau$$

where W is the stored energy in the resonated structure and the integration is taken over the volume of the disc. The perturbation of the disc upon the resonant frequency of a simple rectangular cavity made up of a section of x-band waveguide of length 0.750 inch is shown in Fig. 2-26. The coupling into the cavity is by means of a 0.375 inch diameter aperture in a .063 inch thick plate. Note that due to the extent of the fields outside the coupling plate and due to the finite thickness of the disc the curve shown deviates somewhat from the sine-squared variation that would be expected.

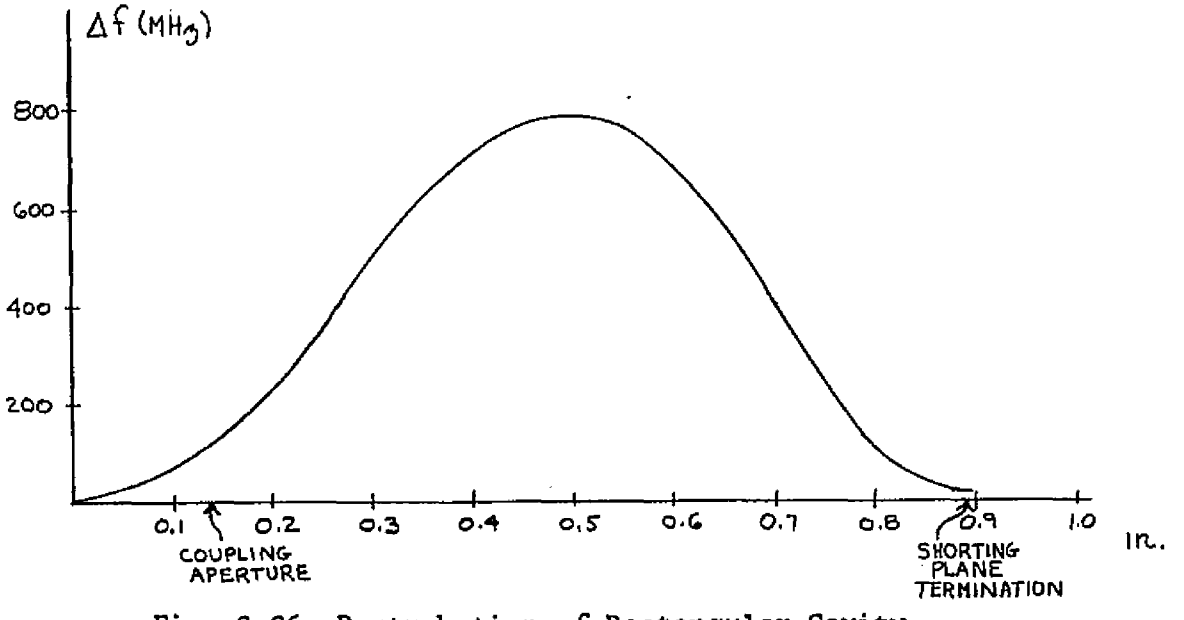

Fig. 2-26 Perturbation of Rectangular Cavity (.400 X .900 X .750 inches)-f_0=9.889GHz

An example of the frequency perturbation curve for a rectangular model is shown in Fig. 2-27. The disc averages the fields so that the space harmonic content is not readily discernible. From the distance between the nulls, however, we may find the value of β_0 corresponding to the resonant frequency, which for the case illustrated is seen to be $\frac{0.4\pi}{L}$. At the shorting plane we note that the frequency shift is not zero and we ascribe this to the finite thickness of the disc. The small modulation pattern imposed upon the envelope of the perturbation curve is ascribed to the space harmonics which combine to form a "beat pattern". By measuring the perturbation of one resonant frequency in the spectrum the β_0 at that point is determined and one may assign one of two values of β_0 to other resonances, provided none are missed by the measurement process. That is, one may assign these values based upon an assumption of a forward or backward wave fundamental. To clarify this ambiguity we therefore measure the perturbation of two resonances to determine the nature of the fundamental. This having been done, the circuit was found experimentally to be forward wave, in agreement with the theoretical results.

Experimental points obtained from the rectangular model are shown in Fig. 2-12 in comparison with the theoretical solution. Agreement between the experimental and theoretical results is seen to be quite good.

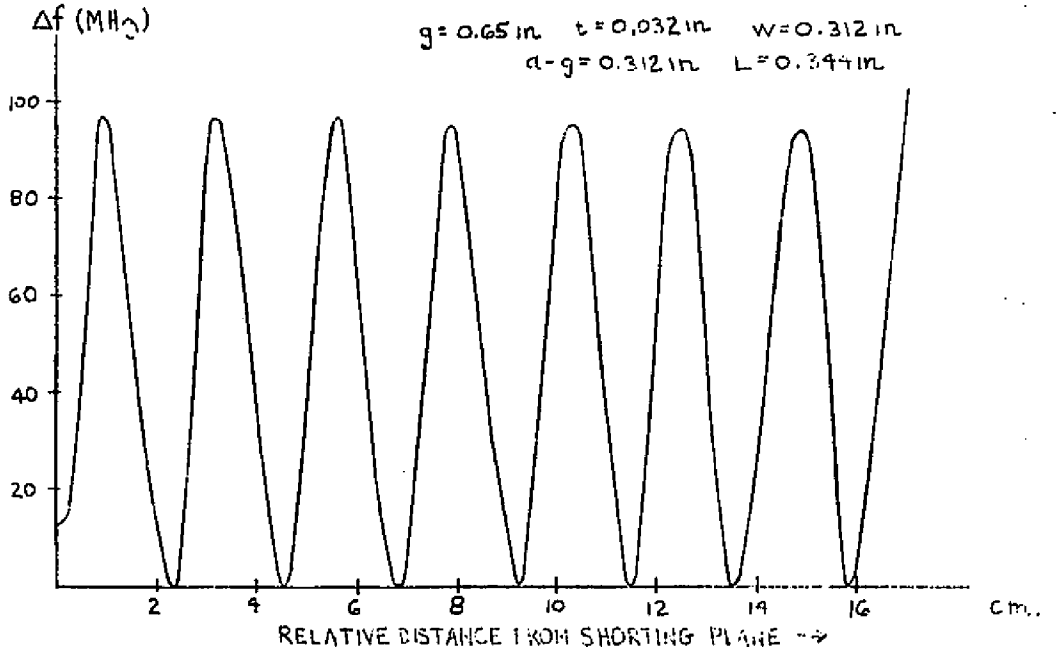

Fig. 2-27 Dielectric Disc Perturbation of Resonant Frequency (f_0=11.086GHz)

Results for the very low β_0 end of the curve could not be obtained due to difficulty in matching to the structure for these values. The upper end of the curve lay outside x-band and therefore beyond the range of the measuring equipment. We note slightly more error at the higher β_0 end of the results and this is attributed to the approximation made in the derivation of the theoretical result.

ω-β curves found experimentally for three different structures are shown in Fig. 2-28. All dimensions of the three cases are the same except for the tooth thickness t and the period L. Again, it is expected that as $t \to 0$ the space harmonic content will be relatively unaffected for thin teeth since E_x must still vanish on the tooth edge. We see from Fig. 2-28 that the change in frequency is not great. We conclude that a useful structure for interaction would be one with teeth as thin as possible; with the limit imposed by mechanical, heat dissipation and electron bombardment considerations. This structure would have the lowest possible synchronous velocity for the range of geometries where the values of t and L are allowed to vary.

The results found from the coaxial model confirmed the presence of the desired mode. The resonant frequencies were somewhat sensitive to the position of the tuning pistons since the position of the coupling plane was questionable in this case. The results were, none-the-less, quite close to the other results. A set of such data is shown in Fig. 2-29,

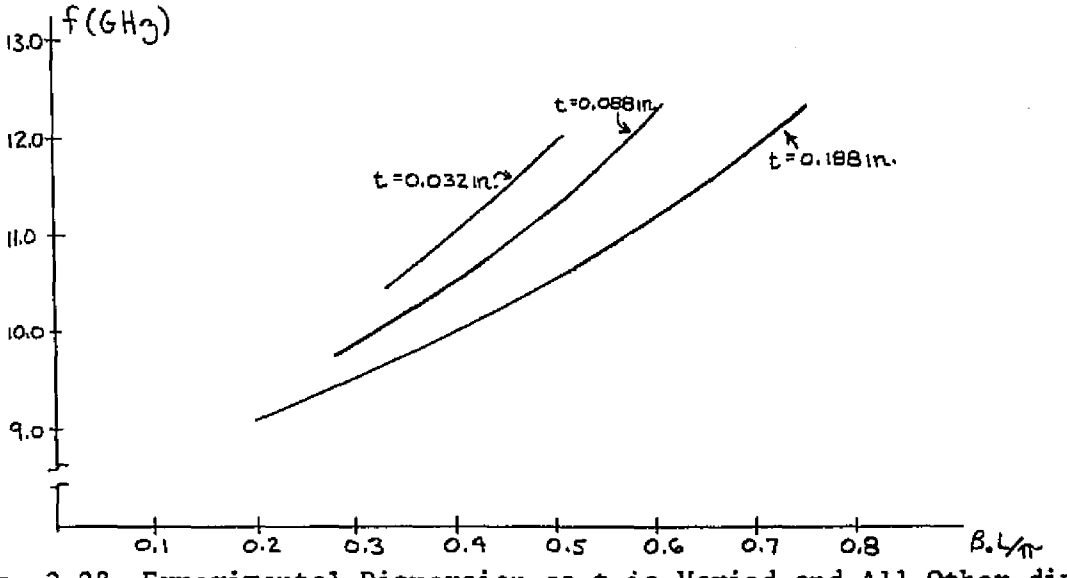

Fig. 2-28 Experimental Dispersion as t is Varied and All Other dimensions Except L Fixed-(Rectangular Model) g=0.650 inch W=d-g=.312 inch

uncorrected for the true position of the entrance plane. Because of the added coupling length, the true values of β_0 will be less than those shown. If the correction is not too large, the experimental points will lie closer to the theoretical results since the experimental points will be moved to the left on the figure.

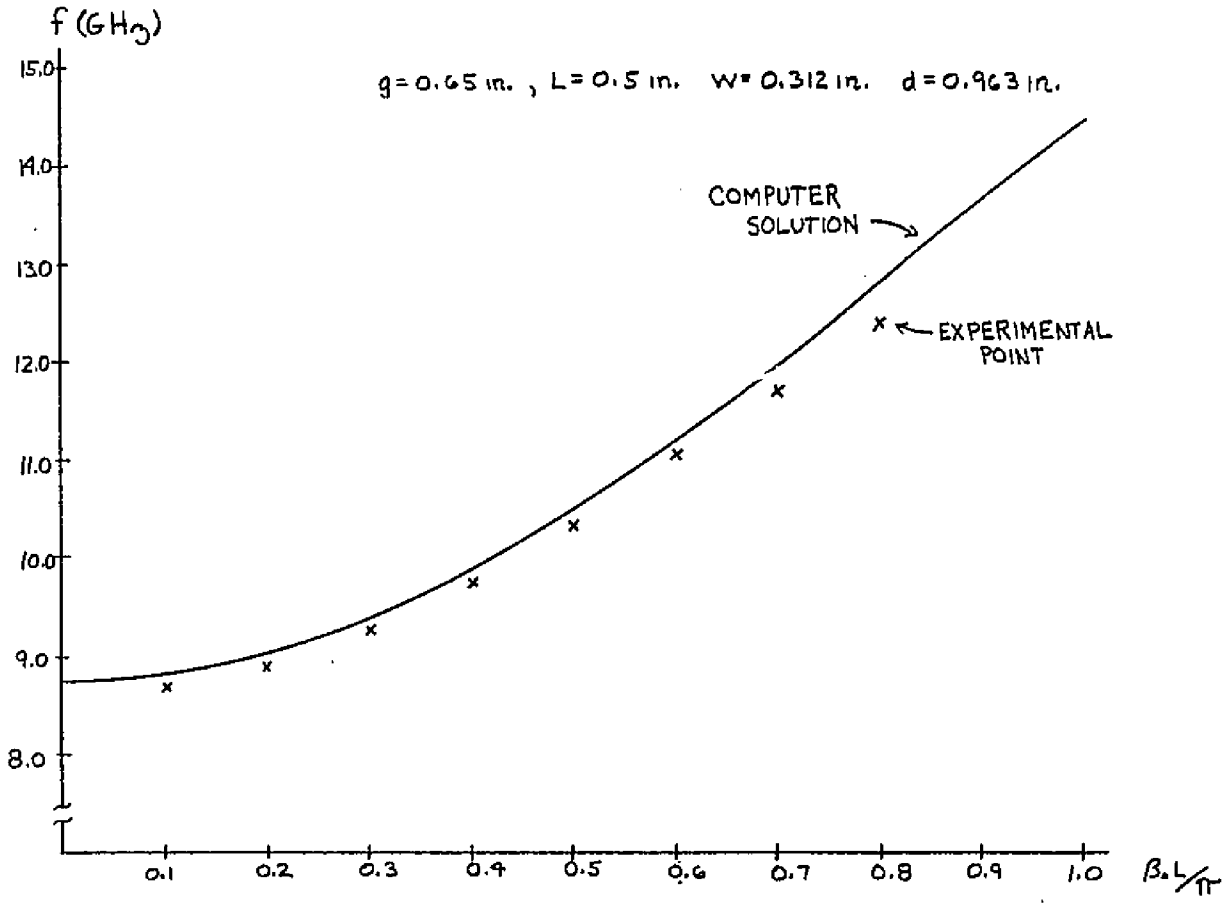

Fig. 2-29 Comparison of Dispersion from Computer Solution and Coaxial Model Experimental Points (Uncorrected Entrance Plane)

The rectangular data is to be regarded as the standard with respect to dispersion although the Q cannot be found from this case because of the presence of the terminating planes. These differentiate the rectangular from the infinite planar case. Experimental determination of matching configurations must also be done on the coaxial model.

CHAPTER 3

THE ELECTROSTATIC PROBLEM

3.1 The Equivalent Problem in the Plane

We inquire now into the solution of Laplace's equation in the structure when the inner and outer boundaries are set at different potentials. The structure is taken to be many periods long and therefore, insofar as the major portion of the structure is concerned, it may be assumed that the structure is infinitely long. The solution obtained for the fields will be accurate except for the immediate vicinity of the ends and in this unbounded region it will be unique if the potential is bounded throughout the region.* This assumption of an infinitely long structure introduces planes of symmetry at the center of each tooth and at the center of each slot. Across these planes we have the boundary condition that the normal derivative of potential is zero.

We have now reduced the problem from an unbounded region to an equivalent bounded one. If we take the region whose boundary consists of the structure and any two planes of symmetry, we have a well defined problem in a bounded region which has a unique solution.† This is known as a mixed boundary value problem. That is, the potential is specified along part of the boundary and the normal derivative is specified along the remainder of the boundary. This type problem is normally quite difficult.[34] An accurate approximate solution will be developed for the geometry of concern. Since the geometry is one of large radius of curvature, following the argument leading to Eq. 2-1B, we must solve Laplace's equation in the plane provided we identify r with one of the rectangular coordinates.

---

* This may be seen by the artifaçe of mapping the plane onto the sphere by the stereographic projection[32] which maps the point at infinity into the north pole of the sphere.

†The boundary conditions consist of specification of the normal derivative and the value of the potential at at least one point. Moreover, the boundary of the region is regular in that it is piecewise differentiable and does not cross itself. Differentiability fails only at the four corners of the rectangle. The solution is therefore unique.[33]

In Chap. 2 it was indicated that the space harmonic content would be affected little as the tooth thickness approached zero for small tooth thickness. This is consistent with lower voltage operation and is therefore to be preferred. The limiting thickness of the tooth is determined therefore by mechanical and thermal considerations and may be only a few percent of the period. Thus, the limiting case of vanishingly small tooth thickness is of practical importance and so the tooth is taken to be a knife edge in the model to be solved. In a physical situation of small but finite thickness, the solution is taken to be good for the region excluding a small band around the edges of the teeth of several tooth thicknesses. The base period may be taken between any of the planes of symmetry. We will take it to be between adjacent teeth. For convenience, we replace the coordinates z and r by x and y, take the width of the base period to be π, and take the inner and outer boundaries to be at potentials 1 and 0 respectively. This rectangular domain is shown in Fig. 3-1.

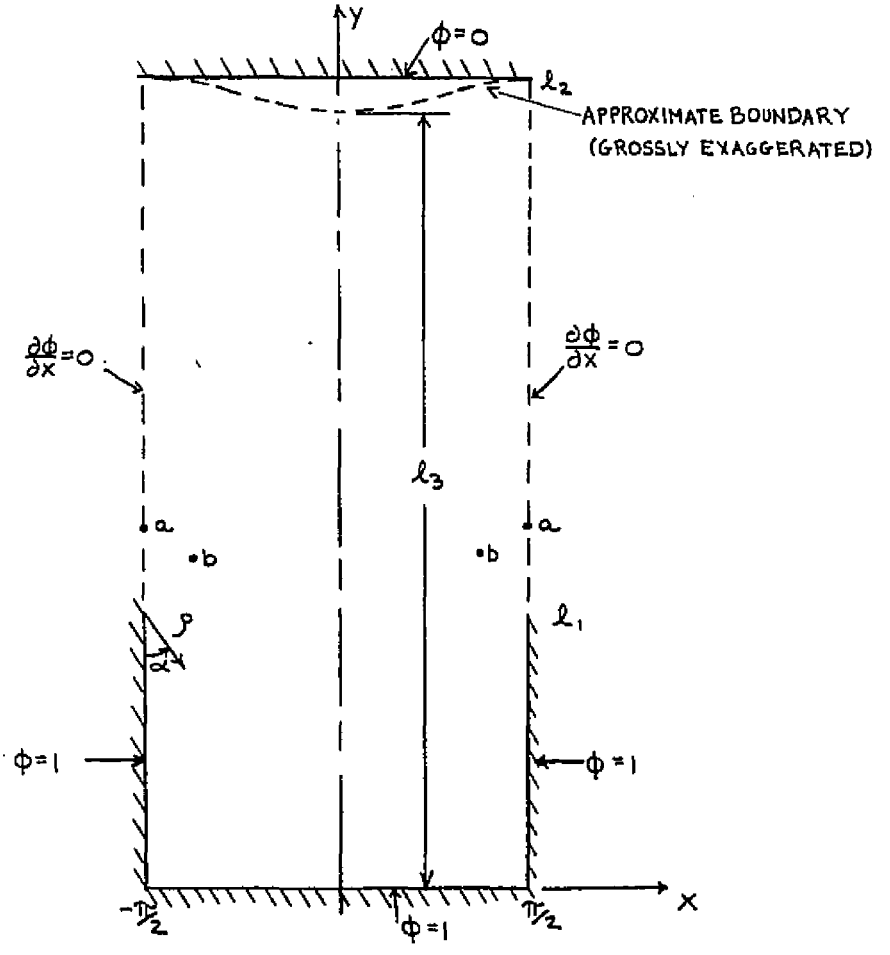

Fig. 3-1 The Rectangular, and Approximate, Domains

3.2 Observations About The Solution

Before proceeding with the solution it is instructive to examine its expected behavior. As y approaches ℓ_2, the differential equation becomes, approximately, $\frac{\partial^2\phi}{\partial y^2} \approx 0$ with solution $\phi \approx a+by$, since a linear solution in x is obviously inconsistent with the boundary requirement on $\frac{\partial\phi}{\partial x}$. The effect of the teeth is therefore neglected close to the outer boundary.

The form of the potential for a circular neighborhood surrounding the edge of the tooth may be arrived at as the radius of the neighborhood approaches zero. As the edge of the tooth is approached, it alone will determine the limiting form of solution as all other boundaries become relatively far away. We consider the case of a semi-infinite conducting plane and describe the position away from the edge in cylindrical coordinates. Application of the method of separation of variables to Laplace's equation in cylindrical coordinates yields the solutions for ϕ in the region defined by $0<\alpha<2\pi$ which have nonzero angular variation as

$$1 + C\rho^{\pm\lambda} \begin{matrix}\sin\\ \cos\end{matrix} \lambda\alpha$$

where ρ and α are defined in Fig. 3-1 and λ is a separation constant. Since we wish solutions which are to be bounded at $\rho=0$ and which approach unity for $\alpha\to 0$ and $\alpha\to 2\pi$ we have $\lambda=\frac{n}{2}$ with n a positive integer. Thus,

$$\phi \sim 1 + \sum_{m=1}^{\infty} C_m \rho^{\frac{m}{2}} \sin\tfrac{m}{2}\alpha \qquad (3\text{-}1)$$

noting that the solutions where n is odd are allowable even though $\frac{\partial\phi}{\partial\alpha}$ is not continuous across $\alpha=0$ since we have the restriction $0<\alpha<2\pi$. Physically, the discontinuity is accounted for by the conducting plane and its surface charge. Observe that as $\rho\to 0$ the leading term, for n=1, approaches zero in the slowest manner. Also if we consider $\frac{\partial\phi}{\partial\rho}$ we note that all terms, except that for n=1, approach zero. That term is unbounded as $\rho\to 0$. We therefore write the limiting form of 3-1 in terms of its dominant term for $\rho\to 0$ as

$$\lim_{\rho\to 0}\phi = 1 + C_1\rho^{1/2}\sin\tfrac{\alpha}{2} \qquad (3\text{-}2A)$$

We write the limiting form of potential as the tooth edge is approached in the plane of the tooth by using 3-2A with $\alpha = \pi$. With reference to Fig. 3-1, we have

$$\lim_{\substack{y \to \ell_1 \\ y > \ell_1}} \phi\left(\pm\frac{\pi}{2}, y\right) = 1 + C_1 (y - \ell_1)^{1/2} \tag{3-2B}$$

Application of 3-1 to the actual geometry of Fig. 3-1 requires satisfaction of the boundary condition $\frac{\partial \phi}{\partial \alpha}(\rho, \pi) = 0$. This leads to

$$C_{2k} = 0, \qquad k = 1, 2, 3, \cdots \tag{3-3}$$

In the neighborhood of the slot corners we use the square function to find the limiting form of the potential. For example, for the corner in the neighborhood of $x = -\frac{\pi}{2}$, $y = 0$ we have

$$\lim_{\substack{x \to -\pi/2 \\ x > -\pi/2 \\ y \to 0 \\ y > 0}} \phi(x, y) = 1 + K \operatorname{Im}\left\{\left[\left(x + \tfrac{\pi}{2}\right) + iy\right]^2\right\} = 1 + 2K\left(x + \tfrac{\pi}{2}\right) y \tag{3-4}$$

3.3 Mapping onto the Half-Plane

Consider the function of a complex variable

$$W = u + iv = \sin Z = \sin(x + iy) = \sin x \cosh y + i \cos x \sinh y \tag{3-5}$$

It is easily shown that W is an entire function, or analytic at every point of the Z plane, since at every point of the Z plane, and at every point of its neighborhood, the derivative of W exists. Sufficient conditions[35] for the existence of the derivative are that u and v are real and single-valued functions of x and y, which together with their partial derivatives of first order are continuous at x_0, y_0; and that those partial derivatives satisfy the Cauchy-Riemann conditions at x_0, y_0

$$\frac{\partial u}{\partial x} = \frac{\partial v}{\partial y} \tag{3-6A}$$

$$\frac{\partial u}{\partial y} = -\frac{\partial v}{\partial x} \tag{3-6B}$$

It is shown that[36] an analytic mapping is isogonal,* or angle preserving, as long as W has a nonvanishing derivative. We shall show that the derivative vanishes only on the boundary of our region of interest but not in the interior. We also show that under the analytic transformation, if ϕ satisfies the Laplace equation in the W plane, it will satisfy Laplace's equation as a function of x and y. Suppose that we have the solution for ϕ in the W plane.

$$\frac{\partial^2\phi}{\partial u^2} + \frac{\partial^2\phi}{\partial v^2} = 0 \tag{3-7}$$

Since,

$$\frac{\partial^2\phi}{\partial u^2} = \frac{\partial\phi}{\partial x}\frac{\partial^2 x}{\partial u^2} + \frac{\partial\phi}{\partial y}\frac{\partial^2 y}{\partial u^2} + \frac{\partial x}{\partial u}\frac{\partial}{\partial x}\left[\frac{\partial\phi}{\partial x}\right] + \frac{\partial y}{\partial u}\frac{\partial}{\partial u}\left[\frac{\partial\phi}{\partial y}\right] \tag{3-8}$$

we have from 3-7, using 3-8 and a similar expression for $\frac{\partial^2\phi}{\partial v^2}$,

$$\frac{\partial\phi}{\partial x}\left[\frac{\partial^2 x}{\partial u^2}+\frac{\partial^2 x}{\partial v^2}\right] + \frac{\partial\phi}{\partial y}\left[\frac{\partial^2 y}{\partial u^2}+\frac{\partial^2 y}{\partial v^2}\right] + \frac{\partial x}{\partial u}\frac{\partial}{\partial u}\left[\frac{\partial\phi}{\partial x}\right] + \frac{\partial y}{\partial u}\frac{\partial}{\partial u}\left[\frac{\partial\phi}{\partial y}\right] + \frac{\partial x}{\partial v}\frac{\partial}{\partial v}\left[\frac{\partial\phi}{\partial x}\right] + \frac{\partial y}{\partial v}\frac{\partial}{\partial v}\left[\frac{\partial\phi}{\partial y}\right] = 0 \tag{3-9A}$$

Where[37] Z is an analytic function of u and v we have that x and y satisfy the Cauchy-Riemann conditions and that the partial derivatives of all orders of x and y exist and are continuous functions of u and v. Then, x and y are harmonic functions of u and v so that together with the Cauchy-Riemann conditions we have from 3-9A

$$\left[\frac{\partial^2\phi}{\partial x^2} + \frac{\partial^2\phi}{\partial y^2}\right]\left[\left(\frac{\partial x}{\partial u}\right)^2+\left(\frac{\partial x}{\partial v}\right)^2\right] = 0 \tag{3-9B}$$

Since $\frac{\partial x}{\partial u}$ and $\frac{\partial x}{\partial v}$ are real

$$\left(\frac{\partial x}{\partial u}\right)^2 + \left(\frac{\partial x}{\partial v}\right)^2 \geq 0 \tag{3-10}$$

---

*The meaning of isogonality is that if two curves intersect at an angle θ in the Z plane, their image curves in the W plane intersect at the same angle at the image point, with respect to magnitude and sense of rotation. The relevance of this to the problem at hand is that the potential lines remain orthogonal to the stream-lines in the mapped region.

where equality holds if and only if x is a constant with respect to u and v, in which case we also have by the Cauchy-Riemann equations that $\frac{\partial y}{\partial u}=0$ and $\frac{\partial y}{\partial v}=0$, so that region in the W plane maps to a single point in the Z plane. Ruling this out we have from 3-9B that ϕ also satisfies Laplace's equation in the Z plane. Note also that with $\frac{\partial x}{\partial u}$ and $\frac{\partial x}{\partial v}$ both zero, the Jacobian

$$\frac{\partial(x,y)}{\partial(u,v)} = \begin{vmatrix} \frac{\partial x}{\partial u} & \frac{\partial x}{\partial v} \\ \frac{\partial y}{\partial u} & \frac{\partial y}{\partial u} \end{vmatrix} \tag{3-11}$$

is zero, so that the mapping is not one-to-one.[38] That is, the one point of the Z plane is the image of the infinity of points in the region of the W plane. Noting that

$$\frac{dZ}{dW} = \frac{\partial x}{\partial u} + i\frac{\partial y}{\partial u} = \frac{\partial x}{\partial u} - i\frac{\partial x}{\partial v} \tag{3-12}$$

we have that 3-9B is

$$\left[\frac{\partial^2\phi}{\partial x^2} + \frac{\partial^2\phi}{\partial y^2}\right]\left|\frac{dZ}{dW}\right|^2 = 0 \tag{3-13}$$

In order that isogonality is maintained we have that $\frac{dZ}{dW}\neq 0$ so that, under the mapping, the differential equation is left unchanged, except on the boundary where the derivative may vanish. However, we do not require $\nabla^2\phi = 0$ on the boundary of the region, but only at interior points. We have already expected from 3-2 that the derivative of ϕ will not exist at the edge of the tooth.

It is shown[39] by the Schwartz-Christoffel formula that consideration of the half-strip of width π, described by $-\frac{\pi}{2}<Re\{Z\}<\frac{\pi}{2}$, $Im\{Z\}>0$, as a limiting case of a triangle, produces the mapping of 3-5 which takes the half-strip onto the upper half-plane, $Im\{W\}>0$. From 3-5 we have

$$u = \sin x \cosh y \tag{3-14A}$$

$$v = \cos x \sinh y \tag{3-14B}$$

If we set y=0, we see that the entire x axis maps onto the segment $-1 \leq u \leq 1$, v=0 in the W plane. This mapping is not one-to-one, however the segment $-\frac{\pi}{2} \leq x \leq \frac{\pi}{2}$, y=0 does map uniquely on the above line segment of the W plane. By setting $x = \pm\frac{\pi}{2}$ we find that the two lines $x=\frac{\pi}{2}$ and $x=-\frac{\pi}{2}$ map onto the remainder of the real axis of the W plane, that is $u \geq 1$, v=0; and $u \leq -1$, v=0, respectively. Since cosh y is an even function, the upper and lower halves of the lines $x = \pm\frac{\pi}{2}$ map onto the same segments of the real axis of the W plane. Therefore, this mapping is not one-to-one, but if we take either of the half-strips, $-\frac{\pi}{2} < Re\{Z\} < \frac{\pi}{2}$ and either $Im\{Z\} > 0$ or $Im\{Z\} < 0$, the vertical boundaries map onto the real axis of the W plane in a one-to-one manner. The half-strip which lies in the upper half of the Z plane maps onto the upper half of the W plane and the half-strip which lies in the lower half of the Z plane maps onto the lower half of the W plane. The complete strip, described by $-\frac{\pi}{2} < Re\{Z\} < \frac{\pi}{2}$, is mapped onto the W plane with cuts or slits in the u axis extending from $-\infty$ to -1 and from 1 to ∞ as is shown in Fig. 3-2. The potential values on the boundary of the strip are mapped onto the appropriate edges of the slits. The upper and lower halves of the y axis map onto the upper and lower halves of the v axis, respectively. Fig. 3-3 indicates how other half-strips map. The shaded half-strips map onto the upper half-plane and the unshaded ones map onto the lower half-plane. In all cases the boundary of each of the half-strips maps onto the real axis.

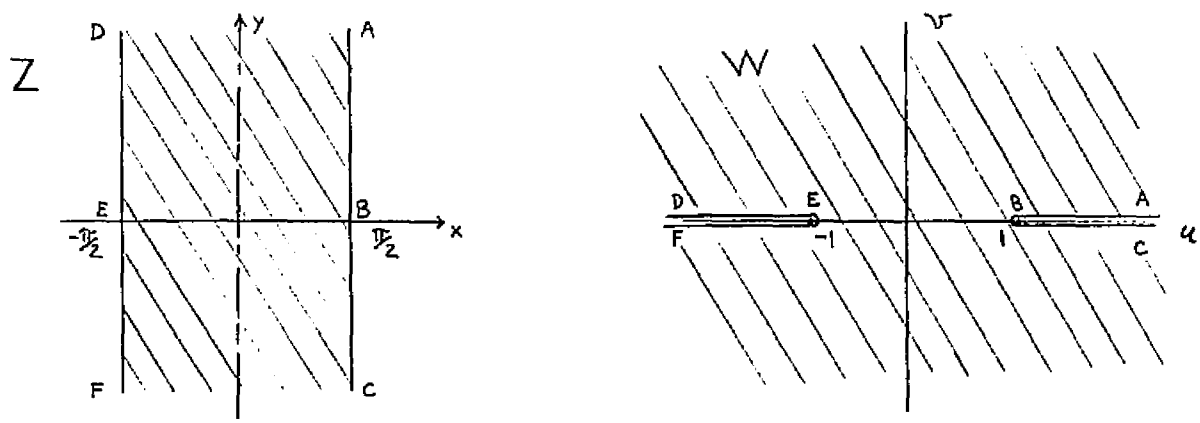

Fig. 3-2 Complete Strip

From 3-14 we obtain

$$\frac{u^2}{\cosh^2 y} + \frac{v^2}{\sinh^2 y} = 1 \qquad (3\text{-}15A)$$

$$\frac{u^2}{\sin^2 x} - \frac{v^2}{\cos^2 x} = 1 \qquad \text{(3-15B)}$$

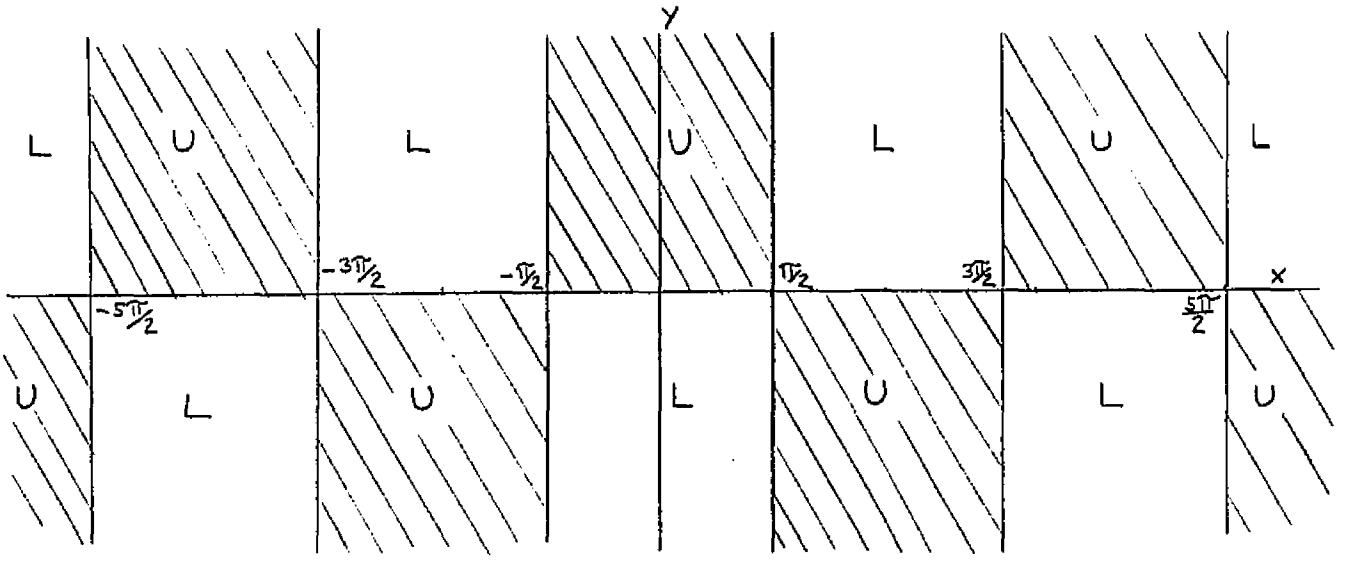

Fig. 3-3 Mapping of Half-Strips

Therefore, the mapping W=sin Z transforms the lines y=constant and x=constant into confocal ellipses and hyperbolas, respectively, whose common foci are at W=±1. An ellipse is transversed an infinity of times if the image point z describes the entire straight line y=constant and a segment of that line of length 2π corresponds to the perimeter of the ellipse. Therefore, the line segment $-\frac{\pi}{2} \leq x \leq \frac{\pi}{2}$, $y=y_0$, maps onto a semi-ellipse. The line $x=x_0$ has as its image the right-hand half of the hyperbola of 3-15B if $0<x_0<\frac{\pi}{2}$ and the left-hand half if $-\frac{\pi}{2}<x_0<0$. It is easily seen that for $y_0=0$ the degenerate ellipse is the segment of the real axis [-1,1] and for $x_0=0$ the degenerate hyperbola is the imaginary axis. Also if $x_0 \rightarrow \pm\frac{\pi}{2}$ the hyperbolas degenerate into the semi-infinite sections of the real axis $[1,\infty)$ and $(-\infty,-1]$. Thus, a rectangular region in the Z plane described by the open set

$$-\frac{\pi}{2} \leq x_1 < \mathrm{Re}\{Z\} < x_2 \leq \frac{\pi}{2}$$

$$0 \leq y_1 < \mathrm{Im}\{Z\} < y_2$$

maps under sin Z into the region between two ellipses and two hyperbolas. If we let x_1 and x_2 and y_1 take on their limiting values the boundaries take on the degenerate forms discussed above and the mapping is shown in

Fig. 3-4. We note that the regions of Fig. 3-1 and Fig. 3-4 are the same.

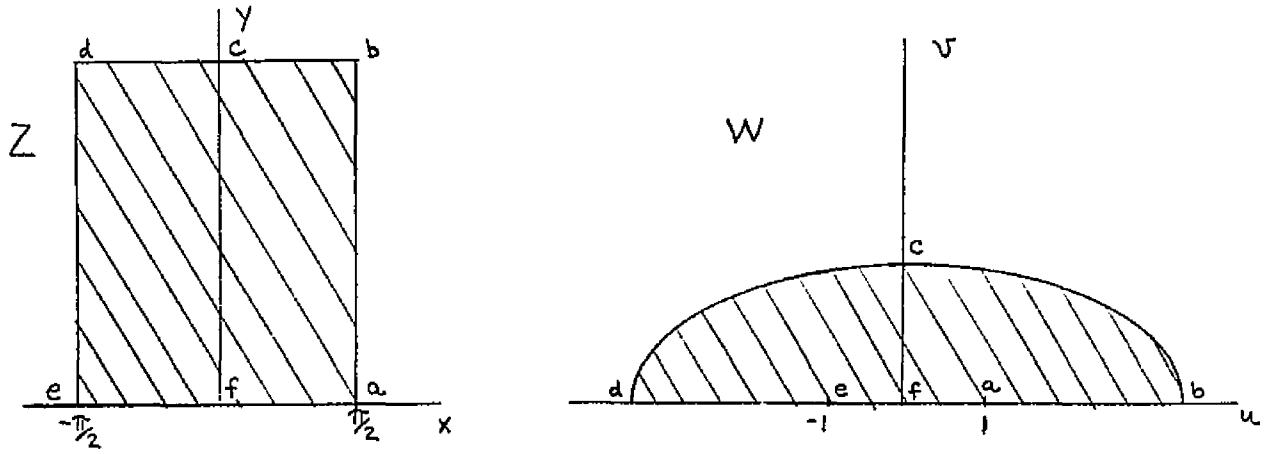

Fig. 3-4 Mapping With Degenerate Hyperbolas and One Degenerate Ellipse

The points where the derivative of the mapping function vanishes, or where $W'(Z)=0$, are known as critical points of the transformation. It is easily shown by the definition of sin Z in terms of exponential functions that

$$\frac{d}{dZ}[\sin Z] = \cos Z = \cos x \cosh y - i \sin x \sinh y \tag{3-16}$$

so that the critical points are the complex zeros of cos Z. The real part of 3-16 vanishes at the zeros of cos x where sin $x \neq 0$ so that in order for the imaginary part of 3-16 to vanish we must have y=0. The zeros of cos Z are therefore purely real and are given by

$$\begin{aligned} x &= (2m+1)\frac{\pi}{2}, \quad m = 0, \pm 1, \pm 2, \cdots \\ y &= 0 \end{aligned} \tag{3-17}$$

The critical points of the mapping, therefore, lie at the corners of the half-strips of Fig. 3-3 and at the bottom corners of the rectangle of Fig. 3-4. As was mentioned earlier, a necessary condition for isogonality is that W has a nonvanishing derivative. Also[40], at the critical points the mapping ceases to be conformal. With reference to Fig. 3-4 it is seen that in the Z plane the rotation of lines d-e into e-a and the rotation of lines e-a into a-b involve angles of $\frac{\pi}{2}$. However, the images of these lines in the W plane involve no rotations, verifying the loss of isogonality at the critical points. However, at the upper corners of the rectangle,

points b and d of Fig. 3-4, isogonality is maintained and the angles there, $\frac{\pi}{2}$, are carried over in the W plane at points b and d. Since the critical points occur on the boundary there is no problem presented with respect to the loss of the harmonic nature of the transformed potential.

If[41] $W(z)$ is analytic at a point and $W'(Z)$ is nonzero at that point then there exists a neighborhood of the image of that point in the W plane in which $W(Z)$ has a unique inverse, $Z(W)$, in the sense that $Z(W)$ is single valued and analytic there and moreover $Z'(W)=\frac{1}{W'(Z)}$. The Jacobian is

$$\frac{\partial(u,v)}{\partial(x,y)} = \begin{vmatrix} \frac{\partial u}{\partial x} & \frac{\partial u}{\partial y} \\ \frac{\partial v}{\partial x} & \frac{\partial v}{\partial y} \end{vmatrix} = \left|W'(Z)\right|^2 = \tfrac{1}{2}[\cos 2x + \cosh 2y] \tag{3-18}$$

and is zero only at the critical points. The mapping is therefore one-to-one in-the-small but not in-the-large.[42] With reference to Fig. 3-3, for any noncritical point there exists a neighborhood which lies totally in a "U" or "L" region. For a critical point, there is no neighborhood which exists for which this is so and in which the inverse is unique. The inverse of 3-5 is, from the exponential definition of sin Z,

$$Z = \sin^{-1} W = -i \ln\left[iW + (1-W^2)^{1/2}\right] \tag{3-19}$$

Owing to the multi-valuedness of the square root and logarithmic function, the multi-valuedness of Z is displayed. Also, by application of the theorem quoted above, it is easily shown that $\sin^{-1} W$ is analytic at all points except ± 1.

In light of the above, the mapping Eq. 3-5 may be used to map the interior of the rectangle of Fig. 3-1 onto the upper half-plane with critical points at the lower corners. Since the potential remains harmonic in the half-plane under the transformation, solution of Laplace's equation in the half-plane is equivalent to solving it in the rectangle. We seek the solution to Laplace's equation in the mapped region of Fig. 3-5, the region bounded by the real axis and a semiellipse with foci at $W=\pm 1$. The boundary conditions,[43] ϕ=constant and $\frac{\partial \phi}{\partial n}=0$, remain unchanged under an analytic

mapping, where the derivative of the analytic function is nonzero. Therefore, the boundary conditions $\phi=0$ and $\phi=1$ carry over as shown and the condition on the normal derivative becomes $\frac{\partial\phi}{\partial y}=0$ on the part of the boundary consisting of the open intervals of the real axis between $\pm\cosh\ell_1$ and $\pm\cosh\ell_2$.

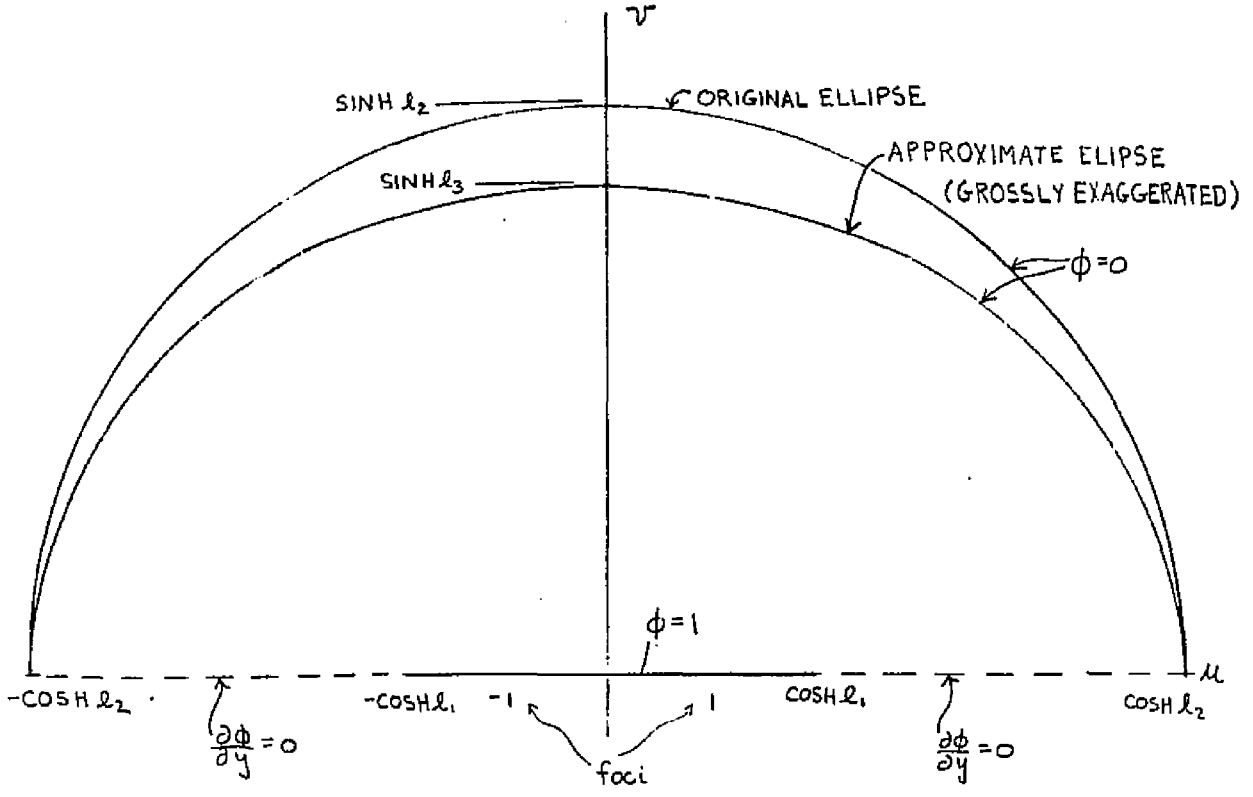

Fig. 3-5 The Mapped Region Corresponding to the Region of Fig. 3-1

3.4 Approximate Solution for Potential

We now consider the mapping 3-5 in a somewhat different manner. For an analytic function, the partial derivatives of all orders exist and are continuous.[44] We may therefore reverse the order of partial differentiation[45] and by use of the Cauchy-Riemann equations, 3-6, it is easily shown that the real and imaginary parts of the analytic function are harmonic. Therefore, for equations similar to 3-5, 3-14, and 3-15, if y were to represent potential, equipotential curves would be confocal ellipses, and if x were to represent potential, the equipotentials

would be confocal hyperbolas. As was developed in Sec. 3.3, a segment of the real axis between -1 and +1 is to be considered a degenerate ellipse. Therefore, with respect to Fig. 3-5, by a suitable scaling, we may consider the section of the real axis extending between $\pm\cosh\ell_1$ as a degenerate ellipse of a confocal system. The boundary condition on this segment is that the potential is constant and therefore it behooves us to represent potential in such a way that the equipotentials are confocal ellipses. The foci of this system of ellipses lie at $\pm\cosh\ell_1$. The foci of the ellipse, however, which forms the closing boundary of Fig. 3-5, lie at ± 1, and therefore this ellipse is not consistent with the system just discussed.

Suppose, however, that this closing boundary is replaced by another ellipse which does in fact have foci at $\pm\cosh\ell_1$. This ellipse may be made to have any points in common with the original ellipse that we wish. We arbitrarily ask that the second, or approximate, ellipse have the intersections with the real axis in common with the original one, as is shown in Fig. 3-5. We apply the same boundary condition to the approximate ellipse, as is carried by the original ellipse, namely, that of constant potential.

The semi-minor axis of the approximate ellipse, is given by the square root of the difference of the squares of the semi-major axis and the focus, in this case

$$v_{max} = \sqrt{\cosh^2\ell_2 - \cosh^2\ell_1} = \sqrt{(\cosh\ell_2 - \cosh\ell_1)(\cosh\ell_2 + \cosh\ell_1)} < \sqrt{\cosh^2\ell_2 - 1} = \sinh\ell_2 \quad (3\text{-}20)$$

Therefore, the vertical excursion of the approximate ellipse is less than that of the original, as is shown in Fig. 3-5.

From Fig. 3-1, ℓ_1 lies in $[0,\ell_2]$. For $\ell_1=0$ we have from 3-20 that $v_{max}=\sinh\ell_2$, the approximate and original ellipses are identical, and therefore the solution is exact. For this limiting case the rectangle of Fig. 3-1 has degenerated into two segments of parallel infinite planes of separation ℓ_2 and therefore the solution is obviously the linear one. If $\ell_1=\ell_2$ we have from 3-20 that $v_{max}=0$ and therefore the approximate ellipse takes on the degenerate role and becomes the section of the real axis between $\pm\cosh\ell_1$. The area between the boundaries has therefore collapsed to zero and there is no solution for the approximate ellipse. The solution

to the exact problem is well-known[46] in terms of an infinite summation of rectangular harmonics with a Fourier sine decomposition of a constant. Thus, the accuracy of the approximate solution will depend upon the ratio of ℓ_2 to ℓ_1 and as this ratio approaches unity the approximate solution derived with the approximate ellipse becomes less accurate. The validity of solution will be discussed later.

It follows from 3-20 that for $\cosh\ell_2 \gg \cosh\ell_1 \gg 1$ we have $v_{max} \approx \cosh\ell_2 \approx \sinh\ell_2$ and the approximate and original ellipses are close. The eccentricity, the ratio of the distance between foci to the major axis, approaches zero and the ellipse becomes approximately a circle.

If the curves representing constant potential are a system of confocal ellipses, it is obvious from symmetry that at the real axis of Fig. 3-5, $\frac{\partial\phi}{\partial\beta}=0$ and the boundary condition on the normal derivative is satisfied. The above represents an outline of an approximate solution to the mixed boundary value problem of Fig. 3-1. Before proceeding with the solution let us ask the obvious question as to the necessity for an approximate solution, accurate as it may turn out to be. It is known[47] that by means of elliptic functions the interior of the rectangle, Fig. 3-1, may be mapped onto the half-plane exactly. If the potential was known on all four sides of the rectangle, we could, in principle, find the solution in the half-plane by means of Green's function for the half-plane and then transform back to the rectangle. We have, however, a mixed boundary-value problem and so the preceding method would not be applicable. As it turns out, the method being presented yields highly accurate results for the geometries which are consistent with results of Chap. 2.*

Let us ascertain to what boundary in the almost-rectangular region the approximate ellipse corresponds to and examine the extent of the perturbation. The equation of the approximate ellipse is

---

* The vanishingly thin tooth provides lower interaction velocity without deleteriously affecting the space harmonic content. The scaled dimension ℓ_1 is taken so as to make ℓ_1 by π a square while frequency and bandwidth considerations prevent the difference between ℓ_2 and ℓ_1 from becoming too small.

$$\frac{u^2}{\cosh^2 \ell_2} + \frac{v^2}{\sinh^2 \ell_3} = 1 \tag{3-21A}$$

$$\sinh^2 \ell_3 \equiv \cosh^2 \ell_2 - \cosh^2 \ell_1 \tag{3-21B}$$

From 3-21 and from 3-14

$$\frac{\sin^2 x[1+\sinh^2 y]}{\cosh^2 \ell_2} + \frac{[1-\sin^2 x]\sinh^2 y}{\sinh^2 \ell_3} = 1 \tag{3-22A}$$

yielding the equation of the transformed boundary,

$$y(x) = \sinh^{-1} \sqrt{\frac{\cosh^2 \ell_2 \sinh^2 \ell_3 - \sinh^2 \ell_3 \sin^2 x}{\cosh^2 \ell_2 - [\cosh^2 \ell_2 - \sinh^2 \ell_3]\sin^2 x}} \tag{3-22B}$$

From 3-22B, we have easily

$$y(0) = \ell_3 \leq \ell_2 = y(\pm \tfrac{\pi}{2}) \tag{3-23}$$

We find from 3-22B

$$\frac{dy}{dx}(x) = \frac{1}{2} \frac{\sinh \ell_3 \cosh \ell_2 \sin 2x [\sinh^2 \ell_2 - \sinh^2 \ell_3]}{[\cosh^2 \ell_2 \cos^2 x + \sinh^2 \ell_3 \sin^2 x] \sqrt{\cosh^2 \ell_3 - \sin^2 x} \sqrt{\cosh^2 \ell_2 - \sin^2 x}} \tag{3-24}$$

If $0 < \ell_1 < \ell_2$ it is easily shown that the denominator of 3-24 does not vanish and the zeros of 3-24 occur at the center and edges of the rectangle. In view of the evenness of y(x) those points are points of extrema. Thus, from 3-23 it follows that $y_{min} = y(0) = \ell_3$ and $y_{max} = y(\pm \frac{\pi}{2}) = \ell_2$. The approximate boundary is shown grossly exaggerated in Fig. 3-1. It is obvious that this perturbed upper boundary corresponds physically to moving the straight upper boundary infinitely far away and then redefining the potential level so that the equipotential which intersects the lines $x = \pm \frac{\pi}{2}$ at $y = \ell_2$ has value zero.

The extent of the perturbation of the upper boundary may be viewed as the difference between ℓ_2 and ℓ_3.

$$\delta \equiv \ell_2 - \ell_3 = \sinh^{-1}[\sinh \ell_2] - \sinh^{-1}\sqrt{\cosh^2 \ell_2 - \cosh^2 \ell_1}$$
$$= \sinh^{-1}\left\{\sinh \ell_2 \sqrt{\cosh^2 \ell_2 - \sinh^2 \ell_1} - \cosh \ell_2 \sqrt{\sinh^2 \ell_2 - \sinh^2 \ell_1}\right\} \qquad (3\text{-}25)$$

since[48]

$$\sinh^{-1} z_1 \pm \sinh^{-1} z_2 = \sinh^{-1}\left\{z_1(1+z_2^2)^{1/2} \pm z_2(1+z_1^2)^{1/2}\right\}$$

and

$$\cosh^2 \ell_2 - \cosh^2 \ell_1 = \sinh^2 \ell_2 - \sinh^2 \ell_1$$

For the values of ℓ_1 and ℓ_2 which are scaled from dimensions consistent with the solution of the electrodynamic problem

$$\ell_1 = \pi$$
$$\ell_2 = 3.08\pi$$
$$\cosh \ell_2 \approx 7.97 \times 10^3$$
$$\cosh \ell_1 \approx 11.59$$

For these dimensions, Eq. 3-25 exhibits that the perturbation of the boundary is smaller than that which would be expected in variation of surface finish when the geometry would actually be constructed, (cf., Sec. 3.7). The approximation is therefore found to be an extremely accurate one.

In solving the potential problem of Fig. 3-5 with the approximate ellipse, we introduce constants to set the scale of potential, the reference level for potential, and the scale of physical dimension. Taking the inverse of 3-5 with incorporation of the above constants and using primes in the new plane to differentiate from the Z plane we have

$$Z' = x' + iy' = \alpha \sin^{-1} \beta W + \gamma + i\delta \qquad (3\text{-}26)$$

with W=u+iv and γ and δ real. Solving for W we have

$$u = \frac{1}{\beta} \sin \frac{x'-\gamma}{\alpha} \cosh \frac{y'-\delta}{\alpha} \qquad (3\text{-}27A)$$

$$v = \frac{1}{\beta} \cos\frac{x'-\gamma}{\alpha} \sinh\frac{y'-\delta}{\alpha} \tag{3-27B}$$

from which it follows that

$$\frac{\beta^2 u^2}{\cosh^2\frac{y'-\delta}{\alpha}} + \frac{\beta^2 v^2}{\sinh^2\frac{y'-\delta}{\alpha}} = 1 \tag{3-28A}$$

and

$$\frac{\beta^2 u^2}{\sin^2\frac{x'-\gamma}{\alpha}} - \frac{\beta^2 v^2}{\cos^2\frac{x'-\gamma}{\alpha}} = 1 \tag{3-28B}$$

We see from the above that y'=constant defines an ellipse and that x' =constant defines a hyperbola. Thus, the variable y' is chosen to represent potential for the required solution. The semi-major and semi-minor axes are obtained from 3-28A by setting v and u equal to zero respectively.

$$u_{max} = \frac{\cosh\frac{y'-\delta}{\alpha}}{\beta} \tag{3-29A}$$

$$v_{max} = \frac{\sinh\frac{y'-\delta}{\alpha}}{\beta} \tag{3-29B}$$

For the ellipse which degenerates into the line segment, we have v_{max}=0, sine the potential equals unity there we have from 3-29B, with y'=1, that δ=1. Since the maximum excursion of this line segment is $\cosh\ell_1$ we have from 3-29A, with δ=1, that $\beta = \frac{1}{\cosh\ell_1}$, the reciprocal of the focus. From the condition that the potential be zero on the outer ellipse, whose semi-major axis is $\cosh\ell_2$, we find from 3-29A that $\alpha = \frac{1}{\cosh^{-1}\left[\frac{\cosh\ell_2}{\cosh\ell_1}\right]}$. The solution for potential is now determined. The constant γ, which sets the level of the stream function, is left undetermined.

We may eliminate x' from 3-27 and find

$$\sinh\frac{y'-\delta}{\alpha} = \frac{\beta v}{\sqrt{1 - \frac{\beta^2 u^2}{\cosh^2\frac{y'-\delta}{\alpha}}}} \tag{3-30A}$$

whose solution is equivalent to solving a quadratic equation in $\sinh^2\frac{y'-\delta}{\alpha}$. We find,

$$\sinh^2\frac{y'-\delta}{\alpha} = \frac{-\left[1-\beta^2u^2-\beta^2v^2\right]\pm\sqrt{\left[1-\beta^2u^2-\beta^2v^2\right]^2+4\beta^2v^2}}{2} \qquad (3\text{-}30B)$$

The left-hand side of Equation 3-30B is ≥ 0 and since $\sqrt{\left[1-\beta^2u^2-\beta^2v^2\right]^2+4\beta^2v^2} \geq \left[1-\beta^2u^2-\beta^2v^2\right]$, it follows that the positive sign is taken in Eq. 3-30B, and we have

$$\sinh\frac{y'-\delta}{\alpha} = \pm\frac{1}{\sqrt{2}}\sqrt{\sqrt{\left[1-\beta^2u^2-\beta^2v^2\right]^2+4\beta^2v^2}-\left[1-\beta^2u^2-\beta^2v^2\right]} \qquad (3\text{-}31)$$

We ascertain the range of y' to fix the choice of sign in 3-31. A harmonic function, in a bounded and connected open region which is continuous in the closure of the region, assumes its maximum and minimum values on the boundary of the region but never at an interior point unless the function is a constant.[49] By virtue of the theorem, the maximum of y' must occur on the boundary of Fig. 3-1 and obviously $y'_{max} \geq 1$. y'_{max} is attained on the lower portion of the boundary where $y'=1$ and/or on the sides of the rectangle where $\frac{\partial y'}{\partial x}=0$. Assume the latter is true at point a of Fig. 3-1. Then

$$y'(a) > y'(b) \qquad (3\text{-}32A)$$

and

$$y'(a) \geq 1 \qquad (3\text{-}32B)$$

$y'(a)$ is strictly greater than $y'(b)$, where b is any interior point of the rectangle. We may always find a circular neighborhood of a which does not intersect the part of the boundary where $y'=1$ is given. The maximum of y' in the neighborhood and its circular boundary occurs on the circular boundary by the theorem. Such a point can be an interior point of the rectangle or an adjacent rectangle or it can be another point of the boundary of the rectangle where $\frac{\partial y'}{\partial x}=0$. Because of 3-32A the former is not possible and the assumption that a is the maximum point on the boundary makes the latter

impossible. Thus, by contradiction we have shown that y' attains its maximum, equal to unity, on the part of the boundary where y'=1 is given. Similarly, we may show that $y'_{min}=0$.

We have, therefore, that $0<y'<1$ in the interior of the rectangle. We arbitrarily take α as the positive value of $\frac{1}{\cosh^{-1}\left[\frac{\cosh \ell_2}{\cosh \ell_1}\right]}$ and since $\delta=1$, so that $-1<y'-\delta<0$ inside the region, we must take the negative sign for the square root in 3-31. From the above and the oddness of sinh we have

$$y'(u,v)=1-\frac{1}{\cosh^{-1}\left[\frac{\cosh \ell_2}{\cosh \ell_1}\right]}\sinh^{-1}\left\{\frac{1}{\sqrt{2}}\sqrt{\sqrt{\left[1-\frac{u^2+v^2}{\cosh^2 \ell_1}\right]^2+\frac{4v^2}{\cosh^2 \ell_1}}-\left[1-\frac{u^2+v^2}{\cosh^2 \ell_1}\right]}\right\} \tag{3-33}$$

Finally, we obtain the solution by use of 3-14 and 3-33 with the notation that $y'(u,v)\rightarrow\phi(x,y)$.

$$\phi(x,y)=1-\frac{1}{\cosh^{-1}\left[\frac{\cosh \ell_2}{\cosh \ell_1}\right]}\sinh^{-1}\left\{\frac{1}{\sqrt{2}}\sqrt{\sqrt{\left[1-\frac{\sin^2 x+\sinh^2 y}{\cosh^2 \ell_1}\right]^2+4\frac{\cos^2 x \sinh^2 y}{\cosh^2 \ell_1}}-\left[1-\frac{\sin^2 x+\sinh^2 y}{\cosh^2 \ell_1}\right]}\right\} \tag{3-34}$$

and we observe in 3-34 the term

$$|\sin Z|^2=\sin^2 x\cosh^2 y+\cos^2 x\sinh^2 y=\sin^2 x+\sinh^2 y$$

It can be shown that 3-34 satisfies the boundary conditions of the approximate region of Fig. 3-1 and $\nabla^2\phi=0$. In particular, consider the boundary lines $x=\pm\frac{\pi}{2}$. Then, from 3-34

$$\lim_{x\rightarrow\pm\frac{\pi}{2}}\phi(x,y)=1-\frac{1}{\cosh^{-1}\left[\frac{\cosh \ell_2}{\cosh \ell_1}\right]}\sinh^{-1}\left\{\frac{1}{\sqrt{2}}\sqrt{\sqrt{\left[1-\frac{\cosh^2 y}{\cosh^2 \ell_1}\right]^2}-\left[1-\frac{\cosh^2 y}{\cosh^2 \ell_1}\right]}\right\} \tag{3-35}$$

We have $\sqrt{\left[1-\frac{\cosh^2 y}{\cosh^2 \ell_1}\right]^2}=\pm\left[1-\frac{\cosh^2 y}{\cosh^2 \ell_1}\right]$, the positive sign holding when $y\leq\ell_1$, and the negative sign holding for $y\geq\ell_1$. Thus, for $0<y\leq\ell_1$,

$$\lim_{x\rightarrow\pm\frac{\pi}{2}}\phi(x,y)=1 \tag{3-36}$$

as is required. For $\ell_1\leq y<$ upper boundary

$$\lim_{X\to\pm\frac{\pi}{2}} \phi(x,y) = 1 - \frac{1}{\cosh^{-1}\left[\frac{\cosh\ell_2}{\cosh\ell_1}\right]} \sinh^{-1}\left\{\sqrt{\frac{\cosh^2 y}{\cosh^2\ell_1}-1}\right\} \qquad (3\text{-}37A)$$

Because, taking the positive root

$$\sinh z = \sqrt{\cosh^2 z - 1}$$

so that

$$z = \sinh^{-1}\sqrt{\cosh^2 z - 1}$$

and so 3-37A becomes

$$\lim_{X\to\pm\frac{\pi}{2}} \phi(x,y) = 1 - \frac{\cosh^{-1}\left[\frac{\cosh y}{\cosh\ell_1}\right]}{\cosh^{-1}\left[\frac{\cosh\ell_2}{\cosh\ell_1}\right]} \qquad (3\text{-}37B)$$

The equipotential plot, obtained from 3-34 with $\phi(x,y)$=constant, found by computer*, is shown for the values $\ell_1=\pi$ and $\ell_2=3.08\pi$ in Fig. 3-6. We note at once that the approximate solution would be valid for geometries where the outer boundary is placed at a value of y not less than approximately 1.5π since for values of y greater than approximately 1.5π the equipotential lines exhibit negligible curvature.

The solution obtained is checked experimentally by the method of analog field plotting. In such a method current flow lines in a high resistance sheet, deposited on paper, are the analog of electric field lines. Equivoltage lines are analogous to equipotentials. The equipotential boundaries are simulated by low resistance metal shapes placed in contact with the paper or by painting on the boundaries with high conductivity silver paint. In the experiment which was performed, the shapes were painted in, and copper blocks were placed upon them to assure low resistance. The boundary condition, $\frac{\partial\phi}{\partial n}=0$, was simulated by cutting the paper at those boundaries so that current flow, and hence electric field, must be tangent to such boundaries.

---

* The inverse hyperbolic functions are computed from the logarithmic representations[50]

$$\sinh^{-1} X = \ln\left[X+(X^2+1)^{1/2}\right]$$

$$\cosh^{-1} X = \ln\left[X+(X^2-1)^{1/2}\right]$$

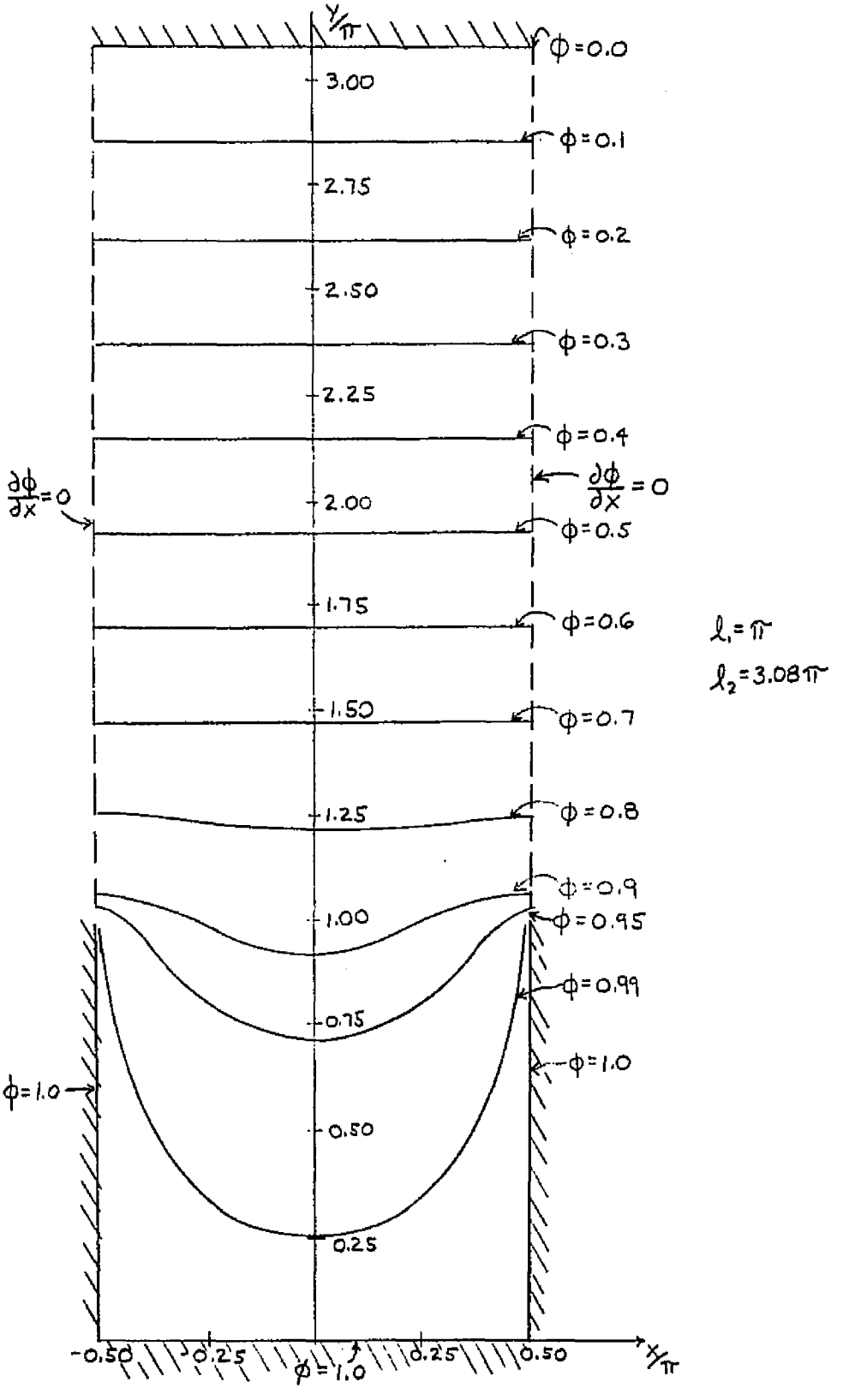

Fig. 3-6 Equipotential Plot For rf Dimensions

$\nabla\phi$ is tangent to those boundaries and so $\frac{\partial\phi}{\partial n}=0$ there. Equipotential lines are searched for by sensing the voltage of the sheet with a probe and comparing this with a bridge configuration to a predetermined proportion of the full potential difference. Null values sensed by the bridge correspond to points (x,y) where the potential has the value required. Since the center line of a unit cell also has the condition $\frac{\partial\phi}{\partial n}=0$ by symmetry, the experiment is carried out on such a half cell. The experimental configuration is shown in Fig. 3-7. The potential profile is found for the two symmetry planes, at the mid-slot plane and at the plane of the tooth. These results are shown in Fig. 3-8. Superimposed upon these curves are points obtained from the theoretical result, Eq. 3-34. The agreement between the experimental and theoretical results is evident from inspection of the figure. We make note of the linearity of potential near the upper boundary as well as $\left|\frac{\partial\phi}{\partial y}\right|$ at the tooth edge becoming very large--theoretically infinite.

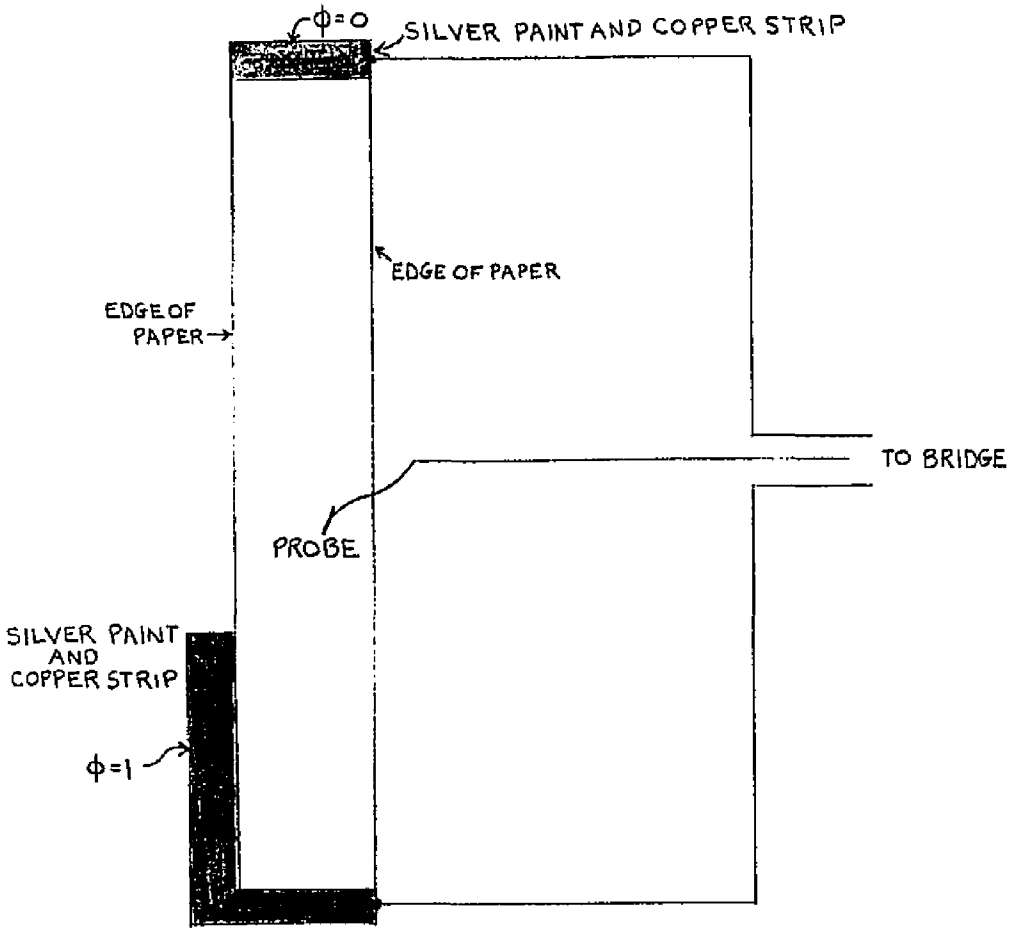

Fig. 3-7 Experimental Configuration for Analog Field Plot

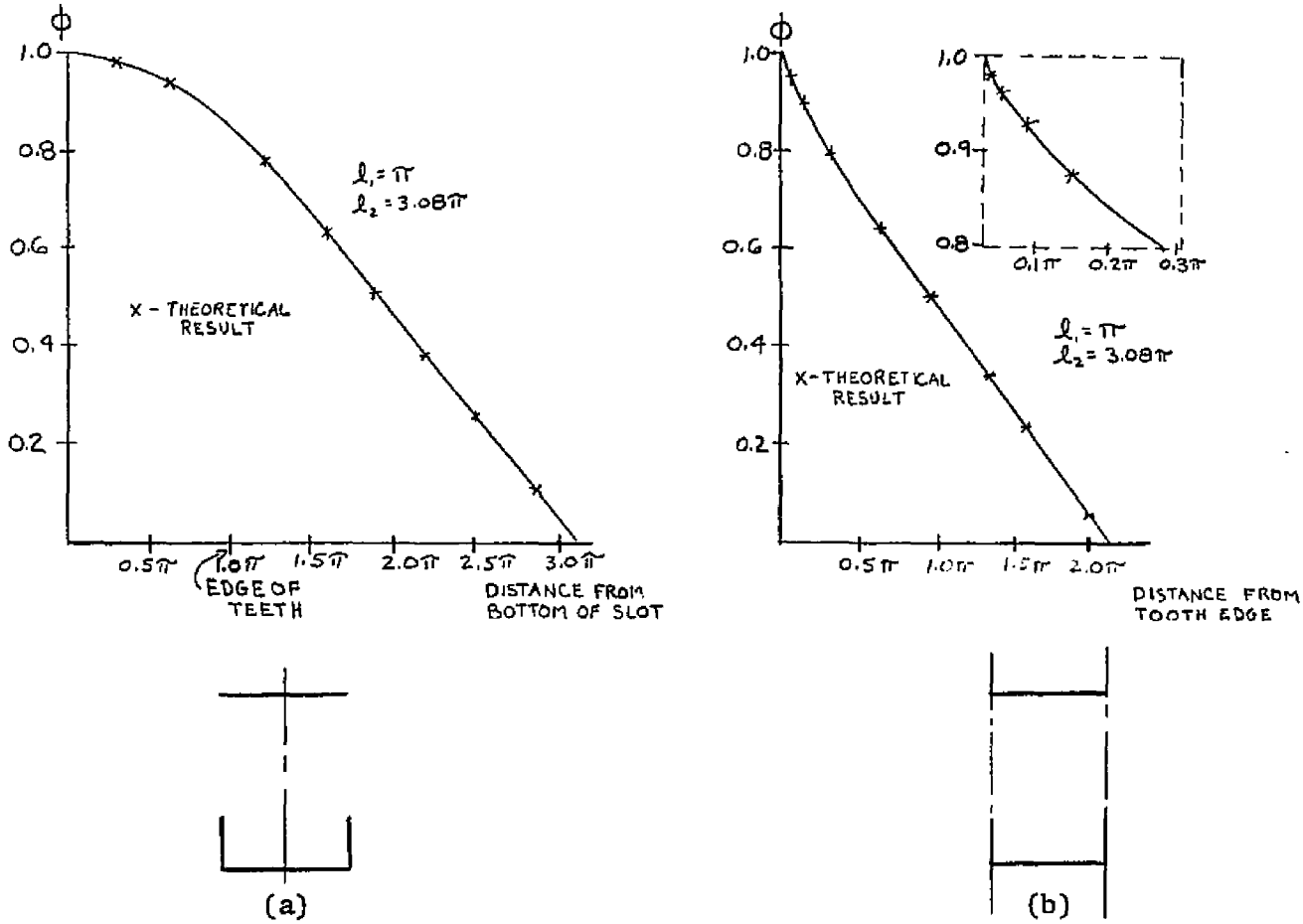

Fig. 3-8 Analog Field Results Along Symmetry Planes
(a) Center of Slot (b) Plane of Tooth

From 3-34 for sinh y≫1, and for $y \gg \ell_1$ so that sinh $y \gg \cosh \ell_1$, we have

$$\Phi(x,y) \approx 1 - \frac{1}{\cosh^{-1}\left[\frac{\cosh \ell_2}{\cosh \ell_1}\right]} \sinh^{-1}\left[\frac{\sinh y}{\cosh \ell_1}\right] = 1 - \frac{1}{\cosh^{-1}\left[\frac{\cosh \ell_2}{\cosh \ell_1}\right]} \ln\left[\frac{\sinh y}{\cosh \ell_1} + \left(\frac{\sinh^2 y}{\cosh^2 \ell_1} + 1\right)^{1/2}\right]$$

$$\approx 1 - \frac{1}{\cosh^{-1}\left[\frac{\cosh \ell_2}{\cosh \ell_1}\right]} \ln\left[2\,\frac{\sinh y}{\cosh \ell_1}\right] \approx 1 - \frac{1}{\cosh^{-1}\left[\frac{\cosh \ell_2}{\cosh \ell_1}\right]} \left[y - \ln(\cosh \ell_1)\right] \qquad (3\text{-}38)$$

which is the form of the potential predicted in Sec. 3.2. The slope in the linear region is given by $-\frac{1}{\cosh^{-1}\left[\frac{\cosh \ell_2}{\cosh \ell_1}\right]}$ and is consistent with the results of Fig. 3-8.*

* For $\ell_1 = \pi$ and $\ell_2 = 3.08\pi$, $\cosh^{-1}\left[\frac{\cosh \ell_2}{\cosh \ell_1}\right] \approx 7.22$.

Consider the behavior of $\phi(x,y)$ near the lower corners. Near the corner in the neighborhood of $x=-\frac{\pi}{2}$, $y=0$ we take $x=\tilde{x}-\frac{\pi}{2}$. For small $\tilde{x}$ and y we have

$$\sin^2 x \approx 1-\tilde{x}^2 \tag{3-39A}$$

$$\cos^2 x \approx \tilde{x}^2 \tag{3-39B}$$

$$\sinh^2 y \approx y^2 \tag{3-39C}$$

In order for $\phi(x,y)$ to be constant consistent with 3-39 we have

$$\left[1-\frac{1}{\cosh^2 \ell_1}+\frac{\tilde{x}^2-y^2}{\cosh^2 \ell_1}\right]\left\{\sqrt{1+\frac{4\tilde{x}^2y^2}{\cosh^2\ell_1\left(1-\frac{1}{\cosh^2\ell_1}+\frac{\tilde{x}^2-y^2}{\cosh^2\ell_1}\right)^2}}-1\right\}=\text{Constant} \tag{3-40}$$

For sufficiently small $\tilde{x}$ and y, $\ell_1 \neq 0$, the square root can be approximated by the first two terms of the binomial series and we find the form predicted in Eq. 3-4. In the neighborhood of the tooth edge, we have from 3-37B, with $y=\ell_1+\epsilon$, $\epsilon>0$ and small

$$\lim_{\substack{x\to\pm\frac{\pi}{2}\\ 0<\epsilon\ll 0}} \phi(x,\ell_1+\epsilon) \approx 1-\frac{\cosh^{-1}\left[1+\epsilon\tanh\ell_1\right]}{\cosh^{-1}\left[\frac{\cosh\ell_2}{\cosh\ell_1}\right]} \tag{3-41}$$

Now $\cosh^{-1} z$ has no derivative at $z=1$ therefore, the Taylor series of $\cosh^{-1}[1+\epsilon\tanh\ell_1]$ does not exist around $\epsilon=0$. However, using the logarithmic representation of $\cosh^{-1}$ we have, for small ϵ,

$$\cosh^{-1}\left[1+\epsilon\tanh\ell_1\right]=\ln\left[(1+\epsilon\tanh\ell_1)+\left[(1+\epsilon\tanh\ell_1)^2-1\right]^{1/2}\right]$$

$$=\ln\left\{1+\epsilon\tanh\ell_1+(2\epsilon\tanh\ell_1)^{1/2}\left[1+\frac{\epsilon\tanh\ell_1}{2}\right]^{1/2}\right\}\approx\ln\left\{1+(2\epsilon\tanh\ell_1)^{1/2}\right\}\approx(2\epsilon\tanh\ell_1)^{1/2} \tag{3-42}$$

Thus, from 3-41,

$$\lim_{\substack{x\to\pm\frac{\pi}{2}\\ y\to\ell_1\\ y>\ell_1}}\phi(x,y)=1-\frac{\sqrt{2\tanh\ell_1}}{\cosh^{-1}\left[\frac{\cosh\ell_2}{\cosh\ell_1}\right]}\sqrt{y-\ell_1} \tag{3-43}$$

agreeing with Eq. 3-2B.

As was mentioned at the beginning of this section, if x were chosen to represent potential, the equipotentials would be a system of confocal hyperbolas instead of the system of ellipses utilized above. As was developed in Sec. 3.3 the degenerate forms of the hyperbolas are the imaginary axis and the sections of the real axis for which $u^2 \geq 1$. Thus, by use of the other conjugate function to represent potential we may find the solution when the boundaries consist of two mutually perpendicular planes separated by a unit gap, g=1, as shown in Fig. 3-9. By symmetry $\frac{\partial \phi}{\partial m}=0$ along the extension of the horizontal plane shown dotted in the figure. It is obvious that by rotation of Fig. 3-9 by $\frac{\pi}{2}$ and by suitable scaling, we may find the solution for potential for one tooth of infinite extent and ascertain the effects of the lower edge of the rectangle and adjacent teeth. For the dimensions of Fig. 3-6, it is seen that the lower edge of the rectangle may be moved infinitely far away and one would not expect a large change in potential since the height of the teeth already equals the width of the slot. In this case one examines the effect of adjacent teeth. The boundary potential is fixed as indicated in Fig. 3-9. Utilizing a general scaling, and proceeding with the solution in a manner similar to that followed previously, except that in this case potential is represented by the family of hyperbolas, we obtain

$$\phi(x'',y'') = \mathrm{Re}\left\{1 - \frac{2}{\pi}\cos^{-1}\left[\frac{x''+iy''}{g}\right]\right\} \tag{3-44}$$

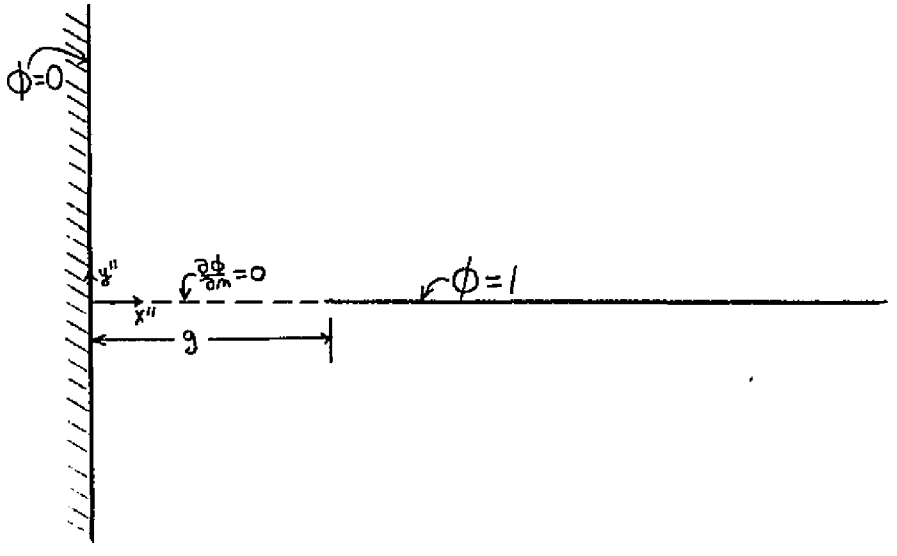

Fig. 3-9 Mutually Perpendicular Planes

We may show in a manner similar to that used before that ϕ is bounded by 0 and 1, dictating the branch taken for $\cos^{-1}$. The point (g,0), the edge of the tooth, is a focus of the hyperbolas which form the equipotentials. For the sake of comparison, we require the potential along the x'' axis and therefore, from 3-44,

$$\phi(x'',0) = 1 - \frac{2}{\pi}\cos^{-1}\frac{x''}{g}, \qquad 0 < x'' < g \tag{3-45A}$$

$$\lim_{\substack{y''\to 0 \\ x''>g}} \phi(x'',y'') = \lim_{\substack{y''\to 0 \\ x''>g}} Re\left\{1 - \frac{2}{\pi}\cos^{-1}\left[\frac{x''+iy''}{g}\right]\right\} = 1 \tag{3-45B}$$

to make these results applicable simply rotate Fig. 3-9 by $\frac{\pi}{2}$ and define the distance from, and in the plane of, the tooth edge as ζ.

$$x'' = g - \zeta$$

Potential in the plane of the tooth is defined as u

$$u = 1 - \frac{2}{\pi}\cos^{-1}\left[1 - \frac{\zeta}{g}\right], \qquad 0 < \zeta < g \tag{3-46}$$

The variation of u is shown in Fig. 3-10 for g=.650, the dimension applicable for the rf geometry. The potential displays* linear variation near the upper wall and infinite derivative at the tooth edge, both expected in light of previous discussion. Comparison of Figs. 3-10 and 3-8 reveals that the actual potential is higher at all interior points due to the shielding effects of the other teeth. As the teeth become relatively

---

* In view of[51]

$$\sin^{-1}\left[1-\zeta\right] = \frac{\pi}{2} - (2\zeta)^{1/2}\left[1 + \sum_{k=1}^{\infty} \frac{1\cdot 3\cdot 5\cdots(2k-1)}{2^{2k}(2k+1)\,k!}\zeta^k\right], \quad |\zeta|<2$$

and since $\cos^{-1}(1-z)+\sin^{-1}(1-z)=\frac{\pi}{2}$ we have

$$\cos^{-1}\left[1-\frac{\zeta}{g}\right] = \left[2\frac{\zeta}{g}\right]^{1/2}\left[1 + \sum_{k=1}^{\infty} \frac{1\cdot 3\cdot 5\cdots(2k-1)}{2^{2k}(2k+1)\,k!}\left[\frac{\zeta}{g}\right]^k\right], \quad \left|\frac{\zeta}{g}\right|<2$$

so that from 3-46 for $\frac{\zeta}{g}$ vanishingly small

further spaced, the model of Fig. 3-9 becomes somewhat more appropriate. It is interesting to note that we have used two different and distinct aspects of the same mapping to obtain the result 3-34 and the above approximation.

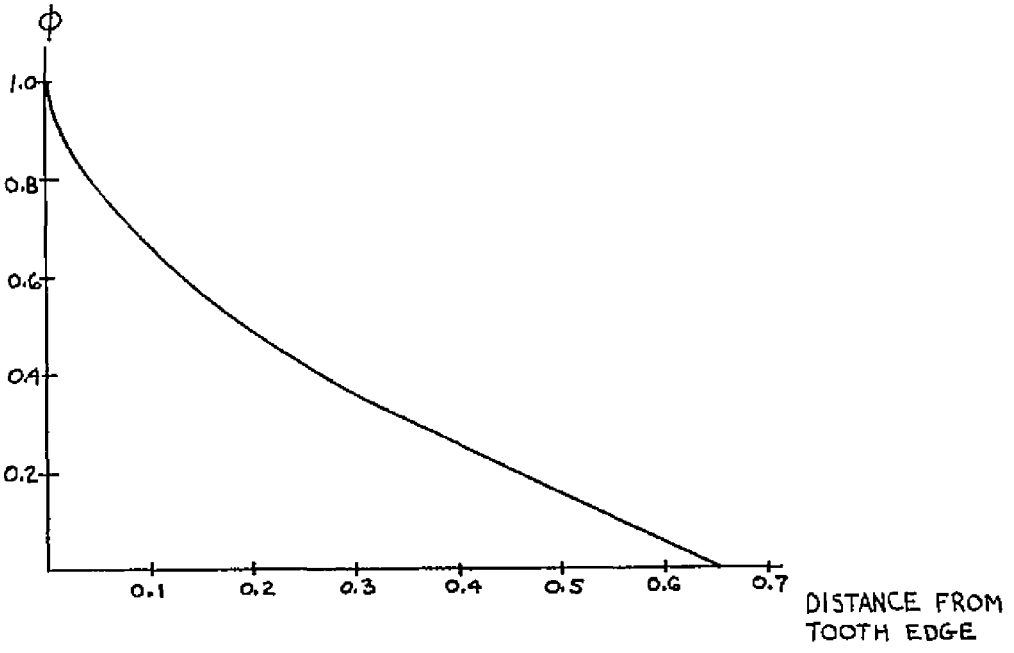

Fig. 3-10 $u=1-\frac{2}{\pi}\cos^{-1}(1-\frac{\eta}{g})$, g=.650

$$u \approx 1-\frac{2^{3/2}}{\pi}\left[\frac{z}{g}\right]^{1/2}$$

(cf. Eqs. 3-43 and 3-2B). Also,[52]

$$\sin^{-1}z = z+\tfrac{1}{2}\tfrac{z^3}{3}+\tfrac{1\cdot3}{2\cdot4}\tfrac{z^5}{5}+\cdots \quad , |z|<1$$

so that

$$\cos^{-1}\left[1-\tfrac{z}{g}\right]=\tfrac{\pi}{2}-\left[1-\tfrac{z}{g}\right]-\tfrac{1}{2}\tfrac{\left[1-\frac{z}{g}\right]^3}{3}-\tfrac{1\cdot3}{2\cdot4}\tfrac{\left[1-\frac{z}{g}\right]^5}{5}-\cdots \quad , \left|1-\tfrac{z}{g}\right|<1$$

For $\frac{z}{g}=1-\epsilon$, ϵ small and positive, we have from 3-46

$$u \approx 1-\frac{2}{\pi}\left[\frac{\pi}{2}-\left(1-\frac{z}{g}\right)\right]=\frac{2}{\pi}\epsilon$$

the linear variation expected near the wall.

We perform a successive mapping and obtain a result which allows the evaluation of the effect of the lower boundary of the rectangle, a further use of the basic mapping, 3-5. As was shown one of the conjugate functions represents a system of confocal ellipses, whose degenerate member is a symmetrical segment of the real axis. This leads to the solution for potential about an equipotential segment of the real axis. If we map this geometry by the logarithmic mapping[53]

$$\zeta + i\gamma = \ln Z = \ln r + i\theta \tag{3-47A}$$

$$\zeta = \ln \sqrt{x^2 + y^2} \tag{3-47B}$$

$$\gamma = \tan^{-1} \frac{y}{x} \tag{3-47C}$$

The upper half-plane maps into the open region between the lines $\gamma = 0$ and $\gamma = \pi$, the strip of width π, as shown in Fig. 3-11. The positive part of the real axis of the Z plane maps into the real axis of the $\zeta\gamma$ plane, the segment between the origin and 1 mapping into the negative part of the ζ axis, and the part from 1 to infinity mapping into the positive part of the ζ axis. Similarly, the negative part of the x axis maps into the line $\gamma = \pi$. In this case the segment between the origin and -1 maps into the negative half of this line and the rest of the negative x axis maps into the positive part. Therefore, if potential is constant on the line $|x| \leq 1$ in the Z plane, potential will be constant[54] along the lines $-\infty < \zeta \leq 0$, $\gamma = 0$ and along $-\infty < \zeta \leq 0$, $\gamma = \pi$. Also, the condition $\frac{\partial \phi}{\partial n} = 0$ existing along the open remainder of the real axis of the Z plane, transforms over. This is true since $\ln Z$ is analytic except at the origin and its derivative is

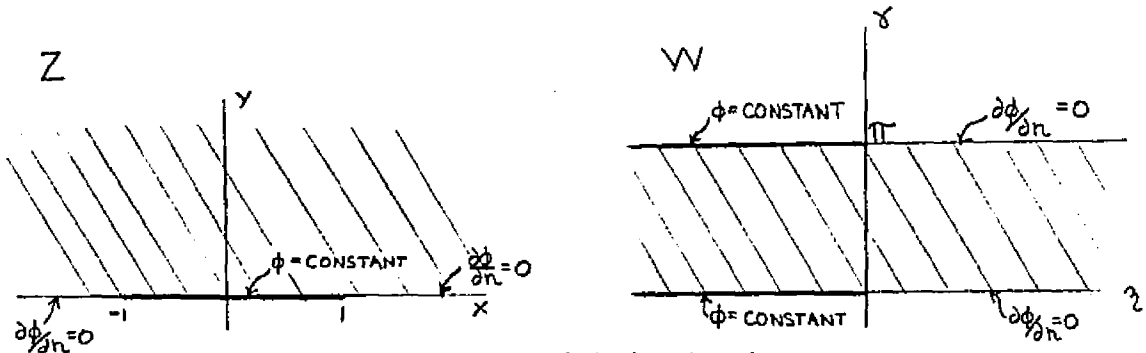

Fig. 3-11 Logarithmic Mapping

nonzero at all finite points. We find from 3-5

$$\zeta = \tfrac{1}{2}\ln\tfrac{1}{2}[\cosh 2\Phi + \cos 2\Psi] \tag{3-48A}$$

$$\gamma = \tan^{-1}[\tanh\Phi \tan\Psi] \tag{3-48B}$$

Φ and Ψ are the two conjugate functions, either of which may be chosen to represent potential. Φ is taken to be the potential function and the geometry consists of an infinite number of parallel semi-infinite planes separated by a distance equal to π. We obtain easily from 3-48

$$2e^{2\zeta} = \cosh 2\Phi + \cos 2\Psi \tag{3-49A}$$

$$\tan\gamma = \tanh\Phi \tan\Psi \tag{3-49B}$$

Eliminate Ψ from 3-49 and obtain

$$2e^{2\zeta} - \cosh 2\Phi = \frac{2}{1+\frac{\tan^2\gamma}{\tanh^2\Phi}} - 1 \tag{3-50}$$

and note that Φ is a periodic function of γ. We restrict ourselves to $0 \le \gamma \le \pi$. For $\gamma = 0$; or $\gamma = \pi$ and $\Phi \neq 0$; we obtain from 3-50

$$\Phi = \cosh^{-1}[e^{\zeta}] \tag{3-51}$$

which holds for $\zeta > 0$. For $\gamma = \frac{\pi}{2}$ we obtain from 3-50

$$\Phi = \sinh^{-1}[e^{\zeta}] \tag{3-52}$$

For Φ large and positive we have that $\sinh\Phi \approx \cosh\Phi \approx \frac{1}{2}e^{\Phi}$ so that

$$\Phi \approx \zeta - \ln\tfrac{1}{2} = \zeta + \ln 2 \tag{3-53}$$

for both symmetry planes. Therefore, for sufficiently large ζ relative to the spacing π, equipotentials are parallel to the γ axis. Thus, in Fig. 3-1, if the lower edge of the rectangle is move infinitely far away, we have the geometry of Fig. 3-11 with a suitable rotation. This yields a

way of determining the effect of the lower edge of the rectangle of Fig. 3-1 in setting potential. We solve 3-50, a quadratic equation in $\sinh^2\Phi$.

$$\sinh^2\Phi = \tfrac{1}{2}\left[e^{2\zeta}-1\right]\left\{1 \pm \sqrt{1+\frac{e^{2\zeta}\sin^2\gamma}{\frac{1}{4}\left[e^{2\zeta}-1\right]^2}}\right\} \tag{3-54}$$

For real Φ the left-hand of the equation is ≥ 0 and the positive sign is appropriate.

$$\Phi = \sinh^{-1}\left\{e^{\frac{\zeta}{2}}\sinh^{1/2}\zeta\sqrt{1+\sqrt{1+\frac{\sin^2\gamma}{\sinh^2\zeta}}}\right\} \tag{3-55}$$

We scale 3-55 by again making the arbitrary requirement that the boundary condition on the upper boundary be satisfied at the edges of the "rectangle", in this case for $\zeta=\ell_2-\ell_1$. We find the solution to Fig. 3-1 with the lower edge of the rectangle removed to $-\infty$ and the upper boundary being similar but not quite the same.

$$\Phi = 1 - \frac{1}{\cosh^{-1}\left[e^{\ell_2-\ell_1}\right]}\sinh^{-1}\left\{e^{\frac{\zeta}{2}}\sinh^{1/2}\zeta\sqrt{1+\sqrt{1+\frac{\sin^2\gamma}{\sinh^2\zeta}}}\right\} \tag{3-56}$$

Along the symmetry planes *

$$\Phi = 1 - \frac{\sinh^{-1}\left[e^{\zeta}\right]}{\cosh^{-1}\left[e^{\ell_2-\ell_1}\right]} \quad , \quad \gamma = \frac{\pi}{2} \tag{3-57A}$$

---

* In 3-57B, with $e^{\zeta}=1+\delta$, $\delta \approx \zeta$

$$\Phi = 1 - \frac{1}{\cosh^{-1}\left[e^{\ell_2-\ell_1}\right]}\ln\left[(1+\delta)+\left[(1+\delta)^2-1\right]^{1/2}\right]$$

$$= 1 - \frac{1}{\cosh^{-1}\left[e^{\ell_2-e^{\ell_1}}\right]}\ln\left[(1+\delta)+(2\delta)^{1/2}\left[1+\tfrac{1}{2}\delta\right]^{1/2}\right]$$

For small δ we find

$$\Phi \approx 1 - \frac{1}{\cosh^{-1}\left[e^{\ell_2-e^{\ell_1}}\right]}\ln\left[1+(2\delta)^{1/2}\right]$$

$$\approx 1 - \frac{1}{\cosh^{-1}\left[e^{\ell_2-e^{\ell_1}}\right]}(2\delta)^{1/2} \approx 1 - \frac{1}{\cosh^{-1}\left[e^{\ell_2-e^{\ell_1}}\right]}(2\zeta)^{1/2}$$

(cf. Eqs. 3-43 and 3-2B).

$$\Phi = 1 - \frac{\cosh^{-1}[e^{\xi}]}{\cosh^{-1}[e^{\ell_2-\ell_1}]} \quad , \quad \gamma = 0,\pi \; ; \; \xi > 0 \tag{3-57B}$$

Writing 3-56 in terms of the x and y of Fig. 3-1 we have by

$$\xi = y - \ell_1$$
$$\gamma = \tfrac{\pi}{2} - x$$

that

$$\phi(x,y) = 1 - \frac{1}{\cosh^{-1}[e^{\ell_2-\ell_1}]} \sinh^{-1}\left\{ e^{\frac{y-\ell_1}{2}} \sinh^{1/2}(y-\ell_1) \sqrt{1+\sqrt{1+\frac{1+\cos 2x}{2\sinh^2(y-\ell_1)}}} \right\} \tag{3-58}$$

It can be shown that as ℓ_1, ℓ_2 and y become large, the more exact solution, 3-34, which accounts for the lower boundary of the rectangle, becomes identical with 3-58. We compare the potential profiles along the symmetry planes for the two solutions to see what effect the lower boundary of the rectangle has upon the potential. These profiles are given by Eqs. 3-57 for the solution of semi-infinite planes. Such a comparison is shown in Fig. 3-12 for the configuration $\ell_1 = \pi$, $\ell_2 = 3.08\pi$. It is seen that with this geometry there is virtually no difference in the solutions for y larger than the plane of the teeth edges. The only difference is found within the slot. Of course, for smaller values of ℓ_1 one would expect larger differences in the solution.

Maxwell[55] points out that for the system of equipotentials Ψ, corrections for the thickness of the corresponding plate may be found by taking a non-degenerate equipotential to represent the plate. It may be possible to gain insight into the effects of a nonzero thickness tooth by a similar consideration here.

The maximum excursion of potential, as x is varied for a given value of y, normalized with respect to the arithmetic average of the two values, is used as a measure to determine the rate that ϕ becomes uniform with increasing y. By use of[56]

$$\sinh^{-1}\left[\frac{\sinh y}{\cosh \ell_1}\right] \pm \cosh^{-1}\left[\frac{\cosh y}{\cosh \ell_1}\right] = \sinh^{-1}\left\{ \frac{\sinh y \cosh y}{\cosh^2 \ell_1} \pm \left[\left(1+\frac{\sinh^2 y}{\cosh^2 \ell_1}\right)\left(\frac{\cosh^2 y}{\cosh^2 \ell_1} - 1\right)\right]^{1/2} \right\} \tag{3-59}$$

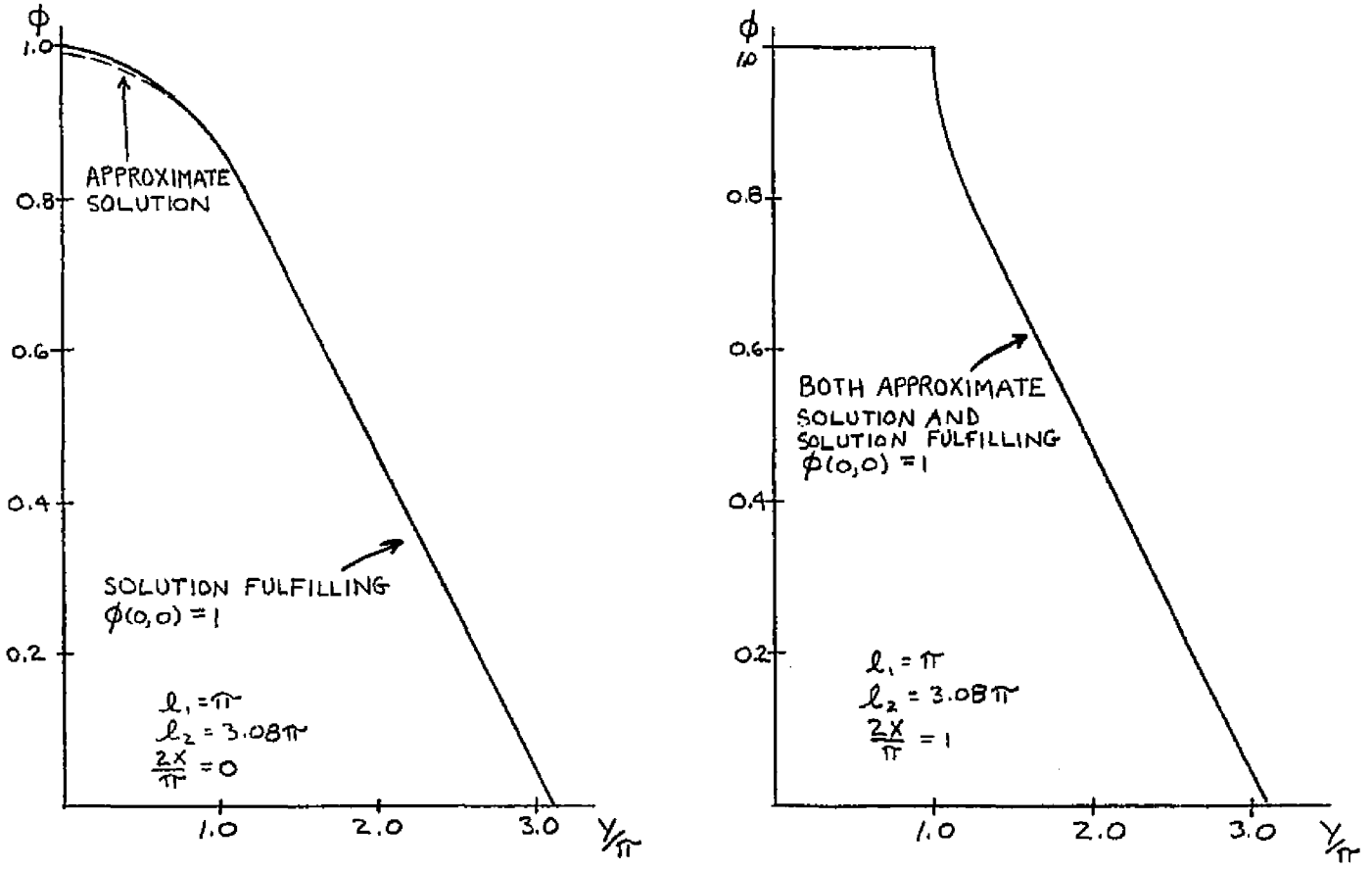

Fig. 3-12 Comparison of Solutions

we may show

$$\frac{\phi(\pm\frac{\pi}{2},y)-\phi(0,y)}{\frac{1}{2}\left[\phi(\pm\frac{\pi}{2},y)+\phi(0,y)\right]} = \frac{2\sinh^{-1}\left[\frac{\sinh y}{\cosh\ell_1}\right]}{2\cosh^{-1}\left[\frac{\cosh\ell_2}{\cosh\ell_1}\right]-\sinh^{-1}\left[\frac{\sinh y}{\cosh\ell_1}\right]}\ ,\ 0\le y\le\ell_1 \qquad (3\text{-}60A)$$

$$\frac{\phi(\pm\frac{\pi}{2},y)-\phi(0,y)}{\frac{1}{2}\left[\phi(\pm\frac{\pi}{2},y)+\phi(0,y)\right]} = \frac{2\sinh^{-1}\left\{\frac{\sinh 2y}{2\cosh^2\ell_1}\left[1-\sqrt{1-\left(\frac{\sinh 2\ell_1}{\sinh 2y}\right)^2}\right]\right\}}{2\cosh^{-1}\left[\frac{\cosh\ell_2}{\cosh\ell_1}\right]-\sinh^{-1}\left\{\frac{\sinh 2y}{2\cosh^2\ell_1}\left[1+\sqrt{1-\left(\frac{\sinh 2\ell_1}{\sinh 2y}\right)^2}\right]\right\}}\ ,\ \ell_1\le y\le\ell_2 \qquad (3\text{-}60B)$$

Results of Eqs. 3-60 are shown for the dimensions $\ell_1=\pi$, $\ell_2=3.08\pi$, in Fig. 3-13. For these dimensions, the normalized excursion of potential attains a maximum value of 13% at the plane of the tooth edges where the

curve exhibits a discontinuous slope.*

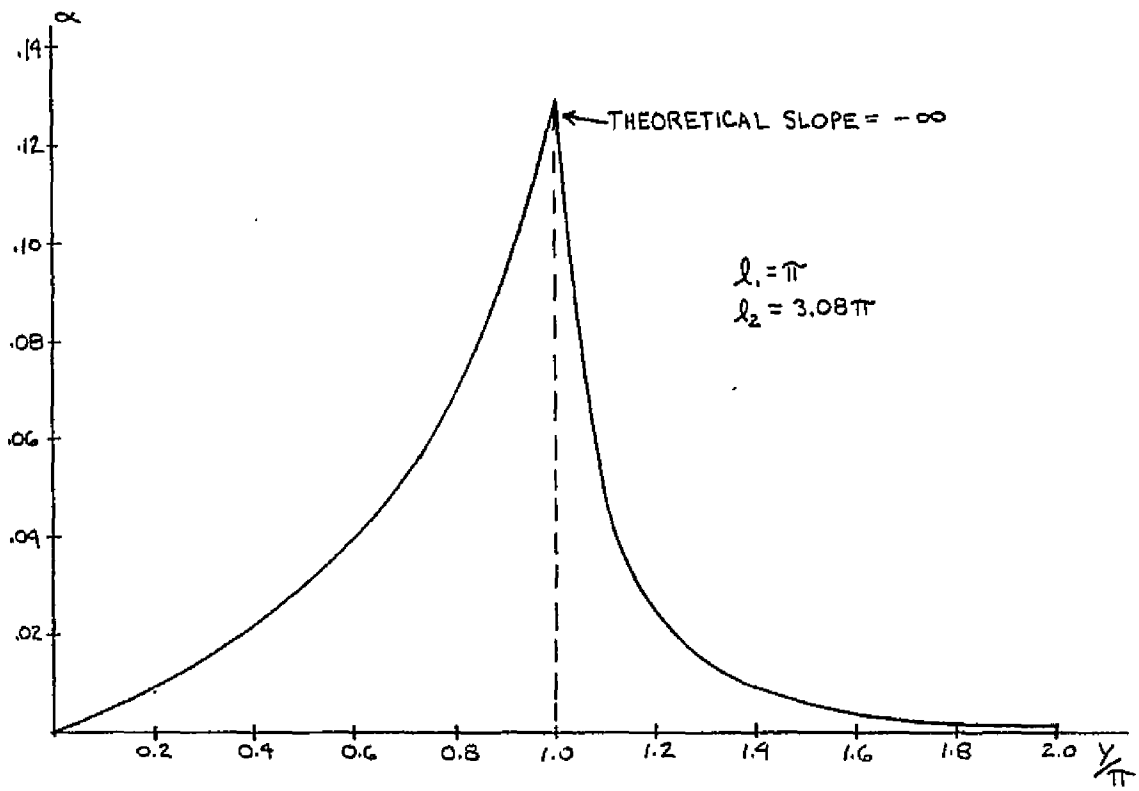

Fig. 3-13 Potential Excursion

---

*

$$\frac{d}{dy}\left\{\frac{\phi(\pm\frac{\pi}{2},y)-\phi(0,y)}{\frac{1}{2}\left[\phi(\pm\frac{\pi}{2},y)+\phi(0,y)\right]}\right\} = 4\,\frac{\frac{\partial\phi}{\partial y}(\pm\frac{\pi}{2},y)\,\phi(0,y)-\frac{\partial\phi}{\partial y}(0,y)\,\phi(\pm\frac{\pi}{2},y)}{\left[\phi(\pm\frac{\pi}{2},y)+\phi(0,y)\right]^2}$$

At $y=\ell_1$, $\frac{\partial\phi}{\partial y}(0,y)$ is continuous.

$$\frac{\partial\phi}{\partial y}(0,\ell_1) = -\frac{1}{\cosh^{-1}\left[\frac{\cosh\ell_2}{\cosh\ell_1}\right]\left[1+\frac{\sinh^2\ell_1}{\cosh^2\ell_1}\right]^{1/2}}$$

and equals -.098 for the dimensions of Fig. 3-13. On the other hand, since $\phi(\pm\frac{\pi}{2},y)=1$ for $0\le y\le\ell_1$, we have

$$\frac{\partial\phi}{\partial y}(\pm\tfrac{\pi}{2},y) = 0\,, \qquad 0<y<\ell_1$$

Since,

$$\lim_{\substack{y\to\ell_1\\ y>\ell_1}}\frac{\partial\phi}{\partial y}(\pm\tfrac{\pi}{2},y) = -\infty$$

we observe that $\frac{\partial\phi}{\partial y}(\pm\frac{\pi}{2},\,y)$ is discontinuous at $y=\ell_1$ accounting for the discontinuous slope of Fig. 3-13.

3.5 First and Second Derivatives of Potential

Defining

$$h(x,y) \equiv \frac{\sin^2 x + \sinh^2 y}{\cosh^2 \ell_1} \tag{3-61A}$$

$$B(x,y) \equiv [1-h(x,y)]^2 + \frac{4\cos^2 x \sinh^2 y}{\cosh^2 \ell_1} \tag{3-61B}$$

$$f(x,y) \equiv h(x,y) + \sqrt{B(x,y)} \tag{3-61C}$$

$$g(x,y) \equiv \sqrt{\left\{h(x,y)\sqrt{B(x,y)} + B(x,y) - 1 + \frac{1-\cosh 2y \cos 2x}{2\cosh^2 \ell_1}\right\}\sqrt{B(x,y)}}$$

$$= \frac{1}{\sqrt{2}}\sqrt{B(x,y)\left[f^2(x,y)-1\right]} \tag{3-61D}$$

it can be shown from 3-34 that the components of $\nabla\phi$ are given by

$$\frac{\partial \phi}{\partial x}(x,y) = -\frac{\sin 2x}{2^{3/2}\cosh^{-1}\left[\frac{\cosh \ell_2}{\cosh \ell_1}\right]\cosh^2 \ell_1}\,\frac{f(x,y)-\cosh 2y}{g(x,y)} \tag{3-61E}$$

$$\frac{\partial \phi}{\partial y}(x,y) = -\frac{\sinh 2y}{2^{3/2}\cosh^{-1}\left[\frac{\cosh \ell_2}{\cosh \ell_1}\right]\cosh^2 \ell_1}\,\frac{f(x,y)+\cos 2x}{g(x,y)} \tag{3-61F}$$

Observing that the functions h(x,y), B(x,y), f(x,y) and g(x,y) have even symmetry about x=0 we note from 3-61 that $\frac{\partial \phi}{\partial x}$ is an odd, and $\frac{\partial \phi}{\partial y}$ is an even, function of x about x=0. Since $\frac{\partial \phi}{\partial x}$ is continuous at x=0, $\frac{\partial \phi}{\partial x}(0,y)=0$ and ϕ has even symmetry about x=0. We may show for $y-\ell_1$ small and positive

$$\frac{\partial \phi}{\partial y}\left(\pm\frac{\pi}{2},y\right) \approx -\frac{\sqrt{\tanh \ell_1}}{\sqrt{2}\cosh^{-1}\left[\frac{\cosh \ell_2}{\cosh \ell_1}\right]\sqrt{y-\ell_1}} \tag{3-62}$$

agreeing with 3-43. For y sufficiently large, it can be shown that

$$h(x,y) \approx \frac{\sinh^2 y}{\cosh^2 \ell_1}$$

$$B(x,y) \approx h^2(x,y)$$

$$f(x,y) \approx 2h(x,y)$$

$$g(x,y) \approx \sqrt{2}\, B(x,y)$$

so that

$$\frac{\partial \phi}{\partial x}(x,y) \approx 0 \tag{3-63A}$$

$$\frac{\partial \phi}{\partial y}(x,y) \approx -\frac{1}{\cosh^{-1}\left[\frac{\cosh \ell_2}{\cosh \ell_1}\right]} \tag{3-63B}$$

The way that $\frac{\partial \phi}{\partial y}(0,y)$ approaches this limit is shown in Fig. 3-14 for $\ell_1=\pi$, $\ell_2=3.08\pi$. For the same dimensions, a logarithmic plot of $\frac{\partial \phi}{\partial y}$ in the plane of the tooth is shown in Fig. 3-15, where a comparison is made with the asymptotic line of slope $-\frac{1}{2}$, as given by Eq. 3-62. We find from 3-61

$$\frac{\partial^2 \phi}{\partial y^2}(x,y) = -\frac{\partial^2 \phi}{\partial x^2}(x,y) = -\frac{f(x,y)+\cos 2x}{\cosh^{-1}\left[\frac{\cosh \ell_2}{\cosh \ell_1}\right]\cosh^2 \ell_1 \sqrt{f^2(x,y)-1}\, B(x,y)} \left\{ \sqrt{B(x,y)}\cosh 2y \right.$$
$$\left. -\frac{1}{2}\frac{\sinh^2 2y}{\cosh^2 \ell_1}\left[f(x,y)+\cos 2x\right]\left[\frac{f(x,y)}{f^2(x,y)-1}+\frac{1}{\sqrt{B(x,y)}}\right]+\frac{\sinh^2 2y}{\cosh^2 \ell_1}\right\} \tag{3-64}$$

verifying that at all points where 3-64 exists, $\nabla^2 \phi = 0$. We compare $\frac{\partial^2 \phi}{\partial (y/\pi)^2}$ as a function of x for three parametric values of y in Fig 3-16.

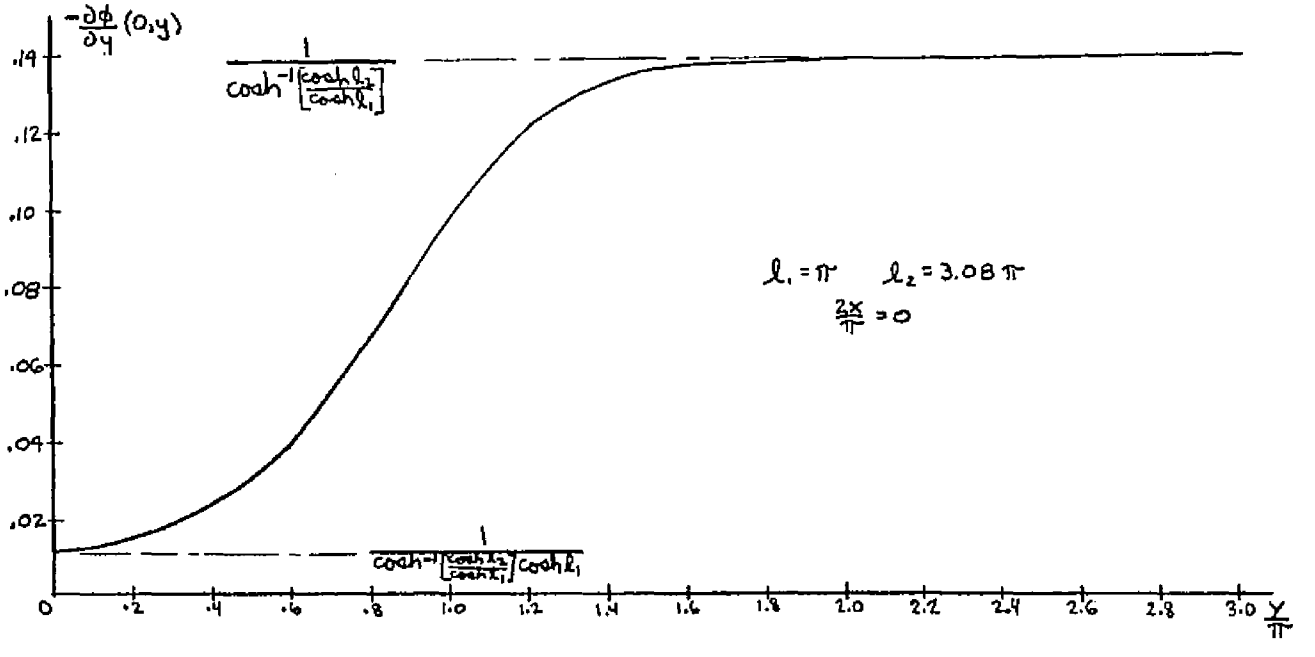

Fig. 3-14 $-\frac{\partial \phi}{\partial y}(0,y)$

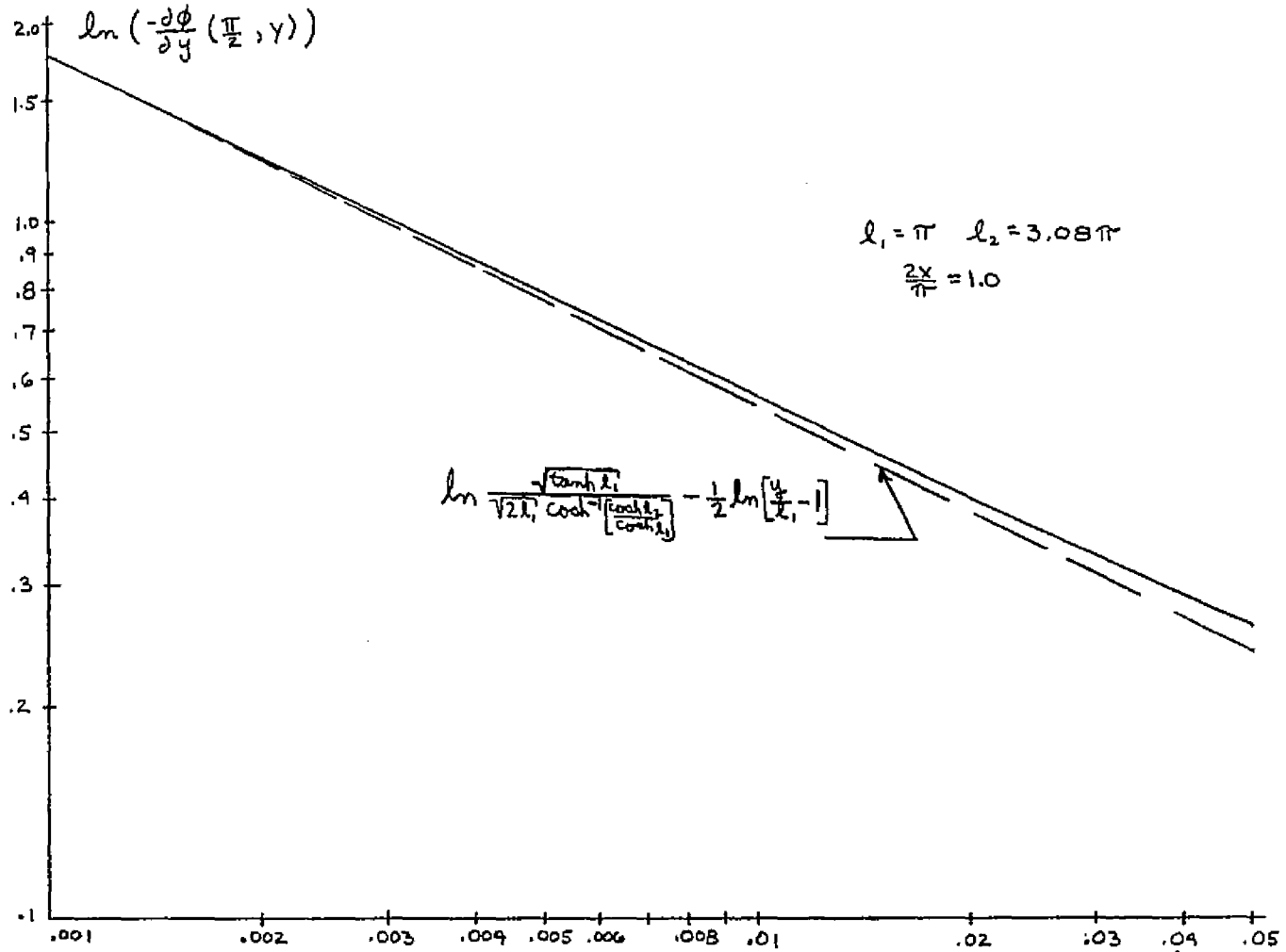

Fig. 3-15 $\ell n[-\frac{\partial\phi}{\partial y}(\pm\frac{\pi}{2}, y)]$ versus $\ell n[\frac{y}{\ell_1}-1]$

Observe that sufficiently far from the teeth a single sinusoid would adequately represent the function while closer to them higher order sinusoids are necessary. This is true since the higher order rectangular harmonics of the expansion attenuate more rapidly away from $\frac{y}{\pi}=1$. Thus for an electron relatively close to the teeth, consistent with stronger interaction, the potential should not be approximated by a single harmonic. Note that the slope of the curves is zero at $x=\pm\frac{\pi}{2}$, even for $\frac{y}{\pi}$ very close to one as in Fig. 3-16C. Thus, for $y > \ell_1$

$$\frac{\partial}{\partial x}\left[\frac{\partial^2\phi}{\partial y^2}(\pm\tfrac{\pi}{2}, y)\right] = \frac{\partial^2}{\partial y^2}\left[\frac{\partial\phi}{\partial x}(\pm\tfrac{\pi}{2}, y)\right] = 0$$

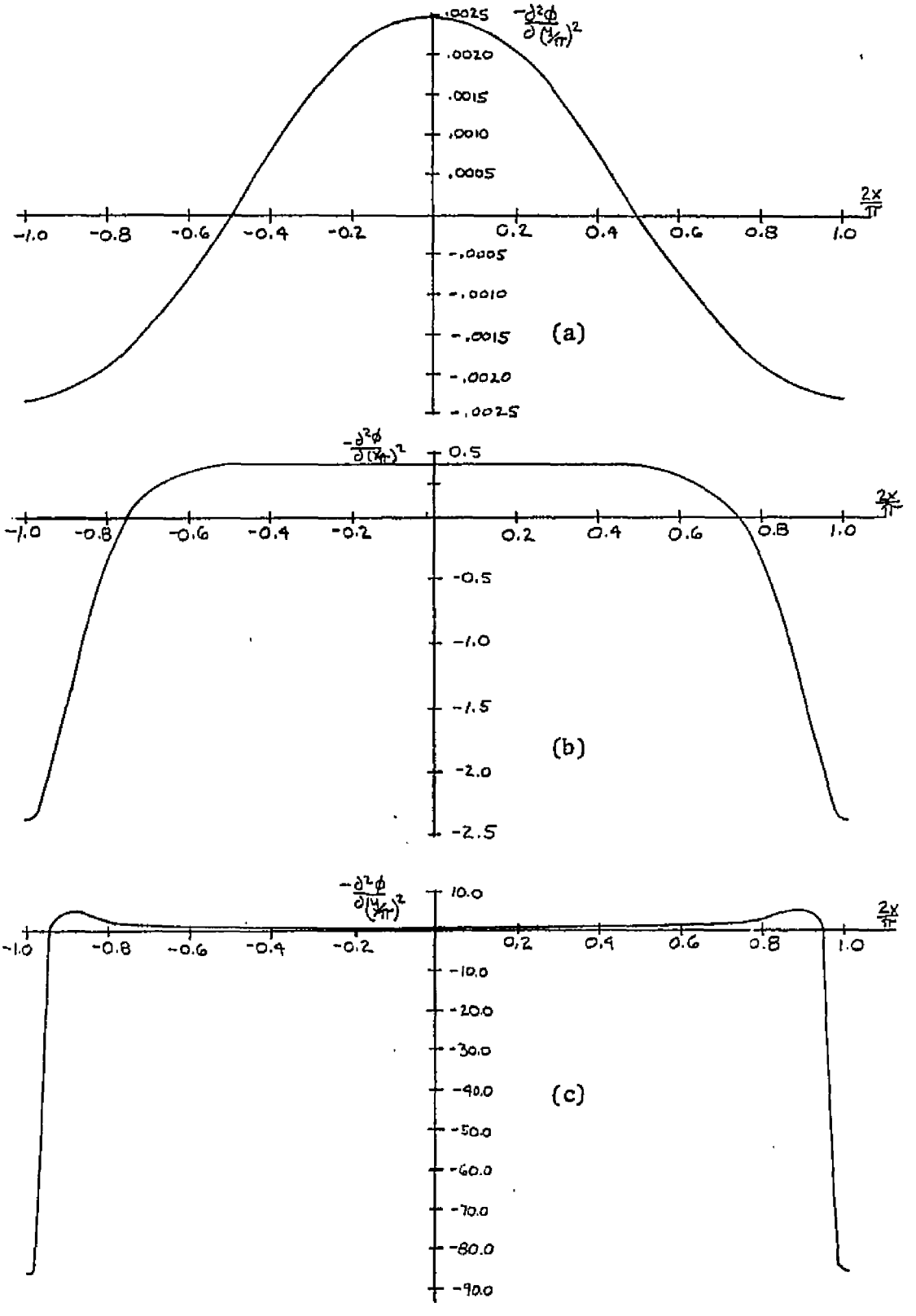

Fig. 3-16 $-\frac{\partial^2\phi}{\partial(\frac{y}{\pi})^2}$ versus $\frac{2x}{\pi}$; $\ell_1=\pi$, $\ell_2=3.08\pi$
a) $\frac{y}{\pi}=2.0$ b) $\frac{y}{\pi}=1.1$ c) $\frac{y}{\pi}=1.01$
(Note Change of Scale)

since $\frac{\partial\phi}{\partial x}(\pm\frac{\pi}{2},y)=0$ for $y>\ell_1$ is a given of the problem.* It is easily seen that

$$\lim_{\substack{y\to\ell_1\\ y>\ell_1}} \frac{\partial^2\phi}{\partial y^2}(\pm\tfrac{\pi}{2},y)=\infty$$

whereas,

$$\lim_{\substack{y\to\ell_1\\ y<\ell_1}} \frac{\partial^2\phi}{\partial y^2}(\pm\tfrac{\pi}{2},y)=0$$

The derivatives with respect to x also exhibit discontinuous behavior with the roles of $y<\ell_1$ or $y>\ell_1$ being reversed. For example,

$$\lim_{\substack{y\to\ell_1\\ y>\ell_1}} \frac{\partial\phi}{\partial x}(\pm\tfrac{\pi}{2},y)=0$$

and

$$\lim_{\substack{y\to\ell_1\\ y<\ell_1}} \left|\frac{\partial\phi}{\partial x}(\pm\tfrac{\pi}{2},y)\right|=\infty$$

3.6 Averages Over The Period

In consonance with the naming of regions in Chap. 2, we call, with respect to the exactly rectangular region of Fig. 3-1

Region I $\{x,y\}\ni$: $|x|<\frac{\pi}{2}$ and $\ell_1<y<\ell_2$

Region II $\{x,y\}\ni$: $|x|<\frac{\pi}{2}$ and $0<y<\ell_1$

Because of the different boundary conditions in the two regions a single eigenfunction expansion cannot hold for the entire rectangle and so we consider each region separately. We have†

---

* The interchange of order of differentiation is possible since $\phi(x,y)$ is the real or imaginary part of an analytic function for $x\neq\pm\frac{\pi}{2}$, $y>\ell_1$ and therefore the partial derivatives of $\phi(x,y)$ of all orders are continuous functions[57] of x and y. By virtue of this property, the interchange is possible.[58]

† The symmetry and boundary conditions fix the form of ϕ^{I} and ϕ^{II}. In the exact rectangle $\phi^{I}(x,\ell_2)=0$. Note the even and odd nature of the eigenvalues for regions I and II, respectively.

$$\phi^{I}(x,y) = a^{I}\left[1-\frac{y}{\ell_2}\right] + \sum_{m=1}^{\infty} C_m^{I} \cos 2mx \sinh 2m(y-\ell_2) \tag{3-65A}$$

$$\phi^{II}(x,y) = 1 + \sum_{m=1}^{\infty} C_m^{II} \cos(2m-1)x \sinh(2m-1)y \tag{3-65B}$$

Thus*

$$\overline{\phi^{I}}(y) \equiv \frac{1}{\pi}\int_{-\frac{\pi}{2}}^{\frac{\pi}{2}} \phi(x,y)dx = a^{I}\left[1-\frac{y}{\ell_2}\right] + \frac{1}{\pi}\sum_{m=1}^{\infty} C_m^{I} \sinh 2m(y-\ell_2)\int_{-\frac{\pi}{2}}^{\frac{\pi}{2}} \cos 2mx\,dx = a^{I}\left[1-\frac{y}{\ell_2}\right] \tag{3-66A}$$

$$\overline{\phi^{II}}(y) = \frac{1}{\pi}\int_{-\frac{\pi}{2}}^{\frac{\pi}{2}} \left\{1+\sum_{m=1}^{\infty} C_m^{II} \cos(2m-1)x \sinh(2m-1)y\right\} dx = 1+\frac{1}{\pi}\sum_{m=1}^{\infty} C_m^{II} \sinh(2m-1)y \int_{-\frac{\pi}{2}}^{\frac{\pi}{2}} \cos(2m-1)x\,dx = 1+\frac{1}{\pi}\sum_{m=1}^{\infty} \frac{(-1)^{m-1}}{m-\frac{1}{2}} C_m^{II} \sinh(2m-1)y \tag{3-66B}$$

$\overline{\phi}(y)$ is shown for $\ell_1=\pi$, $\ell_2=3.08\pi$ using the solution 3-34 in Fig. 3-17. Note that $\overline{\phi^{I}}(y)$ is linear while $\overline{\phi^{II}}(y)$ is not, as found in Eqs. 3-66. The slope of the linear portion, $-\frac{a^{I}}{\ell_2}$, is equivalent to the asymptotic value of Fig. 3-14. We have†

$$\overline{\frac{\partial \phi}{\partial y}}(y) = \frac{1}{\pi}\lim_{a\to\frac{\pi}{2}}\int_{-a}^{a} \frac{\partial \phi}{\partial y}(x,y)dx = \frac{d}{dy}\overline{\phi}(y) \tag{3-67}$$

---

* The interchange of summation and integration in 3-66A and B is possible since[59] if a function f is piecewise continuous on its period then the Fourier series corresponding to f may be integrated term by term to obtain the integral of f, whether or not the Fourier series corresponding to f converges or not. We know that ϕ is continuous therefore the order may be reversed.

†The interchange of differentiation and integration is permissible under conditions of the Leibniz rule.[60] To satisfy these conditions we must have that $\phi(x,y)$ be an integrable function of x for each value of y and that $\frac{\partial \phi}{\partial y}(x,y)$ exists and is a continuous function of x and y in a rectangle formed by $-a \le x \le a$, and y bounded by the interval of interest. $\phi(x,y)$ is integrable in the above sense since it is continuous.[61] In regions I and II separately $\frac{\partial \phi(x,y)}{\partial y}$ exists and is continuous. That is, the points $x=\pm\frac{\pi}{2}$, $y=\ell_1$ are avoided since they lie on the common boundary of the two regions. As was shown previously $\frac{\partial \phi}{\partial y}(x,y)$ does not exist at those points.

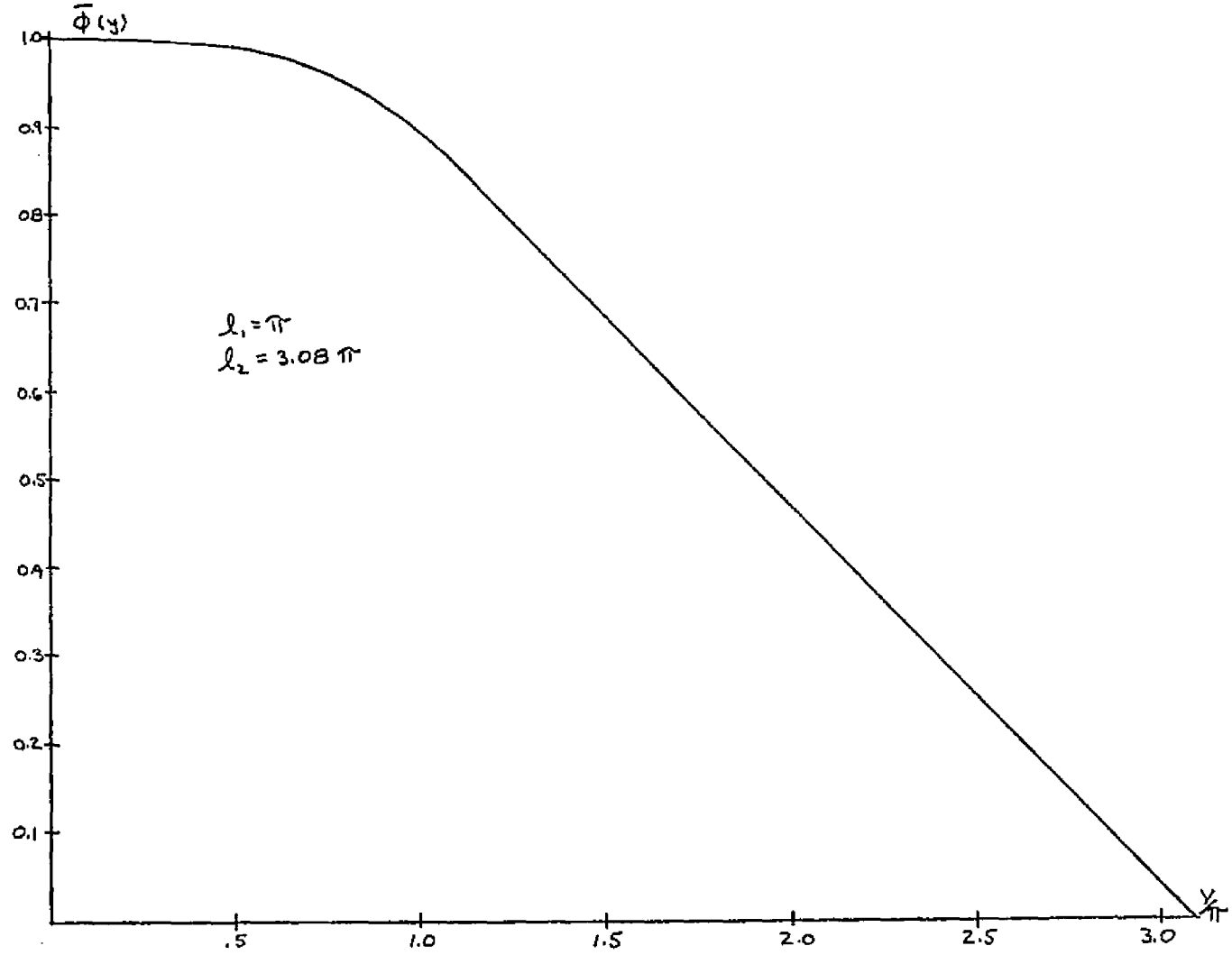

Fig. 3-17 Average Potential

$\overline{\frac{\partial\phi}{\partial y}}$ is continuous across the common boundary, $y=\ell_1$. This is true since $\frac{\partial\phi}{\partial y}$ is continuous across the boundary as long as the end points, $x=\pm\frac{\pi}{2}$, are excluded, so that $\int_{-a}^{a}\frac{\partial\phi}{\partial y}dx$ is the same for both sides of the boundary for $a<\frac{\pi}{2}$. For the remaining parts of the integral, between $-\frac{\pi}{2}$ and -a and between a and $\frac{\pi}{2}$, we have shown earlier that both $\frac{\partial\phi}{\partial y}$ and $\frac{\partial\phi}{\partial x}$ vary approximately as $(\frac{\pi}{2}+x)^{-\frac{1}{2}}$ and as $(\frac{\pi}{2}-x)^{-\frac{1}{2}}$ near the left and right teeth, respectively. We make the substitution $\varsigma=\frac{\pi}{2}+x$ in the first case and $\varsigma=\frac{\pi}{2}-x$ in the second to obtain an approximate integral

$$\int_0^{\frac{\pi}{2}-a}\varsigma^{-\frac{1}{2}}d\varsigma$$

for the parts left of the original integral. Now,

$$\int_0^{b}\varsigma^{-\frac{1}{2}}d\varsigma$$

is an improper integral but is convergent.[62] Thus,

$$\lim_{a\to\frac{\pi}{2}} \int_0^{\frac{\pi}{2}-a} y^{-\frac{1}{2}}\,dy = 0$$

so that $\frac{\partial\phi}{\partial y}$ and $\frac{\partial\phi}{\partial x}$ are continuous across the boundary. We have also proved that $\frac{\partial\phi}{\partial y}$ and $\frac{\partial\phi}{\partial x}$ are bounded at $y=\ell_1$ since the integrals of the parts of the functions which become unbounded go to zero as the interval of integration approaches zero. We have by virtue of the periodicity of $\phi(x,y)$

$$\overline{\frac{\partial\phi}{\partial x}}(y) \equiv \frac{1}{\pi}\int_{-\frac{\pi}{2}}^{\frac{\pi}{2}} \frac{\partial\phi}{\partial x}(x,y)\,dx = \frac{1}{\pi}\left[\phi(\tfrac{\pi}{2},y) - \phi(-\tfrac{\pi}{2},y)\right] = 0 \qquad (3\text{-}68)$$

In Fig. 3-18 $\overline{\frac{\partial\phi}{\partial y}}$ is presented as found from 3-61F. Now,

$$\frac{d}{dy}\overline{\frac{\partial\phi}{\partial y}}(y) = \overline{\frac{\partial^2\phi}{\partial y^2}}(y) \equiv \frac{1}{\pi}\lim_{a\to\frac{\pi}{2}}\int_{-a}^{a}\frac{\partial^2\phi}{\partial y^2}(x,y)\,dx = -\frac{1}{\pi}\lim_{a\to\frac{\pi}{2}}\int_{-a}^{a}\frac{\partial^2\phi}{\partial x^2}(x,y)\,dx = -\overline{\frac{\partial^2\phi}{\partial x^2}}(y)$$

$$= -\frac{1}{\pi}\lim_{a\to\frac{\pi}{2}}\left[\frac{\partial\phi}{\partial x}(a,y) - \frac{\partial\phi}{\partial x}(-a,y)\right] = -\frac{2}{\pi}\lim_{a\to\frac{\pi}{2}}\frac{\partial\phi}{\partial x}(a,y) = -\frac{2}{\pi}\frac{\partial\phi}{\partial x}(\tfrac{\pi}{2},y) \qquad (3\text{-}69)$$

where the interchange of integration and differentiation is permissible by reasoning similar to that used above and where $\nabla^2\phi=0$ for $a<\frac{\pi}{2}$. In region I, $\frac{\partial\phi}{\partial x}(\frac{\pi}{2}, y)=0$ because of the boundary conditions and therefore the slope of Fig. 3-18 is zero for $y>\ell_1$. As $y\to\ell_1$ in region II, $\frac{\partial\phi}{\partial x}(\frac{\pi}{2},y)$ approaches infinity and therefore the slope of Fig. 3-18 approaches infinity for $y\to\ell_1$. Thus Fig. 3-18 has a 90° corner at $y=\ell_1$.

$$\overline{\frac{\partial^2\phi}{\partial y^2}}(y) = -\overline{\frac{\partial^2\phi}{\partial x^2}}(y) = 0, \quad y>\ell_1 \qquad (3\text{-}70A)$$

$$\overline{\frac{\partial^2\phi}{\partial y^2}}(y) = -\overline{\frac{\partial^2\phi}{\partial x^2}}(y) = -\frac{2}{\pi}\frac{\partial\phi}{\partial x}(\tfrac{\pi}{2},y), \quad 0<y<\ell_1 \qquad (3\text{-}70B)$$

Observe in Fig. 3-16 that as $y\to\ell_1$ the zeros of $-\frac{\partial^2\phi}{\partial y^2}$ move towards $\pm\frac{\pi}{2}$. In view of 3-70A, for $y\to\ell_1$, the area under the relatively narrow portion of the curve between the zero and $\frac{\pi}{2}$ must equal the area under the broad portion between x=0 and the zero. In the limit the portions of $\frac{\partial^2\phi}{\partial y^2}$ between the zeros and $\pm\frac{\pi}{2}$ approach δ functions since the integral under these portions is finite although the interval of integration vanishes in the limit.

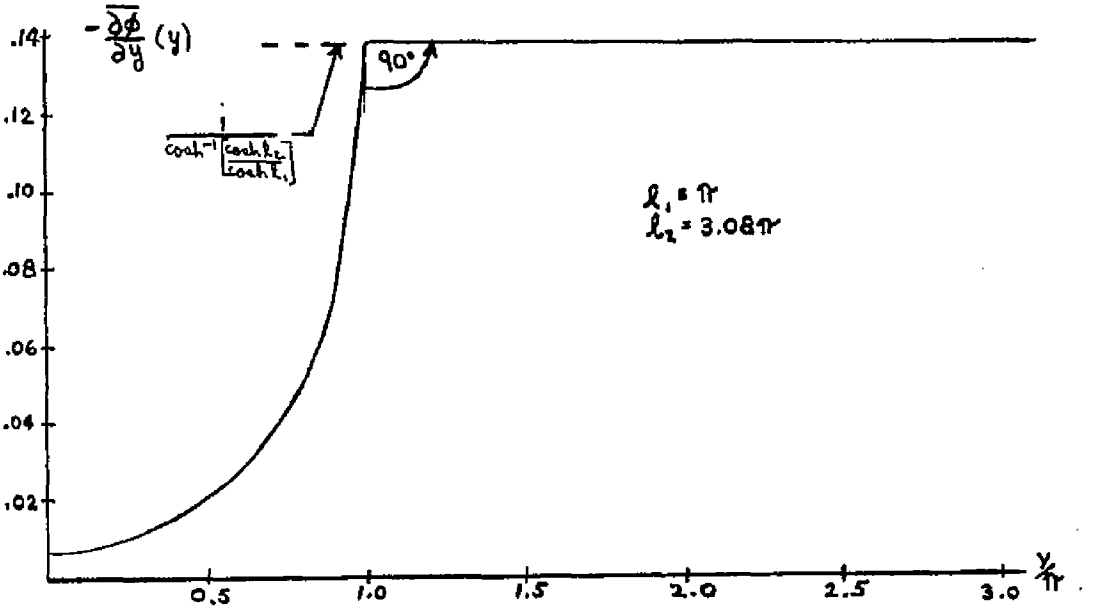

Fig. 3-18 Average Derivative

3.7 Limits of Validity of the Solution

It was noted previously that the dimensions of the structure consistent with the electrodynamic solution are such that the solution presented for $\Phi(x,y)$ is an excellent approximation. That is, not only is the zero tooth width limit in agreement with lower velocity but we have that the gap g is about twice the period L, a favorable situation. The question is asked as to the range of geometries for which 3-34 is an accuarate approximation. One therefore asks how small the dimension ℓ_2 may be made for any given ℓ_1 such that the approximate upper boundary has less than a given allowable perturbation, $\delta = \ell_2 - \ell_3$, as given in 3-25. It may easily be shown that δ is bounded by 0 and ℓ_1, with the upper limit occurring for $\ell_1 = \ell_2$. From 3-25 we have

$$\sinh(\ell_2 - \delta) = \pm\sqrt{\cosh^2 \ell_2 - \cosh^2 \ell_1}$$

where the positive sign is appropriate since $0 < \delta < \ell_2$. This equation is equivalent to a quadratic equation in cosh $2\ell_2$, viz.,

$$\cosh^2 2\ell_2 + [1 - \cosh 2\ell_1]\cosh 2\ell_2 + \frac{1}{2}\frac{(1-\cosh 2\ell_1)^2 + \sinh^2 2\delta}{1-\cosh 2\delta} = 0 \quad (3\text{-}71A)$$

whose solution is

$$\cosh 2\ell_2 = \sinh^2\ell_1\left\{1 \pm \sqrt{1+\frac{1}{\sinh^2\delta}+\frac{\cosh^2\delta}{\sinh^4\ell_1}}\right\} \qquad (3\text{-}71B)$$

It may easily be seen that the positive sign is the correct choice. Thus,

$$\ell_2 = \tfrac{1}{2}\cosh^{-1}\left\{\sinh^2\ell_1\left[1+\sqrt{1+\frac{1}{\sinh^2\delta}+\frac{\cosh^2\delta}{\sinh^4\ell_1}}\right]\right\} \qquad (3\text{-}72)$$

The solutions are presented on logarithmic scales in Fig. 3-19. The physical limit of the solution, for $\ell_1=\ell_2=\delta$, is shown and it is seen that in the physical range δ increases for decreasing ℓ_2. For sufficiently small δ *

$$\ell_2 \approx \tfrac{1}{2}\cosh^{-1}\left[\frac{\sinh^2\ell_1}{\sinh\delta}\right] \approx \tfrac{1}{2}\cosh^{-1}\left[\frac{\sinh^2\ell_1}{\delta}\right] = \tfrac{1}{2}\ln\left\{\frac{\sinh^2\ell_1}{\delta}+\sqrt{\left(\frac{\sinh^2\ell_1}{\delta}\right)^2-1}\right\}$$

$$\approx \tfrac{1}{2}\ln\left[\frac{2\sinh^2\ell_1}{\delta}\right] = \ln\sqrt{2}+\ln[\sinh\ell_1]-\ln\sqrt{\delta} \qquad (3\text{-}73)$$

If, in addition, ℓ_1 is large, $\ln[\sinh\ell_1]\approx\ln[\frac{1}{2}]+\ell_1$ so that

$$\ell_2 \approx \ell_1 - \ln\sqrt{2} - \ln\sqrt{\delta} \qquad (3\text{-}74)$$

The above and Fig. 3-19 may be used as indications as to whether a particular geometry may be adequately described by the solution $\phi(x,y)$ presented.

3.8 Fourier Expansion of the Solution

We write the solution 3-34 as

$$\phi(x,y) \equiv 1 - \psi(x,y) \qquad (3\text{-}75)$$

---

* For $\ell_1=\pi$ and $\ell_2=3.08\pi$ we find $\delta\approx 10^{-6}$

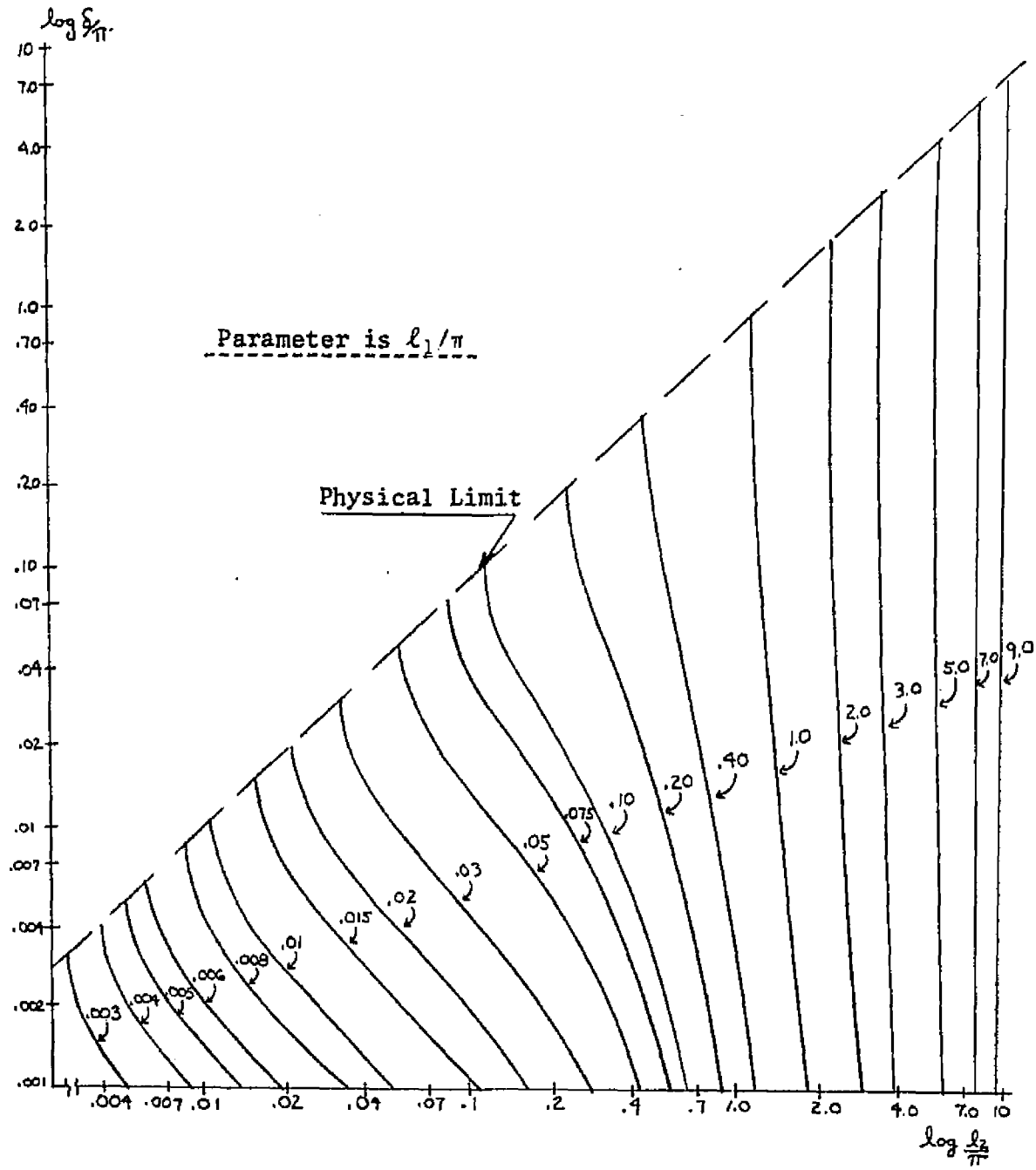

Fig. 3-19 Limit of Validity of Solution

and note that the ratio of the n^{th} harmonic of the Fourier expansion of $\Psi(x,y)$ to the average value of $\Psi(x,y)$ is independent of ℓ_2. We have from 3-65A that for region I

$$\Psi^I(x,y) = 1 - \phi^I(x,y) = 1 - a^I\left[1 - \frac{y}{\ell_2}\right] - \sum_{m=1}^{\infty} C_m^I \cos 2mx \sinh 2m(y-\ell_2) \quad (3\text{-}76)$$

so that

$$- \frac{C_n^I \sinh 2n(y-\ell_2)}{1 - a^I\left[1 - \frac{y}{\ell_2}\right]} \quad (3\text{-}77)$$

must be independent of ℓ_2. This is only possible through the dependence of the Cn^I and a^I upon ℓ_2. This conclusion is drawn subject to the limits of the approximate nature of the solution, 3-34. That is, 3-76 holds for the exact rectangle while 3-34 holds for the approximate one. We set y to be a fixed value away from the plane of the tooth edges, $y=\ell_1$, and compare the normalized spectrum, Eq. 3-77, for different values of $\frac{\ell_1}{\pi}$. The result for $\frac{y-\ell_1}{\pi}=.1$, $1 \leq n \leq 4$, is shown on a logarithmic scale in Fig. 3-20. We note that the harmonics become more important as ℓ_1 increases, with the insensitivity to ℓ_1 taking place near the square slot condition.

3.9 Solution in Another Geometry

The solution which has heretofore been presented has been for the geometry where ℓ_2 cannot be allowed to approach ℓ_1 too closely, as indicated in Sec. 3.7. Suppose the problem involved finding the solution in a configuration where this was violated. For the sake of completeness we indicate a method of solution for a geometry where we have approximately $\ell_1 > \pi$ and ℓ_2 is too small to use the above solution. The geometry is shown in Fig. 3-21a, where the base rectangle has been inverted from that of Fig. 3-1. Since $\ell_1 > \pi$ we may remove the top of the rectangle as in Fig. 3-21b. We next map this inverted case onto the half-plane as was done in the original solution to obtain Fig. 3-21c. By a simple contraction we transform to Fig. 3-21d. Finally we map back to the half-strip in Fig. 3-21e. The geometry of Fig. 3-21e has been solved in connection with a problem in microwave integrated circuits by a rather complex series of transformations.[63] That solution may be applied here.

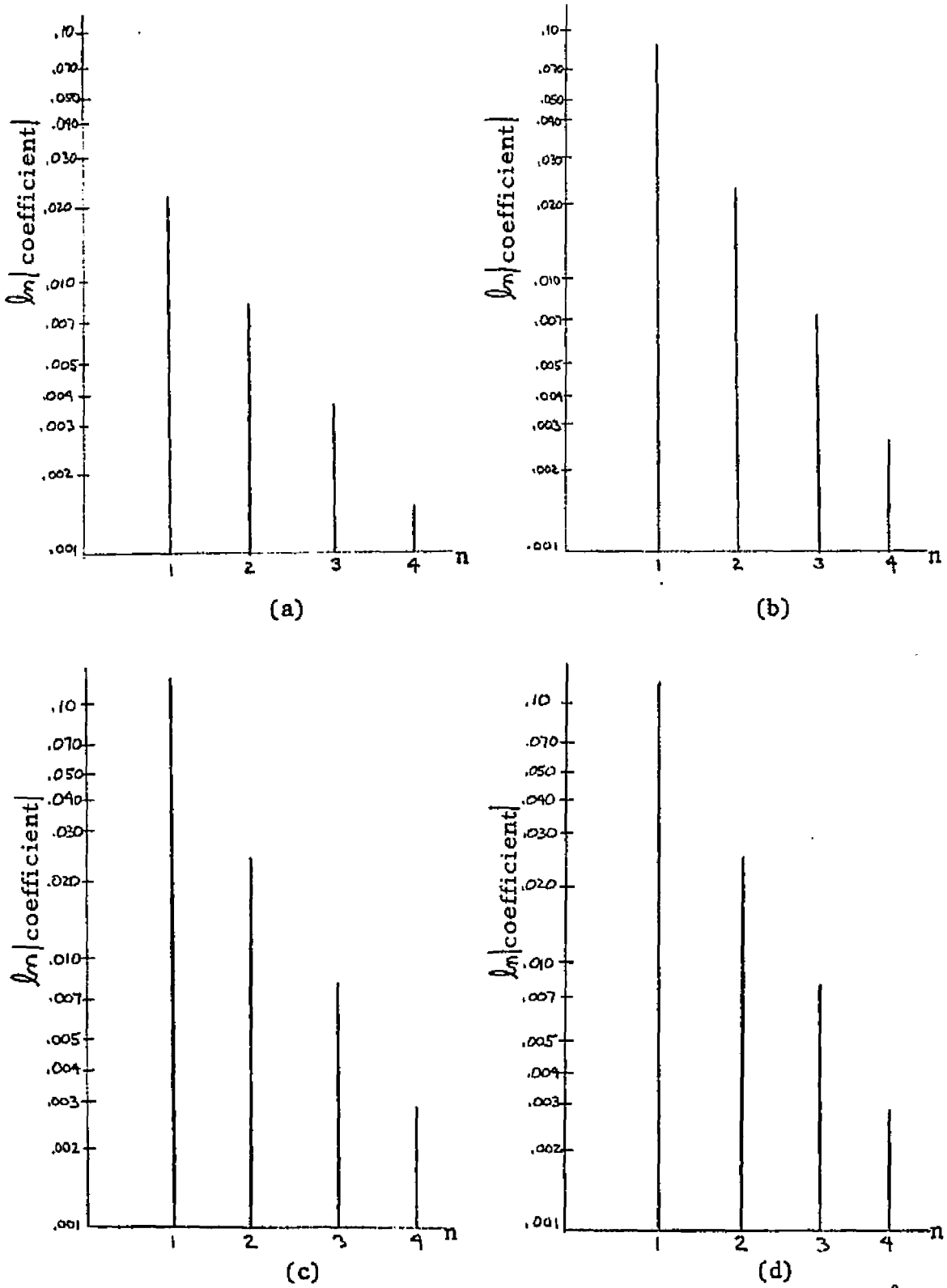

Fig. 3-20 Normalized Fourier Expansion of $\psi(x,y)=1-\phi(x,y)$, $\frac{y-\ell_1}{\pi}=.1$
(a) $\ell_1=.05\pi$ (b) $\ell_1=0.2\pi$ (c) $\ell_1=0.6\pi$ (d) $\ell_1=\pi$

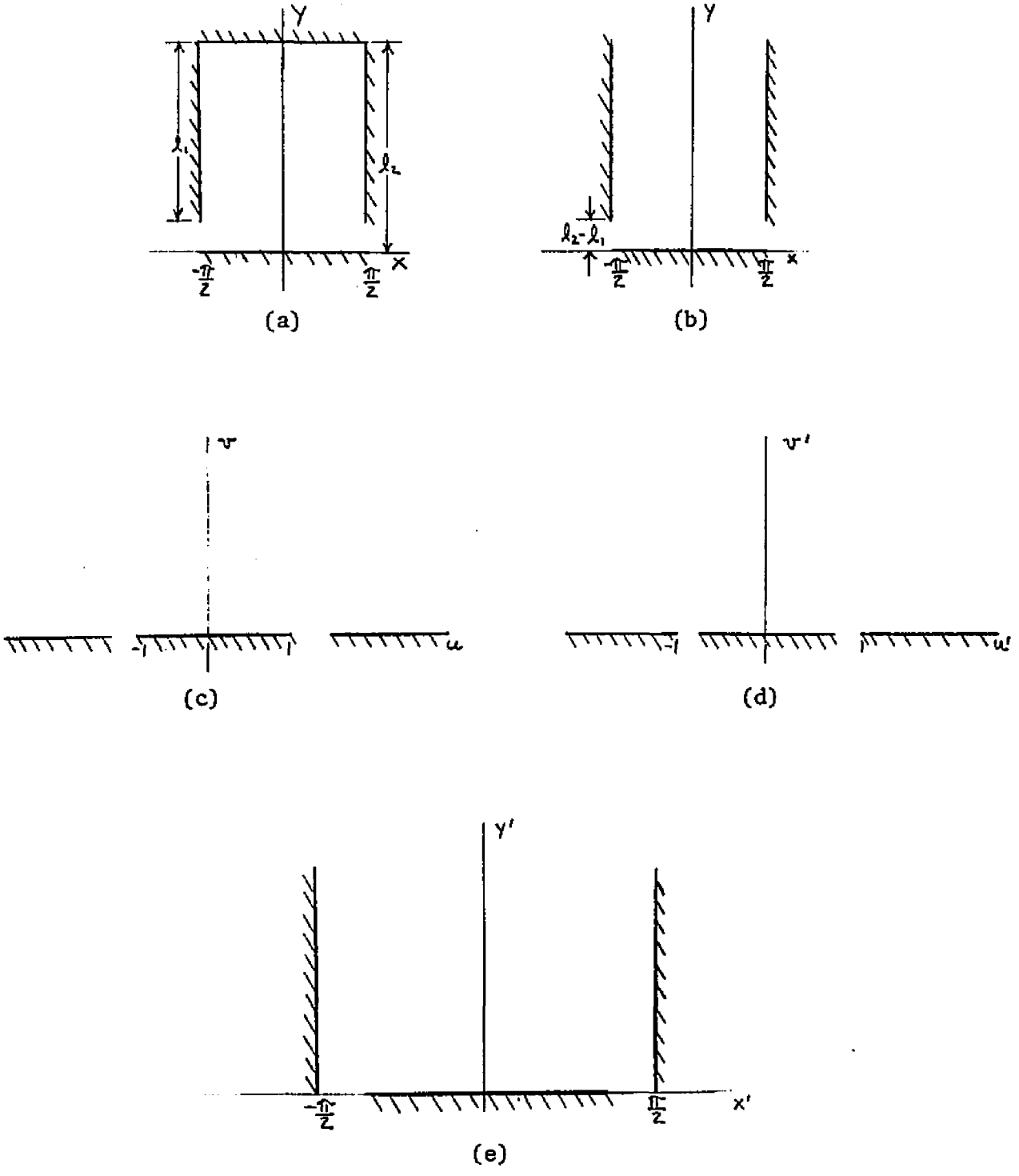

Fig. 3-21 Another Rectangular Configuration

CHAPTER 4

ELECTRON DYNAMICS FOR THE STATIC FIELD CASE

4.1 The Equations of Motion

We consider, in this chapter, the dynamics of the electron motion in the presence of static fields only. These static fields are produced by application of different potentials to the inner and outer boundaries of the slow wave circuit. Electrons are assumed to be injected into this region by an electron gun which accelerates them from a unipotential cathode. Part of the energy is in the form of rotational energy and we do not focus our attention on how this is accomplished. We further assume that all electrons have the same longitudinal velocity so that they are all synchronous with the chosen space harmonic of the rf wave. We will consider to some extent the interaction of the electrons with each other in the form of space charge forces but most of our attention will focus on the space charge free case where the electrons move independently of each other. With regard to the boundaries we will consider two cases. The first involves taking the inner boundary as smooth so that in effect we reduce the problem to one in the plane since $\frac{\partial}{\partial z}=0$. The second considers the effects of the corrugated inner boundary which is necessary to produce the slow waves. For this case, in which $\frac{\partial}{\partial z}\neq 0$, we consider a zero thickness beam of noninteracting electrons for simplicity. The kinetic energy for an electron in cylindrical coordinates, and the potential energy ignoring magnetic forces*, are

$$T = \tfrac{1}{2}m\left(\dot{r}^2 + r^2\dot{\theta}^2 + \dot{z}^2\right) \tag{4-1A}$$

$$V = q\phi = -e\phi \tag{4-1B}$$

where ϕ is the electrostatic potential of Chap. 3, suitably scaled and

---

*Magnetic forces may arise only due to electron-electron interactions in this case, and are small.

adjusted to cylindrical coordinates. The Lagrangian[64] is therefore

$$\mathcal{L} = T - V = \sum_{k=1}^{N} \left[\tfrac{1}{2} m \left(\dot{r}_k^2 + r_k^2 \dot{\theta}_k^2 + \dot{z}_k^2 \right) + e\phi(\bar{r}_k) \right] \tag{4-2A}$$

The equations of motion are contained in the formulation

$$\frac{d}{dt}\left[\frac{\partial \mathcal{L}}{\partial \dot{q}_i}\right] - \frac{\partial \mathcal{L}}{\partial q_i} = 0 \tag{4-2B}$$

where the generalized coordinates q_j, q_{j+1}, q_{j+2} are r_m, θ_m, z_m, the cylindrical coordinates of the m^{th} electron. For N electrons, the system has 3N degrees of freedom, 3N differential equations of second order from 4-2B, and therefore 6N constants. From 4-1A, T is θ-independent. Because the boundaries are axially symmetric, V is also independent of θ. The coordinate θ does not appear in the Lagrangian, θ is a cyclic coordinate,[65] and the canonical or generalized momentum conjugate to θ is conserved. The system is invariant under rotation about the z axis. Thus,

$$p_\theta = \frac{\partial \mathcal{L}}{\partial \dot{\theta}} = mr^2\dot{\theta} = \text{constant} \equiv \mathcal{l} \tag{4-3}$$

conservation of angular momentum, which may be used to formally remove the coordinate θ from the problem.

It is easily shown[66] that for a conservative system where the force is derived from a scalar velocity independent potential and where the constraints are time independent, the Hamiltonian

$$H = \sum_{j=1}^{3N} \dot{q}_j \frac{\partial \mathcal{L}}{\partial \dot{q}_j} - \mathcal{L} \tag{4-4A}$$

is conserved and further that the Hamiltonian is the total energy.

$$H = T + V = \text{constant} \tag{4-4B}$$

Application of Eqs. 4-2 for q=r, and 4-3, yields

$$m\ddot{r} - mr\dot{\theta}^2 = m\ddot{r} - \frac{\mathcal{l}^2}{mr^3} = e\frac{\partial \phi}{\partial r} \tag{4-5}$$

Finally, from Eqs. 4-2 with q=z,

$$m\ddot{z} = e\frac{\partial \phi}{\partial z} \tag{4-6}$$

From 4-3 and 4-4B

$$H = \tfrac{1}{2}m\left[\dot{r}^2 + \dot{z}^2\right] + \frac{1}{2}\frac{l^2}{mr^2} - e\phi = \text{constant} \tag{4-7}$$

Observe from 4-7 that the problem has been reduced to one in the two variables r and z provided that we define a new potential energy

$$V' = \frac{1}{2}\frac{l^2}{mr^2} - e\phi \tag{4-8}$$

Part One--Smooth Inner Boundary

4.2 Stability Condition

The case of smooth inner boundary implies $\frac{\partial}{\partial z}=0$ and we obtain from 4-6

$$z = z_0 + v_{oz}t \tag{4-9}$$

where v_{oz} is the constant axial velocity of the electrons. The equivalent force, $-\frac{\partial V'}{\partial r}$, found from 4-8, is zero for an electron at equilibrium for all z. The motion is helical, or as viewed in cross section, circular.

At the equilibrium radius, r_0, we find the required angular momentum necessary to make the equivalent force zero.

$$l^2 = -em\frac{\partial \phi}{\partial r}(r_0)r_0^3 = em E_r(r_0)r_0^3 \tag{4-10}$$

Then, from 4-5

$$\ddot{r} = \eta\left[E_r(r_0)\left[\frac{r_0}{r}\right]^3 - E_r(r)\right] \tag{4-11A}$$

$$\eta = \frac{e}{m} \tag{4-11B}$$

Taking variations of radius about r_0 defined by

$$\delta \equiv r - r_0 \tag{4-12}$$

we expand E_r abour r_0 in a Taylor series, which is assumed to converge.

$$E_r(r) = E_r(r_0) + \frac{dE_r}{dr}(r_0)\,\delta + \frac{d^2E_r}{dr^2}\frac{\delta^2}{2} + \cdots \tag{4-13}$$

Now,[67]

$$E_r(r_0)\left(\frac{r_0}{r}\right)^3 = \frac{E_r(r_0)}{\left[1+\frac{\delta}{r_0}\right]^3} = E_r(r_0)\left[1 - 3\frac{\delta}{r_0} + 6\left(\frac{\delta}{r_0}\right)^2 - \cdots\right], \quad \left|\frac{\delta}{r_0}\right| < 1 \tag{4-14}$$

Thus, from 4-11A, for sufficiently small $\left|\frac{\delta}{r_0}\right|$,

$$\ddot{\delta} = -\eta\left[\left(3\frac{E_r(r_0)}{r_0} + \frac{dE_r}{dr}(r_0)\right)\delta - \left(6\frac{E_r(r_0)}{r_0^2} - \frac{1}{2}\frac{d^2E_r}{dr^2}(r_0)\right)\delta^2 + \cdots\right] \tag{4-15}$$

An approximate differential equation for small $\left|\frac{\delta}{r_0}\right|$ is therefore

$$\ddot{\delta} + \eta\left[3\frac{E_r(r_0)}{r_0} + \frac{dE_r}{dr}(r_0)\right]\delta \equiv \ddot{\delta} + \Omega\delta \approx 0 \tag{4-16}$$

The solutions of 4-16 are bounded for $\Omega > 0$ and unbounded for $\Omega < 0$. The transitional solution, of form a+bt, for $\Omega = 0$, may be of either type, but the next higher term in the differential equation, 4-15, must be considered for a meaningful result. We may state the stability criterion as the requirement

$$\Omega > 0 \tag{4-17}$$

with $\Omega = 0$ requiring further investigation for the particular case. A requirement of the form of 4-17 has been given previously.[68]

4.3 Preliminary Considerations for a Single Electron

Consider the geometry shown in Fig. 4-1. It is easily shown that

$$\phi = \phi_1 + \frac{\phi_2 - \phi_1}{\ln \frac{r_2}{r_1}} \ln \frac{r}{r_1}, \qquad r_1 < r < r_2 \tag{4-18A}$$

$$E_r = -\frac{\partial \phi}{\partial r} = \frac{\phi_1 - \phi_2}{\ln \frac{r_2}{r_1}} \frac{1}{r} \tag{4-18B}$$

From 4-10 and 4-18B it is obvious that $\phi_1 > \phi_2$. We find* for Ω of 4-16

$$\Omega = \frac{2\eta}{r_0^2} \frac{\phi_1 - \phi_2}{\ln \frac{r_2}{r_1}} \tag{4-19}$$

For $\phi_1 > \phi_2$, $\Omega > 0$, and therefore by criterion 4-17 we are assured that a single electron will be stable. If the electron originated at a cathode at potential ϕ_c we have that the energy of the electron is, from 4-7,

$$H = -e\phi_c \tag{4-20}$$

The potential equivalent of the longitudianl energy is written as in Eq. 2-8A, a constant for the smooth inner boundary case. From 4-7 and 4-18A

$$\dot{r}^2 = 2\eta\left[\phi_1 - \phi_c - \phi_3 - \frac{\phi_1 - \phi_2}{\ln \frac{r_2}{r_1}} \ln \frac{r}{r_1}\right] - \frac{l^2}{m^2 r^2} \tag{4-21}$$

The right-hand side of 4-21 is never negative and the points where equality to zero occurs correspond to the turning points, or apsidal radii, considered in Sec. 4.7. Either $\dot{r}=0$ identically, corresponding to helical motion; or there are two roots corresponding to $\dot{r}^2=0$, no matter what the choice of parameters in 4-21. The motion is constrained between two cylinders, therefore bounded. This is contrasted with motion in a gravitational field[70] where the solution for the orbit is a conic section and may be a circle, ellipse, parabola or hyperbola. The first two are bounded motions while the second two are unbounded, the solution depending upon the energy of the particle. While it has been shown that for a single electron the orbit is bounded this is not enough assurance that there will be no electron interception on the walls of the structure.

---

* Showing the convergence of 4-13 here is equivalent to showing that the series for $\left[1 + \frac{\delta}{r_0}\right]^{-1}$ converges, which it does[69] for $\left|\frac{\delta}{r_0}\right| < 1$.

For example, in Fig. 4-1 we must determine that the turning points lie in the range (r_1, r_2).

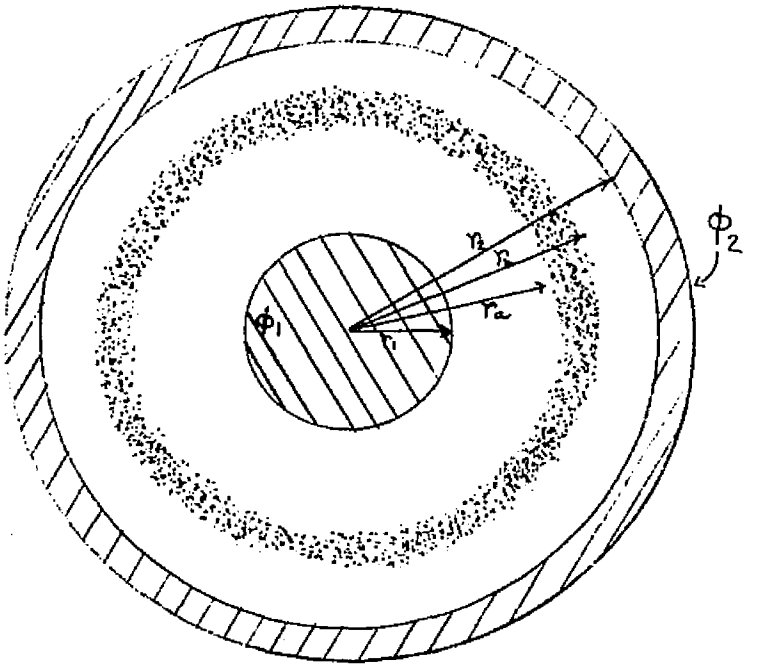

Fig. 4-1 Cross Section of the Beam-Boundary System (Smooth Inner Boundary)

4.4 Finite Space Charge--Required Density

We now inquire into the question of maintaining a beam of electrons in equilibrium in the geometry of Fig. 4-1, the electrons interacting through space charge forces. This is known[71] as Harris flow. We require all electrons to have the same translational velocity and require all electrons be in equilibrium and describe helical orbits. For equilibrium we have from 4-5, 4-7, and 4-20 the differential equation and solution for ϕ inside the beam

$$\frac{d\phi}{dr} + \frac{2}{r}\left[\phi - \phi_c - \phi_z\right] = 0, \quad r_a \le r \le r_b \tag{4-22A}$$

$$\phi = \frac{\kappa}{r^2} + \phi_c + \phi_z, \quad r_a \le r \le r_b \tag{4-22B}$$

Observe that there is no logarithmic term present in 4-22B so that care must be taken with the selection of boundary potentials, ϕ_1 and ϕ_2, such that

such a term is not introduced into the solution. From Poisson's equation in cylindrical coordinates, with $\frac{\partial}{\partial\theta}=\frac{\partial}{\partial z}=0$, viz.,

$$\nabla^2\phi = \frac{1}{r}\frac{\partial}{\partial r}\left[r\frac{\partial\phi}{\partial r}\right] = -\frac{\rho}{\epsilon} \tag{4-23A}$$

we have using 4-22B

$$\rho = -\frac{4K\epsilon}{r^4} \equiv \rho_o\frac{r_o^4}{r^4} \tag{4-23B}$$

as is known for Harris flow. We have,

$$\phi = \phi_c + \phi_z - \frac{\rho_o r_o^4}{4\epsilon}\frac{1}{r^2}\,, \quad r_a \le r \le r_b \tag{4-24A}$$

$$E_r = -\frac{\partial\phi}{\partial r} = -\frac{\rho_o r_o^4}{2\epsilon}\frac{1}{r^3}\,, \quad r_a \le r \le r_b \tag{4-24B}$$

For the beam-free regions, $r_1 < r < r_a$ and $r_b < r < r_2$, we have solutions similar to Eqs. 4-18. We require that ϕ and E_r be continuous at r_a and r_b. This yields for the beam-free regions

$$\phi = \phi_c + \phi_z - \frac{\rho_o r_o^4}{4\epsilon}\frac{1}{r_a^2}\left[1+\ln r_a^2\right] + \frac{\rho_o r_o^4}{2\epsilon}\frac{1}{r_a^2}\ln r, \quad r_1 < r < r_a \tag{4-25A}$$

$$\phi = \phi_c + \phi_z - \frac{\rho_o r_o^4}{4\epsilon}\frac{1}{r_b^2}\left[1+\ln r_b^2\right] + \frac{\rho_o r_o^4}{2\epsilon}\frac{1}{r_b^2}\ln r, \quad r_b < r < r_2 \tag{4-25B}$$

We have then the boundary potentials required to yield the desired situation.

$$\phi_1 = \phi_c + \phi_z - \frac{\rho_o r_o^4}{4\epsilon}\frac{1}{r_a^2}\left[1+\ln\frac{r_a^2}{r_1^2}\right] \tag{4-26A}$$

$$\phi_2 = \phi_c + \phi_z - \frac{\rho_o r_o^4}{4\epsilon}\frac{1}{r_b^2}\left[1-\ln\frac{r_2^2}{r_b^2}\right] \tag{4-26B}$$

The total current through the cross section is, from 4-23B and 4-26A,

$$I = \int_{r_a}^{r_b} 2\pi\rho v_z r\,dr = \pi r_o^4\rho_o\sqrt{2\eta}\,\phi_z^{1/2}\left[\frac{1}{r_a^2}-\frac{1}{r_b^2}\right] = \pi r_o^4\rho_o\sqrt{2\eta}\left[\phi_1-\phi_c+\frac{\rho_o r_o^4}{4\epsilon}\frac{1}{r_a^2}\left(1+\ln\frac{r_a^2}{r_1^2}\right)\right]^{1/2}\left[\frac{1}{r_a^2}-\frac{1}{r_b^2}\right] \tag{4-27}$$

If the geometry and the potentials ϕ_1 and ϕ_c are kept fixed, consider the

problem of maximizing the current as $\rho_0 < 0$ is varied. From $\frac{\partial I}{\partial \rho_0}=0$ we obtain the value of ρ_0 leading to a maximum. With this value we find

$$I_{max} = -4\pi\epsilon\sqrt{\eta}\left[\frac{2}{3}\right]^{3/2} \frac{1-\left[\frac{r_a}{r_b}\right]^2}{1+\ln\left[\frac{r_a}{r_1}\right]^2} \left[\phi_1 - \phi_c\right]^{3/2} \tag{4-28}$$

where the negative sign refers to electron current. We may define a perveance,[72] and find

$$I \equiv P_{1c}\left[\phi_1 - \phi_c\right]^{3/2} \approx -25.4 \times 10^{-6} \frac{1-\left[\frac{r_a}{r_b}\right]^2}{1+\ln\left[\frac{r_a}{r_1}\right]^2} \tag{4-29}$$

The maximum value of P_{1c} occurs when the beam completely fills the space. Then,

$$P_{1c} \longrightarrow -25.4\times10^{-6}\left[1-\left(\frac{r_1}{r_2}\right)^2\right] \tag{4-30}$$

As $\frac{r_2}{r_1}\to\infty$, P_{1c} approaches the maximum value of -25.4 10^{-6}, the maximum perveance for a Brillouin focused beam.[73] Consider an electron within the beam at radius r_e. We have, from 4-11A and 4-24B using the notation r_e in place of r_0 to avoid confusion

$$\ddot{r} = \eta\left[E_r(r_e)\left[\frac{r_e}{r}\right]^3 - E_r(r)\right] = \eta\left[-\frac{\rho_0 r_0^4}{2\epsilon}\frac{1}{r^3} + \frac{\rho_0 r_0^4}{2\epsilon}\frac{1}{r^3}\right] = 0 \tag{4-31A}$$

Therefore Ω of 4-16, and indeed, all the coefficients of the power series in δ of 4-15 are identically zero. Thus, from 4-31

$$r = r_e + \dot{r}(0)\,t \tag{4-31B}$$

The consequences of 4-31B are clear. An electron within the beam which has no initial radial velocity will remain at its radius, r_e, for all time. However, an electron given a vanishingly small, but nonzero, radial velocity will continue to move unrestricted through the beam at constant radial velocity. We have postulated that a single electron is perturbed and therefore we have taken E_r to be consistent with a full beam in equilibrium. When the electron reaches the boundary of the beam it will cross into the space-charge free region and then be under the influence of the fields derived from logarithmic potentials, 4-25A or B. We have shown that the

orbits are bounded there so that the electron will eventually return to the beam, move through the beam to the other side, emerge, and repeat its motion, provided there is no interception on the boundaries. This situation describes stable motion in that the electron undergoes bounded motion. However, it seems more reasonable to consider this a case of instability in that a disturbed electron will emerge from the beam boundary no matter how small the perturbation. The above condition obtains, no matter what the current density, and therefore there is no critical value below which the beam is stable in the sense discussed.

This instability, coupled with the inherent difficulty involved in producing a beam with the necessary r^{-4} variation in ρ, makes a choice of this situation seem somewhat less than desirable. We have determined, though, that this variation is necessary in order that all electrons be in equilibrium so that any other will necessitate a departure from the ideal situation. In any other situation, the electrons cannot follow helical paths, but the stability situation may prove to be no worse. Another variation, such as ρ independent of radius, will no doubt be far easier to produce.

4.5 Potential Derived from Arbitrary Axially-Symmetric Space-Charge Distribution

We begin by deriving the result for the limiting case, where $r_a \to 0$, and suppose that ρ is given in the form of a power series about the origin.

$$\rho = \sum_{m=0}^{\infty} \rho_m r^m \tag{4-32}$$

Then, from Poisson's equation, 4-23A, we obtain two integrals, each time interchanging[74] the order of summation and integration within the open interval of convergence. We find,

$$\phi = -\frac{1}{\epsilon} \sum_{m=0}^{\infty} \rho_m \frac{r^{m+2}}{(m+2)^2} + C_0 \ln r + C_1 \tag{4-33}$$

For the annular beam shown in Fig. 4-1 we are given a power series about

some reference radius within the beam, r_0.

$$\rho = \sum_{m=0}^{\infty} a_m [r-r_0]^m \tag{4-34}$$

From Poisson's equation, 4-23A, we perform the first integration by parts interchanging the order of summation and integration as was done before to obtain

$$\begin{aligned}\phi &= -\frac{1}{\epsilon}\left[\sum_{m=0}^{\infty} a_m \left\{\frac{(r-r_0)^{m+2}}{(m+1)(m+2)} - \int \frac{(r-r_0)^{m+2}}{r(m+1)(m+2)}\,dr\right\} + K_0 \ln r + K_1\right] \\ &= -\frac{1}{\epsilon}\left[\sum_{m=0}^{\infty} \frac{a_m}{(m+1)(m+2)}\left\{(r-r_0)^{m+2} + (-r_0)^{m+2}\left[r - r_0 \ln r\right] - \sum_{k=1}^{m+1}(-r_0)^{m+1-k}\frac{(r-r_0)^{k+1}}{k+1}\right\} + K_0 \ln r + K_1\right] \\ &= -\frac{1}{\epsilon}\left[b_0 \ln r + b_1 + \sum_{m=0}^{\infty} \frac{a_m}{(m+1)(m+2)}\left\{\frac{m+1}{m+2}(r-r_0)^{m+2} + \sum_{k=0}^{m}(-1)^{m-k} r_0^{m+1-k}\frac{(r-r_0)^{k+1}}{k+1}\right\}\right]\end{aligned} \tag{4-35}$$

where the integral was evaluated by use of[75]

$$\int \frac{(a+bx)^p}{x}\,dx = \frac{(a+bx)^p}{p} + a\int \frac{(a+bx)^{p-1}}{x}\,dx$$

We apply this formula repeatedly until we reduce the integral in 4-35 to one which may be evaluated easily. We find

$$\frac{1}{(m+1)(m+2)}\int \frac{(r-r_0)^{m+2}}{r}\,dr = \frac{1}{(m+1)(m+2)}\left\{\sum_{k=1}^{m+1}(-1)^{m+1-k} r_0^{m+1-k}\frac{(r-r_0)^{k+1}}{k+1} + (-1)^{m+1} r_0^{m+1}\left[r - r_0 \ln r\right]\right\}$$

In the limit as r_0 approaches zero

$$\lim_{r_0 \to 0} \phi = -\frac{1}{\epsilon}\left[b_0 \ln r + b_1 + \sum_{m=0}^{\infty} \frac{a_m}{(m+2)^2} r^{m+2}\right] \tag{4-36}$$

which is of the same form as 4-33. It is also easily seen that 4-35 reduces to the result given in Sec. 4.6 if $a_n = 0$ for $n \geq 1$.

4.6 The Beam of Constant Charge Density

We now consider the simplest case of 4-34, $a_n = 0$ for $n > 0$. This condition, of charge density which is independent of radius, would presumably be relatively easy to produce with an actual electron gun. Furthermore, even if ρ would have another variation, the results presented here would be

a first approximation to the actual situation, found by truncating the series of 4-34 and 4-35 after n=0. Such an electron beam may not be held in equilibrium as was shown earlier, but assume that the changes in the beam take place slowly with respect to the overall length of the electron tube and thereby justify the assumption of a purely annular beam of constant charge density. Let the charge density inside the beam of Fig. 4-1 be constant and be given by ρ_0. The solution to Poisson's equation, 4-23A, is easily found to be

$$\phi = C_0 \ln r + C_1 - \frac{\rho_0}{4\epsilon} r^2, \qquad r_a \le r \le r_b \tag{4-37}$$

The solutions to Laplace's equation in the two beam-free regions are taken in the form of a constant plus logarithmic function. After satisfying the boundary conditions at r_1, r_a, r_b and r_2 we find

$$\phi = \phi_1 + \left[\frac{\phi_2-\phi_1+\frac{\rho_0}{4\epsilon}\left\{r_b^2\left(1+\ln\frac{r_2^2}{r_b^2}\right)-r_a^2\left(1-\ln\frac{r_a^2}{r_2^2}\right)\right\}}{\ln\frac{r_2}{r_1}} - \frac{\rho_0}{2\epsilon} r_a^2\right] \ln\frac{r}{r_1}, \quad r_1 \le r \le r_a \tag{4-38A}$$

$$\phi = \phi_1 + \left[\frac{\phi_2-\phi_1+\frac{\rho_0}{4\epsilon}\left\{r_b^2\left(1+\ln\frac{r_2^2}{r_b^2}\right)-r_a^2\left(1-\ln\frac{r_a^2}{r_2^2}\right)\right\}}{\ln\frac{r_2}{r_1}} - \frac{\rho_0}{2\epsilon}\left(r^2+r_a^2-r^2\right)\right] \ln\frac{r}{r_1} + \frac{\rho_0}{2\epsilon}\left(r^2-r_a^2\right), \quad r_a \le r \le r_b \tag{4-38B}$$

$$\phi = \phi_2 + \left[\frac{\phi_2-\phi_1+\frac{\rho_0}{4\epsilon}\left\{r_b^2\left(1+\ln\frac{r_2^2}{r_b^2}\right)-r_a^2\left(1-\ln\frac{r_a^2}{r_2^2}\right)\right\}}{\ln\frac{r_2}{r_1}} - \frac{\rho_0}{2\epsilon} r_b^2\right] \ln\frac{r}{r_2}, \quad r_b \le r \le r_2 \tag{4-38C}$$

$$E_r = -\left[\frac{\phi_2-\phi_1+\frac{\rho_0}{4\epsilon}\left\{r_b^2\left(1+\ln\frac{r_2^2}{r_b^2}\right)-r_a^2\left(1-\ln\frac{r_a^2}{r_2^2}\right)\right\}}{\ln\frac{r_2}{r_1}} - \frac{\rho_0}{2\epsilon} r_a^2\right] \frac{1}{r}, \quad r_1 \le r \le r_a \tag{4-39A}$$

$$E_r = -\frac{\phi_2-\phi_1+\frac{\rho_0}{4\epsilon}\left\{r_b^2\left(1+\ln\frac{r_2^2}{r_b^2}\right)-r_a^2\left(1-\ln\frac{r_a^2}{r_2^2}\right)\right\}}{\ln\frac{r_2}{r_1}} \frac{1}{r} + \frac{\rho_0}{2\epsilon} r, \quad r_a \le r \le r_b \tag{4-39B}$$

$$E_r = -\frac{\phi_2-\phi_1+\frac{\rho_0}{4\epsilon}\left\{r_b^2\left(1+\ln\frac{r_2^2}{r_b^2}\right)-r_a^2\left(1-\ln\frac{r_a^2}{r_2^2}\right)\right\}}{\ln\frac{r_2}{r_1}} - \frac{\rho_0 r_b^2}{2\epsilon}\Bigg] \frac{1}{r}, \quad r_b \le r \le r_2 \tag{4-39C}$$

$$E_r = -\frac{\phi_2-\phi_1+\frac{\rho_0}{4\epsilon}\left\{r_b^2\left(1+\ln\frac{r_2^2}{r_b^2}\right)-r_a^2\left(1-\ln\frac{r_a^2}{r_2^2}\right)\right\}}{\ln\frac{r_2}{r_1}} - \frac{\rho_0 r_b^2}{2\epsilon}\Bigg] \frac{1}{r}, \quad r_b \le r \le r_2 \tag{4-39C}$$

As $\frac{r_2-r_1}{r_1} \to 0$ the radius of curvature becomes large and the system may be approximated by a planar or sheet beam between two conducting planes. It may be shown that the above solutions approach the planar results in the limit.

In the case of a simple solid cylindrical beam it is easy to show by application of Gauss's law at the beam surface that the electric field at the

surface varies as r^{-1}. The presence of an unbounded force in the limit as $r \to 0$ is sufficient to preclude the beam dimension becoming zero, or equivalently, electrons crossing the axis of the beam in a symmetrical manner. For a sheet beam, if we take a Gaussian surface in the beam whose top and bottom faces are tangent to the beam boundaries, we find that the electric field remains constant at the surface of the sheet beam even as its thickness approaches zero. This condition is therefore physically possible and we conclude that for the planar beam, electrons may cross the axis of symmetry of the beam in a symmetrical way, producing a zero-thickness beam. We therefore suspect that for the annular beam, with no restrictions as to radius of curvature, the beam may attain zero thickness. As this happens, the charge per unit length

$$Q \equiv \pi \rho_0 (r_b^2 - r_a^2) \tag{4-40}$$

remains finite and ρ is assumed to remain uniform. In terms of Q

$$E_r = \left[\frac{Q}{2\pi\epsilon} \frac{\left(\frac{r}{r_a}\right)^2 - 1}{\left(\frac{r_b}{r_a}\right)^2 - 1} - \frac{\phi_2 - \phi_1 + \frac{Q}{4\pi\epsilon}\left\{1 + \ln\left(\frac{r_2}{r_b}\right)^2 - \frac{\ln\left(\frac{r_b}{r_a}\right)^2}{\left(\frac{r_b}{r_a}\right)^2 - 1}\right\}}{\ln \frac{r_2}{r_1}} \right] \frac{1}{r}, \quad r_a \le r \le r_b \tag{4-41}$$

It can be shown that in the limit as $\frac{r_b}{r_a} \to 1$, E_r at r_a and r_b as given by 4-41 remains finite. The condition of a zero thickness beam is possible and it will be used in later analyses.

We shall next determine, based upon various models, what current may be passed through the system when ρ is taken independent of radius. We ignore the fact that such a beam may not be in equilibrium for the following analyses and consider other effects.

We begin by asking the question as to what conditions obtain when the electric field becomes zero. It is easily seen that a zero of E_r can occur only in the beam region. From 4-5 for equilibrium, if $E_r = 0$ then $\ell = 0$, defining a limiting case. That is, current may be increased until the electric field just becomes zero in the beam. This is the maximum current for this criterion. We have, setting $E_r = 0$ in 4-41, the value of radius necessary, r_z. Thus,

$$\left(\frac{r_z}{r_a}\right)^2 = 1 + \left\{ \left[\phi_2 - \phi_1\right] \frac{2\pi\epsilon}{Q} + \frac{1}{2}\left[1 + \ln\left(\frac{r_2}{r_b}\right)^2 - \frac{\ln\left(\frac{r_b}{r_a}\right)^2}{\left(\frac{r_b}{r_a}\right)^2 - 1}\right] \right\} \frac{\left(\frac{r_a}{r_a}\right)^2 - 1}{\ln \frac{r_2}{r_1}}, \quad r_a \le r_z \le r_b \tag{4-42A}$$

$$\frac{d\left[\frac{r_2}{r_a}\right]^2}{dQ} = 2\pi\epsilon \frac{\phi_1 - \phi_2}{Q^2} \frac{\left(\frac{r_b}{r_a}\right)^2 - 1}{\ln \frac{r_2}{r_1}} \tag{4-42B}$$

The right-hand side of 4-42B is positive, noting that $\phi_1 > \phi_2$ for electrons. Becuase Q is negative, we find that $[\frac{r_2}{r_a}]^2$ is a decreasing function of the absolute value of Q. We conclude that as the current is increased in magnitude, the beam will first experience a zero of electric field at the outer beam boundary, r_b. We find, by setting $E_r(r_b)=0$ in 4-41, the limiting value of Q which is

$$Q_\alpha = \frac{4\pi\epsilon\left[\phi_1 - \phi_2\right]}{1 - \ln\left(\frac{r_b}{r_1}\right)^2 - \left[\ln\frac{r_b^2}{r_a^2}\right]\frac{1}{\frac{r_b^2}{r_a^2} - 1}} \tag{4-43}$$

where the subscript α refers to the condition for zero electric field at the outer beam boundary. If we substitute the value for Q from 4-43 into 4-38C using 4-40 we find that $\phi(r_b) = \phi_2$ as anticipated.

We next inquire into stability as discussed in Sec. 4.2. Three cases shall be distinguished. The first to be considered will be the stability of a single electron within the beam under the conditions that the remainder of the beam remains in its undisturbed state, as was done in the case of the beam of Sec. 4.4. We then will consider stability of the beam boundaries themselves, taken one at a time. In this model all electrons move together in their oscillations except those of the boundary not being considered. The beam boundary oscillates, the spatial uniformity of ρ is maintained, but Q is held constant so that ρ is a function of time. The three instabilities yield conditions on Q similar to 4-43. First consider the stability of a single electron. We use the solution for E_r as given in 4-41 and apply the criterion given in 4-17. The Taylor series for E_r will be similar to that for an electron in a logarithmic field since if we compare 4-41 to 4-18B we find essentially only the addition of a linear term in r. Therefore, the Taylor series will converge for this case as well. Application of the above yields the following inequality, using the fact that $Q < 0$:

$$\left[\frac{r}{r_a}\right]^2 < \frac{1}{2} + \left\{\pi\epsilon \frac{\phi_2 - \phi_1}{Q} + \frac{1}{4}\left[1 + \ln\left(\frac{r_2}{r_b}\right)^2 - \frac{\ln\left(\frac{r_b}{r_a}\right)^2}{\left(\frac{r_b}{r_a}\right)^2 - 1}\right]\right\} \frac{\left(\frac{r_b}{r_a}\right)^2 - 1}{\ln \frac{r_2}{r_1}} \tag{4-44}$$

All electrons whose radius satisfies 4-44 are stable. Note that $\frac{\phi_2 - \phi_1}{Q} > 0$,

and as $|Q|$ is increased from zero the right-hand side of 4-44 decreases from infinity. The largest value of $|Q|$ which would allow all electrons to be stable is therefore that which makes the limiting radius equal to the outer boundary of the beam, r_b. The first electron to become unstable under this model is an electron at radius r_b. Under this condition we find the bounds on Q necessary for single electron stability, recognizing that $Q<0$, as

$$Q > Q_\beta = \frac{4\pi\epsilon[\phi_1-\phi_2]}{1-\ln\left[\frac{r_b}{r_1}\right]^2-\frac{\ln(r_b/r_a)^2}{\left(\frac{r_b}{r_a}\right)^2-1}-\frac{(r_b/r_a)^2}{\left(\frac{r_b}{r_a}\right)^2-1}\ln\left(\frac{r_2}{r_1}\right)^2} \tag{4-45}$$

Consider next the condition of the outer boundary, r_b, moving as a whole. For this case we may carry out the derivation leading to the stability criterion and find that in this case the condition equivalent to 4-16 and 4-17 is

$$\Omega \equiv \zeta\left[3\frac{E_r(r_b)}{r_b}+\frac{dE_r(r_b)}{dr_b}\right] > 0 \tag{4-46}$$

The difference is seen to be the evaluation of E_r at the boundary, r_b, and then differentiation with respect to r_b. Physically, there is present the additional effect of the compression and expansion of the entire beam and therefore the value of E_r at the boundary changes due to this process. We have from 4-41, as $r\to r_b$,

$$E_r(r_b)=\left[\frac{Q}{2\pi\epsilon}-\frac{\phi_2-\phi_1+\frac{Q}{4\pi\epsilon}\left\{1+\ln\left(\frac{r_2}{r_b}\right)^2-\frac{\ln\left[\frac{r_b}{r_a}\right]^2}{(r_b/r_a)^2-1}\right\}}{\ln\frac{r_2}{r_1}}\right]\frac{1}{r_b} \tag{4-47}$$

In order to apply 4-46 we must show convergence of the Taylor series. Consider first a term of form

$$\frac{\ln(r_b)^2}{r_b}=\frac{2\{\ln r_{bo}+\ln[1+\frac{\delta}{r_{bo}}]\}}{r_{bo}[1+\frac{\delta}{r_{bo}}]} \tag{4-48}$$

It will be sufficient to consider the function $\frac{\ell n(1+\zeta)}{1+\zeta}$. Now the power series for both $(1+\zeta)^{-1}$ and $\ell n(1+\zeta)$ converge[76] for $|\zeta|<1$. If two series are absolutely convergent[77], then the product of the two series is also absolutely convergent and its sum equals the product of the sums of the two series. The products of terms may be arranged in any order. Therefore, the series for $\frac{\ell n(1+\zeta)}{1+\zeta}$, converges absolutely for $|\zeta|<1$. Finally, if a

function[78] is defined by a power series with positive or infinite radius of convergence, the coefficients of the power series are found from the function by the formula $a_n=\frac{f^{(n)}(0)}{n!}$ which means that the power series is the Taylor series, converging absolutely. Consider,

$$\frac{1}{\left(\frac{r_b}{r_a}\right)^2-1}=\frac{1}{\left(\frac{r_{bo}}{r_a}\right)^2-1}\left[\frac{1}{1-\frac{\delta}{r_a\left(1-\frac{r_{bo}}{r_a}\right)}}\right]\left[\frac{1}{1+\frac{\delta}{r_a\left(1+\frac{r_{bo}}{r_a}\right)}}\right] \tag{4-49}$$

of the form of a product of terms of type $(1+x)^{-1}$ which both certainly converge within the smaller of the two radii of convergence with respect to δ. That is, the first term converges for $\left|\frac{\delta}{r_a\left(1-\frac{r_{bo}}{r_a}\right)}\right|<1$ and the second for $\left|\frac{\delta}{r_a\left(1+\frac{r_{bo}}{r_a}\right)}\right|<1$ so they both converge for $|\delta|<r_{bo}-r_a$ and therefore so does their product. Following the preceding line of reasoning, we find that the Taylor series for the term of form

$$\frac{\ln(r_b)^2}{\left(\frac{r_b}{r_a}\right)^2-1}\,\frac{1}{r_b} \tag{4-50}$$

converges absolutely within a nonzero radius of convergence. Thus, using 4-46 and 4-47 we find the necessary condition on Q

$$Q>Q_\gamma=\frac{4\pi\epsilon(\phi_1-\phi_2)}{\frac{\ln\left[\frac{r_b}{r_a}\right]^2}{\left[\left(\frac{r_b}{r_a}\right)^2-1\right]^2}-\frac{1}{\left[\frac{r_b}{r_a}\right]^2-1}-\ln\left(\frac{r_b}{r_1}\right)^2} \tag{4-51}$$

The models involved in finding the limiting values Q_α, Q_β and Q_γ were proposed by others[79] but the results presented there are incorrect. The findings shown above are the corrected results. Consider next the case where the perturbation takes place at the inner boundary of the beam, r_a. We have from 4-41, as $r\to r_a$

$$E_r(r_a)=-\frac{\phi_2-\phi_1+\frac{Q}{4\pi\epsilon}\left\{1+\ln\left(\frac{r_2}{r_b}\right)^2-\frac{\ln\left[\frac{r_b}{r_a}\right]^2}{(r_b/r_a)^2-1}\right\}}{\ln\frac{r_2}{r_1}}\,\frac{1}{r_a} \tag{4-52}$$

We apply this time a formula similar to 4-46 except that E_r is evaluated at r_a and the differentiation is carried out with respect to r_a. Because of the similarity of 4-52 and 4-47 we need not show convergence of its Taylor series. The result is

$$Q>Q_\delta=\frac{4\pi\epsilon\left[\phi_1-\phi_2\right]}{1+\ln\left(\frac{r_2}{r_b}\right)^2+\frac{1}{\left(\frac{r_b}{r_a}\right)^2-1}\left\{1-\frac{2\left(\frac{r_b}{r_a}\right)^2-1}{\left(\frac{r_b}{r_a}\right)^2-1}\ln\left(\frac{r_b}{r_a}\right)^2\right\}} \tag{4-53}$$

From Q we find the current passing through the cross section and define a perveance for this case.

$$I = Q\dot{z} = -\sqrt{2\eta}\, Q\, \phi_z^{1/2} \tag{4-54A}$$

$$I = P(\phi_1 - \phi_2)\, \phi_z^{1/2} \tag{4-54B}$$

We see that due to the difference in assumptions between this model and the one in Sec. 4.4 the definitions of P are quite different. However, we do notice that the current varies as the 3/2 power of potential in the sense that a change in the potential scale is reflected in a change in current given by the scale factor raised to the 3/2 power. This is as expected since it is shown[80] that when potential is changed and the geometry remains fixed, the electron trajectories remain invariant, and the current density varies as potential raised to the 3/2 power. We have found four such perveances as defined in 4-54B. From 4-54A and the various limits given in 4-43, 4-45, 4-51, and 4-53, we find the limits

$$P_\alpha = \frac{\sqrt{2\eta}\, 4\pi\epsilon}{1 - \ln\left(\frac{r_b}{r_1}\right)^2 - \frac{\ln(r_b/r_a)^2}{(r_b/r_a)^2 - 1}} \tag{4-55A}$$

$$P_\beta = \frac{\sqrt{2\eta}\, 4\pi\epsilon}{1 - \ln\left(\frac{r_b}{r_1}\right)^2 - \frac{\ln(r_b/r_a)^2}{(r_b/r_a)^2 - 1} - \frac{(r_b/r_a)^2}{(r_b/r_a)^2 - 1}\ln\left(\frac{r_2}{r_1}\right)^2} \tag{4-55B}$$

$$P_\gamma = \frac{\sqrt{2\eta}\, 4\pi\epsilon}{\frac{\ln(r_b/r_a)^2}{[(r_b/r_a)^2 - 1]^2} - \frac{1}{(r_b/r_a)^2 - 1} - \ln\left(\frac{r_b}{r_1}\right)^2} \tag{4-55C}$$

$$P_\delta = \frac{\sqrt{2\eta}\, 4\pi\epsilon}{1 + \ln\left(\frac{r_2}{r_b}\right)^2 + \frac{1}{(r_b/r_a)^2 - 1}\left\{1 - \frac{2(r_b/r_a)^2 - 1}{(r_b/r_a)^2 - 1}\ln\left(\frac{r_b}{r_a}\right)^2\right\}} \tag{4-55D}$$

where the indices α, β, γ and δ refer respectively to the situations where $E_r \to 0$ at r_b; an electron at r_b becomes unstable; the outer boundary becomes unstable; and finally , where the inner beam boundary loses stability. We compare the values for perveance given in 4-55. The result is that P_β has the smallest value, P_γ is larger than P_β, and both P_α and P_δ are larger than P_β. The relationship between P_α and P_δ depends upon the particular geometry. The conclusion is that a single electron in the outer beam boundary becomes unstable at a lower value of current than that necessary for the other three effects to come into play. The maximum perveance for this model is P_β, the minimum of the four values

found.

$$P_{max} \approx \frac{66 \times 10^{-6}}{1 - \ln\left[\frac{r_b}{r_1}\right]^2 - \frac{\ln(r_b/r_a)^2}{(r_b/r_a)^2 - 1} - \frac{(r_b/r_a)^2}{(r_b/r_a)^2 - 1} \ln\left[\frac{r_2}{r_1}\right]^2} \qquad (4\text{-}56)$$

The value for perveance given in 4-56, as well as the other three values presented in 4-55 for the other effects are to be taken as approximate guidelines for limiting perveance in the system. They can be used together with experimental data for a particular geometry to determine the probable causes of increases in percentage intercepted current as the value of current through the system is raised.

4.7 The Nonzero Thickness Beam - Neglecting Space-Charge Effects

The preceding have dealt with some space-charge effects and will serve as approximations to such effects when other forces are present. The actual solution to the problem is exceedingly difficult since the trajectories of the electrons depend upon the potential which depends, in turn, upon the trajectories. In all the analyses to follow, forces due to space-charge are neglected in comparison to the other forces present. These analyses may be good approximations to the truth when space-charge density is sufficiently low. In higher power beams, by superposing the independent results one may get a feeling for the total solution. Consider a beam of electrons as shown in Fig. 4-1. We take the thickness of the beam, $r_b - r_a$, to be not necessarily vanishingly small, so that we consider effects of the thickness of the beam. We assume that all electrons originated from the same cathode which is held at uniform potential. We neglect noise effects and therefore all electrons have the same total energy, equal to that at the cathode. This energy is only changed by the presence of rf energy but under the influence of the static fields alone, this energy remains constant, as given by Eq. 4-20. Using the definition of axial energy, Eq. 2-8A, we find for the transverse energy

$$\tfrac{1}{2} m v_t^2 = \tfrac{1}{2} m(\dot{r}^2 + r^2\dot{\theta}^2) = \tfrac{1}{2} m(\dot{r}^2 + v_\theta^2) = e[\phi - \phi_c - \phi_3] \qquad (4\text{-}57)$$

We assume that there exists a value of radius such that an electron placed

there with no radial motion remains in equilibrium, that is, maintains a helical orbit. We find from 4-10 the equilibrium condition

$$\frac{m v_\theta^2(r_0)}{r_0} = e E(r_0) \tag{4-58}$$

We use for the electric field in 4-58 the solution for the space-charge free case, 4-18B. This yields a relationship between $v_\theta^2(r_0)$ and the difference of potentials ϕ_1 and ϕ_2, and the ratio $\frac{r_2}{r_1}$, viz.,

$$v_\theta^2(r_0) = \eta \frac{\phi_1 - \phi_2}{\ln \frac{r_2}{r_1}} \tag{4-59}$$

The right-hand-side of 4-59 is a constant independent of r_0. Therefore, if we launch electrons, at different radii, all having values of tangential velocity given by 4-59 with no radial velocity, they will be in equilibrium. However, according to 4-57 the requirement that v_θ^2 be independent of radius implies that ϕz is radius dependent. Therefore, if all electrons are given the same value of v_θ in order to satisfy 4-59 they must necessarily have different longitudinal velocities. If however, they are all to be synchronous with the same rf wave, they must all have the same value of longitudinal velocity. The requirement of synchronization therefore implies that 4-59 may not be satisfied by all electrons. It may be shown from 4-18A, 4-57 and 4-59 that there exists a single solution for equilibrium radius r_0 and from those equations we find the value of potential at the inner boundary, determining the potential all over.

$$\phi_1 = \frac{\phi_1 - \phi_2}{\ln \frac{r_2}{r_1}} \left[\ln \frac{r_0}{r_1} + \frac{1}{2} \right] + \phi_c + \phi_z \tag{4-60A}$$

$$\phi = \frac{\phi_1 - \phi_2}{\ln \frac{r_2}{r_1}} \left[\ln \frac{r_0}{r} + \frac{1}{2} \right] + \phi_c + \phi_z \tag{4-60B}$$

Consider an electron released at radius r' with no radial velocity. The angular momentum of the electron is conserved yielding the following variation for its tangential velocity:

$$v_\theta(r) = v_\theta(r') \frac{r'}{r} \tag{4-61}$$

We find from 4-57, 4-60B and 4-61 together with the condition that $\dot{r}(r')=0$ that

$$\frac{\phi_1-\phi_2}{\ln\frac{r_2}{r_1}}\left[\ln\frac{r_0}{r}+\frac{1}{2}\right]-\frac{\dot r^2}{2\gamma}=\frac{\phi_1-\phi_2}{\ln\frac{r_2}{r_1}}\left[\ln\frac{r_0}{r_1}+\frac{1}{2}\right]\left(\frac{r'}{r}\right)^2 \tag{4-62}$$

As was previously shown, for a non-equilibrium state, there are two solutions* for the turning points where $\dot r=0$. We have specified one value as r'. The second root, r'', satisfies 4-62† with $\dot r=0$.

$$\left[\frac{r'}{r''}\right]^2=\frac{\ln\frac{r_0}{r''}+\frac{1}{2}}{\ln\frac{r_0}{r_1}+\frac{1}{2}}=\frac{1+\ln\left[\frac{r_0}{r''}\right]^2}{1+\ln\left[\frac{r_0}{r_1}\right]^2} \tag{4-63}$$

---

* The net force, given by $-\frac{\partial V'}{\partial r}$ may be shown to have, for the above considerations, the sign of $\ln[\frac{r_0}{r}]$. Thus for $r>r_0$ the force is inward and for $r<r_0$ it is outward. The force therefore acts to return the electron to the equilibrium radius in both cases, a necessary condition for a stable situation with two turning points.

†A physical significance of the constant appearing in 4-62 may be found from the virial theorem[81] for an electron in the force field under consideration.

$$2\overline{T}-\overline{\frac{\partial V}{\partial r}r}=\frac{m}{\tau}\left[r\dot r+z\dot z-r(0)\dot r(0)-z(0)\dot z(0)\right]$$

where the bars indicate averages with respect to time over the time τ. For the smooth inner boundary case $\dot z=\dot z(0)$ so that

$$\frac{m\dot z}{\tau}\left[z-z(0)\right]=m\dot z^2$$

We divide the kinetic energy into its transverse and axial parts, namely,

$$2T=2T_t+m\dot z^2$$

so that

$$\overline{T_t}=\tfrac{1}{2}\overline{\frac{\partial V}{\partial r}r}+\frac{1}{2}\frac{m}{\tau}\left[r\dot r-r(0)\dot r(0)\right]$$

The radial motion is periodic in time so that if τ is made equal to a period the term in the square brackets vanishes. Also, if τ is made very large, not necessarily equal to a multiple of the period, the term approaches zero since, as was shown, the orbits are bounded. Thus,

$$\overline{T_t}=\tfrac{1}{2}\overline{\frac{\partial V}{\partial r}r}=-\tfrac{1}{2}e\,\overline{\frac{\partial\Phi}{\partial r}r}$$

Application to the logarithmic potential yields the result that $\frac{\partial\Phi}{\partial r}r$ is a constant independent of time. In particular,

$$\overline{T_t}=\tfrac{1}{2}e\,\frac{\phi_1-\phi_2}{\ln\frac{r_2}{r_1}}$$

and the recurring constant is proportional to the time-averaged transverse

Note that an electron released at r'' with $\dot{r}(r'')=0$ will have r' as its turning point so that the turning points occur in pairs. The problem is, given $\frac{r_0}{r'}$ to find $\frac{r_0}{r''}$. The solution of 4-63 is equivalent to the solution of

$$G\left(\left[\frac{r_0}{r''}\right]^2\right) = G\left(\left[\frac{r_0}{r'}\right]^2\right) \tag{4-64A}$$

$$G(y) \equiv \frac{y}{1+\ln y} \tag{4-64B}$$

From 4-62 we find that the maximum velocity occurs at radius

$$r_p = r'\sqrt{1+\ln\left[\frac{r_0}{r'}\right]^2} < r_0 \tag{4-65}$$

Note that for r_p to be real, $\ln(\frac{r_0}{r'})^2 > -1$, or

$$\frac{r'}{r_0} < e^{1/2} \tag{4-66}$$

Thus an electron may not violate 4-66. When $\frac{r'}{r_0}=e^{1/2}$, v_θ found from 4-57 and 4-60B equals zero and the electron falls into the inner cylinder. For $\frac{r'}{r_0} > e^{1/2}$, v_θ is imaginary. On the other hand there is no forbidden region for the case when $r' < r_0$, so that an electron may be released at vanishingly small radius, subject of course to the physical limitation imposed by the presence of the inner cylinder. Since the turning points occur in pairs we infer that as $r' \to 0$ the maximum value assumed by the other turning point equals $e^{1/2}r_0$. No matter how close to the axis the electron is released it may never reach $e^{1/2}r_0$. That $r_p < r_0$ may be shown mathematically or by the following physical argument. For non-equilibrium motion, when the electron is at r_0 its value of v_θ is less than that of an equilibrium electron, by Eq. 4-57. Thus, the force due to the electric field is larger in magnitude than the centrifugal force and the net force is inwards. We conclude that $r_p < r_0$. The angular momentum of the electron injected at radius r' with zero radial velocity is

---

kinetic energy of the electron. Since $\overline{T}_t$ is the same for all electrons, all electrons have the same average potential as well.

$$\ell = \sqrt{\frac{em(\phi_1-\phi_2)}{\ln\frac{r_2}{r_1}}}\sqrt{1+\ln\left(\frac{r_0}{r_1}\right)^2}\,r' \tag{4-67}$$

All electrons have different values of ℓ, which is conserved, and have the same value of energy. We find from 4-62

$$\dot{r}^2 = \eta\frac{\phi_1-\phi_2}{\ln\frac{r_2}{r_1}}\left\{\frac{1+\ln\left(\frac{r_0}{r}\right)^2}{\left(\frac{r_0}{r}\right)^2}-\frac{1+\ln\left(\frac{r_0}{r_1}\right)^2}{\left(\frac{r_0}{r_1}\right)^2}\right\}\left(\frac{r_0}{r}\right)^2$$

$$= \eta\frac{\phi_1-\phi_2}{\ln\frac{r_2}{r_1}}\left\{\frac{1}{G\left(\left[\frac{r_0}{r}\right]^2\right)}-\frac{1}{G\left(\left[\frac{r_0}{r_1}\right]^2\right)}\right\}\left(\frac{r_0}{r}\right)^2 \tag{4-68}$$

so that the only allowable solutions are for $G\left(\left[\frac{r_0}{r}\right]^2\right) \leq G\left(\left[\frac{r_0}{r_1}\right]^2\right)$. G(y) has the values 0 and 1 at y=0 and 1 respectively, approaches infinity as y approaches infinity and has a pole at e^{-1}. $\dot{G}$(y) is shown in Fig. 4-2a.

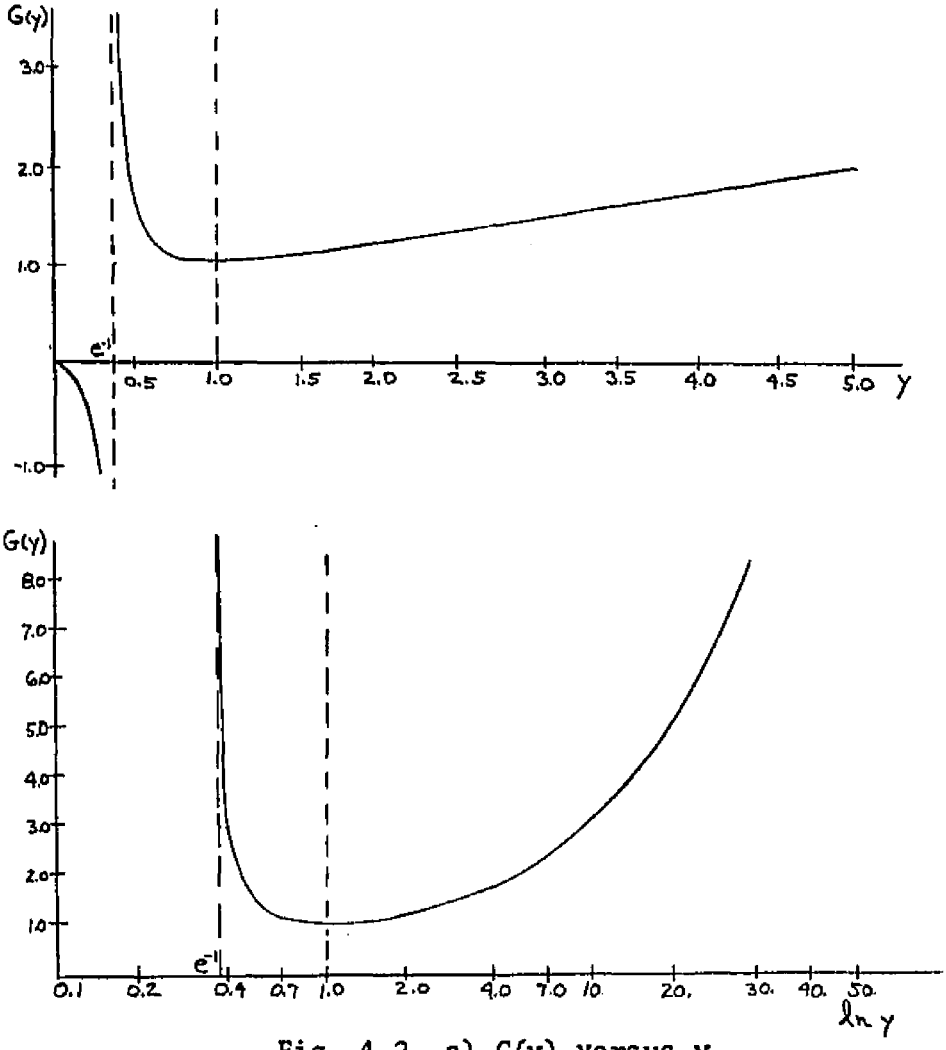

Fig. 4-2 a) G(y) versus y
b) G(y) versus ℓn y. $G(y) \geq 1$

We find the following properties of the concomitant values of y given the range of G:

Table 4-1 Roots of G(y)=Constant

Range of G	Roots
G>1	Two real roots; $e^{-1}<y_1<1$ and $y_2>1$
G=1	One real root; y=1
0<G<1	No real roots
G=0	One real root; y=0
G<0	One real root; $0<y<e^{-1}$

It was shown that two turning points accompany non-equilibrium motion. From Table 4-1, the only case yielding two roots is for $G>1$, the equilibrium case being the limiting one as $G\to 1$. The region of relevancy is seen to be $G(y)\geq 1$ which is shown in Fig. 4-2b.

The problem is to find the second root given one of them. If it were possible to invert Equation 4-64B, that is, to find y(G), then the problem would be solved. If we designate the two roots by y_α and y_β then the inversion formula would allow us to write $y_\beta\,[G(y_\alpha)]$. Attempts to invert G(y) proved to be unsuccessful.* Denote the smaller root by y_1 and

* We do note, however, that inversion is possible for $G'(y)$. We find easily from 4-64B that

$$[\ln y]^2+\left[2-\frac{1}{G'(y)}\right]\ln y+1=0$$

This quadratic equation in $\ln y$ is solved for its two roots and we find for y

the larger by y_2, viz., $e^{-1}<y_1<1$ and $y_2>1$. Expansion of $G(y_1)=G(y_2)$ about $y_1=y_2=1$ and truncation of the series at the quadratic terms yields, for y_1 and y_2 near unity,

$$y_2-1 \approx \pm(y_1-1) \tag{4-69A}$$

From the definitions of the range of y_1 and y_2, we see that the negative sign is appropriate and we find that for small perturbations about unity the roots are symmetrically disposed.

$$\lim_{y_2\to 1}[y_2-1] \approx 1-y_1 \tag{4-69B}$$

Consider the product of the roots, y_1y_2. In the equilibrium limit, $y_1=y_2=1$, we have $y_1y_2=1$. We show that this is the only instance for this to occur. If $y_1y_2=1$ we have from $G(y_1)=G(y_2)$ that

$$y_1^2 = \frac{1+\ln y_1}{1-\ln y_1} = \frac{2+\ln y_1^2}{2-\ln y_1^2} \tag{4-70A}$$

With $y_1^2=1-\delta$, we require, expanding the logarithmic terms,[82]

$$\sum_{m=3}^{\infty} \frac{m-2}{m(m-1)}\delta^m = 0, \qquad -1\le\delta<1 \tag{4-70B}$$

Since $e^{-2}<y_1^2<1$, we have $0<\delta<1-e^{-2}<1$, so the series converges. Because δ is positive, and because for the range $n\ge 3$ the coefficients of the series in 4-70B are positive, the function described by 4-70B is monotonically increasing for the range of δ of interest. Therefore, in that range the only solution for 4-70B is the trivial case, $\delta=0$. Thus, $y_1y_2=1$ if and only if $y_1=y_2=1$. It is easily shown that

$$\lim_{y_1\to e^{-1}}\{y_1y_2\} = \infty \tag{4-71}$$

$$y = e^{-\left\{\left[1-\frac{1}{2G'(y)}\right]\left[1\pm\sqrt{1-\left(1-\frac{1}{2G'(y)}\right)^2}\right]\right\}}$$

There are real solutions for y when the expression appearing under the radical sign is nonnegative. This is equivalent to

$$-\infty < G'(y) \le \tfrac{1}{4}$$

Since, as y_1 varies from 1 to e^{-1}, $y_1 y_2$ varies from 1 to ∞ and never equals one for $y_1 < 1$ we have that

$$y_1 y_2 \geq 1 \tag{4-72A}$$

$$r_o^2 \geq r' r'' \tag{4-72B}$$

with equality occurring only for the case of equilibrium motion. In addition it may be shown, as an extension of 4-69B that*

$$1 - y_1 < y_2 - 1 \tag{4-73}$$

---

* To maintain the equality $G(y_1)=G(y_2)$, we must have

$$\frac{dy_2}{dy_1} = \frac{G'(y_1)}{G'(y_2)}$$

and it is easily seen that

$$\lim_{y_1 \to e^{-1}} \frac{dy_2}{dy_1} = -\infty$$

$$\lim_{y_1 \to 1} \frac{dy_2}{dy_1} = -1$$

We have,

$$\frac{d^2 y_2}{dy_1^2} = \frac{G''(y_1) - G''(y_2)\left[\frac{dy_2}{dy_1}\right]^2}{G'(y_2)}$$

It can be shown that $G'(y_2)$ is zero for $y_2=1$ and ∞ but on the open interval which corresponds to $e^{-1}<y_1<1$, it has no zeros. In order for $\frac{d^2y_2}{dy_1^2}$ to be zero we require

$$G''(y_1) = G''(y_2)\left[\frac{dy_2}{dy_1}\right]^2 = G''(y_2)\left[\frac{G'(y_1)}{G'(y_2)}\right]^2$$

which can be shown to be equivalent to

$$\ln y_1 + \ln y_2 = \ln[y_1 y_2] = \ln y_1 \ln y_2$$

We have, from 4-72A, and the ranges of y_1 and y_2 that

$$\ln(y_1 y_2) > 0 \quad , e^{-1} < y_1 < 1$$

$$\ln y_1 < 0 \quad , e^{-1} < y_1 < 1$$

$$\ln y_2 > 0 \quad , y_2 > 1$$

We have shown that $\frac{d^2y_2}{dy_1^2}$ has no zero on the open interval and so we conclude

It is possible to solve for a root in terms of the ratio of the roots. We find from $G(y_1)=G(y_2)$ that

$$\frac{y_1}{y_2}=\frac{1+\ln y_1}{1+\ln y_2}=1+\frac{\ln\frac{y_1}{y_2}}{1+\ln y_2} \tag{4-74}$$

Solving for the roots,

$$y_2=e^{-1}e^{\frac{\ln y_1/y_2}{(y_1/y_2)-1}}=e^{-1}e^{\ln\left[\frac{y_1}{y_2}\right]^{\frac{1}{\frac{y_1}{y_2}-1}}}=e^{-1}\left[\frac{y_1}{y_2}\right]^{\frac{1}{\frac{y_1}{y_2}-1}} \tag{4-75A}$$

$$y_1=\frac{y_1}{y_2}e^{-1}\left[\frac{y_1}{y_2}\right]^{\frac{1}{\frac{y_1}{y_2}-1}}=e^{-1}\left[\frac{y_1}{y_2}\right]^{\frac{y_1/y_2}{\frac{y_1}{y_2}-1}} \tag{4-75B}$$

It is noted that no specification was made as to which of the two roots is the larger and therefore we may apply Eqs. 4-75 without regard to this.†

$$-\infty<\frac{dy_2}{dy_1}<-1\ ,\quad e^{-1}<y_1<1$$

and varies monotonically. Now,

$$y_2-1=\int_1^{y_1}\frac{dy_2}{dy_1}dy_1=-\int_{y_1}^{1}\frac{dy_2}{dy_1}dy_1$$

and since $\frac{dy_2}{dy_1}$ varies monotonically we may bound the integral as follows:

$$1-y_1<y_2-1<-\left[\frac{dy_2}{dy_1}\right]_{y_1}(1-y_1)$$

† From the limits

$$\lim_{y\to1}y^{\frac{1}{y-1}}=e$$
$$\lim_{y\to0}y^{\frac{1}{y-1}}=\infty$$
$$\lim_{y\to0}y^{\frac{y}{y-1}}=1$$

We obtain from Eqs. 4-75

$$\lim_{\frac{y_1}{y_2}\to1}y_2=1$$
$$\lim_{\frac{y_1}{y_2}\to0}y_2=\infty$$
$$\lim_{\frac{y_1}{y_2}\to0}y_1=e^{-1}$$

We now derive an approximation for the relationship between the two roots. We allow a root, y_α, to take on the values between e^{-1} and infinity, and we seek the value of the other root, y_β. We make some simple observations about the solution. The curve $y_\beta(y_\alpha)$ must pass through the point (1,1) which corresponds to the equilibrium point and must possess symmetry about the line $y_\beta = y_\alpha$ since the designation of a root as y_α is arbitrary and in reality a single pair of roots y_1 and y_2 gives rise to two points. The curve must be asymptotic to the two lines $y_\alpha = e^{-1}$ and $y_\beta = e^{-1}$ since, as was shown earlier, as either root approaches infinity, the other approaches e^{-1}. The above considerations, in conjunction with the monotonic nature of the derivative $\frac{dy_2}{dy_1}$, as found above, suggest that we may approximate the function $y_\beta(y_\alpha)$ by a hyperbola. A hyperbola which passes through the point (1,1) and which has the proper asymptotic behavior is given by*

$$[y_\alpha - e^{-1}][y_\beta - e^{-1}] = [1 - e^{-1}]^2 \tag{4-76A}$$

where we take the branch of the hyperbola such that $y_\alpha > e^{-1}$ and $y_\beta > e^{-1}$. Thus,

$$y_\beta \approx e^{-1} + \frac{[1 - e^{-1}]^2}{[y_\alpha - e^{-1}]} \tag{4-76B}$$

The results of a numerical solution of $G(y_\alpha) = G(y_\beta)$ are shown for the region around the equilibrium point in Fig. 4-3a and for a broad range in Fig. 4-3b, where the results are shown on logarithmic scales. The approximate solution, 4-76, is shown in both cases. We see that the approximation found is a rather good one for the range of values indicated.

We next address ourselves to the following problem: An electron beam is

---

* We may show from Eqs. 4-75 that

$$[y_\alpha e - 1][y_\beta e - 1] = \left\{\left[\frac{y_\alpha}{y_\beta}\right]^{\frac{y_\alpha/y_\beta}{y_\alpha/y_\beta - 1}} - 1\right\}\left\{\left[\frac{y_\alpha}{y_\beta}\right]^{\frac{1}{y_\alpha/y_\beta - 1}} - 1\right\} \approx [e-1]^2$$

the approximation holding for $\frac{y_\alpha}{y_\beta} \approx 1$.

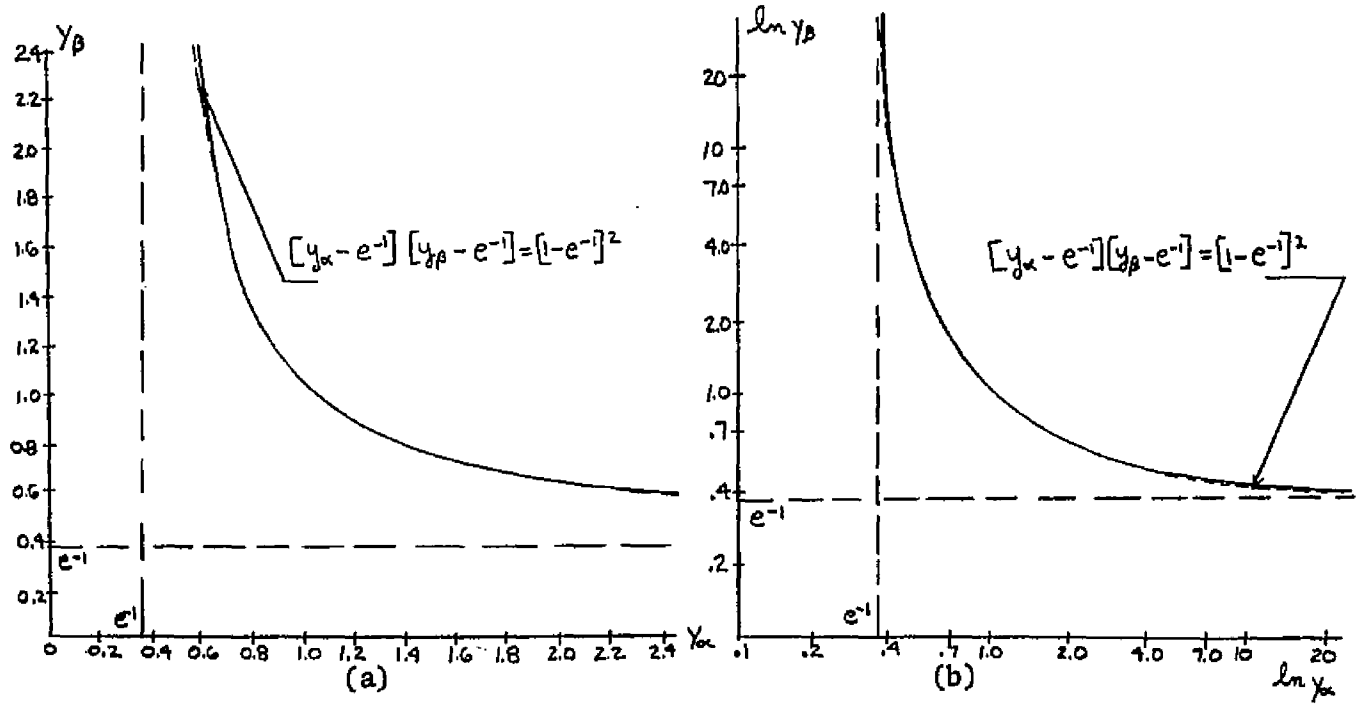

Fig. 4-3 a) y_β versus y_α and approximation
b) $\ell n\ y_\beta$ versus $\ell n\ y_\alpha$ and approximation

launched, as in Fig. 4-1, confined to the annulus $r_a \leq r \leq r_b$. The initial conditions on each electron crossing the entrance plane are such that there is no radial velocity so the energy of each electron is confined, initially, to rotation and pure translation. We ignore space-charge forces and since, as it was shown earlier, there is a single equilibrium radius, all electrons whose initial radius differs from this value will oscillate about radius r_0. The question to be posed is to choose r_0 such that the orbits of all electrons will remain within the bounds $r_a \leq r \leq r_b$. If this is possible we will have a situation in which even though most electrons will execute oscillatory motion, the net locus of paths will maintain the initial beam thickness, $r_b - r_a$. We immediately recognize that $r_a < r_0 < r_b$. We specify y_1 and y_2 according to the range indicated in Table 4-1 and use a single prime to denote an initial value and a double prime to denote a corresponding turning point. Thus,

$$\left(\frac{r_0}{r_b}\right)^2 \equiv \left(\frac{r_0}{r_b'}\right)^2 \equiv y_{1b} \tag{4-77A}$$

$$\left(\frac{r_0}{r_b''}\right)^2 \equiv y_{2b} \tag{4-77B}$$

$$\left(\frac{r_o}{r_a}\right)^2 \equiv \left(\frac{r_o}{r_{a'}}\right)^2 \equiv y_{2a} \tag{4-77C}$$

$$\left(\frac{r_o}{r_{a''}}\right)^2 \equiv y_{1a} \tag{4-77D}$$

The physical requirements we impose are that

$$r_b \geq r_{a''} \tag{4-78A}$$

$$r_{b''} \geq r_a \tag{4-78B}$$

We have,

$$\left(\frac{r_o}{r_b}\right)^2 \leq y_{1a} < y_{2b} \leq \left(\frac{r_o}{r_a}\right)^2 \tag{4-79A}$$

$$G(y_{2b}) = G(y_{1b}) = G\left(\left[\frac{r_o}{r_b}\right]^2\right) \tag{4-79B}$$

$$G(y_{1a}) = G(y_{2a}) = G\left(\left[\frac{r_o}{r_a}\right]^2\right) \tag{4-79C}$$

In the limiting case of small beam thickness we have for the approximate requirement using the approximation 4-69B

$$\left(\frac{r_o}{r_b}\right)^2 \leq 2 - \left(\frac{r_o}{r_a}\right)^2 < 2 - \left(\frac{r_o}{r_b}\right)^2 \leq \left(\frac{r_o}{r_a}\right)^2 \tag{4-80A}$$

We see from 4-80A that $\left[\frac{r_0}{r_b}\right]^2 + \left[\frac{r_0}{r_a}\right]^2$ must be ≤ 2 and ≥ 2 so that equality is the only possibility and we find

$$r_o^2 = 2\frac{r_a^2 r_b^2}{r_a^2 + r_b^2} \tag{4-80B}$$

If in 4-80B we let $r_b - r_a$ be small and use leading terms of the geometric and binomial expansions we find that

$$r_o \approx \tfrac{1}{2}\left[r_a + r_b\right] \tag{4-81}$$

The significance of 4-81 is clear. For small oscillations we have from 4-16 with $\Omega > 0$ that the waveform is sinusoidal and therefore the extrema

of radial motion are equally distributed about equilibrium.

In the nonlimiting situation, we focus our attention upon Eqs. 4-79. Since $e^{-1} < [\frac{r_0}{r_b}]^2 < 1$ and since in this range the function G is monotonically decreasing, we find from the left-hand inequality of 4-79A

$$G\left(\left[\frac{r_0}{r_b}\right]^2\right) \geq G\left(\left[\frac{r_0}{r_a}\right]^2\right) \tag{4-82A}$$

Similarly, since $(\frac{r_0}{r_a})^2 > 1$ and since in this range G is monotonically increasing we have from the right-hand inequality of 4-79A

$$G\left(\left[\frac{r_0}{r_a}\right]^2\right) \geq G\left(\left[\frac{r_0}{r_b}\right]^2\right) \tag{4-82B}$$

In order for both 4-82A and B to be true we must have equality and therefore the condition to be fulfilled is simply

$$G\left(\left[\frac{r_0}{r_a}\right]^2\right) = G\left(\left[\frac{r_0}{r_b}\right]^2\right) \tag{4-83}$$

so that $(\frac{r_0}{r_a})^2$ and $(\frac{r_0}{r_b})^2$ form a pair of roots of the function G, the physical significance being that one is the turning point of the other and they are, in essence, the same trajectory.* We recognize from 4-83 that the ratio of the roots is $[\frac{r_a}{r_b}]^2$, or its reciprocal, which is a constant and which is a given of the problem. This situation was earlier solved, the results formulated in Eqs. 4-75. Thus,

$$r_0 = r_a e^{-\frac{1}{2}\left[\frac{r_a}{r_b}\right]^{\frac{1}{(r_a/r_b)^2-1}}} = r_b e^{-\frac{1}{2}\left[\frac{r_a}{r_b}\right]^{\frac{(r_a/r_b)^2}{(r_a/r_b)^2-1}}}$$

$$= r_a e^{-\frac{1}{2}\left[\frac{r_b}{r_a}\right]^{\frac{(r_b/r_a)^2}{(r_b/r_a)^2-1}}} = r_b e^{-\frac{1}{2}\left[\frac{r_b}{r_a}\right]^{\frac{1}{(r_b/r_a)^2-1}}} \tag{4-84}$$

---

* It is easily demonstrated that the solution 4-83 always exists. As r_0 is varied from r_a to r_b, the left-hand side of 4-83 varies continuously from 1 to $G([\frac{r_b}{r_a}]^2) > 1$. For the same variation in r_0 the right-hand side varies continuously from $G([\frac{r_a}{r_b}]^2) > 1$ to 1. The two continuous functions must therefore intersect in the range $r_a < r_0 < r_b$ to form a solution.

We have therefore found the solution to the problem: given r_a and r_b, to find the proper value of r_0 such that the resultant beam motion is confined to the original bounds.

4.8 The Period of Oscillation

We now consider the period of oscillation of an electron about the equilibrium radius. We consider the electron to be an equilibrium electron in that it satisfies the equilibrium condition, and its oscillatory motion is due to perturbations in radial velocity caused by noise or by radial forces due to the actual nonuniformity of the inner boundary. In the idealization of a zero thickness beam which will be used in the latter part of this chapter, these oscillations represent the "natural" perturbed motion. When the corrugated inner boundary is considered along with its periodic fields it will be seen that the relation of the "natural period" of the electron in the smooth boundary case to the period of the corrugation is important in determining the stability of the motion. We inquire into the variation of the period of oscillation as the deviation from equilibrium is increased. This will involve solving, approximately, a nonlinear differential equation. Perturbation of a variation of 4-5 about radius r_0 for an equilibrium electron, yields, with $\delta \equiv r - r_0$,

$$\ddot{\delta} + \frac{l^2}{m^2 r_0^3}\left[\left(1+\frac{\delta}{r_0}\right)^{-1} - \left(1+\frac{\delta}{r_0}\right)^{-3}\right] = 0 \qquad (4\text{-}85A)$$

We expand both terms appearing within the brackets by the binomial expansion, converging[83] for $-1 < \frac{\delta}{r_0} < 1$, and retain up to linear terms. We have

$$\ddot{\delta} + 2\frac{l^2}{m^2 r_0^4}\delta \approx 0 \qquad (4\text{-}85B)$$

The solution of 4-85B in terms of circular functions is for small oscillations and the period accompanying these linear oscillations is

$$T_0 = \sqrt{2}\,\pi\,\frac{m r_0^2}{l} \qquad (4\text{-}86)$$

From 4-3 we have

$$\frac{d}{dt} = \frac{l}{m r^2}\frac{d}{d\theta} \qquad (4\text{-}87A)$$

so that from 4-85B we have

$$\frac{d^2\delta}{d\theta^2} - \frac{2}{r_0\left(1+\frac{\delta}{r_0}\right)}\left[\frac{d\delta}{d\theta}\right]^2 + 2\delta\left[1+\frac{\delta}{r_0}\right]^4 \approx 0 \qquad (4\text{-}87B)$$

Retaining only the linear terms of 4-87B we have

$$\frac{d^2\delta}{d\theta^2} + 2\delta \approx 0 \qquad (4\text{-}87C)$$

δ is periodic in θ with period $\sqrt{2}\pi$ and the angular spacing between adjacent turning points, or between adjacent crossings of the equilibrium radius, is

$$\Delta\theta = \frac{\pi}{\sqrt{2}} \approx 127^0$$

Noté that since $\sqrt{2}$ is an irrational number the orbit viewed in cross section is not closed, in that m cycles will not bring the electron back to the same value of θ . As the oscillations become larger, however, we expect the period to change. Since we may always find a rational number as close as we wish to an irrational, there exists a vanishingly small perturbation for which we have a closed orbit. The square of angular velocity consistent with the equilibrium electron is, using 4-3,

$$\dot{\theta}_0^2 = \frac{l^2}{m^2 r_0^4} \qquad (4\text{-}88)$$

We normalize δ with respect to r_0 so that

$$\beta \equiv \frac{\delta}{r_0} \qquad (4\text{-}89A)$$

Using 4-88 and 4-89 we arrive at the differential equation

$$\ddot{\beta} + \dot{\theta}_0^2 \frac{\beta(\beta+2)}{(\beta+1)^3} = 0 \qquad (4\text{-}89B)$$

We note from 4-89B that the force is zero at the equilibrium point, $\beta = 0$, so that the maximum radial velocity occurs there, in contrast with the results of Sec. 4.7, Eq. 4-65. This is due to the differences in assumptions for the two situations. The force approaches infinity as the radius approaches zero as is evident from $\beta \to -1$. We see, therefore, that as the depth of perturbation is increased, the reversal of direction

at the smaller turning point should take place more and more rapidly. On the other hand, we note that for large radius, as β approaches infinity, the force approaches zero. From this we infer that at the larger turning point, the reversal of direction will take place more and more slowly. The conclusion is that the period approaches infinity as the depth of perturbation increases. Note that $r \to \infty$ is possible in this case but not possible for the assumptions of Sec. 4.7. Observe also from the above that the time average of the trajectory is a function of initial condition and in particular increases from the equilibrium value as the depth of perturbation increases. We normalize the differential equation 4-89B by setting

$$\dot{\theta}_o^2 = 1 \tag{4-90A}$$

which is equivalent to a time scaling

$$\tau = \dot{\theta}_o t \tag{4-90B}$$

in which case the small perturbation period becomes $\sqrt{2}\pi$ from 4-86.

The differential equation 4-89B subject to 4-90A is solved numerically by computer using the Hamming's modified predictor-corrector method.[84] As an artifice we use an initial displacement, $\beta(0) \equiv \beta_0$ where $\dot{\beta}(0) = 0$ yielding the solutions as functions of off-equilibrium displacement. Some of these solutions are presented in Fig. 4-4 for β_0 on both sides of equilibrium. A single cycle of oscillation is presented for each solution and the curves are normalized with respect to β_0. Note that for large perturbation the direction reversal for the smaller turning point takes place rapidly, whereas the reversal at the other turning point takes place slowly. For these cases, the electron spends most of the time at radius values larger than the equilibrium radius. From numerical results such as these we find the dependence of the period upon β_0. The departure of the period from the value $\sqrt{2}\pi$ is shown in Fig. 4-5. The region $\beta_0 < 0$ is emphasized in Fig. 4-5b. Note the linear dependence* in Fig. 4-5a for $\beta_0 >> 0$. We next obtain appro-

---

* Since the electron spends most of its time at large values of β for the large β case we write an approximate differential equation for most of the

ximate solutions to the differential equation, 4-89B. Carrying the approximation of 4-89B to quadratic terms we obtain the approximate nonlinear differential equation

$$\ddot{\beta} + 2\dot{\theta}_o^2\beta - 5\dot{\theta}_o^2\beta^2 = 0 \tag{4-91}$$

Since $\ddot{\beta} = \frac{d\dot{\beta}}{d\beta}\dot{\beta}$, we obtain the first integral which satisfies the initial conditions $\beta(0)=\beta_0$ and $\dot{\beta}(0)=0$. We find,

$$\dot{\beta} = \pm\sqrt{2}\,\dot{\theta}_o\sqrt{(\beta_o^2-\beta^2)-\tfrac{5}{3}(\beta_o^3-\beta^3)} \tag{4-92A}$$

Since $\beta(0)=\beta_0$ we have

$$t = \pm\frac{1}{\sqrt{2}\dot{\theta}_o}\int_{\beta_o}^{\beta}\frac{d\varsigma}{\sqrt{(\beta_o^2-\varsigma^2)-\tfrac{5}{3}(\beta_o^3-\varsigma^3)}} \tag{4-92B}$$

Now, an integral of the form

$$\int\frac{dx}{\sqrt{P}}$$

can be written in terms of an elliptic integral[85] of the first kind when P is a cubic polynomial. The reduction of the integral depends upon whether the roots of P are all real or whether P has only one real root. We must, therefore, find the roots of the cubic polynomial in ς appearing in 4-92B. Observe that β_0 must be a root of the polynomial. We proceed to remove the

---

period when β is large. From 4-89B, $\ddot{\beta} + \frac{\dot{\theta}_o^2}{\beta^2} \approx 0$, from which we find a first integral

$$\tfrac{1}{2}\dot{\beta}^2 = -\dot{\theta}_o^2\ln\beta + \dot{\theta}_o^2\ln\beta_o = \dot{\theta}_o^2\ln\frac{\beta_o}{\beta}$$

since for $\beta=\beta_0$, $\dot{\beta}=0$. Thus,

$$t = \pm\frac{1}{\dot{\theta}_o}\int_{\beta_o}^{\beta}\frac{d\beta}{\sqrt{\ln\left[\frac{\beta_o}{\beta}\right]^2}}$$

Since most of the time is spent for $\beta\approx\beta_o>>0$ we approximate the period as

$$T \approx \pm\frac{2}{\dot{\theta}_o}\int_{\beta_o}^{0}\frac{d\beta}{\sqrt{\ln\left(\frac{\beta_o}{\beta}\right)^2}} \approx \pm\frac{2}{\dot{\theta}_o}\int_{\beta_o}^{0}\frac{d\beta}{\sqrt{\left[\frac{\beta_o}{\beta}\right]^2-1}} = \mp\frac{2}{\dot{\theta}_o}\beta_o$$

a linear variation. The linear portion of Fig. 4-5a is parallel to this result with $\dot{\theta}_o=1$.

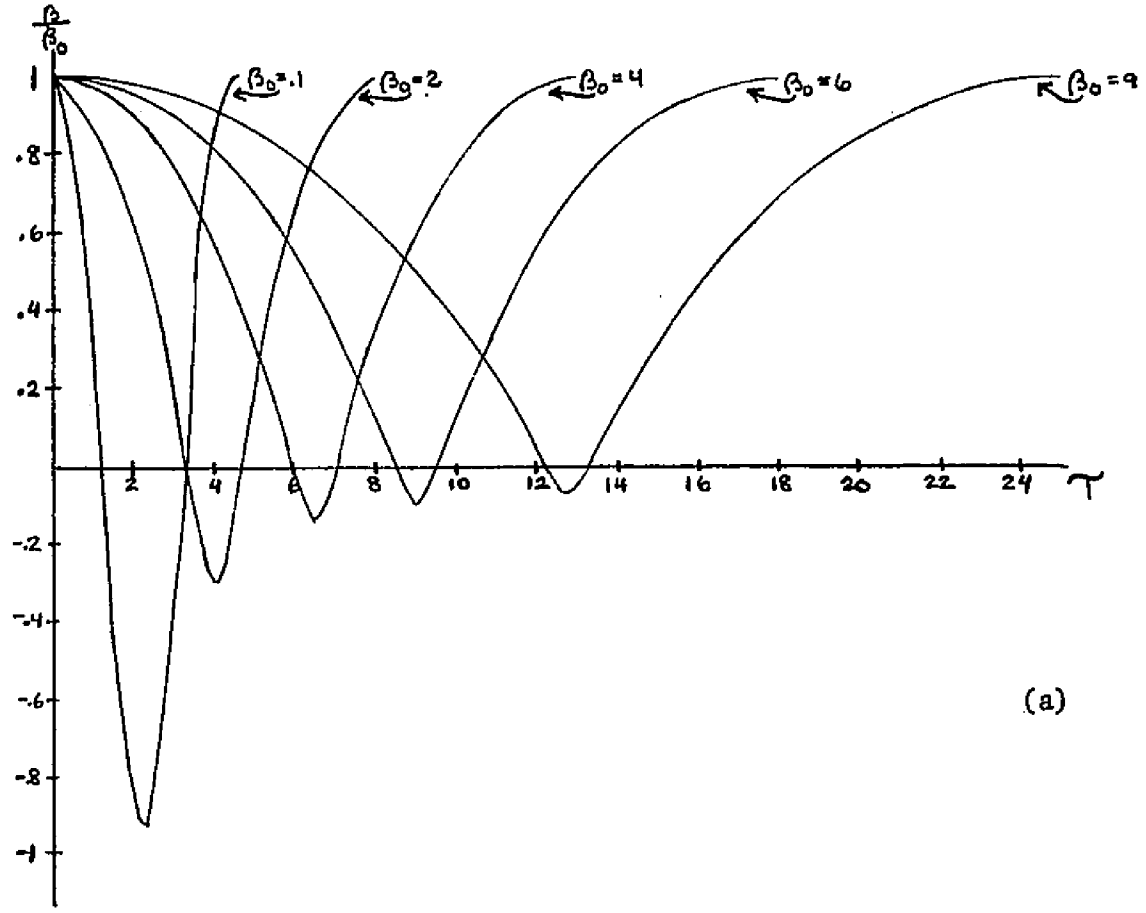

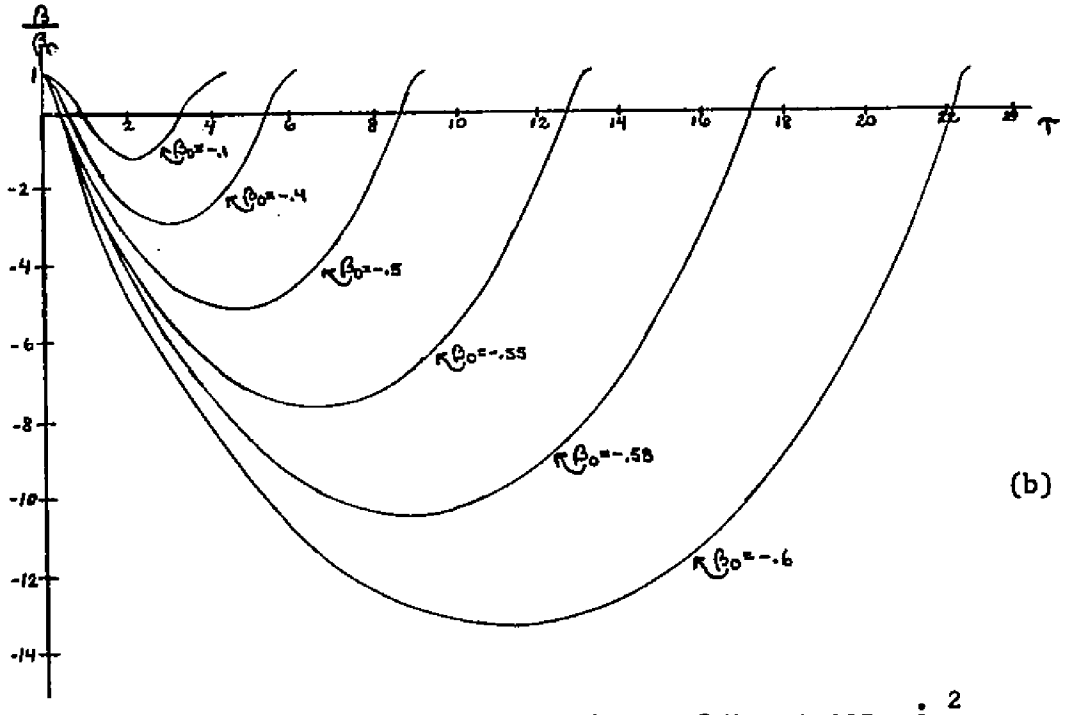

Fig. 4-4 Numerical Solutions of Eq. 4-89B, $\dot{\theta}_0^2 = 1$
a) $\beta_0 > 0$
b) $\beta_0 < 0$

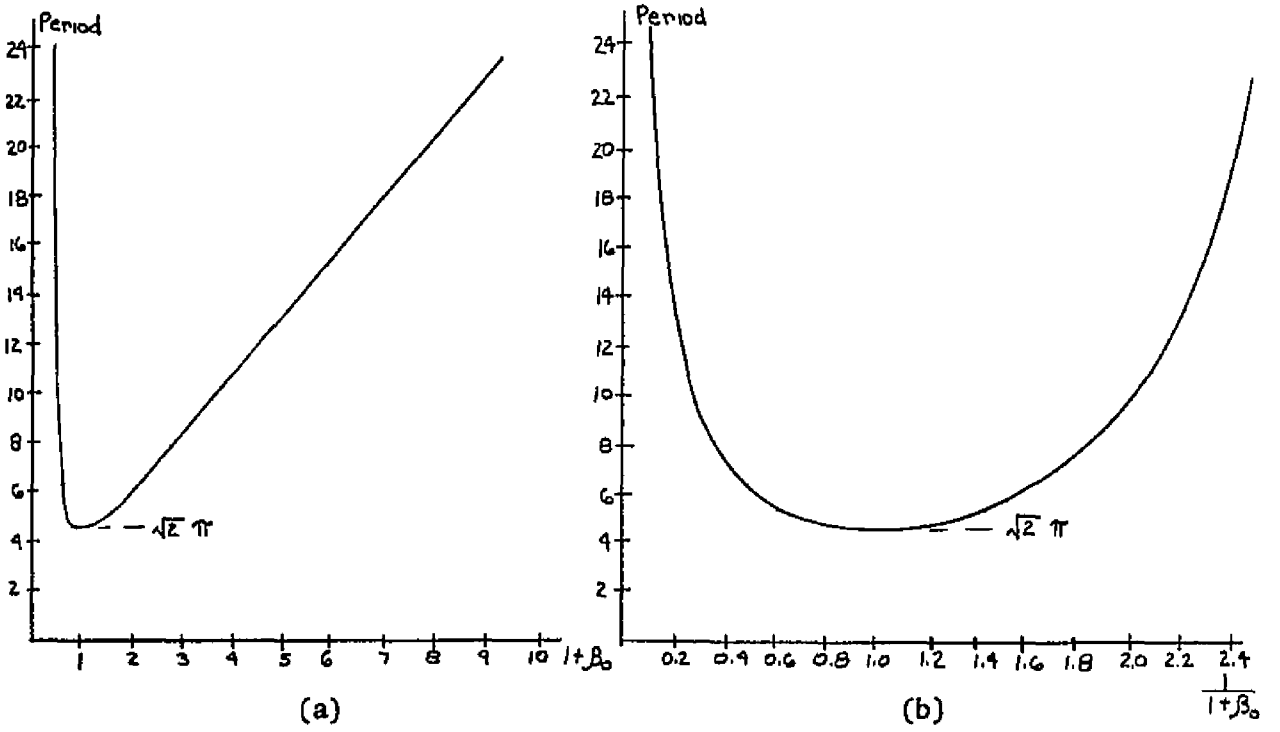

Fig. 4-5 Period Found from Numerical Results, $\dot{\theta}_0^2=1$
a) Period as a Function of $1+\beta_0$
b) Period as a Function of $\frac{1}{1+\beta_0}$

factor $y-\beta_0$ and find the three roots of P are

$$\beta_0,\ \tfrac{1}{2}\left\{\left(\tfrac{3}{5}-\beta_0\right)\left[1+\sqrt{1-\frac{4\beta_0}{\beta_0-\frac{3}{5}}}\right]\right\},\ \tfrac{1}{2}\left\{\left(\tfrac{3}{5}-\beta_0\right)\left[1-\sqrt{1-\frac{4\beta_0}{\beta_0-\frac{3}{5}}}\right]\right\} \qquad (4\text{-}93)$$

By considering the dependence of the term $\frac{4\beta_0}{\beta_0-\frac{3}{5}}$ upon β_0 we find for the character of the roots:

$-\infty<\beta_0<-\frac{1}{5}$: One real and two complex conjugate roots

$-\frac{1}{5}\le\beta_0\le\frac{3}{5}$: Three real roots

$\frac{3}{5}<\beta_0<\infty$: One real and two complex conjugate roots

We expect the solution to be most valid for β_0 near zero so we restrict ourselves, at least, to the case for three real roots. Note that the roots are the values of β for which $\dot{\beta}$ is zero, from 4-92A, so therefore they have the significance of turning points of the orbit. We have shown that the turning points occur in pairs so that the situation for which only one

real root is obtained is not a valid one, occurring for β_0 too far from zero for which the model breaks down. For β_0 near zero we obtain three real roots, yielding one too many turning points. Obviously the approximation made has introduced an additional nonphysical solution. According to the initial assumption about β_0, it itself is one of the turning points. The extraneous root is one of the roots of the quadratic term. Note that for small β_0

$$\frac{1}{2}\left\{\left(\frac{3}{5}-\beta_0\right)\left[1+\sqrt{1-\frac{4\beta_0}{\beta_0-\frac{3}{5}}}\right]\right\}\approx\frac{3}{5} \tag{4-94A}$$

$$\frac{1}{2}\left\{\left(\frac{3}{5}-\beta_0\right)\left[1-\sqrt{1-\frac{4\beta_0}{\beta_0-\frac{3}{5}}}\right]\right\}\approx-\beta_0 \tag{4-94B}$$

We demand that the solution for small β_0, approach the result for the linear oscillations where the turning points are symmetric. Thus, 4-94A represents the extraneous root for sufficiently small β_0. Further, note from 4-91 that $\ddot{\beta}=0$ for $\beta=0$ and $\beta=\frac{2}{5}$. Thus, there are two equilibrium points possible for this model which, of course, is in contrast with the physical situation where only $\beta=0$ qualifies as an equilibrium point. Furthermore, examining $\dddot{\beta}$ we see that

$$\dddot{\beta}>0 \quad \text{for} \quad \beta<0$$
$$\dddot{\beta}<0 \quad \text{for} \quad 0<\beta<\tfrac{2}{5}$$
$$\dddot{\beta}>0 \quad \text{for} \quad \beta>\tfrac{2}{5}$$

so that the motion is bounded for the first two regions and unbounded for the third. We therefore must impose the further restriction that β_0 be less than 2/5. For $\beta_0=\frac{2}{5}$ the physical root, given by 4-94B, yields the value -1/5 for the other turning point. Thus β_0 is restricted between -1/5 and its corresponding turning point, 2/5. In Fig. 4-6 we contrast the turning points as found from 4-94B, the result from the linear approximation, and the results from the numerical solution of the differential equation. We note that the approximation 4-94B yields a rather good improvement over the linear approximation and that the numerically derived results lie between the approximations.

In order to cast 4-92B into a standard form, the roots must be ordered.

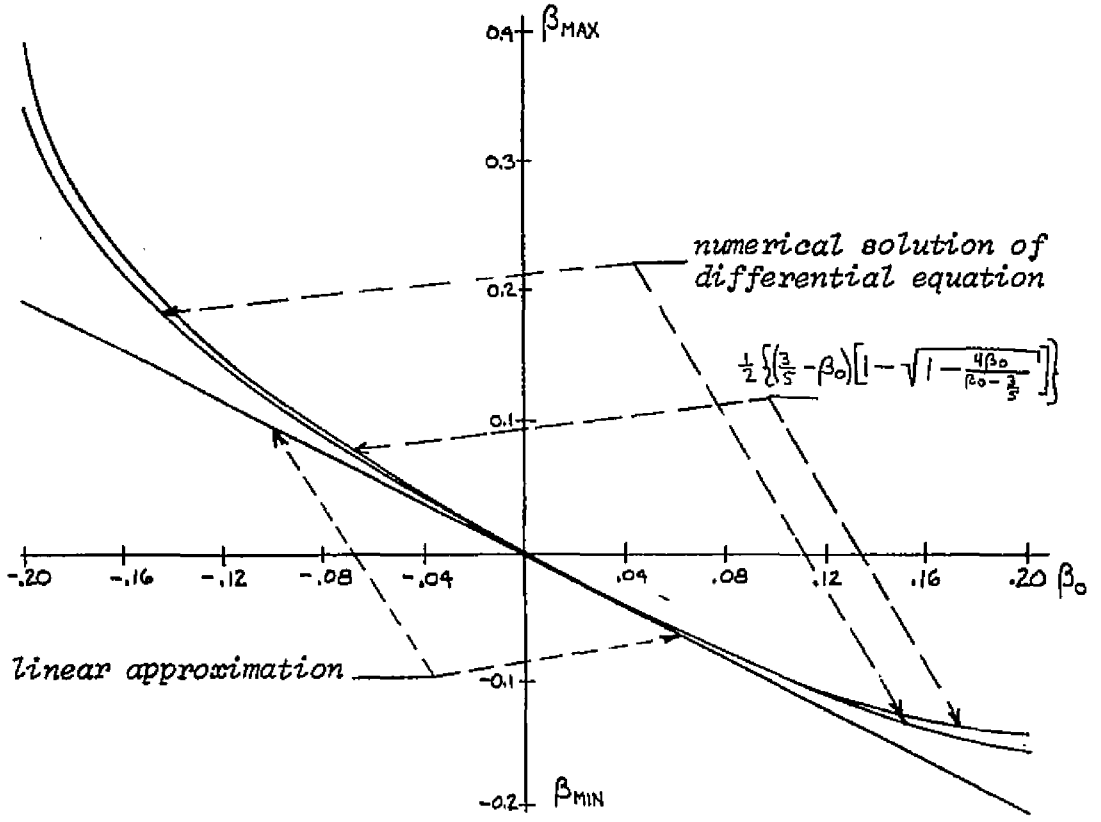

Fig. 4-6 Turning Points, $\dot{\theta}_0^2=1$

We find for the previous restrictions on β_0 that

$$\frac{1}{2}\left\{\left(\frac{3}{5}-\beta_0\right)\left[1-\sqrt{1-\frac{4\beta_0}{\beta_0-\frac{3}{5}}}\right]\right\} < \beta_0 < \frac{1}{2}\left\{\left(\frac{3}{5}-\beta_0\right)\left[1+\sqrt{1-\frac{4\beta_0}{\beta_0-\frac{3}{5}}}\right]\right\}, \quad \beta_0>0 \tag{4-95A}$$

$$\beta_0 < \frac{1}{2}\left\{\left(\frac{3}{5}-\beta_0\right)\left[1-\sqrt{1-\frac{4\beta_0}{\beta_0-\frac{3}{5}}}\right]\right\} < \frac{1}{2}\left\{\left(\frac{3}{5}-\beta_0\right)\left[1+\sqrt{1-\frac{4\beta_0}{\beta_0-\frac{3}{5}}}\right]\right\}, \quad \beta_0<0 \tag{4-95B}$$

We proceed to identify 4-92B as one of two standard forms in accordance with whether β_0 is greater than or less than zero. The solutions have separated naturally into two parts depending upon whether the electron is initially above or below the equilibrium radius. Having cast the solution 4-92B into the two forms we find for $\beta_0>0$

$$\lambda_+ = \frac{1}{2}\sqrt{\left(\frac{3}{5}-\beta_0\right)\sqrt{1-\frac{4\beta_0}{\beta_0-\frac{3}{5}}}} \tag{4-96A}$$

$$m_+ = \sin^2\alpha_+ = \frac{\beta_0-\frac{1}{2}\left(\frac{3}{5}-\beta_0\right)\left[1-\sqrt{1-\frac{4\beta_0}{\beta_0-3/5}}\right]}{\left(\frac{3}{5}-\beta_0\right)\sqrt{1-\frac{4\beta_0}{\beta_0-3/5}}} \tag{4-96B}$$

$$\cos^2\varphi_+ = \frac{\left\{\frac{1}{2}\left(\frac{3}{5}-\beta_0\right)\left[1+\sqrt{1-\frac{4\beta_0}{\beta_0-\frac{3}{5}}}\right]-\beta_0\right\}\left\{\beta-\frac{1}{2}\left(\frac{3}{5}-\beta_0\right)\left[1-\sqrt{1-\frac{4\beta_0}{\beta_0-\frac{3}{5}}}\right]\right\}}{\left\{\beta_0-\frac{1}{2}\left(\frac{3}{5}-\beta_0\right)\left[1-\sqrt{1-\frac{4\beta_0}{\beta_0-\frac{3}{5}}}\right]\right\}\left\{\frac{1}{2}\left(\frac{3}{5}-\beta_0\right)\left[1+\sqrt{1-\frac{4\beta_0}{\beta_0-\frac{3}{5}}}\right]-\beta\right\}} \qquad (4\text{-}96C)$$

$$t = \pm\frac{\sqrt{3/10}}{\theta_0\lambda_+}F(\varphi_+\backslash\alpha_+) = \pm\frac{\sqrt{3/10}}{\theta_0\lambda_+}F(\varphi_+|m_+) \qquad (4\text{-}96D)$$

and for $\beta_0 < 0$

$$\lambda_- = \frac{1}{2}\sqrt{\frac{1}{2}\left(\frac{3}{5}-\beta_0\right)\left[1+\sqrt{1-\frac{4\beta_0}{\beta_0-\frac{3}{5}}}\right]-\beta_0} \qquad (4\text{-}97A)$$

$$m_- = \sin^2\alpha_- = \frac{\frac{1}{2}\left(\frac{3}{5}-\beta_0\right)\left[1-\sqrt{1-\frac{4\beta_0}{\beta_0-3/5}}\right]-\beta_0}{\frac{1}{2}\left(\frac{3}{5}-\beta_0\right)\left[1+\sqrt{1-\frac{4\beta_0}{\beta_0-3/5}}\right]-\beta_0} \qquad (4\text{-}97B)$$

$$\sin^2\varphi_- = \frac{\beta-\beta_0}{\frac{1}{2}\left(\frac{3}{5}-\beta_0\right)\left[1-\sqrt{1-\frac{4\beta_0}{\beta_0-3/5}}\right]-\beta_0} \qquad (4\text{-}97C)$$

$$t = \pm\frac{\sqrt{3/10}}{\theta_0\lambda_-}F(\varphi_-\backslash\alpha_-) = \pm\frac{\sqrt{3/10}}{\theta_0\lambda_-}F(\varphi_-|m_-) \qquad (4\text{-}97D)$$

where $F(\varphi\backslash\alpha)$ and $F(\varphi|m)$ are identified as the elliptic integral of first kind of amplitude φ and modular angle α or parameter m. The stroke in the argument of F indicates which is meant. We note that we have obtained a solution which is presented in an inverse way, that is, it is given in the form $t(\beta, \beta_0)$. There is also an apparent ambiguity in the sign of t obtained by the solutions, yielding values of t for time increasing and decreasing. That they are equal in magnitude is obvious from the fact that β_0 represents a turning point of a symmetric orbit. The values of β introduced into the solutions must lie between β_0 and the other turning point, 4-94B.

In order to find the period we take for β the value of the turning point as given by 4-94B. The value obtained from 4-96D or 4-97D will be half the period since it represents the time between consecutive turning points. Using the value of β given by 4-94B, we find that both φ_+ and φ_- take on the value $\pi/2$ if we take for the range of φ, $0 \leq \varphi \leq \frac{\pi}{2}$. The elliptic

integrals become complete elliptic integrals of the first kind since

$$F\left(\frac{\pi}{2}\middle\backslash\alpha\right) = F\left(\frac{\pi}{2}\middle|m\right) \equiv K(m)$$

We find for the period, in both cases

$$T = \frac{\sqrt{1.2}}{\dot{\theta}_0 \lambda_+} K(m_+) \,, \qquad \frac{2}{5} > \beta_0 > 0 \tag{4-98A}$$

$$T = \frac{\sqrt{1.2}}{\dot{\theta}_0 \lambda_-} K(m_-) \,, \qquad -\frac{1}{5} < \beta_0 < 0 \tag{4-98B}$$

The pair of formulas given in 4-98 give the period if one is given β_0, the choice depending upon the sign of β_0. We realize, however, that either formulation may be used in either case since 4-94B provides us with the other turning point, of opposite sign, which may be used with the companion formula to find the period. As $\beta_0 \to 0$ we have from 4-96 and 4-97 that both m_+ and m_- approach zero. In the same limit both λ_+ and λ_- approach $\frac{1}{2}\sqrt{\frac{3}{5}}$ so that, from 4-98

$$\lim_{\beta_0 \to 0} T = \frac{2\sqrt{2}}{\dot{\theta}_0} \lim_{m \to 0} K(m) = \frac{\sqrt{2}\pi}{\dot{\theta}_0} \tag{4-99A}$$

since[86]

$$K(m) = \frac{\pi}{2}\left[1 + \left(\tfrac{1}{2}\right)^2 m + \left(\frac{1\cdot 3}{2\cdot 4}\right)^2 m^2 + \left(\frac{1\cdot 3\cdot 5}{2\cdot 4\cdot 6}\right)^2 m^3 + \cdots\right], \quad |m| < 1 \tag{4-99B}$$

matching the period of the linear differential equation.

In Fig. 4-7, the period as found by Eqs. 4-98 is compared with the linear approximation and with the results obtained by the numerical solution of the differential equation, 4-89B. It is noted that

$$\lim_{\substack{\beta_0 \to -.2 \\ \beta_0 > -.2}} \frac{\sqrt{1.2}}{\lambda_-} K(m_-) = \lim_{\substack{\beta_0 \to .4 \\ \beta_0 < .4}} \frac{\sqrt{1.2}}{\lambda_+} K(m_+) = \infty$$

since $m_- \to m_+ \to 1$ in the respective limits. These conditions are consistent with the earlier discussion dealing with the bounds of β_0. As the condition for escape is approached the electron requires more and more time to return to its initial value. Again, escape is not physically possible

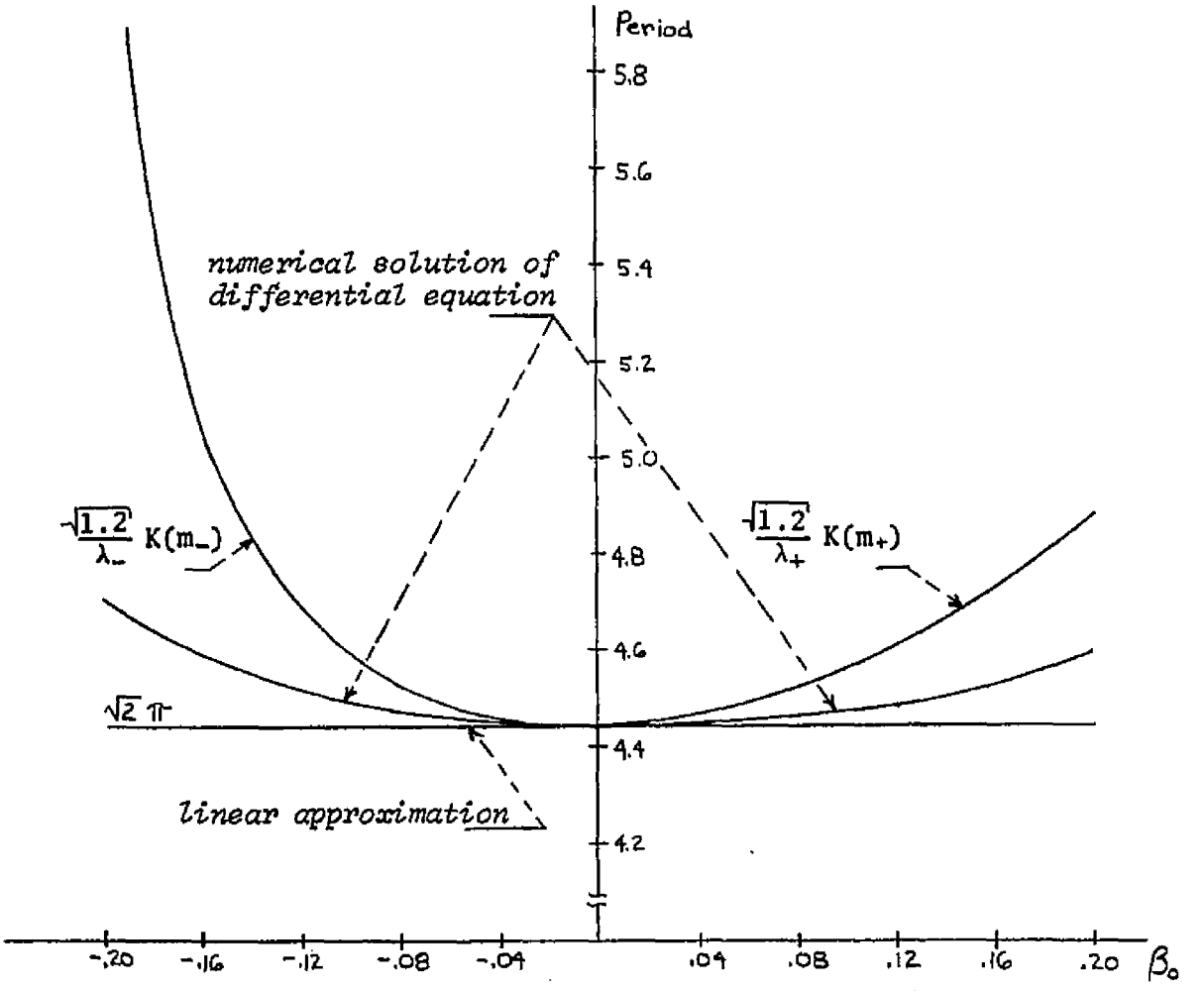

Fig. 4-7 Period as Found by Elliptic Integral, Numerical Solution, and Linear Approximation; $\dot{\theta}_0^2=1$

as was shown in earlier analyses, and we see a breakdown of the model. We observe in Fig. 4-7, as in Fig. 4-6, that the numerical solution lies between the linear approximation and the result in terms of the elliptic integral. The elliptic integral results for the period mirror the shape of the numerical results but diverge from the latter as $|\beta_o|$ increases. The elliptic integral results are due to retention of linear and square terms in the expansion of the force term of the differential equation, 4-89B. Expansion of the differential equation for small enough $|\beta|$, yields

$$\ddot{\beta} + \dot{\theta}_o^2\left\{2\beta + \sum_{m=1}^{\infty}(-1)^m\frac{(m+1)(m+4)}{2}\beta^{m+1}\right\} = 0,\ |\beta|<1 \qquad (4\text{-}100)$$

Note that all odd powers of β have positive coefficients and all even

powers have negative coefficients. If we were to find a solution to the differential equation obtained by retaining up to the third power in β, it is suspected that the period found would be smaller than the elliptic integral period. This is because the cubic term supplies a symmetric restoring force which increases with the magnitude of the displacement as in the case of the hard spring oscillator.[87] In such an oscillator the period is known to decrease as the "hardness" is increased.

We obtain an approximation for the dependence of the period upon initial condition by use of the principle of harmonic balance[88] as applied to the differential equation, 4-89B, since for the physical case the solution is known to be oscillatory. We take for the approximate solution a purely sinusoidal term

$$\beta \approx \beta_0 \cos\omega t \tag{4-101}$$

and use this approximate solution in 4-89B, so that

$$-\omega^2\left\{\beta_0\cos\omega t + \frac{3\beta_0^2}{2}\left[1+\cos 2\omega t\right] + \frac{3}{4}\beta_0^3\left[3\cos\omega t + \cos 3\omega t\right]\right.$$
$$\left. + \frac{\beta_0^4}{8}\left[\cos 4\omega t + 4\cos 2\omega t + 3\right]\right\} + \dot{\theta}_0^2\left[\frac{\beta_0^2}{2}\cos 2\omega t + 2\beta_0\cos\omega t + \frac{\beta_0^2}{2}\right] \approx 0 \tag{4-102}$$

According to the principle, we require that only the terms in $\cos\omega t$ satisfy exactly the equation. This leads to

$$T = \frac{2\pi}{\omega} \approx \frac{\sqrt{2}\,\pi}{\dot{\theta}_0}\sqrt{1 + \frac{9}{4}\beta_0^2} \tag{4-103}$$

The approximate period as found from 4-103 is compared with the numerical solution result in Fig. 4-8. The approximate period is seen to be quite a good approximation relative to the results found by elliptic integral. The approximation is symmetrical in β_0 while the numerical solution is asymmetrical. The approximation is seen to be closer for $\beta_0 > 0$.

We make an observation concerning the stability of the system. The system, oscillating, follows a closed path in the phase or $\beta\dot{\beta}$, plane. If it is disturbed slightly the system will follow a different closed path close to the original one. As the disturbance is made vanishingly small, the

paths come vanishingly close together. In this sense the system is stable. However, we showed that the periods of the two oscillations will be slightly different for a small but nonzero disturbance. The system point therefore travels around the phase plane trajectories at slightly different rates. The system points will therefore become far apart as time increases indefinitely no matter how small the perturbation. In this sense the system is not stable due to the "slip" between the trajectories.

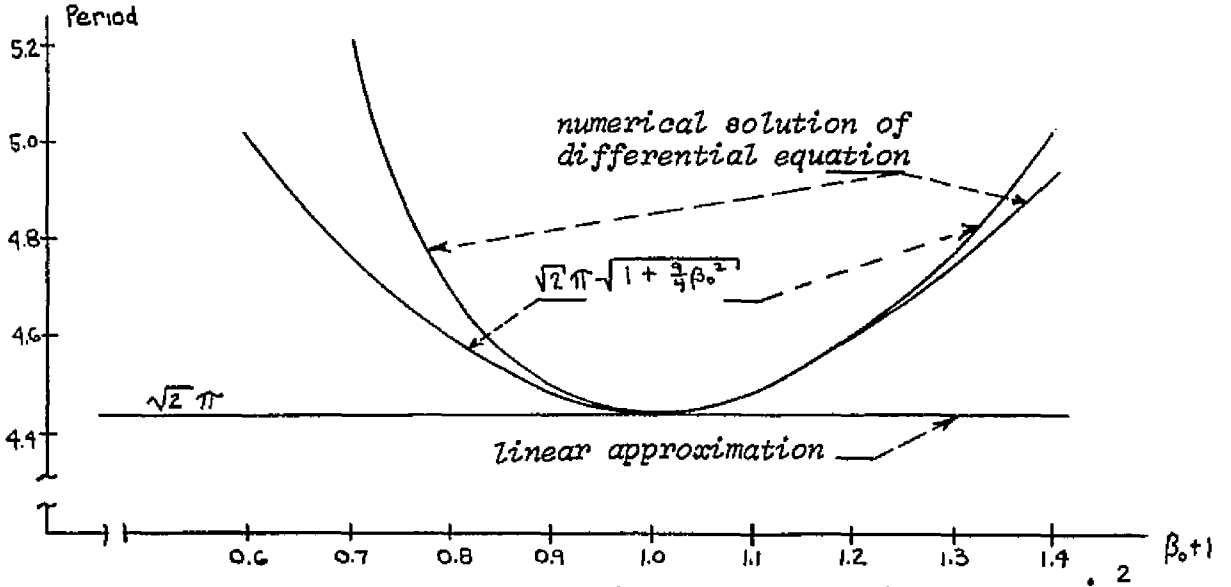

Fig. 4-8 Analysis by Priniciple of Harmonic Balance, $\dot{\theta}_0^2 = 1$

Part Two--Corrugated Inner Boundary

4.9 The Differential Equation

In considering the motion of electrons under the influence of the spatially periodic static fields we make the simplifying assumptions that the electrons do not interact with each other and that the electron beam is of vanishingly small thickness. The problem is therefore equivalent to considering the motion of a single electron in these fields. We assume that the beam is confined to region I of Fig. 2-1. For the rectangular geometry we

found, as in Eq. 3-65A, that the potential in this region may be written as a constant plus linear term plus a function whose average value is zero over the period. With this in mind we may divide the potential in region I in the nonuniform cylindrical geometry into two parts. The first part consists of the solution to Laplace's equation if the inner boundary were smooth and the second part contains the effect of the corrugations. That is,

$$\phi(r,z) \equiv C_0 + C_1 \ln r + \tilde{\phi}(r,z) \tag{4-104}$$

We expand $\tilde{\phi}(r,z)$ in a Taylor series about the radius r_0 which holds for neighborhoods excluding boundary points. This radius is the equivalent of the equilibrium radius which we dealt with in Part One of this chapter. The beam is injected at this value of radius and if the motion is stable the electrons will execute small motions about it. We have,*

$$\tilde{\phi}(r,z) = \sum_{m=0}^{\infty} Q_m(z)\frac{(r-r_0)^m}{m!} \equiv \sum_{m=0}^{\infty} \frac{Q_m(z)\rho^m}{m!} \tag{4-105A}$$

$$\frac{\partial\tilde{\phi}}{\partial r}(r,z) = \sum_{m=0}^{\infty} \frac{Q_{m+1}(z)\rho^m}{m!} \tag{4-105B}$$

$$\frac{\partial\tilde{\phi}}{\partial z}(r,z) = \sum_{m=0}^{\infty} \frac{Q_m'(z)\rho^m}{m!} \tag{4-105C}$$

We have from 4-5 using 4-104 and 4-105B

$$\ddot{r} - \frac{l^2}{m^2 r^3} = \zeta\left[\frac{C_1}{r} + \sum_{m=0}^{\infty} Q_{m+1}(z)\frac{\rho^m}{m!}\right] \tag{4-106}$$

Observe from 4-106 that for $r=r_0$ we may balance the centrifugal and uniform electric forces as was done in Part One of this chapter but there will still be a force proportional to $Q_1(z)$. Obviously r_0 cannot represent an equilibrium radius in the sense that there exists a set of conditions leading to $r=r_0$ for all z. $Q_1(z)$, as well as all the $Q_n(z)$, has zero average value so that in consonance with the development in Part One, we

---

* The order of summation and differentiation may be interchanged because ϕ is the real or imaginary part of an analytic function, whose derivatives of all orders are analytic functions[89] with unique power series.

demand

$$-\frac{\ell^2}{m^2 r_0^3} = \zeta \frac{C_1}{r_0} \tag{4-107}$$

We expand 4-106, subject to 4-107, about $r=r_0$ and retain only up to linear terms in ρ. In terms of $\dot{\theta}_0$ defined in 4-88 we have

$$\ddot{\rho} + 2\dot{\theta}_0^2 \rho = \zeta \left[Q_1(\zeta) + Q_2(\zeta)\rho\right] \tag{4-108}$$

We view the left-hand side of 4-108 as the natural system without the presence of the periodic potential. The right-hand side gives the effects of that perturbation. We express the longitudinal velocity of the electron as a constant plus a varying quantity, viz.,

$$\dot{\zeta} \equiv v_{0\zeta} + \tilde{v}_\zeta \tag{4-109}$$

From 4-6, 4-105C and 4-109, to first order,

$$\frac{d\tilde{v}_\zeta}{dt} = \zeta\left[Q_0'(\zeta) + Q_1'(\zeta)\rho\right] \tag{4-110}$$

In the differential equation for ρ, 4-108, we change the independent variable from time to axial position. Toward this end we have

$$\dot{\rho} = \frac{d\rho}{d\zeta}\left[v_{0\zeta} + \tilde{v}_\zeta\right] \tag{4-111A}$$

$$\ddot{\rho} = \frac{d\rho}{d\zeta^2}\left[v_{0\zeta} + \tilde{v}_\zeta\right]^2 + \frac{d\rho}{d\zeta}\frac{d\tilde{v}_\zeta}{dt} \tag{4-111B}$$

We find from 4-108, 4-110, and 4-111B with retention of first order terms

$$v_{0\zeta}^2 \frac{d^2\rho}{d\zeta^2} + \zeta Q_0'(\zeta)\frac{d\rho}{d\zeta} + \left[2\dot{\theta}_0^2 - \zeta Q_2(\zeta)\right]\rho = \zeta Q_1(\zeta) \tag{4-112}$$

recognized as a nonhomogeneous linear differential equation with periodic coefficients. It is easily seen that in the absence of the nonuniform boundary the solution of 4-112 reduces to the "natural" oscillations of the linear differential equation discussed in Sec. 4.8. Defining the

"wavelength" of these natural oscillations of the electron in the logarithmic potential as

$$\lambda_0 = \sqrt{2}\,\pi \frac{v_{0z}}{\theta_0} \tag{4-113A}$$

we have

$$\frac{d^2\rho}{dz^2} + \frac{2}{v_{0z}^2} Q_0'(z) \frac{d\rho}{dz} + \left[\left(\frac{2\pi}{\lambda_0}\right)^2 - \frac{2}{v_{0z}^2} Q_2(z)\right]\rho = \frac{2}{v_{0z}^2} Q_1(z) \tag{4-113B}$$

We change the dependent variable in order to produce a differential equation which has no first derivative term.[90] Let

$$\sigma \equiv \rho\, e^{\frac{1}{2}\frac{2}{v_{0z}^2}\int Q_0'(z)\,dz} = \rho\, e^{\frac{1}{2}\frac{2}{v_{0z}^2} Q_0(z)} \tag{4-114A}$$

The differential equation for σ is then found to be

$$\frac{d^2\sigma}{dz^2} + \left\{\left(\frac{2\pi}{\lambda_0}\right)^2 - \frac{2}{v_{0z}^2} Q_2(z) - \frac{1}{4}\left[\frac{2}{v_{0z}^2} Q_0'(z)\right]^2 - \frac{1}{2}\frac{2}{v_{0z}^2} Q_0''(z)\right\}\sigma$$
$$= \frac{2}{v_{0z}^2} Q_1(z)\, e^{\frac{1}{2}\frac{2}{v_{0z}^2} Q_0(z)} \tag{4-114B}$$

Observe that since $Q_0(z)$ is periodic so will be the function

$$e^{\frac{1}{2}\frac{2}{v_{0z}^2} Q_0(z)}$$

which transforms ρ into σ and modifies the forcing function of the differential equation. We conclude that ρ and σ are together both bounded or unbounded functions of z. In considering the stability of ρ it is sufficient to examine the stability of σ.

The physical period of the structure equals L but it is convenient to change the independent variable such that the period becomes π. This is motivated by the twofold reason that Laplace's equation was solved in Chap. 3 for a base period equal to π as a natural consequence of the mapping used; and because the most studied periodic differential equation, Mathieu's equation, has a period equal to π. Therefore, we define

$$\zeta = \frac{\pi}{L} z \tag{4-115A}$$

$$\zeta = \frac{\pi}{L}\rho \tag{4-115B}$$

For large radius of curvature the coefficients appearing in the differential equation will be derived from the solution of the Laplace equation in the rectangular approximation of Chap. 3. That solution may be expanded about $y=y_0$, where y_0 is the rectangular equivalent of r_0, and $y-y_0$ is the ζ of Eq. 4-115B. The form of the expansion is noted from 3-65A and is the equivalent of 4-104 and 4-105A. Thus,

$$\Psi(\zeta,\varsigma) = a + b\zeta + \sum_{m=0}^{\infty} \frac{f_m(\varsigma)}{m!}\zeta^m \tag{4-116}$$

where the $f_n(\varsigma)$ have zero average value over the period, π. The potential will be normalized with respect to the constant b of 4-116, which can be related to the constant c_1 of Eq. 4-104. If we expand[91] the logarithmic term of 4-104 about r_0 we have, in terms of ζ

$$C_1 \ln r = C_1 \left\{ \ln r_0 + \sum_{m=1}^{\infty} \frac{(-1)^{m+1}}{m} \left[\frac{L}{\pi} \frac{\zeta}{r_0} \right]^m \right\}; \qquad \left| \frac{L}{\pi} \frac{\zeta}{r_0} \right| \leq 1, \ \frac{L}{\pi} \frac{\zeta}{r_0} \neq -1 \tag{4-117}$$

For small ζ we truncate the series at the linear term and comparison of 4-116 and 4-117 yields

$$b = \frac{C_1}{r_0} \frac{L}{\pi} = -2\pi \frac{r_0}{\lambda_0} \frac{L}{\lambda_0} \frac{v_{0\zeta}^2}{\zeta} \tag{4-118}$$

using 4-107, 4-88 and 4-113A. In addition, we have from 4-116 that

$$f_0(\varsigma) = \Psi(0,\varsigma) - a \tag{4-119A}$$

$$f_2(\varsigma) = \frac{\partial^2 \Psi}{\partial \zeta^2}(0,\varsigma) \tag{4-119B}$$

so that

$$f_0''(\varsigma) = \frac{\partial^2 \Psi}{\partial \varsigma^2}(0,\varsigma) = -\frac{\partial^2 \Psi}{\partial \zeta^2}(0,\varsigma) = -f_2(\varsigma) \tag{4-119C}$$

since Ψ satisfies Laplace's equation in ζ and ς. Normalizing σ with respect

to r_0, viz.,

$$\delta \equiv \frac{\rho}{r_0} \tag{4-120}$$

and using 4-115, 4-118, 4-119C, 4-120 and 4-114 we arrive at the differentiated equation

$$\frac{d^2\delta}{d\varphi^2} + \left[\frac{2L}{\lambda_0}\right]^2 \left\{ 1 + \frac{\pi}{4}\frac{r_0}{L}\frac{f_2(\varphi)}{b} - \left(\frac{2L}{\lambda_0}\right)^2 \left(\frac{\pi}{4}\right)^2 \left(\frac{r_0}{L}\right)^2 \left[\frac{f_0'(\varphi)}{b}\right]^2 \right\} \delta = -\frac{1}{2}\left(\frac{2L}{\lambda_0}\right)^2 \frac{f_1(\varphi)}{b} e^{-\frac{\pi}{4}\frac{r_0}{L}\left[\frac{2L}{\lambda_0}\right]^2 \frac{f_0(\varphi)}{b}} \tag{4-121A}$$

$$\rho = r_0 \delta \, e^{\frac{\pi}{4}\frac{r_0}{L}\left[\frac{2L}{\lambda_0}\right]^2 \frac{f_0(\varphi)}{b}} \tag{4-121B}$$

Observe that 4-121 obeys the general characteristics of a trajectory in a static electric field in that the path is independent of the charge and mass, magnitude of the field, absolute dimensions and direction of travel. Consider the exponential function which appears in the transformation equation relating ρ to δ, viz.,

$$e^{\frac{\pi}{4}\frac{r_0}{L}\left[\frac{2L}{\lambda_0}\right]^2 \frac{f_0(\varphi)}{b}}$$

A similar function appears in the forcing function of the differential equation, 4-121A, with a negative exponent. Referring to 3-65A we see that we may write $\frac{f_0(\varphi)}{b}$ as

$$\frac{f_0(\varphi)}{b} = \sum_{m=1}^{\infty} a_m \cos 2m\varphi \tag{4-122A}$$

Therefore*

$$e^{\frac{\pi}{4}\frac{r_0}{L}\left[\frac{2L}{\lambda_0}\right]^2 \frac{f_0(\varphi)}{b}} = \prod_{m=1}^{\infty} e^{\frac{\pi}{4}\frac{r_0}{L}\left[\frac{2L}{\lambda_0}\right]^2 a_m \cos 2m\varphi} \tag{4-122B}$$

---

* A sufficient condition for the infinite product to converge is that[92]

$$\sum_{m=1}^{\infty} \ln\left\{ e^{\frac{\pi}{4}\frac{r_0}{L}\left[\frac{2L}{\lambda_0}\right]^2 a_m \cos 2m\varphi} \right\} = \sum_{m=1}^{\infty} \frac{\pi}{4}\frac{r_0}{L}\left[\frac{2L}{\lambda_0}\right]^2 a_m \cos 2m\varphi$$

converges, which it does.

Now, from the generating function series for the modified Bessel function of the first kind[93]

$$e^{\gamma\cos\theta} = I_0(\gamma) + 2\sum_{k=1}^{\infty} I_k(\gamma)\cos k\theta$$

we have the Fourier series decomposition

$$e^{\frac{\pi}{4}\frac{r_0}{L}\left[\frac{2L}{\lambda_0}\right]^2\frac{f_0(y)}{b}} = \prod_{m=1}^{\infty}\left\{I_0\left(a_m\tfrac{\pi}{4}\tfrac{r_0}{L}\left[\tfrac{2L}{\lambda_0}\right]^2\right) + 2\sum_{k=1}^{\infty} I_k\left(a_m\tfrac{\pi}{4}\tfrac{r_0}{L}\left[\tfrac{2L}{\lambda_0}\right]^2\right)\cos 2mky\right\} \qquad (4\text{-}123A)$$

Since[94]

$$I_\nu(\gamma) = \left(\tfrac{1}{2}\gamma\right)^\nu \sum_{k=0}^{\infty} \frac{\left(\frac{1}{4}\gamma^2\right)^k}{k!\,\Gamma(\nu+k+1)}$$

we have for the negative exponential

$$e^{-\frac{\pi}{4}\frac{r_0}{L}\left[\frac{2L}{\lambda_0}\right]^2\frac{f_0(y)}{b}} = \prod_{m=1}^{\infty}\left\{I_0\left(a_m\tfrac{\pi}{4}\tfrac{r_0}{L}\left[\tfrac{2L}{\lambda_0}\right]^2\right) + 2\sum_{k=1}^{\infty}(-1)^k I_k\left(a_m\tfrac{\pi}{4}\tfrac{r_0}{L}\left[\tfrac{2L}{\lambda_0}\right]^2\right)\cos 2mky\right\} \qquad (4\text{-}123B)$$

Far from the circuit the first term of 4-122A will suffice to represent $\frac{f_0(y)}{b}$. In this case we take

$$e^{\frac{\pi}{4}\frac{r_0}{L}\left(\frac{2L}{\lambda_0}\right)^2\frac{f_0(y)}{b}} \approx I_0\left(a_1\tfrac{\pi}{4}\tfrac{r_0}{L}\left[\tfrac{2L}{\lambda_0}\right]^2\right) + 2\sum_{k=1}^{\infty} I_k\left(a_1\tfrac{\pi}{4}\tfrac{r_0}{L}\left[\tfrac{2L}{\lambda_0}\right]^2\right)\cos 2ky \qquad (4\text{-}124A)$$

$$e^{-\frac{\pi}{4}\frac{r_0}{L}\left[\frac{2L}{\lambda_0}\right]^2\frac{f_0(y)}{b}} \approx I_0\left(a_1\tfrac{\pi}{4}\tfrac{r_0}{L}\left[\tfrac{2L}{\lambda_0}\right]^2\right) + 2\sum_{k=1}^{\infty}(-1)^k I_k\left(a_1\tfrac{\pi}{4}\tfrac{r_0}{L}\left[\tfrac{2L}{\lambda_0}\right]^2\right)\cos 2ky \qquad (4\text{-}124B)$$

The constant of normalization b is found from the solution of Laplace's equation of Chap. 3. Comparing 4-116 to the value shown in Fig. 3-18 we have

$$b = -\frac{1}{\cosh^{-1}\left[\frac{\cosh\ell_2}{\cosh\ell_1}\right]} \qquad (4\text{-}125A)$$

Therefore the function from which the varying coefficients are derived, is, from 3-34,

$$\frac{\Psi(\zeta,\gamma)}{b} = \sinh^{-1}\left\{\frac{1}{\sqrt{2}}\sqrt{\sqrt{\left(1-\frac{\sin^2\gamma+\sinh^2(y_0+\zeta)}{\cosh^2\ell_1}\right)^2+\frac{4\cos^2\gamma\sinh^2(y_0+\zeta)}{\cosh^2\ell_1}}-\left[1-\frac{\sin^2\gamma+\sinh^2(y_0+\zeta)}{\cosh^2\ell_1}\right]}\right\}-\cosh^{-1}\left[\frac{\cosh\ell_2}{\cosh\ell_1}\right] \quad (4\text{-}125B)$$

The homogeneous differential equation is obtained from 4-121A by setting the forcing function equal to zero. The varying coefficients for this equation may be obtained, for a given value of y_0, from 4-125B. Thus,

$$\frac{f_2(\gamma)}{b} = \frac{1}{b}\frac{\partial^2\Psi}{\partial\zeta^2}(0,\gamma) \quad (4\text{-}126A)$$

$$\left[\frac{f_0'(\gamma)}{b}\right]^2 = \frac{1}{b^2}\left[\frac{\partial\Psi}{\partial\gamma}(0,\gamma)\right]^2 = \frac{1}{b^2}\left\{\overline{\left[f_0'(\gamma)\right]^2}+\widetilde{\left[f_0'(\gamma)\right]^2}\right\} \quad (4\text{-}126B)$$

where in 4-126B the term has been separated into its average and varying parts. For the geometry $\frac{\ell_1}{\pi}=1$ and $\frac{\ell_2}{\pi}=3.08$, we compare the functions of interest as found from 4-125B and 4-126A and B, both with regard to wave-shape and relative magnitude, for values of $\frac{y_o}{\pi}$ equal to 1.1, 1.25 and 1.5. These results are shown in Fig. 4-9. The average value of $\left[\frac{f_o'(\gamma)}{b}\right]^2$ is equal to the negative of $\overline{\left[\frac{f_o'(0)}{b}\right]^2} = \overline{\left[\frac{f_o'(\pi/2)}{b}\right]^2}$ since these planes are planes of symmetry for the potential and therefore f_0' is zero there. Observe that the zeros of $\frac{f_2(\gamma)}{b}$ and the maximum points of $[\frac{f_o'(\gamma)}{b}]^2$ coincide, agreeing with 4-119C. Far from the circuit we have, from 4-122A,

$$\frac{f_2(\gamma)}{b} \approx 4a_1\cos 2\gamma$$

$$\widetilde{\left[\frac{f_o'(\gamma)}{b}\right]^2} \approx -2a_1^2\cos 4\gamma$$

evident for Fig. 4-9c. Observe for Fig. 4-9 a through c

$$\left|\widetilde{\left[\frac{f_o'(\gamma)}{b}\right]^2}\right|_{max} << \left|\frac{f_2(\gamma)}{b}\right|_{max}$$

Comparing, then, the two varying terms of the homogeneous differential equation we have from 4-121A that the ratio of their magnitudes is given by

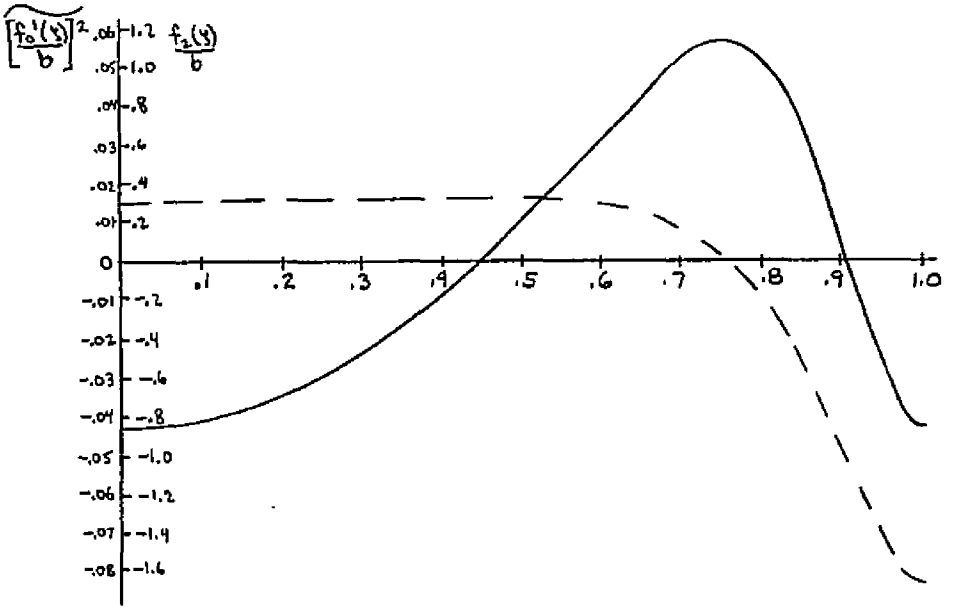

(a)

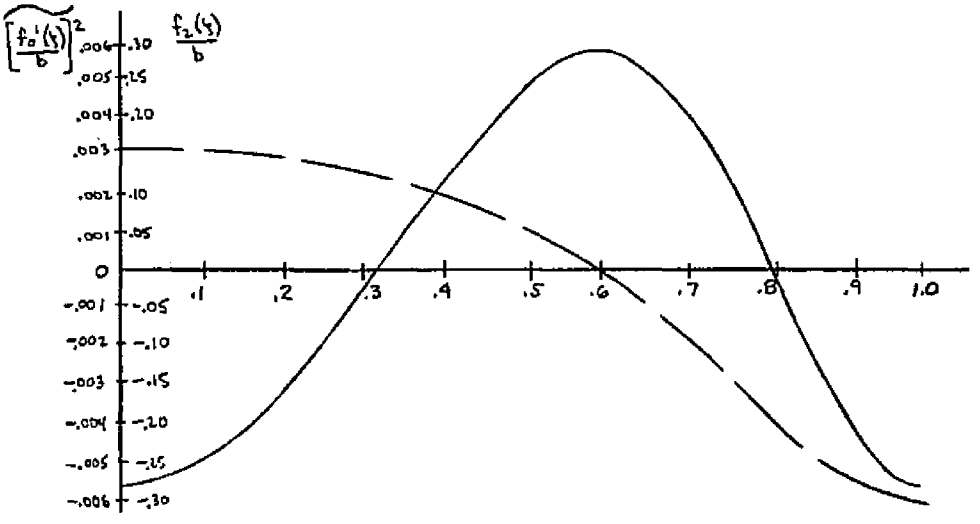

(b)

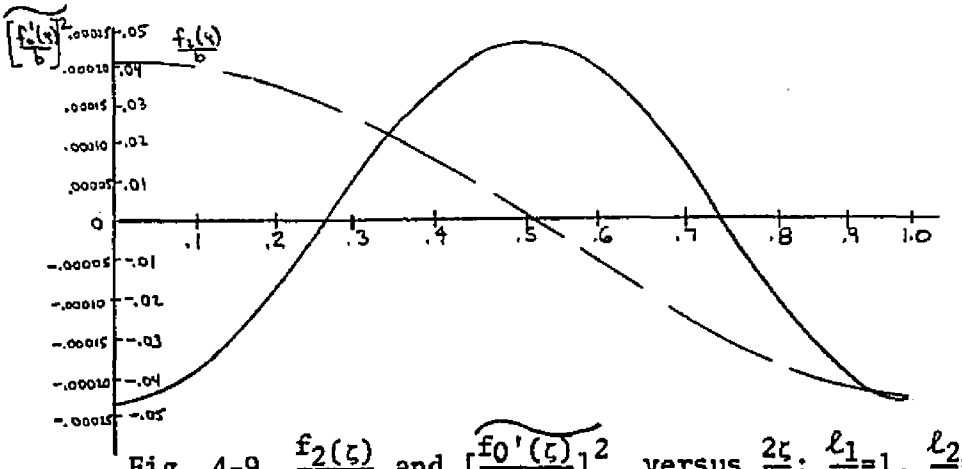

(c)

Fig. 4-9 $\frac{f_2(\zeta)}{b}$ and $\left[\frac{f_0'(\zeta)}{b}\right]^2$ versus $\frac{2\zeta}{\pi}$; $\frac{\ell_1}{\pi}=1$, $\frac{\ell_2}{\pi}=3.08$

a) $\frac{y_o}{\pi}=1.1$, b) $\frac{y_o}{\pi}=1.25$, c) $\frac{y_o}{\pi}=1.5$

--- $\frac{f_2(\zeta)}{b}$ — $\left[\frac{f_0'(\zeta)}{b}\right]^2$

$$\frac{\pi}{4}\frac{r_o}{L}\left[\frac{2L}{\lambda_o}\right]^2\left|\frac{\left[\frac{f_o'(\varsigma)}{b}\right]^2}{\frac{f_2(\varsigma)}{b}}\right| = \frac{Lr_o}{2\pi}\frac{\dot{\theta}_o^2}{v_{oz}^2}\left|\frac{\left[\frac{f_o'(\varsigma)}{b}\right]^2}{\frac{f_2(\varsigma)}{b}}\right| = \frac{1}{2\pi\frac{r_o}{L}}\frac{v_{\theta_o}^2}{v_{oz}^2}\left|\frac{\left[\frac{f_o'(\varsigma)}{b}\right]^2}{\frac{f_2(\varsigma)}{b}}\right| \qquad (4\text{-}127)$$

For large radius of curvature we have that $\frac{r_o}{L}$ is large. The term $v_{\theta_o}^2/v_{oz}^2$ is the ratio of the angular energy to the longitudinal energy of the electrons when they are injected into the system. Becuase of synchronous velocity requirements v_{oz}^2 is large and therefore to moderate the high voltage requirements the energy ratio will be kept less than one. Thus, we may neglect the second varying term in the homogeneous differential equation. In a similar manner we may show that the average value of the second varying term may be neglected with respect to one. Thus, we take for the homogeneous differential equation

$$\frac{d^2\delta}{d\varsigma^2} + \left(\frac{2L}{\lambda_o}\right)^2\left\{1 + \frac{\pi}{4}\frac{r_o}{L}\frac{f_2(\varsigma)}{b}\right\}\delta = 0 \qquad (4\text{-}128)$$

To avoid electron interception we will not allow the electron beam to come excessively close to the circuit. Thus, for the geometry of the example we will not take $\frac{y_o}{\pi}$ less than 1.1. In addition, the zero tooth width solution for potential will not be accurate close to the teeth for any physical geometry of small, but finite, width. With reference to Fig. 4-9a we see that for the lower limit of $\frac{y_o}{\pi}$ the function $\frac{f_2(\varsigma)}{b}$ appears parabolic in form. With reference to Fig. 4-9c we note that for larger values of $\frac{y_o}{\pi}$ it would be appropriate to approximate $\frac{f_2(\varsigma)}{b}$ by a cosinusoidal term. We distinguish, therefore, two cases. The varying term in the homogeneous differential equation, 4-128, will be taken to be parabolic or cosinusoidal depending upon the choice of $\frac{y_o}{\pi}$. In the case of the parabolic approximation the parabolas join at the boundaries of each period so that the resulting function appearing in the differential equation is piecewise smooth, having cusps at the period boundaries.

4.10 The Piecewise Quadratic Hill's Equation

We consider the following homogeneous differential equation

$$u'' + J(\vartheta)\, u = 0 \tag{4-129A}$$

where

$$J(\vartheta) = \eta + \gamma\left[\frac{\pi^2}{12} - \vartheta^2\right], \qquad |\vartheta| \le \frac{\pi}{2} \tag{4-129B}$$

and

$$J(\vartheta) = J(\vartheta \pm n\pi), \quad \text{n an integer} \tag{4-129C}$$

so that $J(\vartheta)$ is a periodic function of ϑ with period π and is given by 4-129B in the base period $-\frac{\pi}{2} \le \vartheta \le \frac{\pi}{2}$. The period of $J(\vartheta)$ is taken to be π so that the periodic differential equation 4-129A will be in consonance with Mathieu's equation, the most studied periodic differential equation. The function $J(\vartheta)$ is even and therefore we may expand it in a Fourier series*

$$J(\vartheta) = \Theta_0 + \sum_{r=1}^{\infty} 2\Theta_r \cos 2r\vartheta \tag{4-130}$$

The value of γ may be taken to be positive or negative in the general case so that we obtain an "invected" or "engrailed"† $J(\vartheta)$ respectively, as is shown in Fig. 4-10. Reference to Fig. 4-9a indicates that the case of interest is of the "invected" type, $\gamma > 0$, so we will focus our attention there.

We have taken pains to express $J(\vartheta)$ in the form 4-129B to be similar to 4-128, that is, in the form of a constant plus a varying function whose average value is zero. This obviously may always be done without loss of

---

* If $\Theta_r = 0$ for $r \ge 1$ the differential equation is simply the harmonic equation. If Θ_1 is nonzero and $\Theta_r = 0$ for $r \ge 2$ the differential equation is the Mathieu equation which has been studied extensively.[95,96] If $\Theta_r = 0$ for $r \ge 3$ and Θ_1 and Θ_2 are nonzero the equation is called the Whittaker-Hill equation, the Whittaker equation or Ince's equation. The general case is called Hill's equation after Hill's work on the motion of the moon[97] Hill's method for determining the characteristic exponent involves the solution of an infinite determinant.[98] We present a finite solution in terms of special functions for the case under consideration.

† The classification is taken from names of similar curves in heraldic

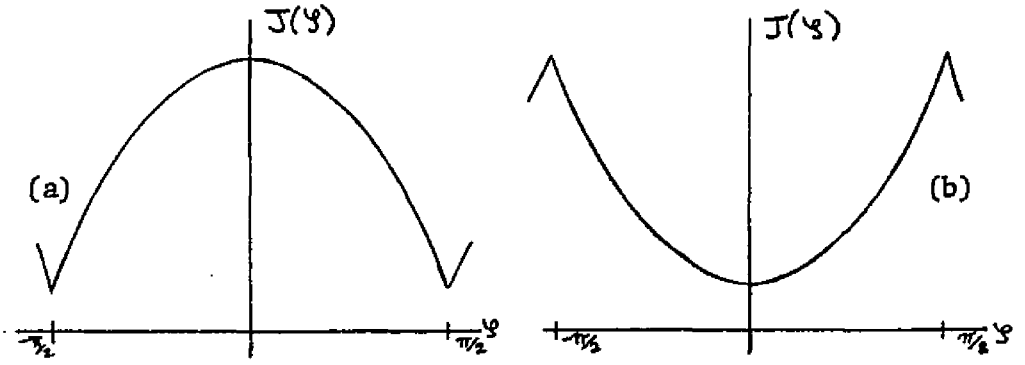

Fig. 4-10 $J(\zeta)$
a) Invected, $\gamma>0$
b) Engrailed, $\gamma<0$

generality. This form for $J(\vartheta)$ is also suggested in the literature[99] to divide the stability plane into three regions of general behavior for each sign of γ. According to those results if we write the differential equation 4-129A in the form

$$u'' + [\eta + \gamma f(\vartheta)]u = 0 \tag{4-131A}$$

$$\overline{f(\vartheta)} = 0 \tag{4-131B}$$

Then if f_M and $-f_m$ are the maximum and minimum values of $f(\vartheta)$ we may divide the $\eta\gamma$ plane into regions by the lines

$$\eta = -\gamma f_M \tag{4-132A}$$

$$\eta = \gamma f_m \tag{4-132B}$$

For the case at hand we obtain the lines

$$\gamma = \frac{6}{\pi^2}\eta \tag{4-133A}$$

$$\gamma = -\frac{12}{\pi^2}\eta \tag{4-133B}$$

The division of the $\eta\gamma$ plane is shown in Fig. 4-11 where the regions I, II and III correspond to, respectively, domains of unstable solutions;

---

symbolism.

narrow domains of stable solutions and broad regions of instability; and narrow regions of instability and broad stable domains. The asymmetrical division of the plane for positive and negative δ indicates the differences in the results for the invected and engrailed cases. This is contrasted with the result for the Mathieu equation which produces symmetrical results for positive or negative δ . This is easily seen to be true in that case since a translation of $\frac{\pi}{2}$ will result in a negative δ and translation cannot affect the stability of the equation. This division of the plane compares very well with the results of the solution of 4-129 with $\delta > 0$ to be presented later. The regions may be understood when it is realized that for region I $J(\vartheta)$ is always negative and for region III $J(\vartheta)$ is always positive. We therefore expect that for region I the solutions will resemble the hyperbolic functions for the most part, while for region III the solutions will be similar to the circular functions, mainly.

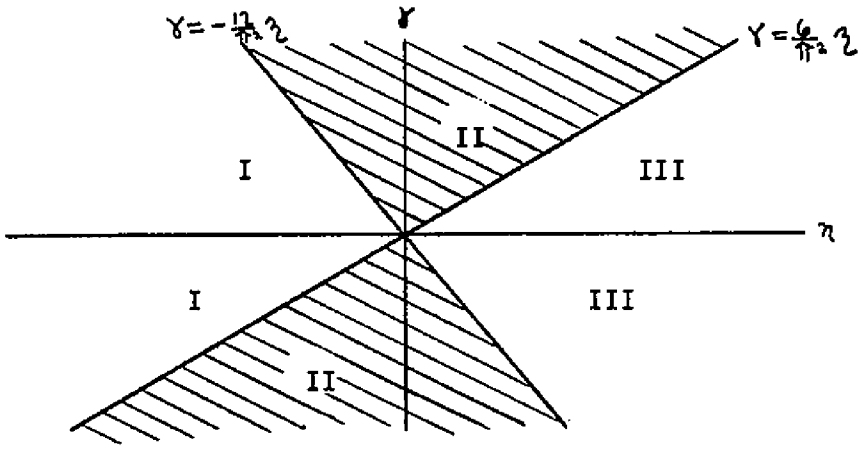

Fig. 4-11 Division of the $\eta\gamma$ Plane

The fundamental result in the theory of Hill's equation is Floquet's theorem. The $J(\vartheta)$ in 4-129A has minimum period π so that for all ϑ , $J(\vartheta+\pi)=J(\vartheta)$, and if s is a number such that $0<s<\pi$ then there exists at least one real interval such that

$$J(\vartheta+s) \neq J(\vartheta)$$

for ϑ in that interval. There exist normalized solutions to the differential equation which are independent and which have the properties that

$$u_1(0) = 1 \tag{4-134A}$$

$$u_1'(0) = 0 \tag{4-134B}$$

$$u_2(0) = 0 \tag{4-134C}$$

$$u_2'(0) = 1 \tag{4-134D}$$

The characteristic equation[100] is

$$\sigma^2 - [u_1(\pi) + u_2'(\pi)]\sigma + 1 = 0 \tag{4-135}$$

and we note that the product of the roots of 4-135, σ_1 and σ_2, equals unity. Either they both have unit magnitude or one of them has magnitude greater than unity. We therefore may, without loss of generality, define

$$e^{\mu\pi} = \sigma_1 \tag{4-136A}$$

$$e^{-\mu\pi} = \sigma_2 \tag{4-136B}$$

where μ is the characteristic exponent. Observe that $\sigma_1 = \sigma_2$ if and only if $\sigma = \pm 1$. Since the sum of the roots equals the bracketed term in 4-135 we may write

$$2\cosh\mu\pi = u_1(\pi) + u_2'(\pi) \tag{4-137}$$

Floquet's theorem[101] states that we may always find a solution of the differential equation such that

$$u(\zeta + \pi) = \sigma u(\zeta) \tag{4-138}$$

If σ_1 and σ_2 are different from each other then Hill's equation has two linearly independent solutions

$$e^{\mu\zeta} Q_1(\zeta) \tag{4-139A}$$

$$e^{-\mu\zeta} Q_2(\zeta) \tag{4-139B}$$

where $Q_1(\vartheta)$ and $Q_2(\vartheta)$ are periodic with period π . If $\sigma_1=\sigma_2$ then Hill's equation has a nontrivial solution which has period π when $\sigma_1=\sigma_2=1$ or period 2π when $\sigma_1=\sigma_2=-1$. If $f(\vartheta)$ is such a periodic solution then if $g(\vartheta)$ is another solution which is linearly independent of $f(\vartheta)$ then

$$g(\vartheta+\pi) = \sigma_1 g(\vartheta) + \Theta f(\vartheta) \tag{4-140}$$

where Θ is a constant. The case $\Theta=0$ is equivalent to

$$U_1(\pi) + U_2'(\pi) = \pm 2 \tag{4-141A}$$

$$U_2(\pi) = 0 \tag{4-141B}$$

$$U_1'(\pi) = 0 \tag{4-141C}$$

Observe that if $\sigma_1 \neq \sigma_2$ and μ is pure imaginary then the absolute value of every solution of the differential equation is bounded for all ϑ . This bound depends only upon the initial conditions of the equation. If $\sigma_1 \neq \sigma_2$ and μ is not pure imaginary then there exists a nontrivial unbounded solution of the differential equation. We will call the regions where the former situation obtains, stable regions; and those applying to the latter, regions of instability. For the case $\sigma_1=\sigma_2$ we will call the resulting combinations of η and χ boundary, or characteristic, curves. For all solutions[102] of the differential equation to be bounded for $\sigma_1=\sigma_2$ it is necessary and sufficient that $\Theta=0$. We call the solutions such that

$$U(\vartheta+\pi) = \pm U(\vartheta)$$

basically periodic solutions. These solutions have period π or 2π and describe the boundary curves. It is obvious that all basically periodic functions have period 2π but not all functions of period 2π can be basically periodic since 4-138 must be satisfied with $\sigma=-1$. We note, of course, that we cannot have a solution of period π and a solution of period 2π coexisting since this implies $\sigma_1\sigma_2=-1$.

It is known[103] that if the differential equation has a nontrivial periodic solution of period $s\pi$, with $s>2$, but no solution with period π or 2π then all solutions are periodic with period $s\pi$. It is easily seen that

μ is purely imaginary with magnitude equal to a rational number, an even integer divided by s. Also, if μ is purely imaginary with irrational magnitude, the solutions are bounded but aperiodic.

The $J(\vartheta)$ of the case at hand is an even function of ϑ. For such a symmetric case if $u(\vartheta)$ is a solution so is $u(-\vartheta)$ and we may write the set of linearly independent solutions equivalent to Eqs. 4-139, for $\sigma_1 \neq \sigma_2$, as

$$e^{\mu\vartheta} Q(\vartheta) \tag{4-142A}$$

$$e^{-\mu\vartheta} Q(-\vartheta) \tag{4-142B}$$

In addition, for the symmetric case[104]

$$u_1(\pi) = 2u_1(\pi/2)u_2'(\pi/2) - 1 = 1 + 2u_1'(\pi/2)u_2(\pi/2) \tag{4-143A}$$

$$u_2(\pi) = 2u_2(\pi/2)u_2'(\pi/2) \tag{4-143B}$$

$$u_1'(\pi) = 2u_1(\pi/2)u_1'(\pi/2) \tag{4-143C}$$

$$u_2'(\pi) = u_1(\pi) \tag{4-143D}$$

$u_1(\vartheta)$ will be an even function and $u_2(\vartheta)$ will be an odd function of ϑ. A nontrivial solution of period π or 2π will necessarily be a multiple of $u_1(\vartheta)$ or $u_2(\vartheta)$ unless all solutions are periodic with period π or 2π. There exists a nontrivial periodic solution which is:
even and of period π if and only if $u_1'(\frac{\pi}{2})=0$,
odd and of period π if and only if $u_2(\frac{\pi}{2})=0$,
even and of period 2π if and only if $u_1(\frac{\pi}{2})=0$, and
odd and of period 2π if and only if $u_2'(\frac{\pi}{2})=0$

Our basic problem will be to determine the nature of the characteristic exponent, μ, given the values of η and γ. The $\eta\gamma$ plane will be divided into regions of stability and instability and we shall find the characteristic curves which form their boundaries. We state the oscillation theorem due to Liapounoff.[105] To every differential equation of form

$$y'' + [\eta + K(x)]y = 0 \tag{4-144}$$

where K(x) is real and periodic with period π and of bounded variation, there belong two monotonically increasing infinite sequences of real numbers

$$\eta_0, \eta_1, \eta_2, \cdots \tag{4-145A}$$

$$\eta_1', \eta_2', \eta_3', \cdots \tag{4-145B}$$

such that 4-144 has a solution of period π if and only if $\eta = \eta_n$ and a solution of period 2π if and only if $\eta = \eta_n'$. The η_n and η_n' satisfy

$$\eta_0 < \eta_1' \leq \eta_2' < \eta_1 \leq \eta_2 < \eta_3' \leq \eta_4' < \eta_3 \leq \eta_4 < \cdots \tag{4-146A}$$

$$\lim_{n\to\infty} \frac{1}{\eta_n} = 0 \tag{4-146B}$$

$$\lim_{n\to\infty} \frac{1}{\eta_n'} = 0 \tag{4-146C}$$

The solutions of the differential equation are stable in the intervals

$$(\eta_0, \eta_1'), (\eta_2', \eta_1), (\eta_2, \eta_3'), (\eta_4', \eta_3), \cdots \tag{4-147}$$

At the endpoints of the intervals the solutions are unstable, in general. This is always true for η_0. The solutions are stable for η_{2n+1} or η_{2n+2} if and only if $\eta_{2n+1} = \eta_{2n+2}$. Similarly they are stable for η'_{2n+1} or η'_{2n+2} if and only if $\eta'_{2n+1} = \eta'_{2n+2}$. The solutions are always unstable for complex values of η. The η_n are the roots of $\Delta(\eta) = 2$ and the η_n' are the roots of $\Delta(\eta) = -2$ where

$$\Delta(\eta) = y_1(\pi) + y_2'(\pi)$$

Observe that the intervals of instability may disappear, with the exception of the interval $(-\infty, \eta_0)$. The intervals of stability may combine together if, say, $\eta_{2n+1} = \eta_{2n+2}$ or $\eta'_{2n+1} = \eta'_{2n+2}$. All of the intervals of instability except the zeroth one disappear if and only if K(x) is a constant.[106] In addition, it is known that if there are only a finite number of intervals

of instability, then K(x) is infinitely differentiable.[107]

We see at once that as $K(x) \to 0$ the values of η necessary to give the basically periodic solutions will be given by the square of an integer. The characteristic curves therefore leave the η axis at values equal to n^2.

If K(x) has zero average value, as we have normalized 4-129B, then the following is true:[108] either all nontrivial real solutions of the differential equation have only a finite number of zeros, or all real solutions have infinitely many zeros. For $\eta \leq \eta_0$ all nontrivial real solutions have only a finite number of zeros but for $\eta > \eta_0$ every real solution has infinitely many zeros. The value η_0 has a nontrivial solution of period π which has no zeros. We also know that η_0 is not positive and equals zero if and only if K(x) is zero identically. We therefore expect the characteristic curve corresponding to the values of η_0 to pass through the origin in the $\eta\gamma$ plane and remain to the left of the γ axis for all $\gamma > 0$. This will be seen in the solution of Eqs. 4-129.

To the left of the zeroth characteristic curve we may put a lower bound upon the square of the characteristic exponent for the same K(x). That is,[109]

$$\mu^2 \geq \eta_0 - \eta , \qquad \eta < \eta_0 \tag{4-148}$$

There are criteria which may be applied to the differential equation to obtain regions of stability without actually solving for the characteristic exponent. Th earliest example of such a criterion is Liapounoff's theorem,[110] which states that if $J(\varphi)$ in 4-129A is nonnegative and piecewise continuous with period π then all solutions of 4-129A are bounded if

$$\pi \int_0^{\pi} J(\varphi)\, d\varphi \leq 4 \tag{4-149}$$

This condition is best possible in the sense that for any $\epsilon > 0$ there exists a nonnegative piecewise continuous function $J_0(\varphi)$ of period π and not identically zero such that

$$\pi \int_0^{\pi} J_0(\varphi)\, d\varphi \leq 4 + \epsilon$$

and such that at least one solution of

$$u'' + J_0(\zeta)\, u = 0$$

is unbounded.

Application of Liapounoff's theorem to 4-129 yields two conditions to be simultaneously satisfied. From the condition that $J(\zeta)$ be nonnegative we find that

$$\zeta \geq \frac{\pi^2}{6}\gamma \tag{4-150A}$$

where the equal sign corresponds to the cusps of the parabolas just touching the line J=0. This condition is the same found in 4-133A. From the condition 4-149 we find simply that

$$\zeta \leq \frac{4}{\pi^2} \tag{4-150B}$$

The two conditions given in Eqs. 4-150 specify a triangular region of stability as shown in Fig. 4-12. We see that this estimate is quite conservative for this case when we compare it with the linear approximation for the ζ_1' characteristic curve, found later. That is, to a first approximation the entire region bounded by the approximate ζ_1' characteristic curve and the ζ and γ axes will be stable. As we will see later, the linear approximation for this curve is quite good.

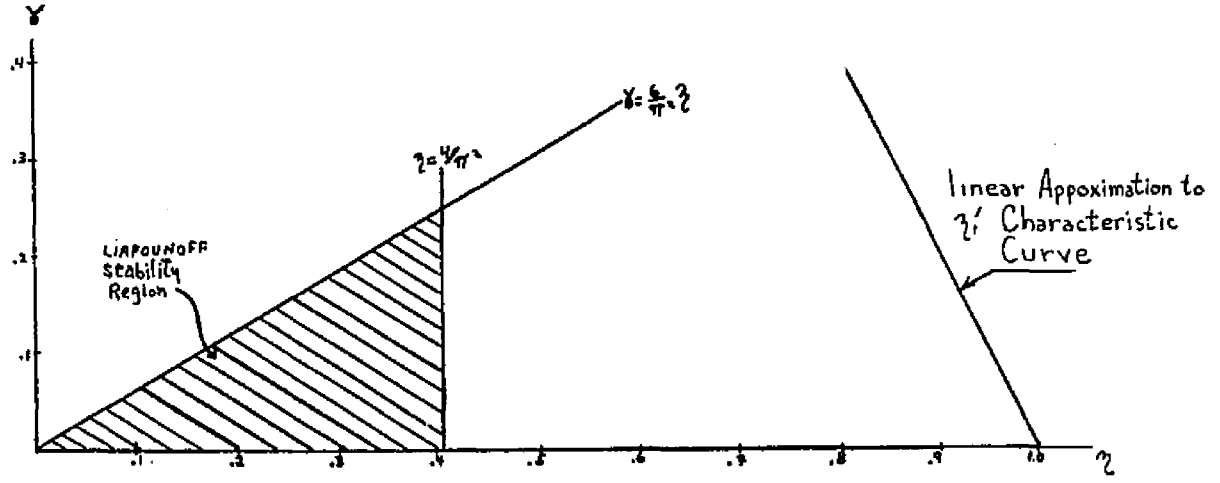

Fig. 4-12 Stability Region of Liapounoff's Theorem

Another stability criterion was given by Beurling in the following form:[111] if, for real a and b

$$a^2 \leq J(\varphi) \leq b^2 \tag{4-151}$$

then the solutions of the differential equation will be stable for all possible $J(\varphi)$ if and only if the interval (a^2, b^2) does not contain the square of an integer. For 4-129B we bound the maximum value of $J(\varphi)$, $\eta + \gamma\frac{\pi^2}{12}$, and the minimum value, $\eta - \gamma\frac{\pi^2}{6}$, between a^2 and b^2 taking successively adjacent integers for a and b. We find triangular regions of stability defined by

$$\gamma \leq \frac{6}{\pi^2}\left[\eta - a^2\right] \tag{4-152A}$$

$$\gamma \leq \frac{12}{\pi^2}\left[b^2 - \eta\right] \tag{4-152B}$$

If we take for the pairs a,b the values 0,1; 1,2; 2,3; and 3,4; we will generate four such regions of stability. These regions are compared, with those found from the exact analysis to follow, in Fig. 4-13. Note that this criterion produces estimates for the higher order stable regions whereas the Liapounoff theorem does not. In addition it is noted that it gives a better stability criterion for the first stable region than does the Liapounoff theorem for 4-129B.

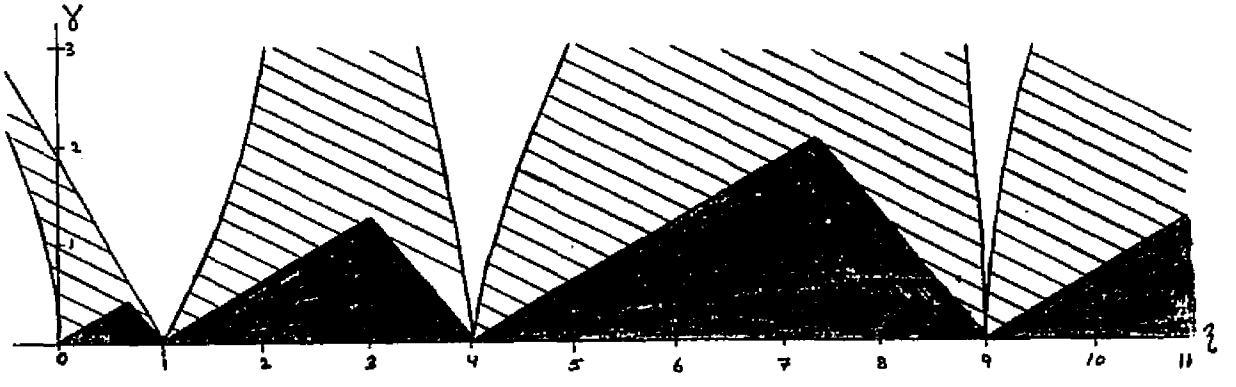

Fig. 4-13 The Beurling Stability Regions Compared to the Exact Solution (The Buerling Stability Region shown shaded)

Near the η axis we find approximate solutions for the characteristic curves by the method of perturbation.[112] For small γ we write u and η in the form

of series in powers of γ.

$$u(\varphi) = \sum_{m=0}^{\infty} u_m(\varphi)\gamma^m \tag{4-153A}$$

$$\zeta = \sum_{m=0}^{\infty} K_m \gamma^m \tag{4-153B}$$

We expand $J(\varphi)$ of 4-129 in a Fourier series

$$J(\varphi) = \zeta + \gamma \sum_{m=1}^{\infty} a_m \cos 2m\varphi \tag{4-154A}$$

$$a_m = \frac{2}{\pi}\int_{-\frac{\pi}{2}}^{\frac{\pi}{2}} \left[\frac{\pi^2}{12} - \varphi^2\right] \cos 2m\varphi \, d\varphi = \frac{(-1)^{m+1}}{m^2} \tag{4-154B}$$

so that the differential equation is

$$u'' + \left[\zeta + \gamma \sum_{m=1}^{\infty} \frac{(-1)^{m+1}}{m^2} \cos 2m\varphi\right] u = 0 \tag{4-154C}$$

Using Eqs. 4-153 in 4-154C and separating the terms according to powers of γ we obtain the differential equations for u_0, u_1, and u_2, viz.,

$$u_0'' + K_0 u_0 = 0 \tag{4-155A}$$

$$u_1'' + K_0 u_1 + K_1 u_0 + u_0 \sum_{m=1}^{\infty} \frac{(-1)^{m+1}}{m^2} \cos 2m\varphi = 0 \tag{4-155B}$$

$$u_2'' + K_2 u_0 + K_1 u_1 + K_0 u_2 + u_1 \sum_{m=1}^{\infty} \frac{(-1)^{m+1}}{m^2} \cos 2m\varphi = 0 \tag{4-155C}$$

As mentioned above, the characteristic curves leave the ζ axis at integer squares plus zero, so we take for K_0 the values 0, 1, 4 and 9. The basically periodic solutions corresponding to these curves will have periods π, 2π, π and 2π respectively. We first consider K_0=0. The solution to 4-155A for this value of K_0 is

$$u_0(\varphi) = b_0 + c_0\varphi \tag{4-156}$$

known as the generating solution. We seek the periodic solution and there-

fore we set $C_0=0$. This is equivalent to removing a secular term in the general perturbation technique. Using the solution 4-156 in 4-155B we have

$$U_1'' + K_1 b_0 + b_0 \sum_{m=1}^{\infty} \frac{(-1)^{m+1}}{m^2} \cos 2m\varphi = 0 \tag{4-157}$$

We remove the secular term by setting $K_1=0$ and obtain

$$U_1(\varphi) = \frac{b_0}{4} \sum_{m=1}^{\infty} \frac{(-1)^{m+1}}{m^4} \cos 2m\varphi \tag{4-158}$$

for the particular solution. Using this solution we have from 4-155C

$$U_2'' + K_2 b_0 + \frac{b_0}{8} \sum_{m,n=1}^{\infty} \frac{(-1)^{m+n}}{m^4 n^2} \left[\cos 2(m+n)\varphi + \cos 2(m-n)\varphi\right] = 0 \tag{4-159}$$

To remove the unbounded solution from 4-159 we set the constant term equal to zero. That part of the constant term derived from the double summation is found by taking m=n. Therefore the secular term will be removed if*

$$K_2 = -\frac{1}{8} \sum_{k=1}^{\infty} \frac{1}{k^6} \tag{4-160}$$

---

* The summation in 4-160 is evaluated by use of the Parseval relation[113] applied to various Fourier series. First, from the Fourier series previously derived in 4-154 we find, at $\varphi = \frac{\pi}{2}$, that

$$\sum_{m=1}^{\infty} \frac{1}{m^2} = \frac{\pi^2}{6} \approx 1.645$$

From the Parseval relation applied to that Fourier series

$$\int_{-\frac{\pi}{2}}^{\frac{\pi}{2}} \left[\frac{\pi^2}{12} - \varphi^2\right]^2 d\varphi = \sum_{m=1}^{\infty} \frac{1}{m^4} = \frac{\pi^4}{90} \approx 1.082$$

If next we find the Fourier sine series for the function φ^3 and apply the Parseval relation to this series we find

$$\sum_{m=1}^{\infty} \left[\frac{72}{m^6} - \frac{24\pi^2}{m^4} + \frac{2\pi^4}{m^2}\right] = \frac{\pi^6}{7}$$

Thus,

$$\sum_{m=1}^{\infty} \frac{1}{m^6} = \frac{\pi^6}{7 \cdot 9 \cdot 15} \approx 1.017$$

For the other characteristic curves we take the value of K_0 to be the square of a nonzero integer. From 4-155A

$$u_0'' + m^2 u_0 = 0, \quad m \neq 0 \tag{4-161A}$$

with solution

$$u_0(\varsigma) = b_0 \cos m\varsigma + C_0 \sin m\varsigma \tag{4-161B}$$

Using this solution in 4-155B we have

$$u_1'' + m^2 u_1 + b_0\left\{K_1 \cos m\varsigma + \frac{1}{2}\sum_{n=1}^{\infty}\frac{(-1)^{n+1}}{n^2}\left[\cos(2n-m)\varsigma + \cos(2n+m)\varsigma\right]\right\}$$
$$+ C_0\left\{K_1 \sin m\varsigma + \frac{1}{2}\sum_{n=1}^{\infty}\frac{(-1)^{n+1}}{n^2}\left[-\sin(2n-m)\varsigma + \sin(2n+m)\varsigma\right]\right\} = 0 \tag{4-162}$$

Therefore, there are two parts to the forcing function in the differential equation for $u_1(\varsigma)$, one being even and one being odd. We may remove the secular term due to each part individually, the secular term due to the other will necessarily remain. This dual situation yields the two characteristic curves emanating from each value m^2. Note that for n=m in the summation a proper term appears to cancel the $K_1\cos(m\varsigma)$ or $K_1\sin(m\varsigma)$ term. Thus,

$$K_1 = \pm \frac{1}{2m^2} \tag{4-163}$$

and the characteristic curves are given approximately by

$$\zeta \approx m^2 \pm \frac{\gamma}{2m^2}, \quad m \neq 0 \tag{4-164A}$$

$$\zeta \approx -\frac{1}{8}\frac{\pi^6}{7\cdot 9\cdot 15}\gamma^2, \quad m = 0 \tag{4-164B}$$

If we had truncated the series given in 4-154A for $n \geq 2$ we would have approximated the Hill's equation by the Mathieu equation. In this case the power series for the characteristic curves are known[114] and it is instructive to compare the two approximate curves, shown in Table 4-2.

Note that only for m=1 the approximations are the same. In particular, for

the Hill's equation linear approximations are obtained for $m \geq 2$ while for the Mathieu equation case the lowest order approximation is quadratic for that range.

Table 4-2 Approximations for Characteristic Curves

m^2	Hill's Equation	Truncation to Mathieu Equation
0	$\eta \simeq -\frac{1}{8} - \frac{\pi^6}{7 \cdot 9 \cdot 15} \gamma^2$	$\eta \simeq -\frac{1}{8}\gamma^2$
1	$\eta \simeq 1 \pm \frac{1}{2}\gamma$	$\eta \simeq 1 \pm \frac{1}{2}\gamma$
4	$\eta \simeq 4 \pm \frac{1}{8}\gamma$	$\eta \simeq 4 + \frac{5}{48}\gamma^2;\ 4 - \frac{1}{48}\gamma^2$
9	$\eta \simeq 9 \pm \frac{1}{18}\gamma$	$\eta \simeq 9 + \frac{1}{64}\gamma^2$

Before turning to the explicit solution we shall consider one final theorem due to Borg.[115] This theorem states that if K(x) in 4-144 has zero average and has period π and if

$$\frac{1}{\pi}\int_0^{\pi} |K(x)|\, dx = A \tag{4-165A}$$

exists, then for any integer $n > \frac{A}{2}$ [sic],

$$\left| \sqrt{\eta_{2m-1}} - 2m \right| \leq \frac{A}{4m} \tag{4-165B}$$

$$\left| \sqrt{\eta_{2m}} - 2m \right| \leq \frac{A}{4m} \tag{4-165C}$$

$$\left| \sqrt{\eta'_{2m-1}} - 2m+1 \right| \leq \frac{A}{4m-2} \tag{4-165D}$$

$$\left| \sqrt{\eta'_{2m}} - 2m+1 \right| \leq \frac{A}{4m-2} \tag{4-165E}$$

Therefore, given a value of n this theorem will generate regions in the stability plane where the characteristic curves generated by that value

of n will lie. For each value of n, A is bounded by 2n and this essentially bounds the value of γ for the approximation. Since $A \geq 0$, we see that bounds for the η_0 curve cannot be generated. We note also that the theorem indicates to what points on the η axis the curves approach. Since the function $\gamma\left[\frac{\pi^2}{12}-\psi^2\right]$ has a simple zero at $\psi=\frac{\pi}{2\sqrt{3}}$ we have

$$A=\frac{2\gamma}{\pi}\int_0^{\frac{\pi}{2}}\left|\frac{\pi^2}{12}-\psi^2\right|d\psi=\frac{2\gamma}{\pi}\left\{\int_0^{\frac{\pi}{2\sqrt{3}}}\left[\frac{\pi^2}{12}-\psi^2\right]d\psi-\int_{\frac{\pi}{2\sqrt{3}}}^{\frac{\pi}{2}}\left[\frac{\pi^2}{12}-\psi^2\right]d\psi\right\}=\frac{\pi^2}{9\sqrt{3}}\gamma \tag{4-166A}$$

We will consider only the curves η_1', η_2', η_1, η_2, η_3' and η_4' and therefore we apply the formula for n=1 and n=2. Thus,

$$\left|\sqrt{\eta_1'}-1\right| \leq \frac{\gamma\pi^2}{18\sqrt{3}}, \quad \gamma < \frac{18\sqrt{3}}{\pi^2} \tag{4-166B}$$

$$\left|\sqrt{\eta_2'}-1\right| \leq \frac{\gamma\pi^2}{18\sqrt{3}}, \quad \gamma < \frac{18\sqrt{3}}{\pi^2} \tag{4-166C}$$

$$\left|\sqrt{\eta_1}-2\right| \leq \frac{\gamma\pi^2}{36\sqrt{3}}, \quad \gamma < \frac{18\sqrt{3}}{\pi^2} \tag{4-166D}$$

$$\left|\sqrt{\eta_2}-2\right| \leq \frac{\gamma\pi^2}{36\sqrt{3}}, \quad \gamma < \frac{18\sqrt{3}}{\pi^2} \tag{4-166E}$$

$$\left|\sqrt{\eta_3'}-3\right| \leq \frac{\gamma\pi^2}{54\sqrt{3}}, \quad \gamma < \frac{36\sqrt{3}}{\pi^2} \tag{4-166F}$$

$$\left|\sqrt{\eta_4'}-3\right| \leq \frac{\gamma\pi^2}{54\sqrt{3}}, \quad \gamma < \frac{36\sqrt{3}}{\pi^2} \tag{4-166G}$$

The resulting triangle-like regions are shown in Fig. 4-14. Comparison of the exact results shows that the theorem gives correct results for all the curves derived except the curve for η_1'. The theorem indicates that the η_1' curve crosses the γ axis for $\gamma \geq \frac{18\sqrt{3}}{\pi^2}$ whereas the exact result is that the η_1' curve crosses the γ axis at $\gamma \approx 1.9$. Application of the theorem to Mathieu's equation shows that the theorem fails there as well for η_1'. The conclusion is that it fails for this particular curve.

We now proceed to solve the Hill's equation given in 4-129. We make the change of variable

$$X=\sqrt{2}\,\gamma^{1/4}\psi \tag{4-167A}$$

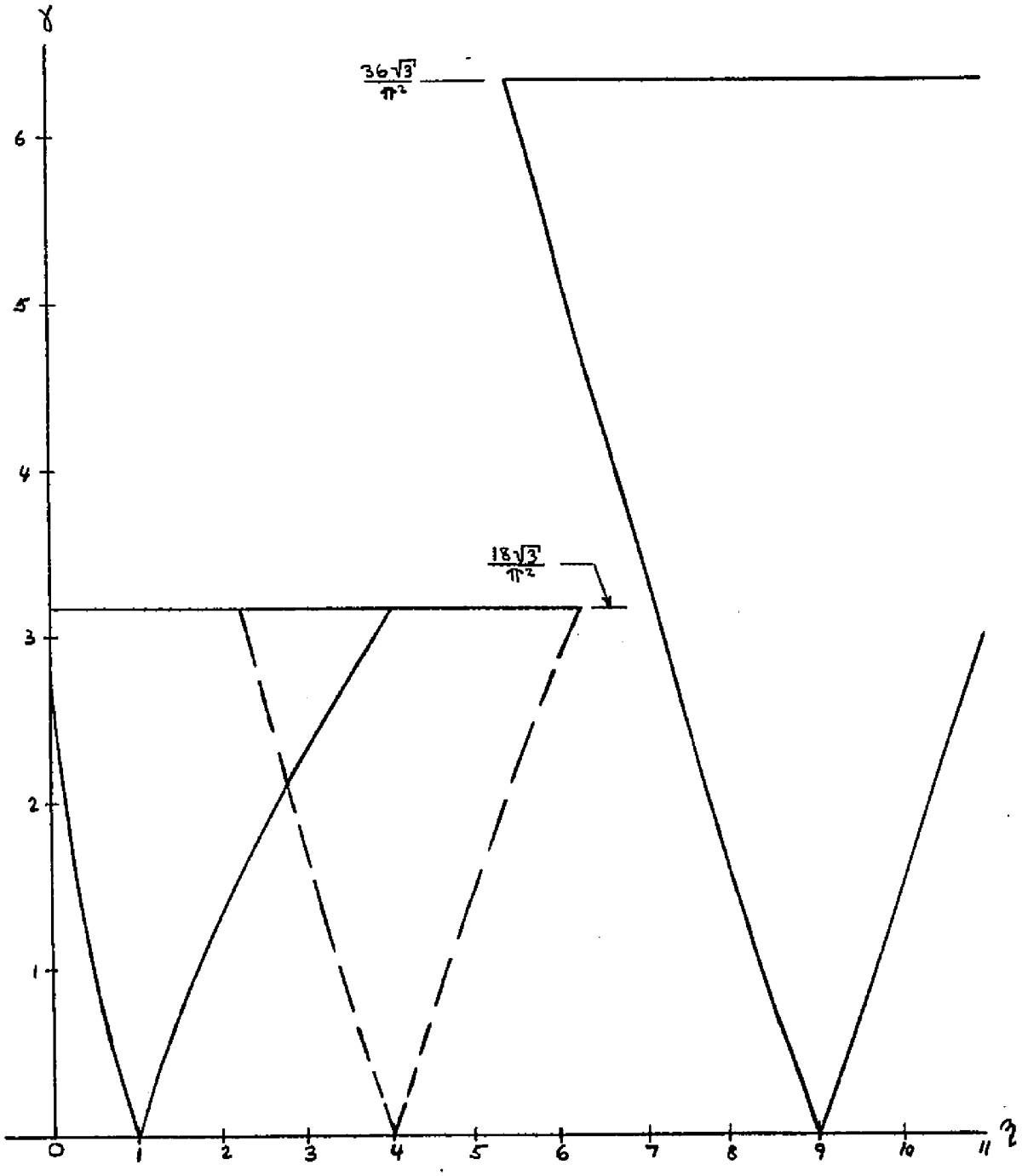

Fig. 4-14 Application of a Theorem Due to Borg

so that the differential equation becomes

$$\frac{d^2u}{dx^2} - \left\{\frac{1}{4}x^2 - \frac{1}{2}\left[\frac{2}{\gamma^{1/2}} + \frac{\pi^2}{12}\gamma^{1/2}\right]\right\}u = 0, \qquad -\frac{\gamma^{1/4}\pi}{\sqrt{2}} \le x \le \frac{\gamma^{1/4}\pi}{\sqrt{2}} \tag{4-167B}$$

The differential equation

$$y'' + f(x)\,y = 0 \tag{4-168A}$$

for f(x) a quadratic function of x, has two distinct standard forms

$$y'' - \left(\frac{1}{4}x^2 + a\right)y = 0 \tag{4-168B}$$

$$y'' + \left(\frac{1}{4}x^2 - a\right)y = 0 \tag{4-168C}$$

which have as their solutions the Parabolic Cylinder Functions.[116] Recognize that 4-167B is of type 4-168B, the invected form. The differential equation given in 4-168C is consistent with the engrailed form. Defining

$$P = -\frac{1}{2}\left[\frac{2}{\gamma^{1/2}} + \frac{\pi^2}{12}\gamma^{1/2}\right] \tag{4-169A}$$

we have for the solution to 4-167B

$$u = AU(P,x) + BV(P,x) \tag{4-169B}$$

where U(P,x) and V(P,x) are the Parabolic Cylinder Functions. We take one of the Floquet solutions given in 4-139 and therefore we have

$$u(\varsigma) = AU(P,\sqrt{2}\,\gamma^{1/4}\varsigma) + BV(P,\sqrt{2}\,\gamma^{1/4}\varsigma) \tag{4-170A}$$

$$u(\varsigma+\pi) = e^{\mu\pi}u(\varsigma) \tag{4-170B}$$

$$u'(\varsigma) = \sqrt{2}\,\gamma^{1/4}\left[AU'(P,\sqrt{2}\,\gamma^{1/4}\varsigma) + BV'(P,\sqrt{2}\,\gamma^{1/4}\varsigma)\right] \tag{4-170C}$$

$$u'(\varsigma+\pi) = e^{\mu\pi}u'(\varsigma) \tag{4-170D}$$

At $\varsigma = \frac{\pi}{2}$ both $u(\varsigma)$ and $u'(\varsigma)$ must be continuous. Setting $\varsigma = \frac{\pi}{2}$ in 4-170A and C

and setting $\xi = -\frac{\pi}{2}$ in 4-170B and D we find, from the continuity demands, a set of homogeneous equations. To obtain a nontrivial solution for the constants A and B we must have the following determinant equal to zero:

$$\begin{vmatrix} U(P,\lambda) - e^{\mu\pi} U(P,-\lambda) & V(P,\lambda) - e^{\mu\pi} V(P,-\lambda) \\ \sqrt{2}\gamma^{1/4}\left[U'(P,\lambda) - e^{\mu\pi} U'(P,-\lambda)\right] & \sqrt{2}\gamma^{1/4}\left[V'(P,\lambda) - e^{\mu\pi} V'(P,-\lambda)\right] \end{vmatrix} = 0 \qquad (4\text{-}171A)$$

$$\lambda \equiv \frac{\gamma^{1/4}\pi}{\sqrt{2}} \qquad (4\text{-}171B)$$

Upon expansion this becomes

$$\begin{aligned} &\left[U(P,-\lambda)V'(P,-\lambda) - U'(P,-\lambda)V(P,-\lambda)\right]e^{2\mu\pi} \\ &-\left[U(P,-\lambda)V'(P,\lambda) + U(P,\lambda)V'(P,-\lambda) - V(P,\lambda)U'(P,-\lambda) - V(P,-\lambda)U'(P,\lambda)\right]e^{\mu\pi} \\ &+\left[U(P,\lambda)V'(P,\lambda) - V(P,\lambda)U'(P,\lambda)\right] = 0 \end{aligned} \qquad (4\text{-}172)$$

Since U(P,x) and V(P,x) both satisfy 4-167B we have that

$$U''(P,x)V(P,x) = V''(P,x)U(P,x) \qquad (4\text{-}173A)$$

Integrating by parts we find

$$U(P,x)V'(P,x) - V(P,x)U'(P,x) = \text{constant} \qquad (4\text{-}173B)$$

which is recognized as the Wronskian[117]

$$W\{U,V\} = \begin{vmatrix} U(P,x) & V(P,x) \\ U'(P,x) & V'(P,x) \end{vmatrix} = \sqrt{\frac{2}{\pi}} \qquad (4\text{-}173C)$$

Using $x = \pm\lambda$ we find

$$e^{2\mu\pi} - \sqrt{\tfrac{\pi}{2}}\left[U(P,-\lambda)V'(P,\lambda) + U(P,\lambda)V'(P,-\lambda) - V(P,\lambda)U'(P,-\lambda) - V(P,-\lambda)U'(P,\lambda)\right]e^{\mu\pi} + 1 = 0 \qquad (4\text{-}174)$$

Note that this equation has been cast in the form of the characteristic equation, 4-135. By use of relations between the functions[118] we find

$$U(p,-\lambda) = \frac{\pi V(p,\lambda)}{\Gamma(p+\frac{1}{2})} - \sin p\pi\, U(p,\lambda) \tag{4-175A}$$

$$V(p,-\lambda) = \frac{\Gamma(p+\frac{1}{2})\, U(p,\lambda)}{\pi \sec^2 p\pi} + \sin p\pi\, V(p,\lambda) \tag{4-175B}$$

$$U'(p,-\lambda) = -\frac{\pi V'(p,\lambda)}{\Gamma(p+\frac{1}{2})} + \sin p\pi\, U'(p,\lambda) \tag{4-175C}$$

$$V'(p,-\lambda) = -\frac{\Gamma(p+\frac{1}{2})\, U'(p,\lambda)}{\pi \sec^2 p\pi} - \sin p\pi\, V'(p,\lambda) \tag{4-175D}$$

Using 4-175 we simplify 4-174 and using 4-137 we have

$$\begin{aligned}\cosh \mu\pi = {} & \frac{\pi^{3/2}}{\sqrt{2}\,\Gamma(p+\frac{1}{2})} V(p,\lambda) V'(p,\lambda) \\ & - \frac{\Gamma(p+\frac{1}{2})}{\sqrt{2\pi}} \cos^2 p\pi\, U(p,\lambda) U'(p,\lambda) \\ & - \sqrt{\tfrac{\pi}{2}} \sin p\pi \left[U(p,\lambda) V'(p,\lambda) + V(p,\lambda) U'(p,\lambda) \right]\end{aligned} \tag{4-176}$$

The derivatives may be found from the relationships[119]

$$U'(p,\lambda) + \tfrac{1}{2}\lambda U(p,\lambda) + (p+\tfrac{1}{2})\, U(p+1,\lambda) = 0 \tag{4-177A}$$

$$U'(p,\lambda) - \tfrac{1}{2}\lambda U(p,\lambda) + U(p-1,\lambda) = 0 \tag{4-177B}$$

$$2U'(p,\lambda) + U(p-1,\lambda) + (p+\tfrac{1}{2})\, U(p+1,\lambda) = 0 \tag{4-177C}$$

$$V'(p,\lambda) - \tfrac{1}{2}\lambda V(p,\lambda) - (p-\tfrac{1}{2})\, V(p-1,\lambda) = 0 \tag{4-177D}$$

$$V'(p,\lambda) + \tfrac{1}{2}\lambda V(p,\lambda) - V(p+1,\lambda) = 0 \tag{4-177E}$$

$$2V'(p,\lambda) - V(p+1,\lambda) - (p-\tfrac{1}{2}) V(p-1,\lambda) = 0 \tag{4-177F}$$

The values of the right-hand side of 4-176 determine the nature of μ and therefore the stability of the differential equation. We arrange a table similar to that used in Chap. 2.

We find the limiting value of 4-176 as $\gamma \to 0$, $\zeta > 0$. We have from their definitions

$$\lim_{\substack{\gamma\to 0\\ \zeta>0}} P = -\infty \tag{4-178A}$$

$$\lim_{\gamma\to 0} \lambda = 0 \tag{4-178B}$$

$$\lim_{\substack{\gamma\to 0\\ \zeta>0}} \sqrt{-P}\,\lambda = \tfrac{\pi}{2}\zeta^{1/2} \tag{4-178C}$$

Table 4-3 Stability of Differential Equation

$\cosh \mu\pi$	μ	Condition
$-\infty<\cosh[\mu\pi]<-1$	$\pm\frac{1}{\pi}\cosh^{-1}[-\cosh\mu\pi]\pm i(2m+1)$	Unstable
$\cosh[\mu\pi]=-1$	$\pm i(2m+1)$	Characteristic Curve
$-1<\cosh[\mu\pi]<1$	$\pm\frac{i}{\pi}\{\cos^{-1}[\cosh\mu\pi]\}\pm i2m$	Stable
$\cosh[\mu\pi]=1$	$\pm i2m$	Characteristic Curve
$1<\cosh[\mu\pi]<\infty$	$\pm\frac{1}{\pi}\cosh^{-1}[\cosh\mu\pi]\pm i2m$	Unstable

From[120] the expansion for $-P \gg \lambda^2$

$$U(P,\lambda)+i\,\Gamma(\tfrac{1}{2}-P)V(P,\lambda) = \frac{e^{i\pi(\frac{1}{4}+\frac{1}{2}P)}\,\Gamma(\frac{1}{4}-\frac{1}{2}P)}{2^{\frac{1}{2}P+\frac{1}{4}}\sqrt{\pi}}\, e^{i\sqrt{-P}\,\lambda}\, e^{v_r+iv_i} \tag{4-179A}$$

$$v_r = \frac{(\frac{1}{2}\lambda)^2}{[2\sqrt{-P}]^2} + \frac{2(\frac{1}{2}\lambda)^4}{[2\sqrt{-P}]^4} - \frac{9(\frac{1}{2}\lambda)^2 - \frac{16}{3}(\frac{1}{2}\lambda)^6}{[2\sqrt{-P}]^6} - \cdots \tag{4-179B}$$

$$v_i = -\frac{\frac{2}{3}(\frac{1}{2}\lambda)^3}{2\sqrt{-P}} + \frac{\frac{1}{2}\lambda + \frac{3}{5}(\frac{1}{2}\lambda)^5}{[2\sqrt{-P}]^3} + \frac{\frac{16}{3}(\frac{1}{2}\lambda)^3 - \frac{4}{7}(\frac{1}{2}\lambda)^7}{[2\sqrt{-P}]^5} - \cdots \tag{4-179C}$$

we find

$$\lim_{\substack{\gamma\to 0\\ \zeta>0}} U(p,\lambda) = \frac{\Gamma(\frac{1}{4}-\frac{1}{2}p)}{2^{\frac{1}{2}p+\frac{1}{4}}\sqrt{\pi}}\cos\pi\left(\tfrac{1}{4}+\tfrac{1}{2}p+\tfrac{1}{2}\zeta^{1/2}\right) \tag{4-180A}$$

$$\lim_{\substack{\gamma\to 0\\ \zeta>0}} V(p,\lambda) = \frac{\Gamma(\frac{1}{4}-\frac{1}{2}p)}{2^{\frac{1}{2}p+\frac{1}{4}}\sqrt{\pi}\,\Gamma(\frac{1}{2}-p)}\sin\pi\left(\tfrac{1}{4}+\tfrac{1}{2}p+\tfrac{1}{2}\zeta^{1/2}\right) \tag{4-180B}$$

Using 4-177B and D we have

$$\lim_{\substack{\gamma\to 0\\ \zeta>0}} U'(p,\lambda) = -\lim_{\substack{\gamma\to 0\\ \zeta>0}} U(p-1,\lambda) \tag{4-180C}$$

$$\lim_{\substack{\gamma\to 0\\ \zeta>0}} V'(p,\lambda) = \lim_{\substack{\gamma\to 0\\ \zeta>0}} (p-\tfrac{1}{2})V(p-1,\lambda) \tag{4-180D}$$

Using these limiting values and the reflection and duplication formulas for the Gamma function[121]

$$\Gamma(z)\Gamma(1-z) = -z\Gamma(-z)\Gamma(z) = \pi\csc\pi z \tag{4-181A}$$

$$\Gamma(2z) = \frac{2^{2z-\frac{1}{2}}}{\sqrt{2\pi}}\Gamma(z)\Gamma(z+\tfrac{1}{2}) \tag{4-181B}$$

we find ultimately from 4-176

$$\lim_{\substack{\gamma\to 0\\ \zeta>0}} \cosh\mu\pi = \cos[\pi\zeta^{1/2}] \tag{4-182A}$$

or,

$$\lim_{\substack{\gamma\to 0\\ \zeta>0}} \mu = \pm i\left[\zeta^{1/2} \pm 2m\right] \tag{4-182B}$$

In particular, for the characteristic curves we see that for a solution of period π we require ζ to be the square of an even integer and for a solution of period 2π, we must have ζ the square of an odd integer. These are the points on the ζ axis where the characteristic curves begin.

We find the asymptotic behavior of the characteristic curves for large γ in the following manner. As γ becomes increasingly large the characteristic

curves enter region II of the stability plane, as given by Eqs. 4-133. The domains for stable solutions become narrow as γ increases so that we expect pairing of the characteristic curves in this region. Members of these pairs should approach the same asymptote as $\gamma \to \infty$. We label these asymptotes in a natural way; s=0, 1, 2, ...; which correspond to the intervals of stability given in 4-147 from Liapounoff's Oscillation theorem. The stability intervals are given by

$$(\zeta_s, \zeta_{s+1}') \quad , \quad s \text{ even} \tag{4-183A}$$

$$(\zeta_{s+1}', \zeta_s) \quad , \quad s \text{ odd} \tag{4-183B}$$

so that for even s the left-hand characteristic curve has period π and the right-hand curve has period 2π. For s odd the reverse situation holds.

In the differential equation 4-162 used in the perturbational analysis of the characteristic curves for m≠0 there are two forcing functions, one even and one odd. The removal of one or the other secular term results in a characteristic curve solution. In either case the remaining forcing function produces an unbounded solution. The term which was removed identifies the symmetry of the periodic solution corresponding to the characteristic curve. Using those results and assuming that the characteristic curves emanating from the same point on the ζ axis do not cross, or assuming no coexistence of solutions, we find that for s even, the basically periodic solutions corresponding to both characteristic curves have even symmetry and for s odd they have odd symmetry. We find, therefore, that for s even the basically periodic solutions for the left-hand and right-hand characteristic curves reduce to multiples of cos $s\psi$, and cos $(s+1)\psi$, respectively, as $\gamma \to 0$. On the other hand, for odd values of s they reduce to multiples of sin $s\psi$, and sin$(s+1)\psi$, respectively. At this point we use a corollary proved in Arscott[122] for Mathieu's equation but which would hold here as well. This corollary states that the basically periodic solutions which reduce to multiples of cos $2n\psi$, cos $(2n+1)\psi$, sin $(2n+1)\psi$ and sin $(2n+2)\psi$ each have n zeros in $0 < \psi < \frac{\pi}{2}$. Applying this theorem to the characteristic curves for even and odd values of s we find that for even s the basically periodic solutions have $\frac{1}{2}$ s

zeros in $0<\varsigma<\frac{\pi}{2}$ while for odd s the number of zeros in that interval is $\frac{1}{2}(s-1)$. Taking note of the fact that for odd s the basically periodic solutions have odd symmetry, and for even s the symmetry is even, we find that for both situations the number of zeros in the open interval $(-\frac{\pi}{2}, \frac{\pi}{2})$ equals s. We see from the relationship between x and ς given in 4-167A that as $\gamma\to\infty$ the interval $-\frac{\pi}{2}<\varsigma<\frac{\pi}{2}$ is transformed to the entire real line, $-\infty<x<\infty$. We therefore require that the basically periodic solutions in the form of 4-169B have s zeros in the interval $(-\infty,\infty)$ and have even or odd symmetry with respect to x in accordance with s being even or odd. In region I of the stability plane $J(\varsigma)$ is always negative and the solutions are always unstable. The asymptotes are therefore expected to lie outside this region, or

$$\zeta > -\frac{\pi^2}{12}\gamma \tag{4-184A}$$

indicating that the bracket in 4-169A is positive and we have that

$$P<0 \tag{4-184B}$$

for the asymptotes. The basically periodic solutions in the limit $\gamma\to\infty$ must be bounded at infinity when written in the form 4-169B. The only values of P which lead to such bounded solutions at $\pm\infty$ are[123]

$$P=-\left[n+\tfrac{1}{2}\right] \tag{4-185}$$

with n a nonnegative integer. For such a value of P the basically periodic solution may be written in terms of Hermite Polynomials[124] of order n. These polynomials have even or odd symmetry according as n is even or odd and have n zeros in $(-\infty,\infty)$. We conclude finally that the asymptote characterized by the value of s=0, 1, 2, ...; is given by

$$-P=\tfrac{1}{2}\left[\frac{\zeta}{\gamma^{1/2}}+\frac{\pi^2}{12}\gamma^{1/2}\right]=S+\tfrac{1}{2} \tag{4-186}$$

the arithmetic average of the two indices of the two characteristic curves bounding the stability interval. Comparison of these asymptotes to the exact solution shows that they are excellent approximations for large γ

(cf. Fig. 4-15). For γ sufficiently large

$$\gamma >> \left[\frac{12}{\pi^2}(s+\tfrac{1}{2})\right]^2 \tag{4-187A}$$

so that from 4-186

$$\zeta \approx -\gamma\frac{\pi^2}{12} \tag{4-187B}$$

and we see that in the limit all the asymptotes are parallel to the boundary between region I and region II.

For each point in the stability plane, $\gamma > 0$, we may find the corresponding value of μ from 4-176 and from this value characterize the stability of the differential equation. The characteristic curves form the boundaries of the stable and unstable regions. We find these curves from 4-176 using the digital computer to evaluate the Parabolic Cylinder Functions according to a computer program given in the Appendix. The results of this computation are given in Fig. 4-15. Comparisons with the division of the plane according to Fig. 4-11 and the asymptotic curves are made on this figure and we see that they are indeed good approximations. It is of interest to compare the stability plane for the parabolic $J(\gamma)$ to that which would be found by truncation of the Fourier series. In this case we find from 4-154C

$$u'' + [\zeta + \gamma\cos 2\eta]u = 0 \tag{4-188}$$

the Mathieu equation. We found earlier from the perturbation analysis that the characteristic curves for the two cases were approximately the same in the vicinity of $\zeta = 1$ for sufficiently small γ. The characteristic curves differed, however, for small and nonzero γ in the vicinity of $\zeta = 0$, 4 and 9 (cf., Table 4-2). This behavior is borne out by comparison with the stability plane for the Mathieu equation, 4-188, as found from tables of the characteristic curves,[125] shown in Fig. 4-16. We note also that the characteristic curves for the two cases differ markedly far from the ζ axis.

By use of Hamming's modified predictor-corrector method[126] and the digital

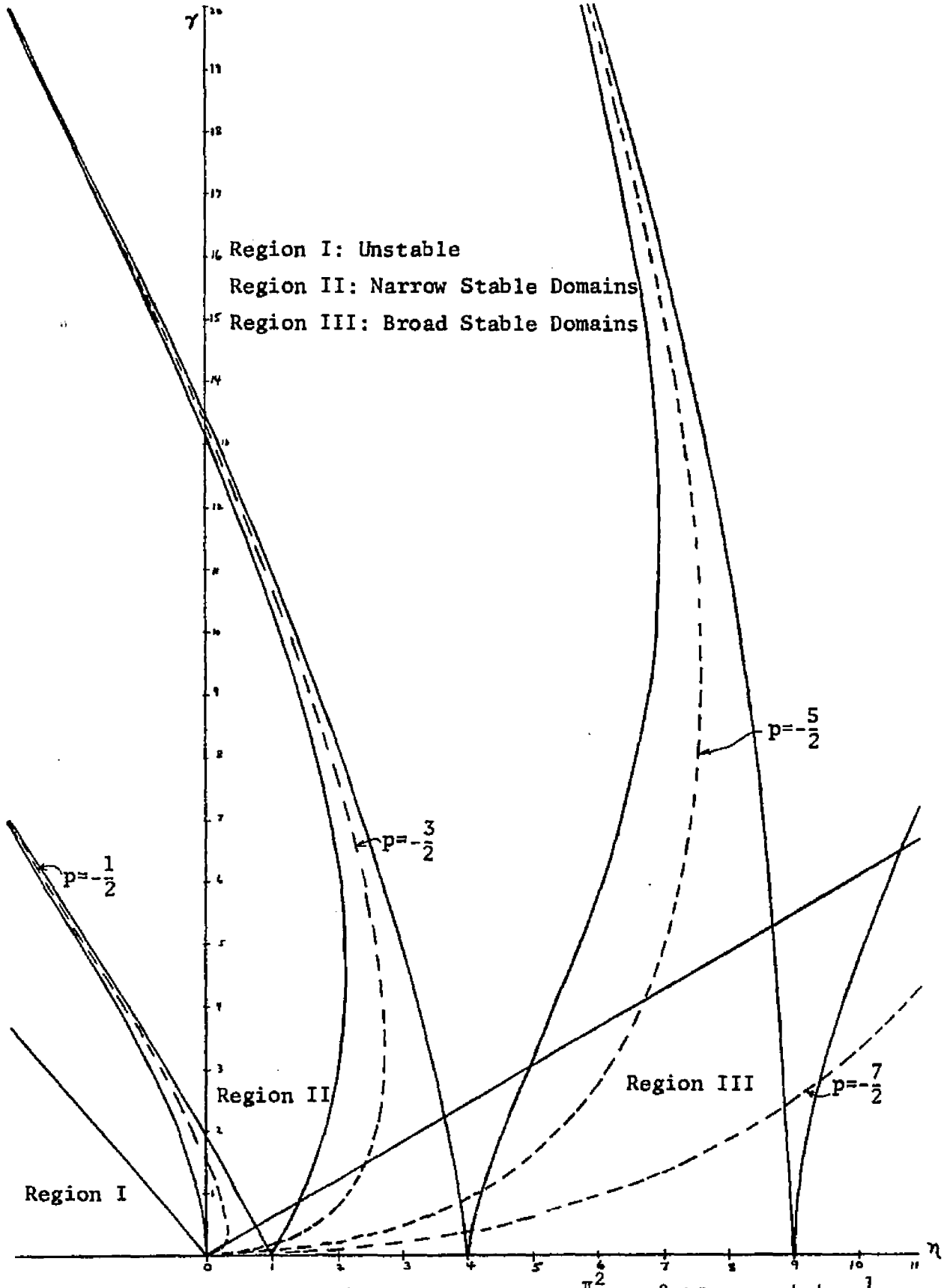

Fig. 4-15 Stability Plane for $u'' + [\eta + \gamma(\frac{\pi^2}{12} - \zeta^2)]\, u=0$, $|\zeta| \leq \frac{1}{2}\pi$
(otherwise periodic extension)

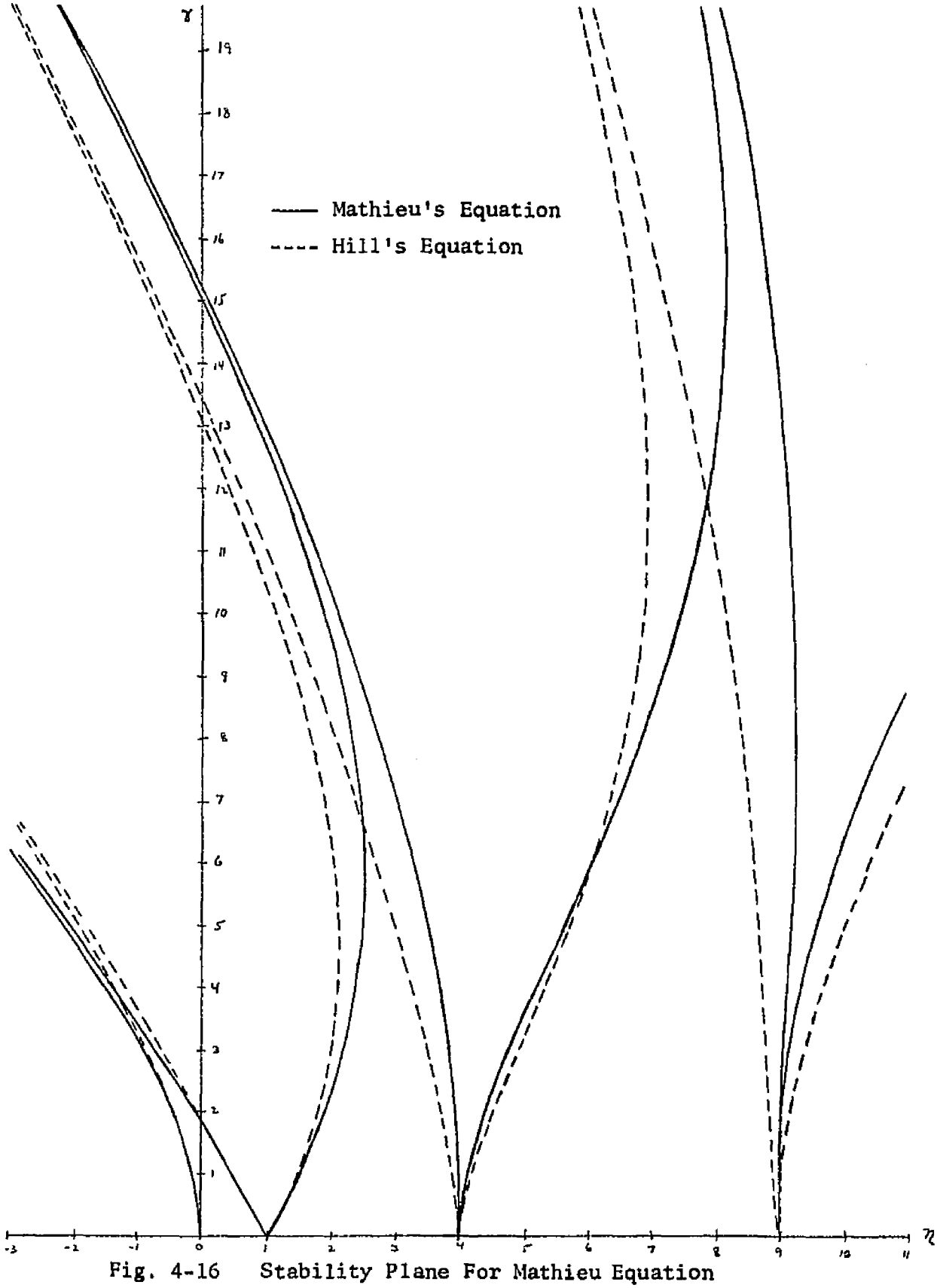

Fig. 4-16 Stability Plane For Mathieu Equation
(First Harmonic of Piecewise Periodic Parabolas)

computer we find some trajectories corresponding to different points of the stability plane. The trajectories are compared with the information found from the stability diagram. We take the initial conditions for all cases to be

$$u(-\tfrac{\pi}{2}) = 1$$
$$u'(-\tfrac{\pi}{2}) = 0$$

We consider first the case $\eta = -3.0$, $\gamma = 4.0$. From Fig. 4-15 we see that this point lies in the instability interval $(-\infty, \eta_0)$. From the previous discussion we have that the solution must have a finite number of zeros. Also, for this region the result quoted in 4-148 holds and we find a lower bound for the characteristic exponent. From Fig. 4-15 we see that $\eta_0 \approx -1.4$ for $\gamma = 4.0$ and we find from 4-148 that

$$\mu \geq 1.265$$

The solution is compared to the exponential function, $e^{1.265\frac{\pi}{2}\left[\frac{2}{\pi}\gamma + 1\right]}$, in Fig. 4-17a. We note that ignoring the periodic part of the solution, and the other linearly independent solution, over the range indicated it represents a lower bound for the solution. It would seem that the instability is verified along with the finiteness of the number of zeros. All the other cases considered lie to the right of the η_0 curve and therefore we expect the solution to have infinitely many zeros for the stable, as well as the unstable, solutions. In the stability interval (η_0, η_1'), the trajectory for $\eta = -1.3$, $\gamma = 4.0$ is shown in Fig. 4-17b. The solution is an example of a stable solution for $J(\varphi)$ having negative average value. Observe that the stability plane yields accurate results in the sense that a small change in η will bring the solution into the unstable region, as noted from Fig. 4-15.

In the (η_1', η_2') instability interval a trajectory is shown for $\eta = 1$, $\gamma = 1$ in Fig. 4-18a, an example of an unstable solution with an infinite number of zeros. In the (η_2', η_1) stability interval the solution is shown for $\eta = 2.5$, $\gamma = 4$ in Fig. 4-18b.

The above work represents an explicit solution for a piecewise parabolic Hill's equation. Other known explicit solutions are the rectangular

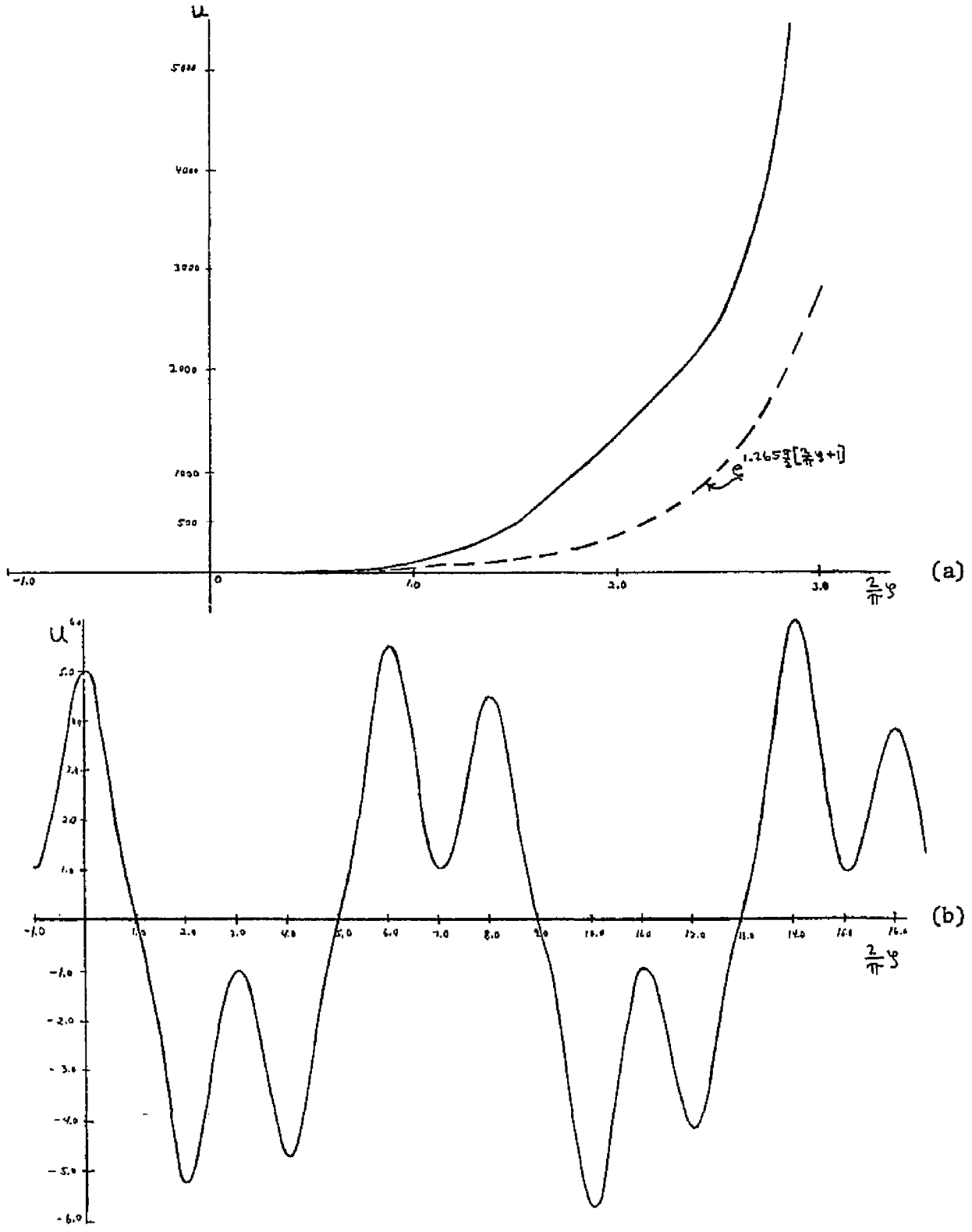

Fig. 4-17 Numerical Solution of Piecewise Parabolic Hill's Equation
$u(-\pi/2)=1.0$ $u'(-\pi/2)=0$
(a) $\eta=-3.0$, $\gamma=4.0$ (b) $\eta=-1.3$, $\gamma=4.0$

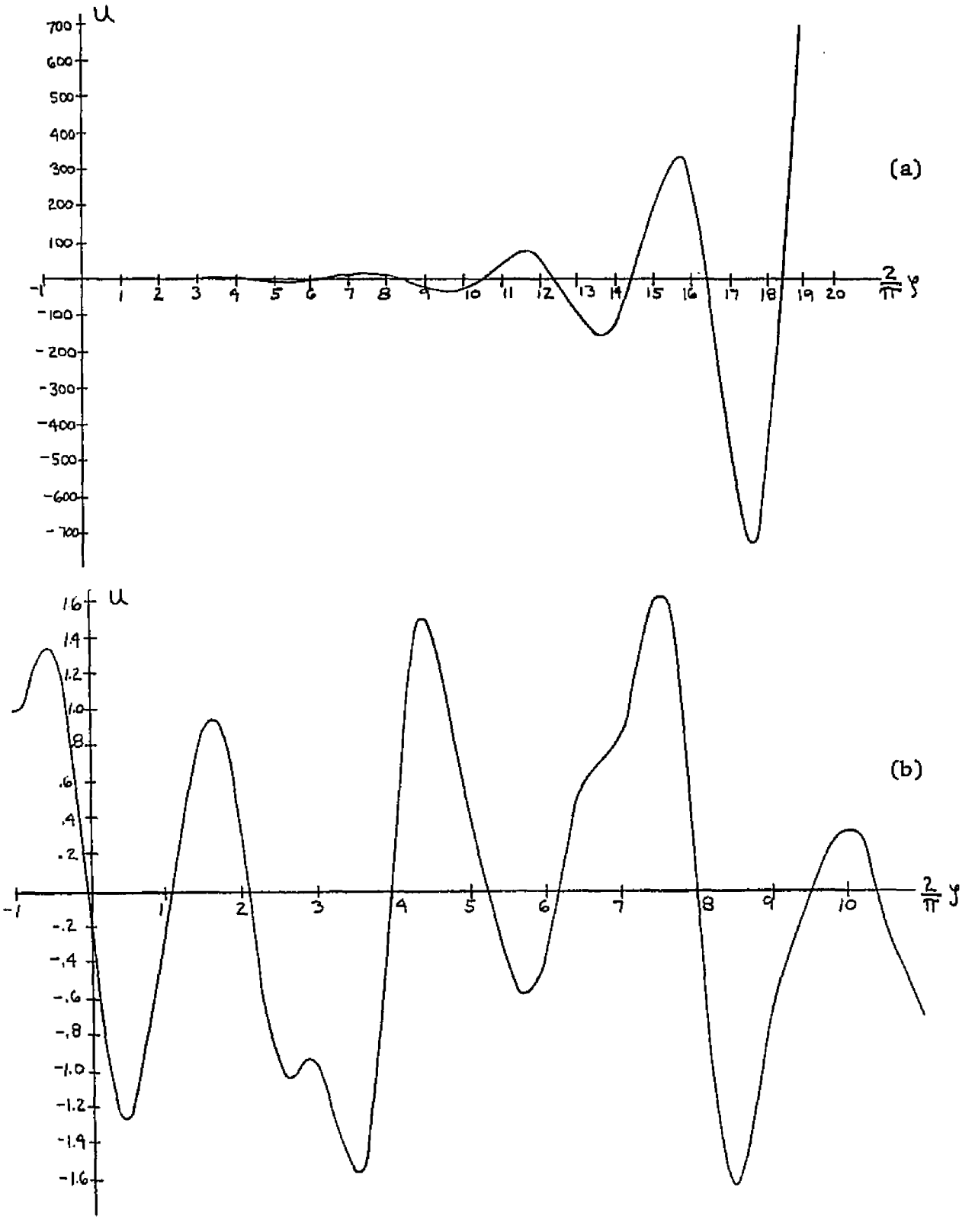

Fig. 4-18 Numerical Solution of Piecewise Parabolic Hill's equation
$u(-\pi/2)=1.0$ $u'(-\pi/2)=0$
(a) $\eta=1.0$, $\gamma=1.0$ (b) $\eta=2.5$, $\gamma=4.0$

wave* and impulse function and the saw-tooth[127] and piecewise linear reciprocal function.[128] This work has therefore carried the range of known explicit solutions a step further to quadratic variation. From Fig. 4-15 we see that for the range of ζ and γ depicted there is no intersection of characteristic curves and thus the instability intervals do not vanish for $\gamma > 0$. If this were to happen we would have an instance of coexistence which is defined as a choice of γ and ζ such that there are two linearly independent solutions of period π or 2π. According to Ince's theorem[129] Mathieu's equation, 4-188, never displays coexistence for $\gamma > 0$ while situations of coexistence for the rectangular wave are known[130] It would be of interest to determine if coexistence could occur for the piecewise parabolic situation, an example of a $J(\vartheta)$ which is continuous but only piecewise differentiable.

4.11 Stability

In order to find the stability of 4-128 by using results of the preceding section we must approximate the function $\frac{f_2(\vartheta)}{b}$ by a parabola proportional to $\frac{\pi^2}{12} - \vartheta^2$. Because the average value of the parabola over the interval $(-\frac{\pi}{2}, \frac{\pi}{2})$ is zero there is only one constant to specify for the approximation. We could set this constant by satisfying any one of a number of arbitrary criteria. We will choose to set the value of the constant by requiring minimum square error between the two functions. That is, we wish to approximate the function $\frac{f_2(\vartheta)}{b}$ by the function

$$g(\vartheta) = A\left[\frac{\pi^2}{12} - \vartheta^2\right], \qquad |\vartheta| \le \frac{\pi}{2} \tag{4-189A}$$

such that

$$\overline{\epsilon^2} = \frac{1}{\pi}\int_{-\frac{\pi}{2}}^{\frac{\pi}{2}} \left[\frac{f_2(\vartheta)}{b} - g(\vartheta)\right]^2 d\vartheta \tag{4-189B}$$

is minimized.

---

* As was used in Chap. 2

Applying the condition

$$\frac{d\overline{\epsilon^2}}{dA} = 0 \tag{4-190}$$

to 4-189B we find for the value of A corresponding to minimum $\overline{\epsilon^2}$

$$A = \frac{\int_{-\pi/2}^{\pi/2} \frac{f_2(\psi)}{b}\left[\frac{\pi^2}{12} - \psi^2\right] d\psi}{\int_{-\pi/2}^{\pi/2}\left[\frac{\pi^2}{12} - \psi^2\right]^2 d\psi} = \frac{180}{\pi^5}\int_{-\frac{\pi}{2}}^{\frac{\pi}{2}} \frac{f_2(\psi)}{b}\left[\frac{\pi^2}{12} - \psi^2\right] d\psi \tag{4-191}$$

The value of A as a function of $\frac{y_0}{\pi}$ is shown in Fig. 4-19 for the geometry $\frac{\ell_1}{\pi}$=1 and $\frac{\ell_2}{\pi}$=3.08, where the integral to find A was calculated using the digital computer. We see that for this example the range of A will be between the approximate limits of 0.1 and 0.6.

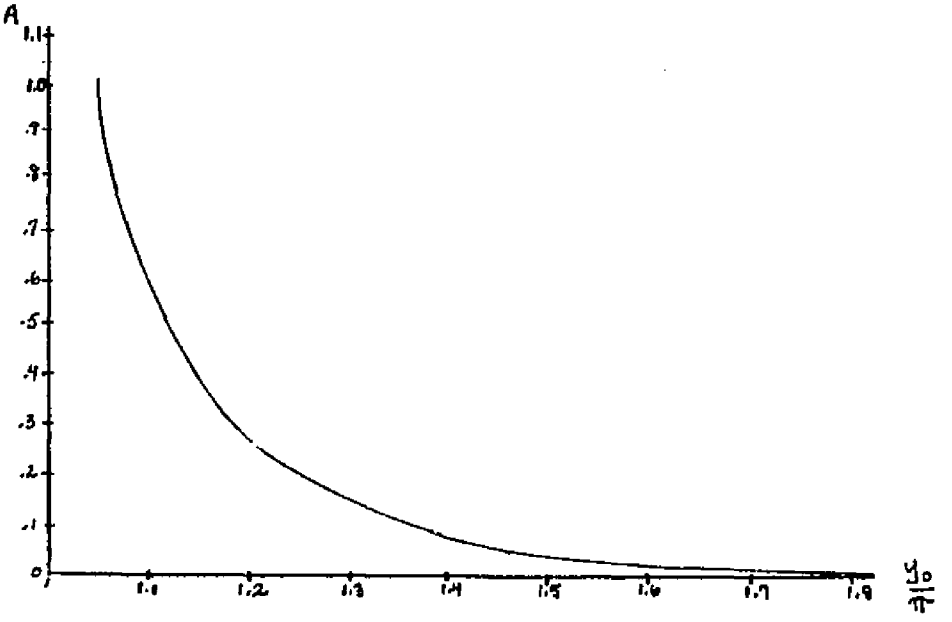

Fig. 4-19 A as a Function of $\frac{y_0}{\pi}$
$\frac{\ell_1}{\pi}$=1.0, $\frac{\ell_2}{\pi}$=3.08

Comparison of 4-128 and 4-129 yields the identification of ζ and γ in terms of the energy and geometric ratios.

$$\zeta = \left(\frac{2L}{\lambda_0}\right)^2 = \frac{2}{\pi^2}\frac{\left[v_{0_0}/v_{0_2}\right]^2}{\left[r_0/L\right]^2} \tag{4-192A}$$

$$\gamma = A\zeta\frac{\pi}{4}\frac{r_0}{L} = \frac{A}{2\pi\left[\frac{r_0}{L}\right]}\left[\frac{v_{\theta_0}}{v_{0z}}\right]^2 \qquad (4\text{-}192B)$$

Observe from 4-192 and Fig. 4-15 for small γ, the values of $\frac{2L}{\lambda_0}$, the ratio of the period of the structure to the half-wavelength of natural oscillations, which lead to instabilities, are integers. Note also that for our physical application we only consider $\zeta > 0$.

Suppose that the linear analysis indicates a point in the stability plane within the first stable region, (ζ_0, ζ_1'), near the ζ_1' curve. We found from the nonlinear analysis of the smooth boundary system that the natural period increases as the oscillations increase in magnitude. The nonlinear analysis therefore predicts that λ_0 will increase as the oscillations increase in strength and therefore both ζ and γ will decrease inversely as the square of λ_0, making the system more stable from this viewpoint alone.

As an example of the application of 4-192 we take $\frac{y_0}{\pi}=1.25$ and investigate the stability as a function of the two parameters $[\frac{v_{\theta_0}}{v_{0z}}]^2$ and $[\frac{r_0}{L}]$. We find that over the range of interest the solutions are stable and the characteristic exponent is purely imaginary. Taking for the principal part of the characteristic exponent

$$\mu = i\beta \quad , \quad 0 < \beta < 1$$

we plot constant β curves as functions of $\frac{r_0}{L}$ and $[\frac{v_{\theta_0}}{v_{0z}}]^2$. This family of curves is shown in Fig. 4-20 for $\frac{y_0}{\pi}=1.25$. We have shown $[\frac{v_{\theta_0}}{v_{0z}}]^2$ up to 10 to indicate the variation, although as was mentioned earlier we would not go beyond the value 1.

4.12 Particular Integral

We turn now to the particular solution of the nonhomogeneous differential equation which we find from 4-121, using the simplifications leading to 4-128, and using 4-123B, to be

$$\frac{d^2\delta}{d\vartheta^2} + \left[\frac{2L}{\lambda_0}\right]^2\left\{1 + \frac{\pi}{4}\frac{r_0}{L}\frac{f_2(\vartheta)}{b}\right\}\delta$$

$$= -\frac{1}{2}\left[\frac{2L}{\lambda_0}\right]^2 \frac{f_1(\vartheta)}{b}\prod_{m=1}^{\infty}\left\{I_0\left(a_m\frac{\pi}{4}\frac{r_0}{L}\left[\frac{2L}{\lambda_0}\right]^2\right) + 2\sum_{R=1}^{\infty}(-1)^R I_k\left(a_m\frac{\pi}{4}\frac{r_0}{L}\left[\frac{2L}{\lambda_0}\right]^2\right)\cos 2mk\vartheta\right\} \quad (4\text{-}193)$$

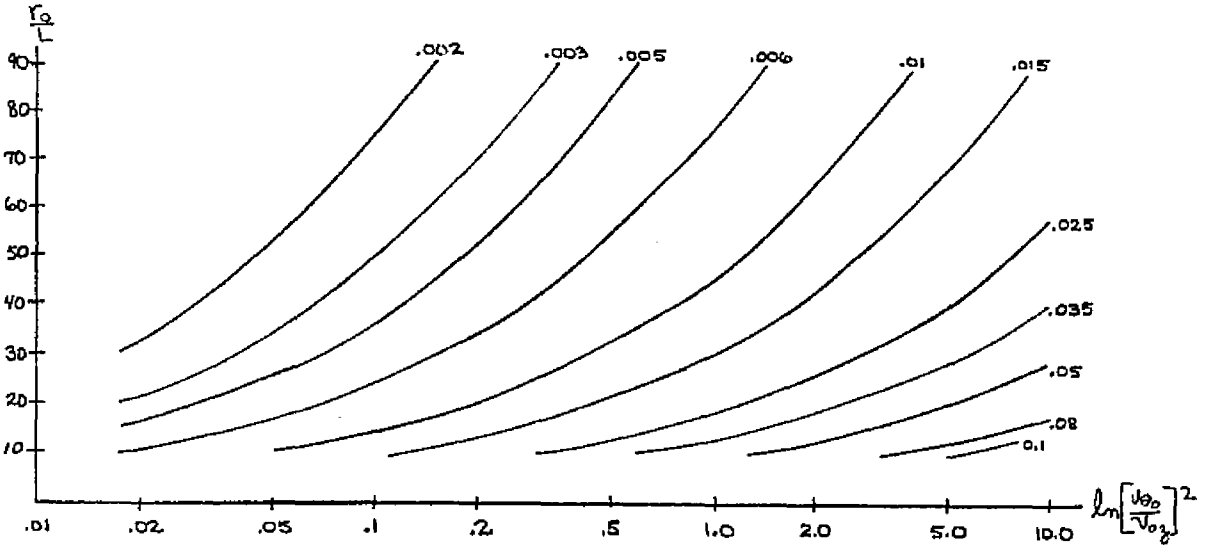

Fig. 4-20 Constant β Curves
$\frac{y_0}{\pi}=1.25$, $\frac{\ell_1}{\pi}=1.0$, $\frac{\ell_2}{\pi}=3.08$

The right-hand side of 4-193, representing the forcing function, is a periodic function with period π. In Sec. 4.10 we found the solutions to the homogeneous equation in the forms given in 4-142. In the stable regions we write the solution in those forms with $\mu=i\beta$ and recall that if β is rational the solution will be periodic with period $s\pi$, with $s>2$. If β is irrational the solution is aperiodic. We write the forcing function of the differential equation as

$$\tfrac{1}{2} g_0 + \sum_{m=1}^{\infty} g_m \cos 2m\varphi = \tfrac{1}{2} \sum_{m=-\infty}^{\infty} g_m e^{i2m\varphi} \tag{4-194}$$

from 4-193, where the approximation given in 4-124B may be applicable. We write the solutions to the homogeneous equation for the stable regions as

$$\delta_1 = \sum_{m=-\infty}^{\infty} q_m e^{i[\beta+2m]\varphi} \tag{4-195A}$$

$$\delta_2 = \sum_{m=-\infty}^{\infty} q_m e^{-i[\beta+2m]\varphi} \tag{4-195B}$$

We may write the particular solution in terms of δ_1 and δ_2 as[131]

$$\delta_p(\varphi) = h_1(\varphi)\delta_1(\varphi) + h_2(\varphi)\delta_2(\varphi) \tag{4-196A}$$

$$h_1(\varphi) = -\tfrac{1}{2} \int \frac{\sum_{m=-\infty}^{\infty} g_m e^{i2m\varphi} \sum_{k=-\infty}^{\infty} q_k e^{-i[\beta+2k]\varphi}}{\delta_1\delta_2' - \delta_1'\delta_2} \, d\varphi \tag{4-196B}$$

$$h_2(\varphi) = \tfrac{1}{2} \int \frac{\sum_{m=-\infty}^{\infty} g_m e^{i2m\varphi} \sum_{k=-\infty}^{\infty} q_k e^{i[\beta+2k]\varphi}}{\delta_1\delta_2' - \delta_1'\delta_2} \, d\varphi \tag{4-196C}$$

By the same reasoning leading to 4-173B we note that the denominator appearing in the integral of 4-196B or 4-196C is constant. Since the forcing function and the solutions to the homogeneous equation are continuous with continuous derivatives the Fourier series in the integrals converge uniformly.[132] If we look at them as power series in the exponential functions, they also converge absolutely and we may interchange multiplication and summation and also integration and summation.[133] The h functions therefore involve integrals of the form

$$\int e^{\pm i[\beta \pm 2j]\varphi} \, d\varphi$$

which is itself exponential unless the exponent is zero. In such a case the integral leads to a term linear in φ which indicates an unbounded term. In the stable region

$$0 < \beta < 1$$

so that such a term cannot be generated. This is equivalent to ruling out a resonance phenomenon when it is recalled that if the solution to the homogeneous equation is periodic in the stable region it has period $s\pi$, with $s > 2$. The forcing function has period π, however, so that resonance at a harmonic of the forcing function may not take place. Thus, we see that if the homogeneous equation is stable then the forced solution is also bounded and we expect a periodic particular solution. We will apply a method similar to the principle of harmonic balance[134] which was used to find the nonlinear variations of the period in Sec. 4.8. We truncate the series of the forcing function and seek a particular solution which is of the same order of truncation. We evaluate the coefficients of the solution by making the equation satisfied for only those orders, discarding the higher order terms which are generated.

To illustrate, suppose the homogeneous equation is approximated by the piecewise parabolic Hill's equation of Sec. 4.10. Further suppose that we truncate the forcing function at n=1 so that we have, using the form given in 4-154C

$$u'' + \left[\eta + \gamma \sum_{m=1}^{\infty} \frac{(-1)^{m+1}}{m^2} \cos 2m\vartheta\right] u = \tfrac{1}{2} g_0 + g_1 \cos 2\vartheta \qquad (4\text{-}197A)$$

We seek an approximate particular solution of form

$$u_p = A \cos 2\vartheta + B \sin 2\vartheta + C \qquad (4\text{-}197B)$$

Substitution of 4-197B into 4-197A, discarding higher order terms, yields, when equality is demanded for the three solution forms separately

$$\left[\eta - 4 - \frac{\gamma}{8}\right] A + \gamma C = g_1 \qquad (4\text{-}198A)$$

$$\left[\eta - 4 + \frac{\gamma}{8}\right] B = 0 \qquad (4\text{-}198B)$$

$$\frac{\gamma}{2} A + \eta C = \tfrac{1}{2} g_0 \qquad (4\text{-}198C)$$

We see from 4-198B that B is identically zero, and there is no odd part

to the solution, provided that

$$\zeta - 4 + \frac{\gamma}{8} \neq 0 \tag{4-199A}$$

Referring to the perturbation analysis of the characteristic curves of Sec. 4.10, given in Table 4-2, we see that the characteristic curve for an odd solution near $\zeta=4$ was approximated by

$$\zeta \approx 4 - \frac{\gamma}{8} \tag{4-199B}$$

Therefore, if 4-199B is true then our results predict the possibility of an odd solution, which is consistent with the characteristic cruve. Within the stable regions 4-199A is satisfied for the approximation so that the particular solution is even. From Table 4-2, the perturbation analysis approximated the characteristic curve for an even solution near $\zeta=4$ as

$$\zeta \approx 4 + \frac{\gamma}{8} \tag{4-199C}$$

so within the approximation the coefficient of A in 4-198A is not zero within the stable region. We find for the approximate particular solution in the stable regions

$$u_p = \frac{g_1 \zeta - \frac{\gamma g_0}{2}}{\Delta} \cos 2\varphi + \frac{\frac{1}{2} g_0 \left[\zeta - 4 - \frac{\gamma}{8}\right] - \frac{\gamma}{2} g_1}{\Delta} \tag{4-200A}$$

$$\Delta = \begin{vmatrix} \zeta - 4 - \frac{\gamma}{8} & \gamma \\ \frac{\gamma}{2} & \zeta \end{vmatrix} \tag{4-200B}$$

To obtain the solution in terms of radial displacement we use the transformation in the form 4-123A or 4-124A. It is obvious that there will be, in general, a shift in the solution given by the constant part obtained after making the transformation. The beam is therefore displaced by the periodic fields.

CHAPTER 5

INTERACTION

5.1 Assumptions

The analysis of the interaction between the electron beam and the rf wave will be a simple one. We attempt to extract the most basic processes which are in force in order to find the gain of the system in a simple way. The analysis will be a linear one, valid for small signal strengths. All equations are linearized and in order to find the gain an exponential variation is assumed, which is consistent with the solution of linear differential equations with constant coefficients.

The results of Chap. 2 are used for the electrodynamic fields existing in the structure for the desired mode. It is assumed that it is the only mode which exists, other modes not being excited by the excitation scheme, being in a cutoff state, or being damped heavily by the stacked ring design. We therefore have assumed that the fields present are the "cold" fields, which are the solution in the absence of the electron beam, the inherent assumption being that the beam current is small enough not to perturb those fields significantly.

The presence of the beam is also ignored insofar as it affects the static fields. We take the solution to be that of Laplace's equation and dispense with the need for a solution to Poisson's equation. The electrons do not interact with each other in this simple analysis and each electron is free to move independently of the others. There is, therefore, no consideration at all of any analog of space change waves.

The static fields which affect the electron motion are taken to be those derived from a logarithmic potential and so the corrugated nature of the inner boundary is ignored in this regard. We use the results of Chaps. 3 and 4 to assure that the beam motion is a stable one. Once this is determined, we ignore the effects upon the electron motion caused by the periodic nature of the inner boundary.

The electron beam is assumed synchronous with a single space harmonic and no direct interaction is considered between the beam and any other than this single harmonic. However, since we take the cold field solution, if a single harmonic is amplified so is every other one amplified since the totality of the field is needed to satisfy the boundary conditions. In this sense the other space harmonics are coupled to the electron beam by the boundary conditions.

The forces on the electrons are therefore taken to be the radial electrostatic force due to the assumed uniform boundaries and the angular electric force due to the synchronous space harmonic. The sign and magnitude of this latter force depends upon the time of entrance of the electron into the structure.

As is uniformly done in electron-wave interaction calculations, we ignore, initially, for the simple model, consequences of the magnetic fields of the rf wave.

5.2 Linearized Interaction

We assume that the electron beam is synchronous with the n=1 space harmonic and therefore 2-46 is relevant. We express the field in terms of the total power transmitted over the $2\pi r_0$ circumference and make the usual remarks as to radius of curvature and coordinates. The dimension y_0 corresponds to r_0 so that from Fig. 2-1 we see that

$$r - r_0 = y_0 - y \tag{5-1}$$

and making the necessary changes in 2-46 we have

$$E_{1\theta}^{I}(r,z) \approx iA\sqrt{P_{Tang}}\,\sinh\gamma_1[y_0 + r_0 - r]\,e^{-i\left[\beta_0 + \frac{2\pi}{L}\right]z} \tag{5-2A}$$

$$A = \sqrt{\frac{\omega\mu}{\pi r_0}}\,\frac{\frac{\cos\pi\frac{W}{L}}{1-4(W/L)^2}\sqrt{\sinh\gamma_0' g}}{\sinh\gamma_1 g\sqrt{\frac{\beta_0}{\sinh\gamma_0' g}\left[\frac{g}{2} - \frac{\sinh 2\gamma_0' g}{4\gamma_0'}\right] - \frac{\cos\pi\frac{W}{L}}{1-4\left[\frac{W}{L}\right]^2}\left[\frac{(\beta_0+\beta_1)(\gamma_1\sinh\gamma_0' g\cosh\gamma_1 g - \gamma_0'\cos\gamma_0' g\sinh\gamma_1 g)}{\sinh\gamma_1 g(\gamma_0'^2+\gamma_1^2)}\right.}} \tag{5-2B}$$

$$\left. + \frac{(\beta_0+\beta_{-1})(\gamma_{-1}\sinh\gamma_0' g\cosh\gamma_{-1} g - \gamma_0'\cos\gamma_0' g\sinh\gamma_{-1} g)}{\sinh\gamma_{-1} g(\gamma_0'^2+\gamma_{-1}^2)}\right]$$

We obtain E_θ as a function of time for each electron by multiplication by $e^{i\omega t}$ and taking the real part, where t for an electron is expressed in terms of its entrance time into the fields and its longitudinal displacement. Since we have assumed uniformity of boundaries, the displacement is simply inversely proportional to the constant longitudinal velocity, given by Eq. 2-14 with m=1.

$$t = t_o + \frac{z}{v_{oz}} \tag{5-3}$$

Thus,

$$E_{1\theta}^{I} \approx -A\sqrt{P_{rfz}}\sinh\gamma_1[y_o + r_o - r]\sin\omega t_o \tag{5-4}$$

For small signal interaction we expand the field about $r=r_0$ and retain only the first two terms of the series. Using the notation of Eq. 4-12 we have

$$E_{1\theta}^{I} \approx -A\sqrt{P_{rfz}}\sin\omega t_o\left[\sinh\gamma_1 y_o - (\gamma_1\cosh\gamma_1 y_o)\delta\right] \tag{5-5}$$

Instead of constant angular momentum, as found in Eq. 4-3, we have that the time derivative of the angular momentum equals the torque[135] which is given by the product of E_θ and -er. We take the angular momentum in the form

$$\ell = \ell_o + \lambda \tag{5-6}$$

where ℓ_0 is the initial value which satisfies the equilibrium conditions in the absence of rf energy. Therefore,

$$\dot{\ell} = \dot{\lambda} \approx eA\sqrt{P_{rfz}}\sin\omega t_o\left[\sinh\gamma_1 y_o - (\gamma_1\cosh\gamma_1 y_o)\delta\right]\left[r_o + \delta\right] \tag{5-7}$$

Taking 5-7 to first order, and since for the uniform case $\frac{d}{dt} = v_{oz}\frac{d}{dz}$, we have

$$\frac{d\lambda}{dz} \approx \frac{eA\sqrt{P_{rfz}}\sin\omega t_o}{v_{oz}}\left\{\left[r_o\sinh\gamma_1 y_o\right] + \left[\sinh\gamma_1 y_o - r_o\gamma_1\cosh\gamma_1 y_o\right]\delta\right\}$$
$$\equiv \sin\omega t_o\sqrt{P_{rfz}}\left[K_o + K_1\delta\right] \tag{5-8}$$

Using logarithmic potential in Eq. 4-5 and demanding equilibrium when the electron enters the system with $r=r_0$, $\dot{r}=0$, and $\ell=\ell_0$, we obtain

$$\ddot{r} - \frac{(\ell_0+\lambda)^2}{m^2 r^3} = -\frac{\ell_0^2}{m^2 r_0^2 r} \tag{5-9}$$

Expansion of 5-9 about r_0 as was done in Chap. 4 and retention of linear terms in δ and λ yields, with $\frac{d}{dt}=v_{oz}\frac{d}{dz}$,

$$\frac{d^2\delta}{dz^2} + 2\frac{\ell_0^2}{m^2 r_0^4 v_{oz}^2}\delta - \frac{2\ell_0}{m^2 r_0^3 v_{oz}^2}\lambda = 0 \tag{5-10}$$

Differentiation of 5-10 and substitution of 5-8 yields

$$\frac{d^3\delta}{dz^3} + 2\frac{\ell_0^2}{m^2 r_0^4 v_{oz}^2}\frac{d\delta}{dz} - \frac{2\ell_0}{m^2 r_0^3 v_{oz}^2}\sin\omega t_0\sqrt{P_{Tavg}}\left[K_0+K_1\delta\right]=0 \tag{5-11}$$

We assume that an exponential solution for power is appropriate to linear interaction and therefore take

$$P_{Tavg} \approx P_0 e^{2\alpha z} \tag{5-12}$$

so that the differential equation for δ is

$$\delta''' + 2\frac{\ell_0^2}{m^2 r_0^4 v_{oz}^2}\delta' - \frac{2\ell_0}{m^2 r_0^3 v_{oz}^2}\sin\omega t_0\sqrt{P_0}\,e^{\alpha z}\left[K_0+K_1\delta\right]=0 \tag{5-13}$$

We solve 5-13 approximately by the method of perturbation[136] which was applied in Chap. 4. We wish a solution which will be accurate for small values of power so that we seek a solution of the form

$$\delta = \delta_0 + P_0^{1/2}\delta_1 + P_0\delta_2 + \cdots \tag{5-14}$$

We substitute 5-14 in 5-13 and separate according to powers of $P_0^{1/2}$. We obtain for the first two equations

$$\delta_0''' + 2\frac{\ell_0^2}{m^2 r_0^4 v_{oz}^2}\delta_0' = 0 \tag{5-15A}$$

$$\delta_1''' + 2\frac{\ell_0^2}{m^2 r_0^4 v_{oz}^2}\delta_1' = 2\frac{\ell_0}{m^2 r_0^3 v_{oz}^2}\sin\omega t_0 e^{\alpha z}\left[K_0+K_1\delta_0\right] \tag{5-15B}$$

The solution to 5-15A is immediately

$$\delta_0 = a_0 \cos \frac{\sqrt{2}\, l_0}{m r_0^2 v_{0z}} z + b_0 \sin \frac{\sqrt{2}\, l_0}{m r_0^2 v_{0z}} z + C_0 \qquad (5\text{-}16)$$

Since the solution 5-14 must satisfy the initial conditions as $P_0^{1/2} \to 0$, the δ_0 solution must carry the initial conditions. At z=0, $\delta_0 = \delta_0' = \delta_0'' = 0$ so that $\delta_0 \equiv 0$.

The particular solution of 5-15B with $\delta_0 \equiv 0$ will be obtained by assuming a solution of form proportional to $e^{\alpha z}$. The homogeneous part of 5-15B is identical with 5-15A so that a solution of form 5-16 is appropriate for the homogeneous solution. We therefore have

$$\delta_1 = a_1 \cos \frac{\sqrt{2}\, l_0}{m r_0^2 v_{0z}} z + b_1 \sin \frac{\sqrt{2}\, l_0}{m r_0^2 v_{0z}} z + C_1 + \frac{K_0 \sin \omega t_0}{\alpha \left[\alpha^2 + \frac{2 l_0^2}{m^2 r_0^4 v_{0z}^2}\right]} \frac{2 l_0}{m^2 r_0^3 v_{0z}^2} e^{\alpha z} \qquad (5\text{-}17)$$

The initial conditions on δ_1 are the same as those for δ_0 so that evaluation of the constants in 5-17, and using 5-14, yields for the approximate solution for δ

$$\delta \approx \frac{K_0 \sin \omega t_0 \, P_0^{1/2}}{\alpha \left[\alpha^2 + \frac{2 l_0^2}{m^2 r_0^4 v_{0z}^2}\right]} \frac{2 l_0}{m^2 r_0^3 v_{0z}^2} \left\{ e^{\alpha z} + \frac{\alpha^2}{\frac{2 l_0^2}{m^2 r_0^4 v_{0z}^2}} \cos \frac{\sqrt{2}\, l_0}{m r_0^2 v_{0z}} z - \frac{\alpha}{\frac{\sqrt{2}\, l_0}{m r_0^2 v_{0z}}} \sin \frac{\sqrt{2}\, l_0}{m r_0^2 v_{0z}} z - \left[1 + \frac{\alpha^2}{\frac{2 l_0^2}{m^2 r_0^4 v_{0z}^2}} \right] \right\} \qquad (5\text{-}18)$$

For large enough z we take the dominant term in 5-18 to be the exponential. Therefore,

$$\delta \approx \frac{K_0 \sin \omega t_0}{\alpha \left[\alpha^2 + \frac{2 l_0^2}{m^2 r_0^4 v_{0z}^2}\right]} \frac{2 l_0}{m^2 r_0^3 v_{0z}^2} P_0^{1/2} e^{\alpha z} \qquad (5\text{-}19)$$

We have from 5-8

$$\frac{d\lambda}{dz} \approx K_0 \sin\omega t_0 P_0^{1/2} e^{\alpha z}\left\{1 + \frac{K_1 \sin\omega t_0}{\alpha\left[\alpha^2 + \frac{2l_0^2}{m^2 r_0^4 v_{0z}^2}\right]} \frac{2l_0}{m^2 r_0^3 v_{0z}^2} P_0^{1/2} e^{\alpha z}\right\} \tag{5-20}$$

We next average $\frac{d\lambda}{dz}$ over all entrance times to obtain the value for the the "average" electron. This will be used to obtain the cumulative effect of all the phases. We find,

$$\frac{1}{2\pi}\int_0^{2\pi} \frac{d\lambda}{dz} d[\omega t_0] \equiv \overline{\frac{d\lambda}{dz}} \approx \frac{K_0 K_1}{\alpha\left[\alpha^2 + \frac{2l_0^2}{m^2 r_0^4 v_{0z}^2}\right]} \frac{l_0}{m^2 r_0^3 v_{0z}^2} P_0 e^{2\alpha z} \tag{5-21}$$

The energy of an electron is given by

$$H = T + V = \tfrac{1}{2} m\left\{\dot{\delta}^2 + \frac{[l_0+\lambda]^2}{m^2[r_0+\delta]^2} + v_{0z}^2\right\} - e\phi \tag{5-22}$$

We find ϕ within a constant from 5-9 and without loss of generality define the energy to be zero at the cathode and when the beam enters the system, setting the value of the constant. Linearizing the potential we find

$$\phi \approx \frac{l_0^2}{2em r_0^2} + \frac{m}{2e} v_{0z}^2 - \frac{l_0^2}{e m r_0^3}\delta \tag{5-23}$$

Similarly we linearize T and find

$$T \approx \tfrac{1}{2} m v_{0z}^2 + \frac{l_0^2}{2m r_0^2} + \frac{l_0}{m r_0^2}\lambda - \frac{l_0^2}{m r_0^3}\delta \tag{5-24}$$

To first order, the energy of an electron is, from 5-22, 5-23, and 5-24

$$H \approx \frac{l_0}{m r_0^2}\lambda \tag{5-25}$$

The power carried by the beam past any cross section is just the product of 5-25 averaged over all phases and the number of electrons flowing past that cross section per second. Therefore

$$P_b = \frac{N l_0}{m r_0^2}\overline{\lambda} \tag{5-26A}$$

$$N = \frac{|I|}{e} \tag{5-26B}$$

The sum of the beam and wave powers flowing through a cross sectional plane at arbitrary value of z is constant and therefore the derivative with respect to z is zero. We have, from 5-12, 5-21, and 5-26A that

$$2\alpha P_0 e^{2\alpha z} + \frac{N l_0^2}{m^3 r_0^5} \frac{K_0 K_1}{\alpha\left[\alpha^2 + \frac{2 l_0^2}{m^2 r_0^4 v_{0z}^2}\right]} \frac{P_0 e^{2\alpha z}}{v_{0z}^2} = 0 \tag{5-27}$$

which is equivalent to, for $P_0 \neq 0$, the quadratic equation in α^2

$$\alpha^4 + \frac{2 l_0^2}{m^2 r_0^4 v_{0z}^2}\alpha^2 + \frac{N l_0^2 K_0 K_1}{2 m^3 r_0^5 v_{0z}^2} = 0 \tag{5-28}$$

If the variations in the electron motion occur much faster due to the effects of the rf forces rather than the natural electron oscillations, so that

$$\alpha^2 >> \frac{2 l_0^2}{m^2 r_0^4 v_{0z}^2} \tag{5-29A}$$

we have from 5-28

$$\alpha^4 \approx -\frac{N l_0^2 K_0 K_1}{2 m^3 r_0^5 v_{0z}^2} \tag{5-29B}$$

From 5-8 we see that for large radius of curvature K_1 will certainly be negative. Under those circumstances α^4 is positive and we have approximately for the four roots of α

$$\alpha_1' = |\alpha'| \tag{5-30A}$$

$$\alpha_2' = -|\alpha'| \tag{5-30B}$$

$$\alpha_3' = i|\alpha'| \tag{5-30C}$$

$$\alpha_4' = -i|\alpha'| \tag{5-30D}$$

$$|\alpha'| = \sqrt[4]{-\frac{N l_0^2 K_0 K_1}{2 m^3 r_0^5 v_{0z}^2}} \tag{5-30E}$$

There will be, therefore, a growing solution, an attenuating solution and an oscillating solution. The solution of interest for these considerations is the growing wave, given by α_1'.

If the above approximation is not made we have from 5-28 that

$$\alpha^2 = -\frac{l_o^2}{m^2 r_o^4 v_{oz}^2}\left\{1 \pm \sqrt{1 - \frac{NK_oK_1 m r_o^3 v_{oz}^2}{2l_o^2}}\right\} \tag{5-31}$$

We see that for K_1 negative the two values of α^2 are both real, one being positive and one negative. We therefore have two purely real values of α, with the same magnitude and opposite sign and for the other two roots a pair of purely imaginary complex conjugate roots. The behavior is basically the same as for the approximated case, the important point being that there is a growing solution. We have

$$\alpha_{1,2} = \pm \frac{l_o}{m r_o^2 v_{oz}} \sqrt{\sqrt{1 - \frac{NK_oK_1 m r_o^3 v_{oz}^2}{2l_o^2}} - 1} \tag{5-32A}$$

$$\alpha_{3,4} = \pm i \frac{l_o}{m r_o^2 v_{oz}} \sqrt{1 + \sqrt{1 - \frac{NK_oK_1 m r_o^3 v_{oz}^2}{2l_o^2}}} \tag{5-32B}$$

We may easily show that Eqs. 5-32 reduce to Eqs. 5-30 when

$$\sqrt{-\frac{NK_oK_1 m r_o^3 v_{oz}^2}{2l_o^2}} \gg 1$$

Of course, we recognize that if the losses of the rf structure are taken into account, the growing wave root of α must be larger than a critical value before actual gain will be noticed.

We may express the value of α consistent with a growing solution given in Eq. 5-32A in terms of the more approximate value given in 5-30A utilizing the wavelength of natural electron oscillations, λ_0, given in 4-113A. We find

$$\alpha_1 = \alpha_1' \sqrt{\sqrt{1 + \frac{4\pi^2}{(\alpha_1'\lambda_o)^4}} - \frac{2\pi}{(\alpha_1'\lambda_o)^2}} \tag{5-33}$$

and we see that for $\alpha_1' \lambda_0$ large the two solutions coalesce. As an example we choose the dimensions and data shown in Fig. 2-28:

$$g=.650 \text{ inch}$$
$$W=.312 \text{ inch}$$
$$t=.032 \text{ inch}$$

and we choose for the operating point on the dispersion diagram

$$\beta_0 L=.4\pi$$
$$f\approx 11 GHz$$

We allow for the zero thickness beam a clearance to the plane of the teeth of .100 inch. For this clearance the interaction fields will be relatively strong without a large possibility of beam interception and the piecewise parabolic Hill's equation is a good approximation. The choice of operating point on the dispersion diagram and the choice for synchronization with the n=1 space harmonic yields from 2-14 and 2-8A

$$\frac{v_e}{c} = \frac{v_{0z}}{c} \approx .267$$

and

$$\phi_z \approx \frac{v_{0z}^2}{2\eta} \approx 18.23 \text{ KV}$$

We find then

$$\alpha_1' \approx .777 \frac{|I|^{1/4}}{\sqrt{\lambda_0}}$$

If we take

$$\frac{r_0}{L}=10$$

and we take

$$\left[\frac{v_{e_0}}{v_{0z}}\right]^2 = .6$$

consistent with the discussion in Chap. 4 so that

$$\left[\frac{v_{e_0}}{v_{0z}}\right]^2 < 1$$

From Fig. 4-20 the beam will be stable with

$$\beta \approx .035$$

We find therefore that the total potential of the electron is

$$V_T \approx 29.175 \text{ KV}$$

since

$$\frac{V_{oz}}{V_T}=\frac{5}{8}$$

For an electron gun of perveance

$$P\approx 10^{-6}$$

We have then

$$|I|\approx 5 \text{ amp}$$

With these values we find

$$\alpha_1'\lambda_0\approx .823$$

and

$$\sqrt{\sqrt{1+\frac{4\pi^2}{(\alpha_1'\lambda_0)^4}}-\frac{2\pi}{(\alpha_1'\lambda_0)^2}}\approx .232$$

so that 5-33 must be used for accuracy. We find for the gain in db

$$G_{db}=10\ell og_{10}e^{2\alpha_1 z}\approx 8.686\alpha_1 z$$

so that

$$G_{db}/\text{period}\approx .029 \text{ db}$$

$$G_{db}/\text{ free space wavelength}\approx .09 \text{ db}$$

We can easily show

$$\alpha_1=\frac{\sqrt{2\pi}}{\lambda_0}\sqrt{\sqrt{1+\frac{(\alpha_1'\lambda_0)^4}{4\pi^2}}-1} \qquad (5\text{-}34)$$

so that for the low gain situation

$$\frac{(\alpha_1'\lambda_0)^4}{4\pi^2}<<1$$

and it is readily shown

$$\alpha_1\approx\frac{(\alpha_1')^2\lambda_0}{2\sqrt{\pi}} \qquad (5\text{-}35)$$

We see, therefore, that in the low gain region the gain varies as

$$|I|^{1/2}$$

so that some improvement in the low gain for this simple model may be realized by increasing the perveance of the gun.

5.3 Large Signal Region

If the beam displacements become appreciable some interception can take

place. If this beam collection occurs at the outer cylinder and not at the inner circuit, electrons which remove energy from the field will be removed entirely from the interaction process. In this way, net interaction can be enhanced according to the simple model.

However, this may require that the initial position of the beam be so close to the outer cylinder that the space harmonic fields will be negligible there. It seems that there will be some optimum arrangement which would give the best results under the conditions of the model presented.

As electrons are removed periodically from interaction a bunched beam will result. Space-charge forces will then tend to make the beam uniform once again. Also, these axial bunches may also excite a modewhich has longitudinal electric field which can then interfere with the interaction process of the model.

5.4 Effects of the Magnetic Field

All of the preceding was predicated upon the omission of the force due to the rf magnetic field as is uniformly done in beam-wave interaction calculations. We will now show that this is a gross error for TE waves.

We transform to a moving coordinate system moving in the axial direction, the direction of propagation and electron translation. The transformation of the field quantities is[137]

$$E_z' = E_z \tag{5-36A}$$

$$E_T' = \left[\frac{\bar{E} + \bar{v} \times \bar{B}}{\sqrt{1-\left(\frac{v}{c}\right)^2}}\right]_T \tag{5-36B}$$

$$B_z' = \left[\bar{B} - \frac{\bar{v}}{c^2} \times \bar{E}\right]_z \tag{5-36C}$$

$$B_T' = \left[\frac{\bar{B} - \frac{\bar{v}}{c^2} \times \bar{E}}{\sqrt{1-\left(\frac{v}{c}\right)^2}}\right]_T \tag{5-36D}$$

where the primed components are written in the coordinate system moving with velocity v in the z direction and the subscript T stands for the transverse components of the fields.

The space harmonic fields obey Maxwell's equations and we can derive the transverse components of the fields from the relevant axial components in the TE and TM cases. We take the axial dependence to be, as usual

$$e^{-i\beta_m z}$$

For the TM wave we have the relation between the fields to be[138]

$$\bar{H}_{m_T} = \frac{k}{\beta_m}\sqrt{\frac{\epsilon}{\mu}}\,\bar{a}_z \times \bar{E}_{mT} \tag{5-37A}$$

where k is the free-space wave number. Therefore,

$$\bar{B}_{m_T} = \frac{v_{\varphi m}}{c^2}\,\bar{a}_z \times \bar{E}_{mT} \tag{5-37B}$$

with $v_{\varphi m}$ given in Eq. 2-14. For a slow wave, a necessary condition is

$$v_{\varphi m} < c \tag{5-38A}$$

and therefore we have from 5-37B that the magnitudes of $\bar{E}_{nT}$ and $\bar{B}_{nT}$ are in the ratio of

$$\frac{c^2}{v_{\varphi m}} > c \tag{5-38B}$$

We therefore see from 5-36B that if the velocity of the moving coordinate system is to be less than c we cannot eliminate the electric field by such a transformation. However, we can eliminate the magnetic field and we take

$$\bar{v} = v_{\varphi m}\,\bar{a}_z \tag{5-39}$$

With 5-39, 5-36D and in view of 5-38A we see that

$$B'_{m_T} = 0 \tag{5-40A}$$

Similarly, from 5-36B we find

$$\bar{E}'_{mT} = \frac{\bar{E}_{mT} + \left(\frac{v_{\varphi m}}{c}\right)^2 \bar{a}_z \times \bar{a}_z \times \bar{E}_{mT}}{\sqrt{1-\left[\frac{v_{\varphi m}}{c}\right]^2}} = \sqrt{1-\left[\frac{v_{\varphi m}}{c}\right]^2}\;\bar{E}_{mT} \tag{5-40B}$$

In this frame of reference, in which the electron is stationary, there is no magnetic field and the transverse electric field is reduced by the factor

$$\sqrt{1-\left[\frac{v_{\varphi m}}{c}\right]^2}$$

tending to zero in the limit as

$$\frac{v_{\varphi m}}{c} \longrightarrow 1$$

For a TE wave the parallel relation to 5-37A is

$$\bar{E}_{mT} = -\frac{k}{\beta_m}\sqrt{\frac{\mu}{\epsilon}}\,\bar{a}_z \times \bar{H}_{mT} = -v_{\varphi m}\bar{a}_z \times \bar{B}_{mT} \qquad (5\text{-}41)$$

For this situation the magnitudes of $\bar{E}_{nT}$ and $\bar{B}_{nT}$ are in the ratio of

$$v_{\varphi m} < c$$

and so a transformation 5-36B can eliminate the electic field. We use the velocity of transformation as in 5-39 obtaining from 5-36B and 5-41 in the light of 5-38A that

$$\bar{E}'_{mT} = 0 \qquad (5\text{-}42A)$$

and from 5-36D

$$\bar{B}'_{mT} = \frac{\bar{B}_{mT} + \left(\frac{v_{\varphi m}}{c}\right)^2 \bar{a}_z \times \bar{a}_z \times \bar{B}_{mT}}{\sqrt{1-\left(\frac{v_{\varphi m}}{c}\right)^2}} = \sqrt{1-\left(\frac{v_{\varphi m}}{c}\right)^2}\,\bar{B}_{mT} \qquad (5\text{-}42B)$$

In this frame of reference, for which the electron is stationary with respect to translation, there is no electric field and the transverse magnetic field is reduced in a manner similar to the reduction of the transverse electric field in the TM case.

The total rf transverse force on the electron for synchronous motion is therefore zero and one cannot expect to find interaction based on the model proposed earlier.

The inclusion of v_θ in the synchronous case produces radial and axial magnetic forces. The radial motion will give rise to an angular magnetic

force, albeit small in view of the radially bounded nature of the geometry. The force for the required mode, still demanding synchronism despite the axial force, is then

$$\bar{f} = -e\mu[v_\theta H_z \bar{a}_r - v_r H_z \bar{a}_\theta - v_\theta H_r \bar{a}_z] \tag{5-43}$$

Despite the magnetic nature of 5-43 there is still power transferred between wave and electron since

$$P = \bar{v}\cdot\bar{f} = -e\bar{v}\cdot[\bar{E} + \bar{v}\times\bar{B}] = -e\bar{v}\cdot\bar{E} = -ev_\theta E_\theta \tag{5-44}$$

The dot product of the purely magnetic force, 5-43, with the velocity vector yields

$$P = e\mu v_\theta v_z H_r \tag{5-45}$$

which is for synchronism easily shown to be identical with 5-44, using 5-41.

It can be that these magnetic forces give rise to net interaction. Moreover, it may be possible that net interaction will result when effects such as space-charge forces and nonsynchronous velocity are considered. A nonsynchronous velocity will no longer result in cancellation of the angular electric force on the electron. Just as nonsynchronous velocity results in net gain for a normal traveling wave tube, so may it here.

Other so-called transverse wave interactions[139] have purely transverse electric fields only at the unperturbed beam position. The longitudinal electric field is nonzero off the axis and this field is crucial to the energy-exchange process in those interaction mechanisms.

APPENDIX

COMPUTATION OF THE PARABOLIC CYLINDER FUNCTIONS

A method of computation of the functions U(a,x) and V(a,x) of Sec. 4.10 was developed for the digital computer using a composite scheme. The method was found to give accurate results when compared to tables[140] for $|a| \leq 5.0$ and $|x| \leq 3.5$ which was a wide enough range to obtain the results given in Sec. 4.10 by use of the digital computer. All of the following is subject to those restrictions on $|a|$ and $|x|$.

The series definitions for the functions[141] are used for $a \leq 0$; for $a \geq 0$ and $|x| \leq 1.5$; and for $a \geq 0$ and $|x| \geq 1.5$ for V(a,x) only. The number of terms taken in the series is greater than a minimum number set in the computer program. This number should not be so great as to cause underflow or overflow in the computer. The series is terminated when either the upper bound for the number of terms is reached or the normalized change in the series is less than some chosen value given by the variable STOP. Cases where the gamma functions have very large negative arguments or poles, are not computed. The latter situation, involving indeterminate cases, involves evaluation in terms of Hermite polynomials and probability and Dawson's Integrals.

The first subroutine uses the recurrence relations easily found from Eqs. 4-177.

$$x U(a,x) - U(a-1,x) + (a+\tfrac{1}{2}) U(a+1,x) = 0 \tag{A-1}$$

$$x V(a,x) - V(a+1,x) + (a-\tfrac{1}{2}) V(a-1,x) = 0 \tag{A-2}$$

For U(a,x) for the range mentioned A-1 is used in a backward recurrence scheme while for V(a,x) it was found that the series was more accurate. The method is initiated for a value of a much larger than the desired value and U(a+1,x) and U(a,x) are set arbitrarily at the values 1 and 2 respectively. The recurrence relation is applied successively until the

value of a lies between 0 and -1. The value of the function is stored at the desired value of a. The functions will differ for this range by a multiplicative constant from the true values since the other solution to the difference equation will be small. The solutions are normalized by evaluating U(a,x) for the value of a between 0 and -1 by the series method, given in the second subroutine. The FORTRAN IV program is given below.

```
C     ********************************************************************  MAIN   10
C     ********************************************************************  MAIN   20
C     ********************************************************************  MAIN   30
C     ********************************************************************  MAIN   40
C     COMPUTATION OF THE PARABOLIC CYLINDER FUNCTIONS                       MAIN   50
C                   U(A,X)  AND  V(A,X)                                     MAIN   60
C     SOLUTIONS TO THE DIFFERENTIAL EQUATION                                MAIN   70
C              Y'' - (0.25*X*X + A)*Y = 0.0                                 MAIN   80
C                                                                           MAIN   90
C     THE METHOD HAS BEEN SHOWN TO BE ACCURATE FOR                          MAIN  100
C     ABSOLUTE VALUE OF A LESS THAN OR EQUAL TO 5.0 AND                     MAIN  110
C     ABSOLUTE VALUE OF X LESS THAN OR EQUAL TO 3.5                         MAIN  120
C                                                                           MAIN  130
C     SET FLAG=1.0 BEFORE CALLING PROGRAM                                   MAIN  140
C     FLAG IS CHANGED TO -1.0 IF THE GAMMA FUNCTION HAS A POLE OR           MAIN  150
C     TOO LARGE A NEGATIVE ARGUMENT.                                        MAIN  160
C     NO VALUE IS RETURNED FOR THESE CASES                                  MAIN  170
C     A POLE CORRESPONDS TO AN INDETERMINATE CASE                           MAIN  180
C                                                                           MAIN  190
C     THE METHOD USED IS A COMPOSITE ONE.......                             MAIN  200
C           FOR NEGATIVE A THE SERIES IS USED                               MAIN  210
C     FOR POS. A THE SERIES IS USED FOR ABS. VALUE OF X LESS THAN 1.5       MAIN  220
C     FOR POS. A AND FOR ABS. VALUE OF X GREATER THAN 1.5                   MAIN  230
C                                  FOR U THE RECURSION METHOD IS USED       MAIN  240
C                                  FOR V THE SERIES IS USED                 MAIN  250
C                                                                           MAIN  260
C     THE NUMBER OF TERMS IN THE SERIES IS SET TO BE WITHIN TWO BOUNDS      MAIN  270
C     THE SERIES IS TERMINATED WHEN THE ABSOLUTE VALUE OF THE               MAIN  280
C     RELATIVE CHANGE IS LESS THAN STOP                                     MAIN  290
C     THE NUMBER OF TERMS TAKEN IS RETURNED IN ZAP                          MAIN  300
C                                                                           MAIN  310
C     THE REFERENCE FOR THE RECURSION METHOD IS FOR A BETWEEN 0 AND -1      MAIN  320
C     THE INITIALIZATION OF THE RECURSION METHOD IS WITH VALUES 1,2         MAIN  330
C     ********************************************************************  MAIN  340
C     ********************************************************************  MAIN  350
C     ********************************************************************  MAIN  360
```

```
      SUBROUTINE FRODO(A,X,U,V,ZAP,FLAG)                                FROD   10
      DIMENSION HOLD(4)                                                 FROD   20
      IF (A .GE. 0.0) GO TO 60                                          FROD   30
      FLAG = 1.0                                                        FROD   40
      CALL BILBO(A,X,UAX,VAX,FLAG,ZAP)                                  FROD   50
      U=UAX                                                             FROD   60
      V=VAX                                                             FROD   70
      GO TO 7                                                           FROD   80
60    ABX=ABS(X)                                                        FROD   90
      IF(ABX .GE. 1.5) GO TO 61                                         FROD  100
      FLAG = 1.0                                                        FROD  110
      CALL BILBO(A,X,UAX,VAX,FLAG,ZAP)                                  FROD  120
      U=UAX                                                             FROD  130
      V=VAX                                                             FROD  140
      GO TO 7                                                           FROD  150
61    DO 922 LAU=1,4                                                    FROD  160
      HOLD(LAU)=0.0                                                     FROD  170
922   CONTINUE                                                          FROD  180
      VALPU1=1.0                                                        FROD  190
      VALPV1=1.0                                                        FROD  200
      VALPU2=2.0                                                        FROD  210
      VALPV2=2.0                                                        FROD  220
      VALPU3=0.0                                                        FROD  230
      VALPV3=0.0                                                        FROD  240
      WAIT=AINT(A)                                                      FROD  250
      WAITA=ABS(WAIT)                                                   FROD  260
      STARTP=(2.0*WAITA)+20.0+A                                         FROD  270
      ARGPU1=STARTP                                                     FROD  280
      ARGPU2=ARGPU1-1.0                                                 FROD  290
      ARGPU3=ARGPU1-2.0                                                 FROD  300
      ARGPV1=STARTP                                                     FROD  310
      ARGPV2=ARGPV1-1.0                                                 FROD  320
      ARGPV3=ARGPV1-2.0                                                 FROD  330
      DO 902 LI=1,500                                                   FROD  340
      VALPU3=X*VALPU2+((ARGPU2+0.5)*VALPU1)                             FROD  350
      VALPV3=(1.0/(ARGPV2-0.5))*(VALPV1-(X*VALPV2))                     FROD  360
      FLI=LI                                                            FROD  370
```

```
      ARGPU1=STARTP-FLI                                                 FROD  380
      ARGPU2=ARGPU1-1.0                                                 FROD  390
      ARGPU3=ARGPU2-2.0                                                 FROD  400
      ARGPV1=STARTP-FLI                                                 FROD  410
      ARGPV2=ARGPV1-1.0                                                 FROD  420
      ARGPV3=ARGPV2-2.0                                                 FROD  430
      VALPU1=VALPU2                                                     FROD  440
      VALPU2=VALPU3                                                     FROD  450
      VALPV1=VALPV2                                                     FROD  460
      VALPV2=VALPV3                                                     FROD  470
      STOPP=ABS(ARGPU2-A)                                               FROD  480
      IF(STOPP .GT. 0.001) GO TO 952                                    FROD  490
      HOLD(1)=VALPU2                                                    FROD  500
      HOLD(2)=VALPV2                                                    FROD  510
  952 RBR=0.0                                                           FROD  520
      IF(ARGPU2 .GE.   RBR ) GO TO  902                                 FROD  530
      HOLD(3)=VALPU2                                                    FROD  540
      HOLD(4)=VALPV2                                                    FROD  550
      FLAG=1.0                                                          FROD  560
      CALL BILBO(ARGPU2,X,TUP,TVP,FLAG,ZAP)                             FROD  570
      IF(FLAG .LT. 0.0) GO TO 7                                         FROD  580
      UAX=(TUP/HOLD(3))*HOLD(1)                                         FROD  590
      VAX=(TVP/HOLD(4))*HOLD(2)                                         FROD  600
      BRACHA=UAX                                                        FROD  610
      VAX=0.0                                                           FROD  620
      FLAG=1.0                                                          FROD  630
      CALL BILBO(A,X,UAX,VAX,FLAG,ZAP)                                  FROD  640
      UAX=0.0                                                           FROD  650
      UAX=BRACHA                                                        FROD  660
      U=UAX                                                             FROD  670
      V=VAX                                                             FROD  680
      GO TO 7                                                           FROD  690
  902 CONTINUE                                                          FROD  700
      PRINT 972                                                         FROD  710
  972 FORMAT(18H A IS TOO POSITIVE)                                     FROD  720
      FLAG=-1.0                                                         FROD  730
      GO TO 7                                                           FROD  740
```

```
7       RETURN                                                  FROD  750
        END                                                     FROD  760
```

```
      SUBROUTINE BILBO(A1,X,UAIX,VAIX,FLAG,ZAP)                          BILB   10
      PI=3.1415927                                                       BILB   20
      FLAG=1.0                                                           BILB   30
      BRAY1S=EXP(-(X*X/4.0))                                             BILB   40
      PRE1=1.0                                                           BILB   50
      BRAY2S=X*(EXP(-(X*X/4.0)))                                         BILB   60
      PRE2=X                                                             BILB   70
      PREU=0.0                                                           BILB   80
      PREV=0.0                                                           BILB   90
      DO 200  I=1,500                                                    BILB  100
      FI=I                                                               BILB  110
      PRE1=((A1+0.5+(2.0* (FI-1.0)))*(PRE1)/((2.0*FI)*((2.0*FI)-1.0)))*X BILB  120
     1*X                                                                 BILB  130
      FINC1=(PRE1)*(EXP(-(X*X/4.0)))                                     BILB  140
      BRAY1S = BRAY1S +FINC1                                             BILB  150
      YS1=BRAY1S                                                         BILB  160
      FK=I                                                               BILB  170
      PRE2=((A1+1.5 +(2.0*(FK-1.0)))*(PRE2)/((2.0*FK)*((2.0*FK)+1.0)))   BILB  180
     1*X*X                                                               BILB  190
      FINC2=(PRE2)*(EXP(-(X*X/4.0)))                                     BILB  200
      BRAY2S=BRAY2S+FINC2                                                BILB  210
      YS2=BRAY2S                                                         BILB  220
      GARG1=0.25-(0.5*A1)                                                BILB  230
      PRE=1.0                                                            BILB  240
      DO 143  M=1,100                                                    BILB  250
      FM=M                                                               BILB  260
      IF (GARG1)  148, 145, 149                                          BILB  270
148   IF(GARG1+FM)  144, 145, 146                                        BILB  280
145   PRINT 147, GARG1                                                   BILB  290
147   FORMAT(30H GAMMA HAS A POLE, 0.25-0.5A1=, F8.3,                    BILB  300
     1  57H THEREFORE FOR THIS VALUE OF A, THE CASE IS INDETERMINATE)     BILB  310
      FLAG=-1.0                                                          BILB  320
      GO TO 77                                                           BILB  330
149   FUN1=GAMMA(GARG1)                                                  BILB  340
      GO TO 150                                                          BILB  350
144   PRE=(1.0/(GARG1+FM-1.0))*PRE                                       BILB  360
      GO TO  143                                                         BILB  370
```

```
146   PRE=(1.0/(GARG1+FM-1.0))*PRE                                          BILB  380
      FUN1= PRE*GAMMA(GARG1+FM)                                             BILB  390
      GO TO 150                                                             BILB  400
150   GO TO 152                                                             BILB  410
143   CONTINUE                                                              BILB  420
152   CONTINUE                                                              BILB  430
      IF (FM .LT. 99.0) GO TO 153                                           BILB  440
      PRINT 154                                                             BILB  450
154   FORMAT (34H ARGUMENT OF GAMMA IS TOO NEGATIVE)                        BILB  460
      FLAG=-1.0                                                             BILB  470
      GO TO 77                                                              BILB  480
153   FNUM1= (YS1)*FUN1                                                     BILB  490
      FDEN1=(SQRT(PI))*(2.0**((0.5*A1)+0.25))                               BILB  500
      YL1= FNUM1/FDEN1                                                      BILB  510
      GARG2=0.75-(0.5*A1)                                                   BILB  520
      PRE=1.0                                                               BILB  530
      DO 243  N=1,100                                                       BILB  540
      FN=N                                                                  BILB  550
      IF (GARG2) 248, 245, 249                                              BILB  560
248   IF(GARG2+FN) 244, 245, 246                                            BILB  570
245   PRINT 247, GARG2                                                      BILB  580
247   FORMAT(30H GAMMA HAS A POLE, 0.75-0.5A1=, F8.3,                       BILB  590
     1  57H THEREFORE FOR THIS VALUE OF A, THE CASE IS INDETERMINATE)       BILB  600
      FLAG=-1.0                                                             BILB  610
      GO TO 77                                                              BILB  620
249   FUN2=GAMMA(GARG2)                                                     BILB  630
      GO TO 250                                                             BILB  640
244   PRE=(1.0/(GARG2+FN-1.0))*PRE                                          BILB  650
      GO TO  243                                                            BILB  660
246   PRE=(1.0/(GARG2+FN-1.0))*PRE                                          BILB  670
      FUN2= PRE*GAMMA(GARG2+FN)                                             BILB  680
      GO TO 250                                                             BILB  690
250   GO TO 252                                                             BILB  700
243   CONTINUE                                                              BILB  710
252   CONTINUE                                                              BILB  720
      IF (FN .LT. 99.0) GO TO 253                                           BILB  730
      PRINT 254                                                             BILB  740
```

```
254   FORMAT (34H ARGUMENT OF GAMMA IS TOO NEGATIVE)                    BILB  750
      FLAG=-1.0                                                         BILB  760
      GO TO 77                                                          BILB  770
253   FNUM2=(YS2)*FUN2                                                  BILB  780
      FDEN2=(SQRT(PI))*(2.0**((0.5*A1)-0.25))                           BILB  790
      YL2=FNUM2/FDEN2                                                   BILB  800
      PREU=UA1X                                                         BILB  810
      UA1X=(YL1)*(COS(PI*(0.25+(0.5*A1))))-(YL2)*(SIN(PI*(0.25+(0.5*A1)) BILB  820
     1))                                                                BILB  830
      GARG3=0.5-A1                                                      BILB  840
      PRE=1.0                                                           BILB  850
      DO 343  L=1,100                                                   BILB  860
      FL=L                                                              BILB  870
      IF(GARG3) 348,345,349                                             BILB  880
348   IF(GARG3+FL) 344,345,346                                          BILB  890
345   PRINT 347, GARG3                                                  BILB  900
347   FORMAT(26H GAMMA HAS A POLE, 0.5-A1=, F8.3,                       BILB  910
     157H THEREFORE FOR THIS VALUE OF A, THE CASE IS INDETERMINATE)     BILB  920
      FLAG=-1.0                                                         BILB  930
      GO TO 77                                                          BILB  940
349   FUN3=GAMMA(GARG3)                                                 BILB  950
      GO TO 350                                                         BILB  960
344   PRE=(1.0/(GARG3+FL-1.0))*PRE                                      BILB  970
      GO TO 343                                                         BILB  980
346   PRE=(1.0/(GARG3+FL-1.0))*PRE                                      BILB  990
      FUN3=PRE*GAMMA(GARG3+FL)                                          BILB 1000
      GO TO 350                                                         BILB 1010
350   GO TO 352                                                         BILB 1020
343   CONTINUE                                                          BILB 1030
352   CONTINUE                                                          BILB 1040
      IF(FL .LT. 99.0) GO TO 353                                        BILB 1050
      PRINT 354                                                         BILB 1060
354   FORMAT(34H ARGUMENT OF GAMMA IS TOO NEGATIVE)                     BILB 1070
      FLAG=-1.0                                                         BILB 1080
      GO TO 77                                                          BILB 1090
353   CONTINUE                                                          BILB 1100
      PREV=VA1X                                                         BILB 1110
```

```
      VA1X=(1.0/  FUN3         )*((YL1)*(SIN(PI*(0.25+(0.5*A1))))      BILB 1120
     1  +(YL2)*(COS(PI* (0.25+(0.5*A1)))))                            BILB 1130
      ZAP=FI+1.0                                                      BILB 1140
      IF(FI .LT.  4.0) GO TO 200                                      BILB 1150
      TESTU= ABS((UA1X-PREU)/UA1X)                                    BILB 1160
      TESTV=ABS((VA1X-PREV)/VA1X)                                     BILB 1170
      STOP=1.0E-15                                                    BILB 1180
      IF (TESTU  .LT. STOP  .AND. TESTV .LT. STOP)  GO TO 70          BILB 1190
200   CONTINUE                                                        BILB 1200
      PRINT 72                                                        BILB 1210
72    FORMAT(48H MORE THAN 500 TERMS NECESSARY FOR THE FUNCTIONS)     BILB 1220
70    CONTINUE                                                        BILB 1230
77    RETURN                                                          BILB 1240
      END                                                             BILB 1250
```

REFERENCES

[1]Chernov, "Methods of focusing electron streams in modern microwave devices," Radiotekhnika i Elektronika, vol. 3, p. 1227, 1958.(English translation by Pergamon Institute:Radio Engineering and Electronics, vol. 3, p. 1.)

[2]Hutter, Beam and Wave Electronics in Microwave Tubes (Princeton: D. Van Nostrand Company, Inc., 1960), chap. 10.

[3] Hansen and Susskind, "Improvement of beam-tube performance by collector potential depression and a novel design," IRE Trans. on Electron Devices, vol. ED-7, p. 282, October 1960.

[4] Enderby and Phillips, "The Ubitron Amplifier--a high power millimeter TWT," Proc. IEEE, vol. 53, p. 1648, October 1965.

[5]Phillips, "The Ubitron, a high power traveling wave tube based on a periodic interaction in unloaded waveguide," IRE Trans. on Electron Devices, vol. ED-7, p. 231, October 1960.

[6]Crumly, "A UHF Traveling Wave Amplifier Tube employing an electrostatically focused hollow beam," IRE Trans. on Electron Devices, vol. ED-3, p. 62, January 1956.

[7]Bernashevskii and Novskova, "Spiratron with backward wave," Radiotekhnika iElektronika, vol. 3, p. 1218, 1958. (English translation by Pergamon Institute:Radio Engineering and Electronics, vol. 3, p. 165, 1958).

[8]Bernashevskii and Novskova, "Experimental investigation of a Backward-Wave Spiratron," Radiotekhnica i Elektronika, vol. 4, p. 1499, 1959. (English translation by Pergamon Institute:Radio Engineering and Electronics, vol. 4, p.135, 1959).

[9]Watkins and Wada, "The Helitron Oscillator," Proc. IRE, vol. 46, p. 1700, October 1958.

[10]Pantell, "Small signal analysis of the Helitron Oscillator," IRE Trans. on Electron Devices, vol. ED-7, p. 22, January 1960.

[11]Guenard and Doehler, "E and C type traveling wave devices," Proc. IRE, vol. 44, p. 261, February 1956.

[12]Heffner and Watkins, "The practicality of E-type traveling wave devices," Proc. IRE, vol. 43, p. 1007, August 1955.

[13]Abramowitz and Stegun, Handbook of Mathematical Functions (New York: Dover Publications, Inc., 1965), p. 364.

[14]Brillouin, Wave Propagation in Periodic Structures (New York: McGraw-Hill Book Company, Inc., 1946).

[15]Collin, Field Theory of Guided Waves (New York: McGraw-Hill Book Company, Inc., 1960), pp. 368-371.

[16]Watkins, Topics in Electromagnetic Theory (New York: John Wiley and Sons, Inc., 1958), chap. 1.

[17]Arscott, Periodic Differential Equations (New York: MacMillan Company, 1964), pp. 29-31.

[18]Collin, Field Theory of Guided Waves, pp. 388-390.

[19]Watkins, Topics in Electromagnetic Theory, pp. 6-7.

[20]Ibid., pp. 76-77.

[21]Ibid., pp. 8-9.

[22]Ibid., pp. 19-20.

[23]Collin, Field Theory of Guided Waves, pp. 371-388.

[24]Hutter, Beam and Wave Electronics in Microwave Tubes, pp. 100-106.

[25]Collin, Field Theory of Guided Waves, p. 16.

[26]Hutter, Beam and Wave Electronics in Microwave Tubes, p. 100.

[27]Kronig and Penny, "Quantum Mechanics of electrons in crystal lattices," Proc of the Royal Soc. of London, Series A, vol 130, p. 499, 1931.

[28]van der Pol and Strutt, "On the stability of the solutions of Mathieu's equation," Philosophical Magazine and Journal of Science, vol. 5, p. 18, 1928.

[29]Brillouin, Wave Propagation in Periodic Structures, pp. 180-186.

[30]Ginzton, Microwave Measurements (New York: McGraw-Hill Book Company, Inc., 1957), chap. 10.

[31]Ibid., pp. 438-440.

[32]Bieberbach, Conformal Mapping (New York: Chelsea Publishing Company, 1953), pp. 21-23.

[33]Stratton, Electromagnetic Theory (New York: McGraw-Hill Book Company, Inc., 1941), p. 196.

[34]Sneddon, Mixed Boundary Value Problems in Potential Theory (New York: John Wiley and Sons, Inc., 1966).

[35]Churchill, Complex Variables and Applications (2d. ed.; New York: McGraw-Hill Book Company, 1960), pp. 34-38.

[36]Bieberbach, Conformal Mapping, pp. 5-13.

[37]Churchill, Complex Variables and Applications, pp. 41-43.

[38]Taylor, Advanced Calculus (Boston: Ginn and Company, 1955), p. 276.

[39]Nehari, Conformal Mapping (New York: McGraw-Hill Book Company, Inc., 1953), pp. 194-196.

[40]Ibid., p. 153.

[41]Churchill, Complex Variables and Applications, pp. 181-183.

[42]Taylor, Advanced Calculus, p. 270.

[43]Churchill, Complex Variables and Applications, pp. 186-187.

[44]Ibid., p. 122.

[45]Taylor, Advanced Calculus, p. 220.

[46]Javid and Brown, Field Analysis and Electromagnetics (New York: McGraw-Hill Book Company, Inc., 1963), pp. 209-219.

[47]Nehari, Conformal Mapping, pp. 280-296.

[48]Abramowitz and Stegun, Handbook of Mathematical Functions, p. 87.

[49]Churchill, Complex Variables and Applications, p. 125.

[50]Abramowitz and Stegun, Handbook of Mathematical Functions, p. 87.

[51]Ibid., p. 81.

[52]Ibid.

[53]Maxwell, A Treatise on Electricity and Magnetism (3d. ed.; New York: Dover Publications, Inc., 1954), pp. 297-301.

[54]Churchill, Complex Variables and Applications, pp. 186-187.

[55]Maxwell, A Treatise on Electricity and Magnetism, p. 301.

[56]Abramowitz and Stegun, Handbook of Mathematical Functions, p. 87.

[57]Churchill, Complex Variables and Applications, p. 122.

[58]Taylor, Advanced Calculus, p. 220.

[59]Churchill, Fourier Series and Boundary Value Problems (2d. ed.; New York: McGraw-Hill Book Company, 1963), pp. 107-109.

[60]Taylor, Advanced Calculus, p. 523.

[61]Ibid., p. 509.

[62]Ibid., p. 642.

[63]Lim and Moore, "Properties of alternately charged coplanar parallel strips by conformal mappings," IEEE Trans. Electron Devices, vol. ED-15, pp. 173-180, March 1968.

[64]Goldstein, Classical Mechanics (Reading, Massachusetts: Addison-Wesley Publishing Company, Inc., 1950), p. 18.

[65]Ibid., pp. 48-49.

[66]Ibid., pp. 53-55.

[67]Taylor, Advanced Calculus, p. 574.

[68]Chernov and Bernashevsky, "Helical Beam Tubes," translation unpublished.

[69]Taylor, Advanced Calculus, p. 574.

[70]Goldstein, Classical Mechanics, pp. 76-80.

[71]Kirstein, Kino, and Waters, Space-Charge Flow (New York: McGraw-Hill Book Publishing Company, 1967), pp. 160-162.

[72]Ibid.

[73]Ibid., p. 154.

[74]Taylor, Advanced Calculus, p. 608.

[75]Bois, Tables of Indefinite Integrals (New YArk: Dover Publications, Inc., 1961), p. 89.

[76]Taylor, Advanced Calculus, pp. 542, 574.

[77]Ibid., p. 577.

[78]Ibid., p. 613.

[79]Chernov and Bernashevsky, "Helical Beam Tubes."

[80]Kirstein, Kino, and Waters, Space-Charge Flow, p. 33.

[81]Goldstein, Classical Mechanics, pp. 69-71.

[82]Abramowitz and Stegun, Handbook of Mathematical Functions, p. 68.

[83]Taylor, Advanced Calculus, p. 574.

[84]Ralston and Wilf, eds., Mathematical Methods for Digital Computers (New York: John Wiley and Sons, Inc., 1960), p. 100-101.

[85]Abramowitz and Stegun, Handbook of Mathematical Functions, p. 597.

[86]Ibid., p. 591.

[87]Cunningham, Nonlinear Analysis (New York: McGraw-Hill Book Company, Inc., 1958), p. 83.

[88]Ibid., pp. 164-168.

[89]Churchill, Complex Variables and Applications, p. 122.

[90]Whittaker and Watson, A Course of Modern Analysis (4th. ed.; London: Cambridge University Press, 1927), p. 194.

[91]Abramowitz and Stegun, Handbook of Mathematical Functions, p. 68.

[92]Whittaker and Watson, A Course of Modern Analysis, p. 32.

[93]Abramowitz and Stegun, Handbook of Mathematical Functions, p. 376.

[94]Ibid., p. 375.

[95]McLachlan, Theory and Application of Mathieu Functions (New York: Dover Publications, Inc., 1964).

[96]Arscott, Periodic Differential Equations, chaps. 1-6.

[97]Hill, "On the part of the motion of the lunar perigee," Acta Math., vol. 8, pp. 1-36, 1886.

[98]Whittaker and Watson, A Course of Modern Analysis, pp. 413-417.

[99]Brillouin, Wave Propagation in Periodic Structures, p. 180.

[100]Magnus and Winkler, Hill's Equation, Interscience Tracts in Pure and Applied Mathematics, No. 20 (New York: Interscience Publishers, 1966), p. 4.

[101]Ibid., pp. 3-7.

[102]Ibid., p. 5.

[103]Ibid.

[104]Ibid., pp. 8-9.

[105]Ibid., pp. 11-12.

[106]Ibid., pp. 112-113.

[107]Ibid., p. 113.

[108]Ibid., p. 56.

[109]Ibid., pp. 61-62.

[110]Ibid., p. 46.

[111]Ibid., p. 68.

[112]Cunningham, Nonlinear Analysis, pp. 270-273.

[113]Taylor, Advanced Calculus, pp. 746-747.

[114]Abramowitz and Stegun, Handbook of Mathematical Functions, p. 724.

[115]Magnus and Winkler, Hill's Equation, pp. 39-40.

[116]Abramowitz and Stegun, Handbook of Mathematical Functions, chap. 19.

[117]Ibid., p. 687.

[118]Ibid.

[119]Ibid., pp. 688-689.

[120]Ibid., p. 689.

[121]Ibid., p. 256.

[122]Arscott, Periodic Differential Equations, p. 47.

[123]Morse and Feshbach, Methods of Theoretical Physics (New York: Mcgraw-Hill Book Company, 1953), Part II, pp. 1641-1642.

[124]Abramowitz and Stegun, Handbook of Mathematical Functions, chap. 22.

[125]United States National Bureau of Standards Computation Laboratory Tables Relating to Mathieu Functions, Characteristic Values, Coefficients and Joining Factors (New York: Columbia University Press, 1951).

[126]Ralston and Wilf, eds., Mathematical Methods for Digital Computers, pp. 100-101.

[127]McLachlan, Theory and Application of Mathieu Functions, pp. 137-138.

[128]Magnus and Winkler, Hill's Equation, pp. 117-118.

[129]Arscott, Periodic Differential Equations, pp. 34-37.

[130]Hochstadt, "A special Hill's equation with discontinuous coefficients," American Mathematical Monthly, vol. 70, pp. 18-26, 1963.

[131]Cunningham, Nonlinear Analysis, pp. 251-252.

[132]Dettman, Mathematical Methods in Physics and Engineering (New York: McGraw-Hill Book Company, Inc., 1962), p. 48.

[133]Taylor, Advanced Calculus, pp. 577-608.

[134]Cunningham, Nonlinear Analysis, pp. 164-168.

[135]Goldstein, Classical Mechanics, p. 2.

[136]Cunningham, Nonlinear Analysis, pp. 123-124, 189-190.

[137]Sommerfeld, Electrodynamics (New York: Academic Press, 1964), III, pp. 238-239.

[138]Collin, Foundations for Microwave Engineering (New York: McGraw-Hill Book Company, 1966), pp. 69-71.

[139]Briggs, Paik, and Gottfried, "Transverse-Wave tubes as high-efficiency microwave amplifiers," IEEE Trans. Electron Devices, vol. ED-18, pp. 511-520, August 1971.

[140]Abramowitz and Stegun, Handbook of Mathematical Functions, pp. 702-711.

[141]Ibid., pp. 686-687.

AUTOBIOGRAPHICAL STATEMENT

Mr. Mitchell Haspel was born in New York City on January 23,1940.

After receiving the Bachelor of Electrical Engineering degree from The City College of New York in February of 1961, he was employed by the Research Department of SFD Laboratories, Inc. of Union, New Jersey. For the next two and one-half years he was engaged in research work on experimental microwave tubes.

In September of 1963 he turned to full time graduate study at The City University of New York, a continuation of the part time study undertaken while employed at SFD Laboratories. In February, 1964 he attained the Master of Engineering (Electrical Engineering) degree. The decision was then taken to continue his education and enroll in the Doctoral Program at The City University of New York. He engaged in research first in plasma oscillations and later in microwave electronics.

Since 1964 he has held positions with the Department of Electrical Engineering of City College as Lecturer, Fellow and Research Assistant and has found that he enjoys teaching very much.

He has co-authored some technical reports at SFD Laboratories and a paper delivered at the High Power Tube Symposium, Fort Monmouth, New Jersey (September, 1962).

Mr. Haspel is a member of the IEEE and Eta Kappa Nu.